Virginia Commonwealth University
VCU Scholars Compass

Theses and Dissertations | Graduate School

2017

TYPE 2 IMMUNE RESPONSES IN THE CONTEXT OF HELMINTH INFECTION, ASTHMA, DENDRITIC CELLS, AND MYELOID DERIVED SUPPRESSOR CELL FUNCTION

Sheela Ruby Damle
Virginia Commonwealth University

Follow this and additional works at: https://scholarscompass.vcu.edu/etd

 Part of the Allergy and Immunology Commons, Immune System Diseases Commons, Immunity Commons, Immunopathology Commons, Neoplasms Commons, and the Parasitic Diseases Commons

© Sheela R. Damle

Downloaded from
https://scholarscompass.vcu.edu/etd/4696

This Dissertation is brought to you for free and open access by the Graduate School at VCU Scholars Compass. It has been accepted for inclusion in Theses and Dissertations by an authorized administrator of VCU Scholars Compass. For more information, please contact libcompass@vcu.edu.

©Sheela R. Damle 2017

All Rights Reserved

TYPE 2 IMMUNE RESPONSES IN THE CONTEXT OF HELMINTH INFECTION, ASTHMA, DENDRITIC CELLS, AND MYELOID DERIVED SUPPRESSOR CELL FUNCTION

A dissertation submitted in partial fulfillment of the requirements for the degree of Doctor of Philosophy at Virginia Commonwealth University

By

Sheela Ruby Damle

B.S., Cornell University, 2008

Director: Daniel H. Conrad, Ph.D., Professor, Department of Microbiology and Immunology

Virginia Commonwealth University

Richmond, Virginia

March, 2017

Acknowledgement

I would like to thank my advisor Dr. Daniel H. Conrad, who interviewed me when I applied to the M.D.-Ph.D. program and invited me to join his lab. Throughout my time in his lab, his door was always open for me to pop in and discuss current and future projects as well as troubleshoot experiments. He gave me the space to come up with and lead projects wherever the science led and gave me the opportunity to help write several grants, which has given me valuable skills that will aid me in my career. I greatly appreciate that he fostered an intellectually demanding lab environment and his willingness to let me explore many different scientific areas.

Dr. Conrad initially had me work with one of his graduate students at the time, Dr. Rebecca Martin. Dr. Martin introduced me to the lab and helped me find my bearings in an environment very different from my previous experiences. Over the past few years, Dr. Martin and I have worked on several projects, papers, and grants together. Within these experiences, she challenged me to think critically about experiments, scientific concepts, and my goals as a researcher. I am indebted to her for her mentorship and friendship during my PhD, and I hope that we will continue to collaborate and have fruitful scientific discussions throughout our careers.

I would also like to acknowledge the rest of the Conrad lab, past and present, for the assistance and guidance with experiments and immunology. I would especially like to thank

Andrea Luker and Joseph Lownik who were great sounding boards for project ideas. I greatly appreciate past Conrad lab members Dr. Sheinei Saleem Alam and Lauren Folgosa Cooley for the scientific work they did while in the lab as well as their guidance for navigating the Ph.D. and M.D.-Ph.D. worlds.

My thesis committee Dr. Harry Bear, Dr. Francine Cabral, Dr. Masoud Manjili, and Dr. Xiang-Yang Wang were instrumental in my success as Ph.D. student. They had constructive criticism for me and pushed me to pursue new ideas and avenues of research. I would particularly like to thank Dr. Bear, who has been a great mentor in the cancer-MDSC projects and a role model as a physician-scientist. The M.D.-Ph.D. committee has been a great advocate for me and other M.D.-Ph.D. students. I am appreciative that the door was always open to discuss the program and the transition back into medical school.

Lastly, I would like to thank my parents, Rohinee and Jayant Damle, and my sisters, Jai Massari and Meera Shier. My parents have encouraged me to pursue my dreams and have given me the opportunities to do so, and for that I am eternally grateful. My sisters are my ever-present support system and sources of inspiration. Without them, I would not be where I am today.

Table of Contents

List of Figures

List of Tables

List of Abbreviations

-/-	Homozygous deletion of a gene
5-LO	5-lipoxygenase
ACA	Active cutaneous anaphylaxis
ADAM	A disintegrin and metalloproteinase
ADAM-TS	ADAM-thrombospondin
Ag	Antigen
AIT	Adoptive immunotherapy
ANOVA	Analysis of variance
AP	Alkaline phosphatase
AP-1	Activator protein 1
APC	Antigen presenting cell
ARE	Antioxidant response element
Arg1	Arginase-1
ASA	Active systemic anaphylaxis
AT	Adoptive transfer
BALF	Bronchoalveolar lavage fluid
BBS	Borate buffered saline
BCR	B cell receptor
BM	Bone marrow
BMDC	Bone marrow derived DC

BMMC	Bone marrow derived mast cell
BMP	Bovine metalloproteinase
BSA	Bovine serum albumin
CCL	CC chemokine ligand
CCR	CC chemokine receptor
CD	Cluster of differentiation
cDC	Conventional dendritic cell
cDNA	Complementary DNA
CFSE	Carboxyfluorescein succinimidyl ester
CFU	Colony forming unit
ChIP	Chromatin immunoprecipitation
CIM	Cimetidine
CLP	Common lymphoid progenitor
CMP	Common myeloid progenitor
CNS	Central nervous system
COX	Cyclooxygenase
CPM	Counts per minute
CR	*Citrobacter rodentium*
Cre	Cre recombinase
CSR	Class switch recombination
CT	Cetirizine
CTL	Cytotoxic T lymphocyte
CU	Chronic urticaria

CXCR	CXC chemokine receptor
CYP	Cyclophosphamide
DC	Dendritic Cell
Dll	Delta-like ligand
DLN	Draining lymph node
DMSO	Dimethylsulfoxide
DNA	Deoxyribonucleic acid
DNP	Dinitrophenol
EGFR	Epidermal growth factor receptor
ELISA	Enzyme-linked immunosorbent assay
EPG	Eggs per gram feces
ERK	Extracellular signal-regulated kinase
FACS	Fluorescence activated cell sorting
FBS	Fetal bovine serum
FcεRI	High affinity IgE receptor
FITC	Fluorescein isothiocyanate
FO	Follicular
FSC	Forward scatter
GATA3	GATA-binding protein 3
GC	Germinal center
GEM	Gemcitabine
GI	Gastrointestinal
GM-CSF	Granulocyte-macrophage colony stimulating factor

GMP	Granulocyte-macrophage progenitor
H	Healthy
H&E	Hematoxylin and eosin
HDC	Histidine decarboxylase
HDM	House dust mite
HR	Histamine receptor
i.d.	Intradermal
i.n.	Intranasal
i.p.	Intraperitoneal
i.v.	Intravenous
ICD	Intracellular domain
ICOS	Inducible costimulator
ICOSL	Inducible costimulator ligand
IFN	Interferon
Ig	Immunoglobulin
IL	Interleukin
ILC	Innate lymphoid cell
IRB	Institutional review board
IRF	Interferon regulator factor
ISM	Indolent systemic mastocytosis
Jab1	c-Jun activation domain-binding protein-1
Jak	Janus kinase
KLF4	Kruppel like factor 4

kuz	Kuzbanian
L-Arg	L-arginine
LB	Luria-Bertani broth
Lin	Lineage
LLC	Lewis lung carcinoma
LN	Lymph node
LPS	Lipopolysaccharide
M1	Classically activated macrophage
M2	Alternatively activated macrophage
mAb	Monoclonal antibody
MACS	Magnetic cell sorting
MAPK	Mitogen activated protein kinase
MC	Mast cell
MCP-1	Monocyte chemotactic factor 1
MDSC	Myeloid derived suppressor cell
MedLN	Mediastinal lymph node
MEF	Mouse embryonic fibroblast
MEP	Megakaryocyte erythroid progenitor
MFI	Mean fluorescence intensity
MHC	Major histocompatibility complex
MIF	Macrophage migration inhibitor factor
MIP2	Macrophage inflammatory protein 2α
MLN	Mesenteric lymph node

MMP	Matrix metalloproteinase
mRNA	Messenger ribonucleic acid
MZ	Marginal zone
N-ICD	Notch intracellular domain
NADPH	Nicotinamide adenine dinucleotide phosphate
ND	Not detected
Neo	Neomycin
NES	*N. brasiliensis* excretory-secretory extract
NF-kB	Nuclear factor kB
NO	Nitric oxide
NP-KLH	4-Hydroxy 3-nitrophenylacetyl keyhole limpet hemocyanin
NS	Not significant
OCT	Optimal cutting temperature medium
OVA	Ovalbumin
PAS	Periodic Acid Schiff
PB	Peripheral blood
PBMC	Peripheral blood mononuclear cell
PBS	Phosphate buffered saline
PC	Plasma cell
PC	Phosphocholine
PCA	Passive cutaneous anaphylaxis
PCR	Polymerase chain reaction
pDC	Plasmacytoid dendritic cell

PE	Phycoerythrin
PGE	Prostaglandin E
PL	Peritoneal lavage
PMN	Polymorphonuclear cell
PNS	Peripheral nervous system
popLN	Popliteal lymph node
PP	Peyer's patch
qRT-PCR	Quantitative reverse transcription polymerase chain reaction
Rag1	Recombination activation gene 1
RBC	Red blood cell
RIP	Regulated intramembrane proteolysis
RNA	Ribonucleic acid
RNS	Reactive nitrogen species
ROS	Reactive oxygen species
RPMI	Roswell Park Memorial Institute medium
s.c.	Subcutaneous
SCF	Stem cell factor
SD	Standard deviation
SEM	Standard error of the mean
SFN	Sulforaphane
SHM	Somatic hypermutation
SSC	Side scatter
STAT	Signal transducer and activator of transcription

TACE	TNF converting enzyme
TCR	T cell receptor
TFH	T follicular helper
Tg	Transgenic
TGFa	Transforming growth factor α
TGFB	Transforming growth factor β
TH	T helper
TIMP	Tissue inhibitor of metalloproteinase
TK	Tyrosine kinase
TLR	Toll-like receptor
TNF	Tumor necrosis factor
Treg	Regulatory T cell
VCU	Virginia Commonwealth University
VEGF	Vascular endothelial growth factor
Wsh	MC-deficient kit$^{Wsh/Wsh}$
WT	Wild type
YFP	Yellow fluorescent protein

Abstract

TYPE 2 IMMUNE RESPONSES IN THE CONTEXT OF HELMINTH INFECTION, ASTHMA, DENDRITIC CELLS, AND MYELOID DERIVED SUPPRESSOR CELL FUNCTION

Sheela Ruby Damle, B.S.

A dissertation submitted in partial fulfillment of the requirements for the degree of Doctor of Philosophy at Virginia Commonwealth University.

Virginia Commonwealth University, 2017

Director: Daniel H. Conrad, Ph.D., Professor, Department of Microbiology and Immunology

Type 2 (T_H2) immune responses evolved to respond to helminth parasite infections by the production of T_H2 cytokines, which stimulate anti-helminth immunity. Macrophage migration

inhibitor factor (MIF) is a pleiotropic cytokine, which is produced by many cell types. We demonstrate that mice deficient in MIF have enhanced clearance of a helminth parasite. MIF deficiency in $CD4^+$ T cells was found to be the most important for mediating parasite clearance. We mimicked MIF deficiency by administering an inhibitor of the MIF tautomerase activity, sulforaphane, and this also increased parasite clearance (Section I).

T_H2 immune responses underlie allergy and allergic asthma, in which the same cytokines that help expel parasites are released in response to innocuous substances. Integral to the initiation of adaptive T_H2 immunity are dendritic cells (DCs), which take up antigen and stimulate antigen-specific $CD4^+$ T cell responses. We found that DC expression of ADAM10, a zinc-dependent metalloproteinase, is critical for the development of T_H2 immune responses and IgE production from B cells. This effect is demonstrated in both allergic airway inflammation and anaphylaxis models. ADAM10-deficient DCs are unable to cleave Notch1 receptors, resulting in reduced IL-6 production and this ultimately results in decreased T_H2 activity. ADAM17 is closely related to ADAM10 in both structure and function. Interestingly, mice from which ADAM10 and 17 are removed from DCs ($ADAM10/17^{DC-/-}$) have a distinct phenotype from both $ADAM10^{DC-/-}$ and $ADAM17^{DC-/-}$ mice in models of allergic airway inflammation (Section I).

We also examined another effect of T_H2 cytokines on the interaction between mast cells and myeloid derived suppressor cells (MDSCs). We sought to understand how histamine and IL-13, mediators made by mast cells, affect the immunoregulatory function of MDSCs. MDSCs in IL-13-deficient mice with tumor are more prevalent in circulation rather than in tumor or organs, which could be due to changes in CCL2/CCR2 chemotaxis. In addition, MDSC function after treatment with the DNA methyltransferase inhibitor, decitabine was examined. This treatment

reduced their suppressive function and increased the expression of molecules needed for antigen presentation. Overall, T_H2 immunity has multifaceted roles in anti-parasite immunity, allergic asthma, and MDSC function (Section II).

Section 1: The initiation and maintenance of type 2 immune responses

Introduction

Type 2 (T_H2) immune responses are characterized by the cytokines interleukin 4 (IL-4), IL-5, IL-9, and IL-13. Innate cells are first to respond to T_H2 signals by producing cytokines that relay the message to other innate cells as well as the adaptive arm of the immune system. These innate cells are innate lymphoid cells type 2 (ILC2), mast cells, eosinophils, basophils, and alternatively activated macrophages, whereas the adaptive response involved $CD4^+$ T cells and B cells[1]. Originally, T_H2 responses were primarily thought to be regulatory responses aimed at countering the inflammation generated by T_H1 immunity[2]. However, advances in the field have elucidated the many new aspects of T_H2 immune responses as well as their complexities.

T_H2 immunity evolved as a protective response against helminth parasites[3]. These responses revolved around enhancing barrier defenses through mucus production, eosinophilia, smooth muscle contractility, intestinal epithelial turnover and alternative macrophage activation[4–7]. Overall the outcome is expulsion of the parasite from the gut. As the initial reports indicated, there is a regulatory function of T_H2 immunity, which dampens the inflammation associated with T_H1 immune responses. T_H2 responses also activate tissue repair mechanisms.

The host protective functions are valuable, but when dysregulated they can lead to many diseases that are becoming increasingly prevalent. Overactivity of T_H2 responses is responsible for allergic asthma, atopic dermatitis, allergic rhinitis, eosinophilic esophagitis, and allergies, including anaphylaxis[8]. An enhancement in T_H2 versus T_H1 immunity in the situation of cancer has been shown to be detrimental for patient prognosis. As T_H2 immune responses antagonize

T_H1, anti-tumor and tumor surveillance activities of T_H1 immunity are largely impaired[9–11]. Given the wide and varied roles of T_H2 immunity in health and disease, a better understanding of the mechanisms of initiation and maintenance of responses is indispensible and may lead to potential targets for therapeutic intervention.

Chapter 1 Macrophage migration inhibitor factor deficiency enhances immune response to *Nippostrongylus brasiliensis*

1.1.1 Introduction

Clinical manifestations and functions

Soil transmitted helminths infect greater than one billion individuals worldwide, particularly in tropical and sub-tropical climates where sanitation is poor. These infections include the species *Ascaris lumbricoides*, *Trichuris trichiura*, *Necator americanus*, and *Ancylostoma duodenale*[12]. Though these infections are not usually fatal, significant morbidity related to the worm burden in the individual remains a problem. Symptoms range from diarrhea and abdominal pain to general malaise and weakness, but can progress to impaired cognition and physical development, especially in children[12]. While current anti-helminthic agents are available and relatively inexpensive, the global coverage of children with these treatments is only 33%[13]. Understanding and enhancing the immune response to soil transmitted helminths could greatly expand potential therapeutic options and reduce helminth associated morbidity.

Nippostrongylus brasiliensis is a rodent helminth that is similar to the human hookworm. *N. brasiliensis* elicits a dominant T_H2 response in mice, including the cytokines IL-4, IL-5, and IL-13 as well as IgE antibody production. Downstream effects include enhanced mucus production, goblet cell hyperplasia, eosinophilia, and enteric nerve stimulation, all of which facilitate expulsion of the intestinal worm. This response has been well-studied, but in recent years elucidating the effect of the innate immune system on T_H2 responses has increased in importance[14,15]. Many of these innate factors alter adaptive immune responses toward a specific T helper subset, thereby altering effective immunity to helminth parasites.

Macrophage migration inhibitor factor

Macrophage migration inhibitory factor (MIF) was one of the first cytokines to be described[16,17]. Since its initial discovery, it has been shown to have many functions, acting as an anterior pituitary hormone[18], a pro-inflammatory cytokine[19–22], and a tautomerase enzyme[23–25], among many others[26]. Consistent with its diverse functions and the large array of cell types that produce it, the downstream effects of MIF are extensive: MIF activates MAPK signaling pathways[27], promotes LPS stimulation through TLR4[28], interacts with Jab1 to increase transcription of AP-1 target genes[29], and activates NF-kB[30]. In addition to these functions and in contrast with other cytokines, MIF encodes an enzymatic activity, acting as a keto-to-enol tautomerase[25]. The role of this enzymatic activity in the biological functions of MIF remains controversial, as no physiological substrate has been identified. However, several groups have characterized inhibitors of this activity, which display efficacy in disease models that are dependent on MIF[31,32].

Given that MIF is involved in many cellular pathways and functions as a pro-inflammatory cytokine, it is not surprising that it has been studied in both human and murine disease, including rheumatoid arthritis[33], atherosclerosis[34], and LPS-induced sepsis[19,22,35]. In infections caused by intracellular pathogens like *Salmonella typhimurium* and *Mycobacterium tuberculosis*, MIF deficiency led to a diminished T_H1 immune response and was detrimental to host[36,37]. MIF has additionally been studied in several parasite infections[38–42]. However, these studies have been limited to models in which a T_H1 response is required for clearance, such as *Leishmania major*[38], *Plasmodium chabaudi*[41,42], and *Taenia crassiceps*[43]. To date, inquiry into the role of MIF in infection with parasites requiring a T_H2 response for clearance has been limited[40].

In this study, we analyzed the role of MIF in the immune response of mice infected with *N. brasiliensis*. We examined how MIF deficiency altered the course of infection and the cellular immune responses using $MIF^{-/-}$ mice. $MIF^{-/-}$ mice had enhanced clearance of *N. brasiliensis* due to a robust T_H2 response. Using an inhibitor of MIF, we demonstrate the importance of the tautomerase enzyme activity in mediating immune alterations and immunity to *N. brasiliensis*.

1.1.2 Materials and Methods

1.1.2.1 Mice

All animal experiments were performed with the approval of the Virginia Commonwealth University Institutional Animal Care and Use Committee. $MIF^{-/-}$ mice were generously provided by Janet Cross at the University of Virginia. Mice were maintained in the Virginia Commonwealth University animal facility in accordance to guidelines for the humane treatment of laboratory animals set forth by the National Institutes of Health and the American Association for the Accreditation of Laboratory Animal Care. $MIF^{-/-}$ Balb/c mice were obtained from cryopreserved stocks at the Jackson Laboratory (Bar Harbor, ME)[35]. These mice were then backcrossed onto C57Bl/6 as described[44]. Female and male mice wild type (WT) C57Bl/6 (Stock No. 000664) and Balb/c (Stock No. 000651) aged 6 to 12 weeks old were purchased from the Jackson Laboratory and used as controls for $MIF^{-/-}$ C57Bl/6 and Balb/c mice, respectively. The C57Bl/6 congenic strain CD45.1 (B6.SJL-*Ptprc*^{a} *Pepc*^{b}/BoyJ, Stock No. 002014) was used as WT recipient and donor in the bone marrow reconstitution experiment. Mice were euthanized by isoflurane inhalation followed by cervical dislocation as per AALAC guidelines. Table 1 lists genotyping primers used to identify mice.

Table 1: Genotyping Primers

Mouse Colony		Primer Name	Sequence
$MIF^{-/-}$	MIF	MIF F	CTTGGGTGGAGAGGCTATTC
		MIF R	AGGTGAGATGACAGGAGATC
	Neo	Neo F	ACGACATGAACGCTGCCAAC
		Neo R	GGTCTCTTATAAACCATTTATTTCTCC

1.1.2.2 Helminth infections

N. brasiliensis and *H. polygyrus bakeri* (L3) larvae were generously provided by Joseph Urban at the USDA and maintained as previously described[45]. Each experimental group of mice was inoculated *s.c.* with either ~600 *N. brasiliensis* or intra-gastric ~200 *H. polygyrus bakeri*. Eggs in the feces were enumerated using a saturated NaCl solution and a McMaster counting chamber. Adult worms (L5) were isolated from the proximal small intestine and counted using a dissecting microscope[45].

1.1.2.3 MLN and splenocyte culture and proliferation measurement

Spleens were crushed manually between two frosted microscope slides, filtered through 40μM cell strainer, and red blood cells (RBCs) were lysed using ACK Lysis Buffer (Quality Biological Inc., Gaithersburg, MD). Splenocytes were washed in PBS and enumerated. Mesenteric lymph nodes (MLNs) were isolated, teased apart with forceps, filtered through a 40μM cell strainer and enumerated. 96-well plates were coated with anti-CD3ε (1μg/mL, clone 145-2C11, Biolegend, San Diego, CA) for 1h at 37°C and then washed with PBS. Splenocytes and MLN cells were seeded at $5x10^5$ cells per ml complete RPMI (cRPMI, RPMI 1640 containing 10% heat inactivated fetal bovine serum (Atlanta Biological Inc., Norcross, GA), 2mM L-glutamine, 50μg/mL penicillin, 50μg/mL streptomycin, 1mM sodium pyruvate, 50μM 2-mercaptoethanol, 1X non-essential amino acids, 20mM HEPES buffer, (all from Invitrogen, San Diego, CA) and with anti-CD28 (2μg/mL, clone 37.51 Biolegend). Cell culture supernatants were harvested after 96h of growth at 37°C with 5% CO_2. For proliferation assessment, 1.25×10^5 cells/mL were plated in cRPMI with anti-CD28 (2μg/mL). After 72h of growth, 1μC of [^{3}H]-Thymidine (Perkin Elmer, Waltham, MA) was added to each well. After 18h, cells were harvested onto GFC plates

using a Filtermate cell harvester and incorporation of [^{3}H]-Thymidine was measured by beta counter (TopCount plate counter PerkinElmer, Waltham, MA).

1.1.2.4 Enzyme-linked immunosorbant assay (ELISA)

Serum was collected at different time points after infection. The following in house ELISA antibodies were used in IgE, IgG1, and IgM ELISAs[46]: anti-IgE capture, biotinylated anti-mouse IgE, anti- mouse IgG1 capture, anti-mouse IgG1 alkaline phosphatase (AP), anti-mouse IgM capture, and anti-mouse IgM AP. The 96-well plate was coated with the capture antibody; serially diluted samples were added and followed by detection antibody. IgE, IgG1, and IgM standards were used to generate a standard curve. Plates were developed by adding alkaline phosphate substrate (Sigma-Aldrich) and read by a spectrophotometer at 405 and 650nm.

Cell culture supernatants were examined for IL-13 and interferonγ (IFN) cytokines. For IL-13, 96-well plates were coated with anti-mouse IL-13 capture antibody (6μg/mL, #MAF413, R&D Systems, Minneapolis, MN) for 1h at 37°C. Plates were blocked for 1h at 37°C with 10% fetal bovine serum in PBS. Samples were added to plates neat and diluted 1:10 for 2hr at 37°C. Recombinant IL-13 was used to generate a standard curve. Biotinylated anti-mouse IL-13 detected antibody (0.2μg/mL, #BAF413, R&D Systems) was added for 1h at 37°C, followed by Streptavidin-AP (Southern Biotech) for 1h at 37°C. Plate was developed as described above. IFNγ was detected in the supernatants using Ready-Set-Go! IFNγ ELISA kit (eBioscience, San Diego, CA) per manufacturer's instructions.

1.1.2.5 qPCR

Tissues were flash frozen in liquid N_2 and total RNA was extracted using TRIzol Reagent (Life Technologies, Grand Island, NY). Cells were homogenized in the TRIzol Reagent and total RNA was isolated per manufacturers instructions. RNA was quantified using the absorbance at 260nm

(ND-100 Nanodrop). 400ng RNA was reverse transcribed into cDNA using iScript cDNA Synthesis Kit (Bio-Rad, Hercules, CA). Real time PCR was performed using the iQ5 system (Bio-Rad). Gene Expression Master Mix and Taqman probes (Table 2) were purchased from Applied Biosystems (Grand Island, NY) and used per manufacturers instructions. Primers for Gata3, Tbx21, and β2 microglobulin (Table 2) were purchased from Integrated DNA Technologies (Coralville, IA) and used with SYBR Green SuperMix (Bio-Rad). Fold change from uninfected samples was calculated using the ΔΔCt method[47].

1.1.2.6 Histology

Small intestines were fixed in 10% formaldehyde. Paraffin sections were cut, mounted on slides, and stained with Periodic Acid Schiff stain (Life Technologies, Carlsbad, CA). Images were taken on an Olympus BX41 microscope.

1.1.2.7 Bone marrow reconstitution

Bone marrow cells were collected from WT CD45.1 and $MIF^{-/-}$ mice as follows: tibiae and femurs were isolated from the mice and then centrifuged in microcentrifuge tubes to retrieve bone marrow, RBCs were lysed with ACK Lysing Buffer and then bone marrow cells were washed in PBS and enumerated. WT CD45.1 and $MIF^{-/-}$ mice were irradiated (MDS Nordion cell 40 research irradiator [^{137}Cs]) with 2 doses of 550cGy separated by a 2h rest period. $5x10^6$ bone marrow cells were then injected intravenously into the irradiated mice[48]. After 6 – 8 weeks of reconstitution, mice were infected with *N. brasiliensis* as described above. Successful reconstitution was indicated by flow cytometric analysis of the spleen, MLN, resident peritoneal cells isolated by lavage, and blood of recipient mice (Figure 11).

1.1.2.8 Rag1$^{-/-}$ Reconstitution

Rag1$^{-/-}$ mice (Stock no. 002216) were obtained from Jackson Laboratory (Bar Harbor, ME). B cells were isolated from WT spleens using B220^{+} magnetic bead selection and WT and MIF$^{-/-}$ splenic CD4^{+} T cells were isolated using L3T4 magnetic bead selection according to manufacturer's instructions (Miltenyi Biotec, Gergisch, Gladbach, Germany). 20 x 10^{6} B cells and 10 x 10^{6} WT or MIF$^{-/-}$ CD4^{+} T cells were *i.v.* injected into Rag1$^{-/-}$ mice. After one week, *N. brasiliensis* was injected as described above.

1.1.2.9 Flow cytometric analyses and FACS

Single cell suspensions were obtained from MLNs, spleens, peritoneal lavage, and peripheral blood after bone marrow reconstitution and *N. brasiliensis* infection. Cells were blocked with unlabeled anti-mouse CD16/32 (clone 2.4G2) for 10min on ice, followed by incubation with fluorochrome labeled antibodies. Antibodies used were as follows Alexa647 anti-mouse CD45.1 (clone A20), PerCP-Cy5.5 anti-mouse CD45.2 (clone 104) (Biolegend), FITC lineage cocktail, CD127 (clone A7R34), ST2 (clone DIH9), CD117 (clone 2B8), and FcεrIα (clone MAR-1) (Biolegend). Cells were analyzed on a BD Canto Flow analyzer; data was analyzed using FlowJo software (version7.6, TreeStar, Ashland, OR). For FACS, single cell suspensions of MLNs were stained with PE anti-mouse CD90.2 (clone 30.H12), APC anti-mouse/human B220 (clone RA3-6B2), PE-Cy7 anti-mouse CD4 (clone GK1.5), and FITC anti-mouse CD11c (clone N418) (Biolegend) and then sorted on a BD FACS Aria cell sorter (BD Biosciences, San Jose, CA).

1.1.2.10 MLN CD4^{+} T cell isolation and western blotting

Single cell suspensions of MLNs were generated as described above. CD4^{+} cells were isolated by positive selection using non-activating CD4^{+} (clone L3T4) magnetic beads (Miltenyi Biotec) per manufacturer's instructions. Total cell lysates from MLN CD4^{+} T cells on day 7 post

infection were obtained using lysis buffer (#9803, Cell Signaling, Danvers, MA) per manufacturer's instruction. Protein was quantified using a Bradford assay (Bio-Rad), read at 595nm on a spectrophotometer. 30µg of protein was loaded onto Novex NuPage 10% Bis-Tris gel, run for 30min at 70V and 1.5h at 100V, and then transferred to a nitrocellulose membrane. Blots were probed with Rabbit anti-phospho ERK1/2 (#4377, Cell Signaling), Rabbit anti-ERK1/2 (#9102, Cell Signaling), Rabbit anti-phospho p65 (#3033, Cell Signaling), Rabbit anti-p65 (#8242, Cell Signaling), and HRP anti-Beta actin (Sigma-Aldrich). Signal was detected using Clarity Western ECL Blotting Substrate (Bio-Rad) and a ChemiDoc MP System (Bio-Rad) was used to measure band densitometry.

1.1.2.11 Sulforaphane administration

Indicated mice were given daily intraperitoneal (*i.p.*) injections of 200µg R,S-sulforaphane ([1-isocyanato-4*R*(methylsulfinyl)butane], SFN) (LKT Labs, St. Paul, MN) in saline in beginning on the day of infection[49].

1.1.2.12 Statistics

All statistical analyses were performed using Prism6 (GraphPad Software Inc., La Jolla, CA). Statistical significance was assessed by two-tailed, unpaired Student's t test (two groups) or one-way ANOVA for multiple groups with a Tukey's post hoc test or Dunnett's multiple comparisons test. Unless otherwise indicated differences are not significant. ****$p<0.0001$, ***$p<0.001$, ** $p<0.01$, * $p<0.05$.

Table 2: Primer and probe list

Gene	Primer/Probe[1]
Tbx21 F	TCCCATTCCTGTCCTTCA
Tbx21 R	GCTGCCTTCTGCCTTTC
Gata3 F	ACCACGGGAGCCAGGTATG
Gata3 R	CGGAGGGTAAACGGACAGAG
β2 micro-globulin F	TCACTGACCGGCCTGTATGCTATC
β2 micro-globulin R	GTGAGGCGGGTGGAACTGTGT
Nqo1 F	AGGATGGGAGGTACTCGAATC
Nqo1 R	TGCTAGAGATGACTCGGAAGG
Sod1 F	AACCAGTTGTGTTGTCAGGAC
Sod1 R	CCACCATGTTTCTTAGAGTGAGG
Hmox1 F	GATAGAGCGCAACAAGCAGAA
Hmox1 R	CAGTGAGGCCCATACCAGAAG
γGcl F	GGACAAACCCCAACCATCC
γGcl R	GTTGAACTCAGACATCGTTCCT
Il13	Mm00434204_m1
Il4	Mm00445259_m1
Il6	Mm00446190_m1
Il17a	Mm00439618_m1
Gapdh	Mm99999915_g1

[1] Product number for Taqman probes purchased from LifeTech.

1.1.3 Results

MIF deficiency enhances clearance of N. brasiliensis

Given the increasing appreciation of the importance of innate immune system factors in the initiation, amplification, and fine-tuning of T_H2 immune responses, we sought to determine if MIF played a role in the immune response to *N. brasiliensis*. WT and $MIF^{-/-}$ C57Bl/6 mice were infected with 600 L3 *N. brasiliensis* larvae. The $MIF^{-/-}$ mice had fewer eggs per gram (EPG) feces (Figure 1A, B) and fewer adult worms (L5 stage) in the proximal small intestine at day 7 post infection (Figure 1C). In contrast, there was no significant difference in the number of L4 stage worms in the lungs at day 2 in $MIF^{-/-}$ mice (Figure 1D). These data suggests that MIF deficiency primarily affects the immune response to *N. brasiliensis* in the gut. A similar decrease in EPG and adults worms was also seen in $MIF^{-/-}$ mice on the Balb/c background (Figure 2A, B). Surprisingly, we do not see an increase in proliferation and T_H2 cytokine production in the Balb/c $MIF^{-/-}$ mice compared to WT (Figure 2C-E), despite the reduction in parasite burden. Thus, MIF deficiency leads to enhanced control of *N. brasiliensis on* both C57Bl/6 and Balb/c backgrounds.

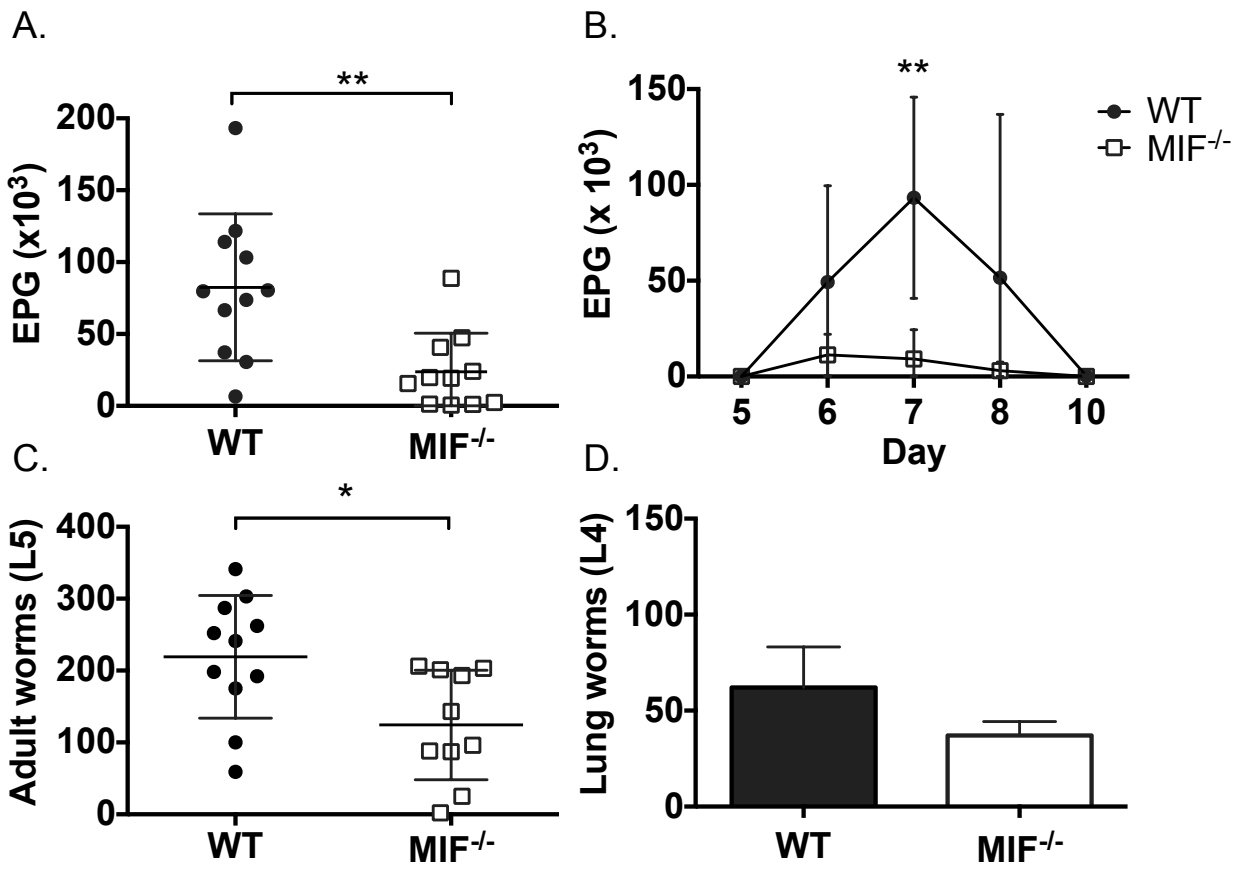

Figure 1: MIF$^{-/-}$ mice exhibit enhanced clearance of *N. brasiliensis* infection.

A. and B. Eggs per gram (EPG) feces were enumerated in WT and MIF$^{-/-}$ mice at day 7 post infection (A) and over the course of infection (B). C. Number of adult worms (L5) in the proximal small intestine were measured at day 7 post infection. D. On day 2 post infection, the lungs were assessed for lung worms (L4). Symbols represent individual mice and data are combined from at least three independent experiments with three mice per group. ** $p<0.01$, *$p<0.05$, unpaired t test.

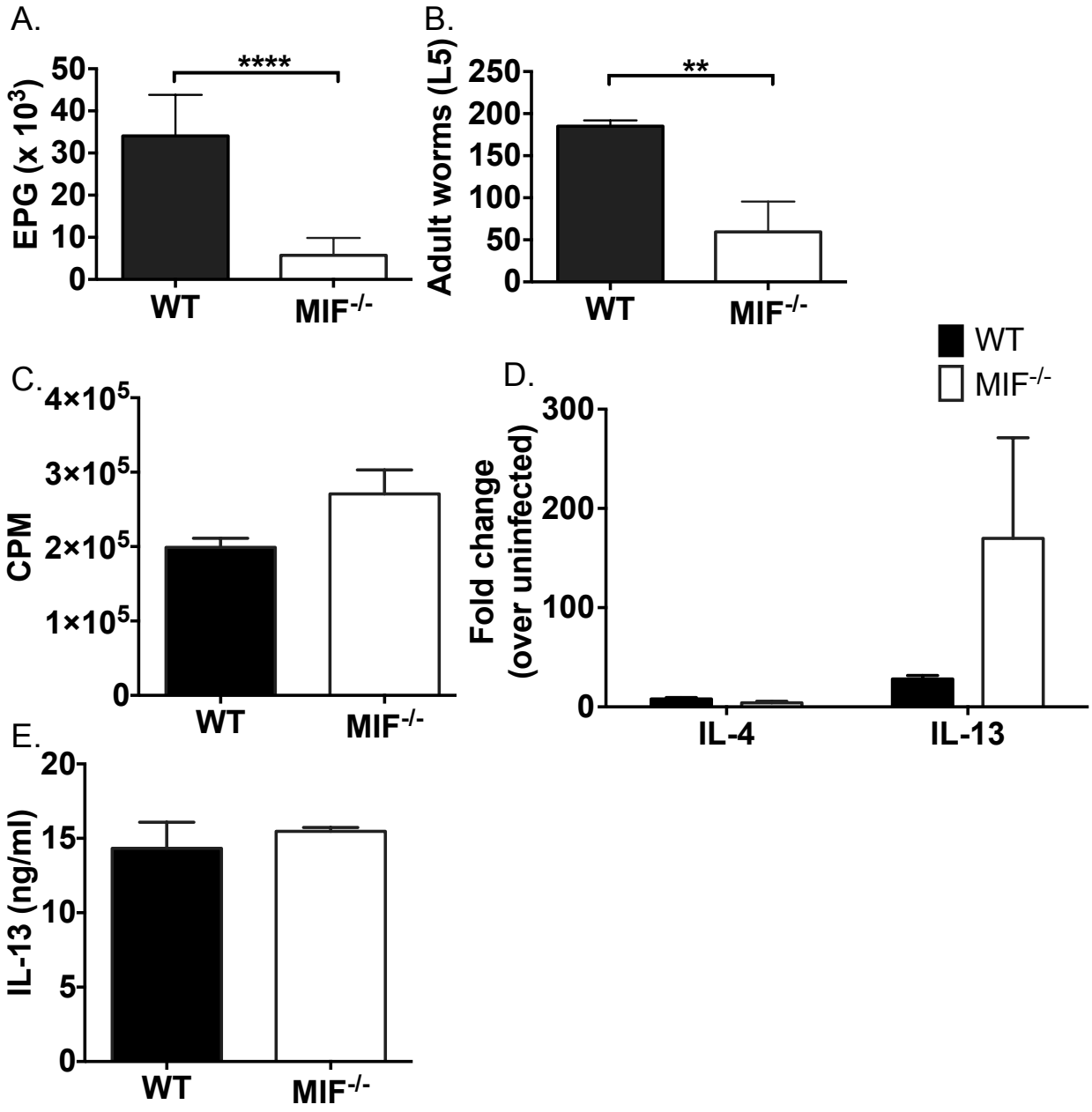

Figure 2: MIF$^{-/-}$ Balb/c mice have enhanced clearance of *N. brasiliensis*.

A. EPG were measured in WT and MIF$^{-/-}$ mice on day 7 post infection. B. In the proximal small intestine, adult worms (L5) were enumerated on day 7 after infection. C. 1.25 x 10^5 MLN cells/mL were seeding in anti-CD3ε coated plates with anti-CD28 in the media. Proliferation was assessed by [^{3}H]-thymidine incorporation after 72h. D. Expression of *Il4* and *Il13* were assessed in MLN on day 7 after infection. D. IL-13 was measured in MLN culture supernatants by

ELISA. Data is combined from two independent experiments, each with at least three mice per group. **** $p<0.0001$, ** $p<0.01$, unpaired t test.

MIF$^{-/-}$ mice develop a heightened T_H2 response

T_H2 responses are critical for clearance of *N. brasiliensis*; we examined the spleen and mesenteric lymph nodes (MLNs, the draining lymph node) for markers of this response. MLNs from MIF$^{-/-}$ mice had significantly increased cellularity when compared to WT MLNs (Figure 3A) and *in vitro* stimulation with anti-CD3ε/anti-CD28 resulted in significantly more proliferation in the MIF$^{-/-}$ cultures, when compared to WT MLN controls (Figure 3B). We measured mRNA expression of transcription factors associated with T_H1 and T_H2 responses (*Tbx21* and *Gata3*, respectively) in MLNs isolated from mice on day 7 post infection. MIF$^{-/-}$ MLNs from infected mice exhibited a 12 fold increase in expression of *Gata3* relative to the uninfected controls, compared to only 7 fold increase in MLNs from WT mice. In contrast, there was no difference in fold induction of *Tbx21* (Figure 3C). We also measured the expression of mRNA for the T_H2 cytokines, *Il4* and *Il13*, which are integral to the clearance of *N. brasiliensis*. There was no difference in the degree of *Il4* induction in the MLNs isolated from WT and MIF$^{-/-}$ mice (Figure 3D). However, *Il13* induction was enhanced in the MIF$^{-/-}$ mice, compared to the WT controls. Next, we measured the production of T_H1 and T_H2 cytokines (IFNγ and IL-13, respectively) in cultured MLNs from infected mice stimulated with anti-CD3ε/anti-CD28. Supernatants from the cultured MLNs from MIF$^{-/-}$ mice contained significantly more IL-13 than did the WT MLN supernatant (Figure 3E). In contrast IFNγ was unchanged (Figure 3F). Given that we see increased IL-13, but not IL-4, we examined MIF$^{-/-}$ and WT mice for ILC2s. We found no differences in the percentage of ILC2s in the lungs, pleural lavage, and peritoneal lavage on day 7 after infection (Figure 4A). Also, we did not see differences in the percentage of mast cells in the peritoneal lavage (Figure 4B). Expression of T_H1 and T_H2 transcription factors and cytokines were not altered in uninfected mice (Figure 4C, D). Further, we did not observe

any differences in ionomycin-mediated bone marrow derived mast cell (BMMC) degranulation as assessed by Lamp1 (CD107a) surface expression by flow cytometry (Figure 4E). Sections of small intestine stained with Periodic Acid Schiff (PAS) demonstrate an increase in PAS^{+} cells in day 7 infected $MIF^{-/-}$ mice compared to WT (Figure 3G), indicating the presence of more mucus producing cells. These results indicate that the $MIF^{-/-}$ mice exhibit a heightened T_H2 response in the draining lymph node and in the gut, which may be responsible for enhanced parasite clearance.

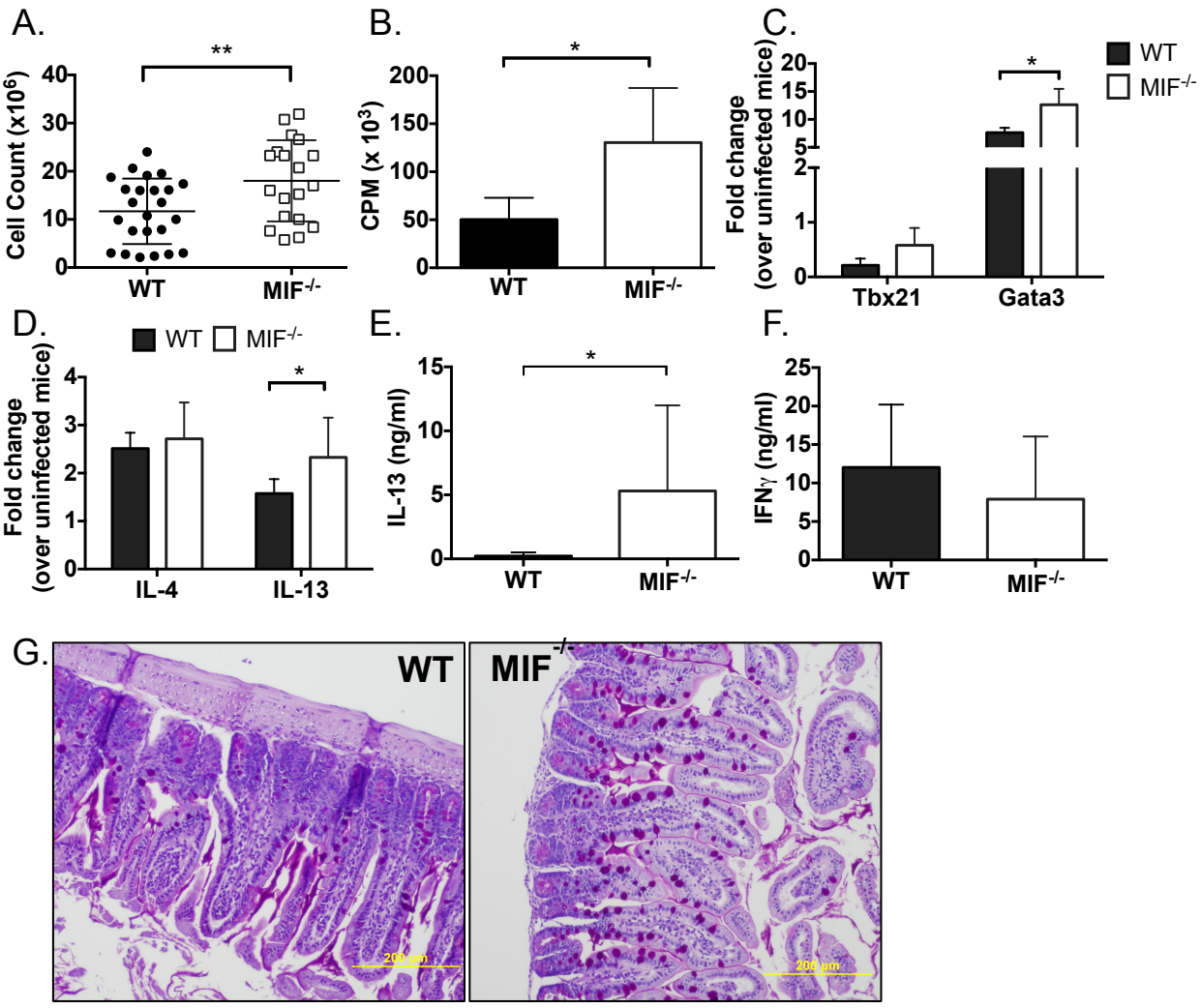

Figure 3: MIF deficiency enhances the adaptive T_H2 response to *N. brasiliensis*.

A. Cells in the MLN were enumerated by trypan blue exclusion on day 7 after infection. B. 1.25 x 10^5 MLN cells/mL were seeding in anti-CD3ε coated plates with anti-CD28 in the media. Proliferation was assessed by [^{3}H]-thymidine incorporation after 72h. C. Fold change in mRNA expression (over uninfected) of transcription factors, *Tbx21* and *Gata3*, was measured in MLN cells on day 7 after infection. D. Fold change in *Il4* and *Il13* mRNA expression was assessed on day 7 post infection in MLN cells. E. and F. 5 x 10^5 cell/mL were cultured with anti-CD3ε/anti-CD28 stimulation for 96h and IL-13 (E) and IFNγ (F) were measured in the culture supernatant by ELISA. G. Sections of the small intestine from day 7 infected WT and MIF$^{-/-}$ mice were

stained with Periodic Acid Schiff. Symbols represent individual mice and data is combined from at least three independent experiments each with three mice per group. ** $p<0.01$, * $p<0.05$, unpaired t test.

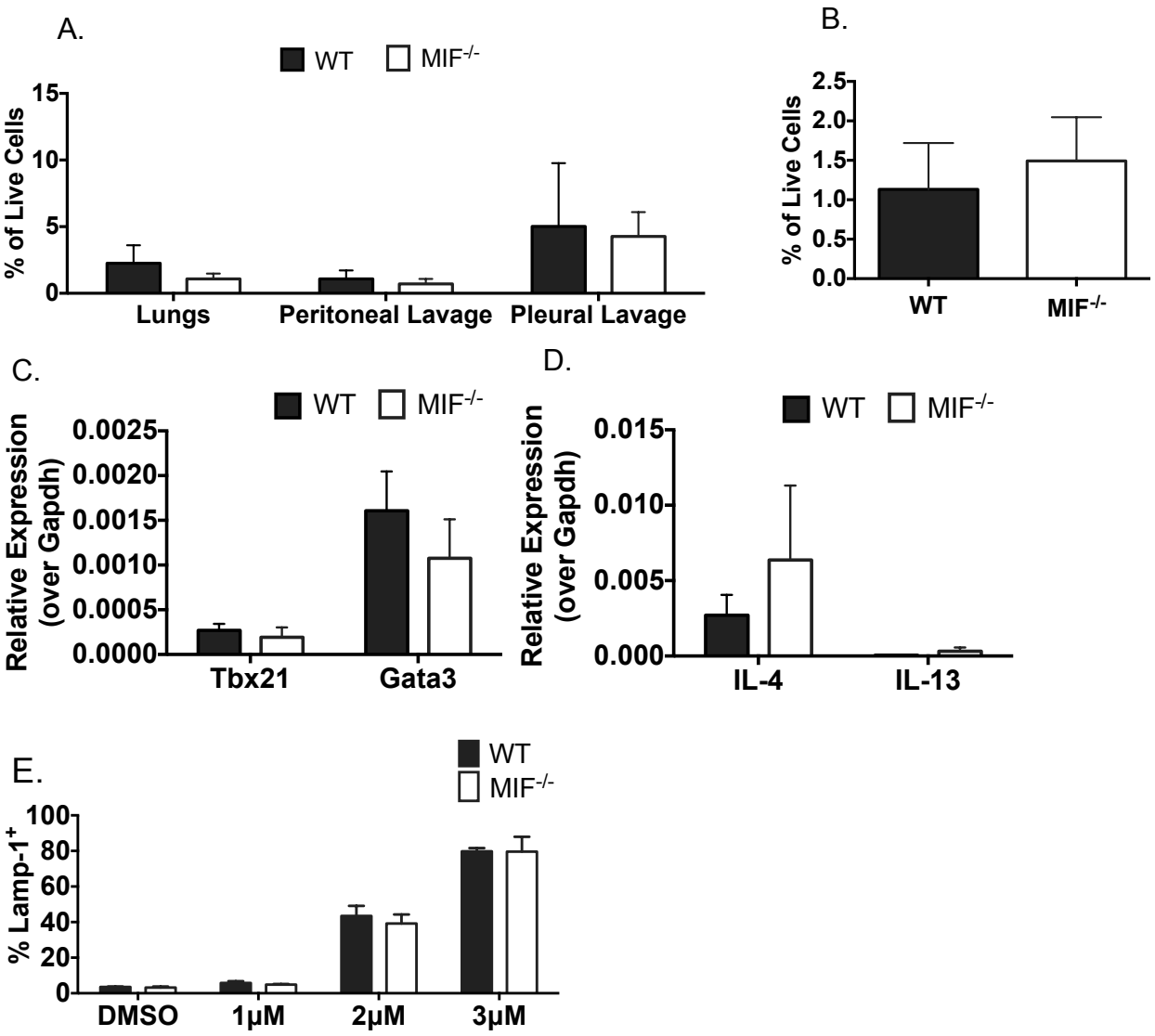

Figure 4: MIF deficiency does not affect ILC2s or mast cell numbers

A. Lungs, peritoneal lavage cells, pleural lavage were isolated from day 7 infected WT and MIF$^{-/-}$ mice. Percent of ILC2 (Lineage^{-} CD127^{+} ST2^{+}) were analyzed by flow cytometry. B. Mast cells (CD117^{+} FcεRIα^{+}) were measured by flow cytometry in the peritoneal lavage from day 7 infected WT and MIF$^{-/-}$ mice. C. and D. Relative expression of *Tbx21* and *Gata3* (C) and *Il4* and *Il13* (D) in MLNs from naïve WT and MIF$^{-/-}$ mice. E. Ionomycin-mediated degranulation was assessed by surface Lamp1 (CD107a) expression by flow cytometry at indicated concentrations in BMMCs from WT and MIF$^{-/-}$ mice.

Enhanced T_H2 cytokine response of MIF$^{-/-}$ mice to infection with the helminth H. polygyrus bakeri

We also examined the effect of infection with another T_H2 helminth *H. polygyrus bakeri*, which unlike *N. brasiliensis* has its complete life cycle in the gastrointestinal tract and requires a longer time frame for clearance[45]. We found no difference in eggs per gram feces over the course of infection with *H. polygyrus bakeri* (Figure 5A) or the expression of T_H1 or T_H2 transcription factors, *Tbx21* or *Gata3* in re-stimulated MLN cultures (Figure 5B). However, we did find that the expression of *Il4* and *Il13* were increased in MLN cultures from day 14 infection MIF$^{-/-}$ mice compared to WT (Figure 5C).

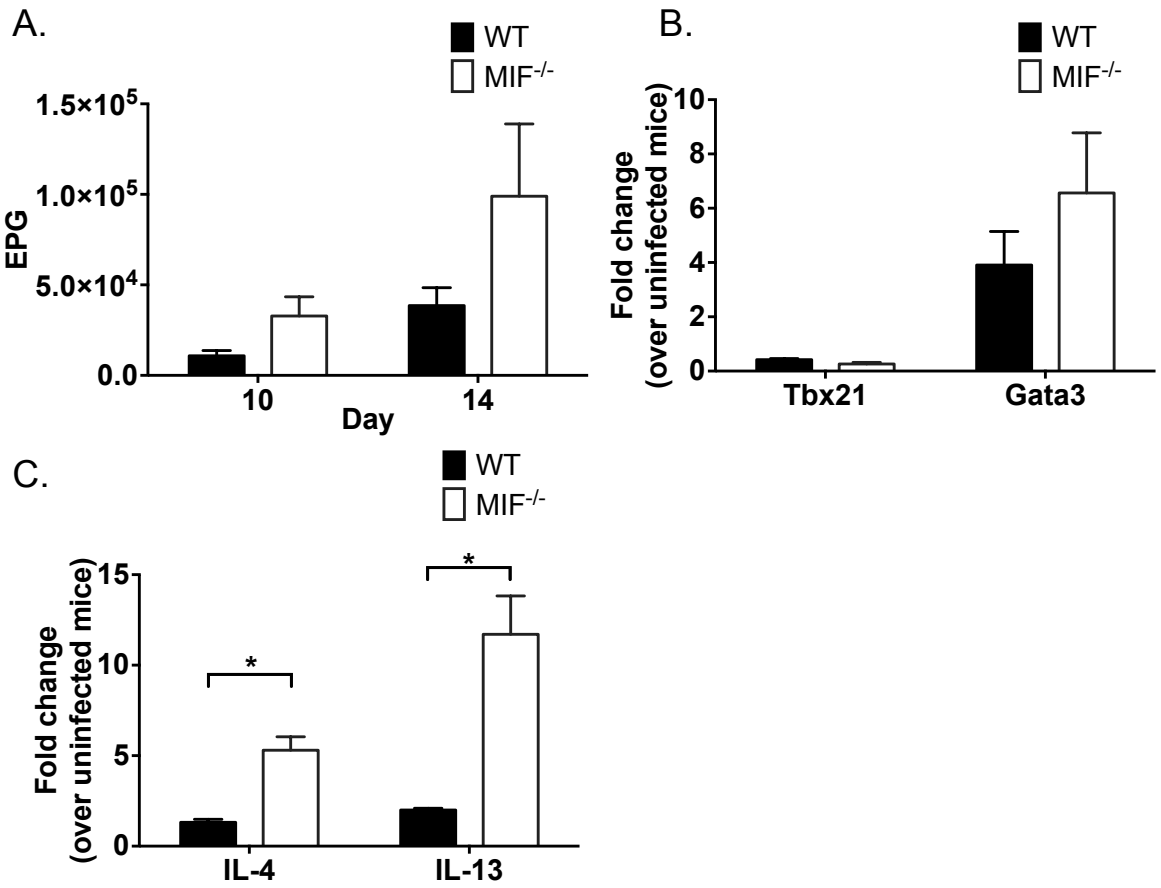

Figure 5: Heightened T_H2 response to *H. polygyrus bakeri* infection in $MIF^{-/-}$ mice.

WT and $MIF^{-/-}$ mice were inoculated with *H. polygyrus bakeri* by intragastric administration. A. EPG were assessed at indicated days after infection. B. – D. MLNs were isolated from day 14 infected mice and re-stimulated. mRNA expression of *Tbx21* and *Gata3* (B) and *Il4* and *Il13* (C).

MIF deficiency does not impact splenic T_H2 response or serum antibody production

Since $MIF^{-/-}$ mice infected with *N. brasiliensis* exhibited a distinct increase in the T_H2 response in the MLN, we investigated the adaptive immune responses in the spleen during infection to determine if the phenomenon observed in the MLN was present in non-draining secondary lymphoid structures. To accomplish this, antibody levels were measured in the serum of *N. brasiliensis* infected mice at various time points post infection. We found no difference in either serum IgM or the T_H2 associated antibodies, IgE and IgG1 (Figure 6A-C) as a function of MIF deficiency. In addition, there were no differences in proliferation and cytokine production in cells isolated from the spleen of $MIF^{-/-}$ mice compared to WT. Splenocytes isolated from $MIF^{-/-}$ mice at day 7 after infection proliferated to the same extent as than WT and did not produce more IL-13 (Figure 7A, B). Moreover, the fold induction of *Tbx21*, *Gata3*, *Il4*, and *Il13* mRNA in the splenocytes following infection was also similar between WT and $MIF^{-/-}$ mice (data not shown). This indicates that the T_H2 response was specifically enhanced in the draining LNs of $MIF^{-/-}$ mice, and not in the spleen.

We also examined any intrinsic B cells effects of MIF deficiency by culturing splenic $B220^+$ cells with anti-CD40 and IL-4 or LPS and IL-4 for 9 days[50]. We did not observe any differences in proliferation between WT and $MIF^{-/-}$ B cells stimulated with either anti-CD40/IL-4 or LPS/IL-4 (Figure 8A, B). Interestingly, we found trending lower IgG1 levels in the supernatants of $MIF^{-/-}$ B cells, but increased IgE (Figure 8C, D).

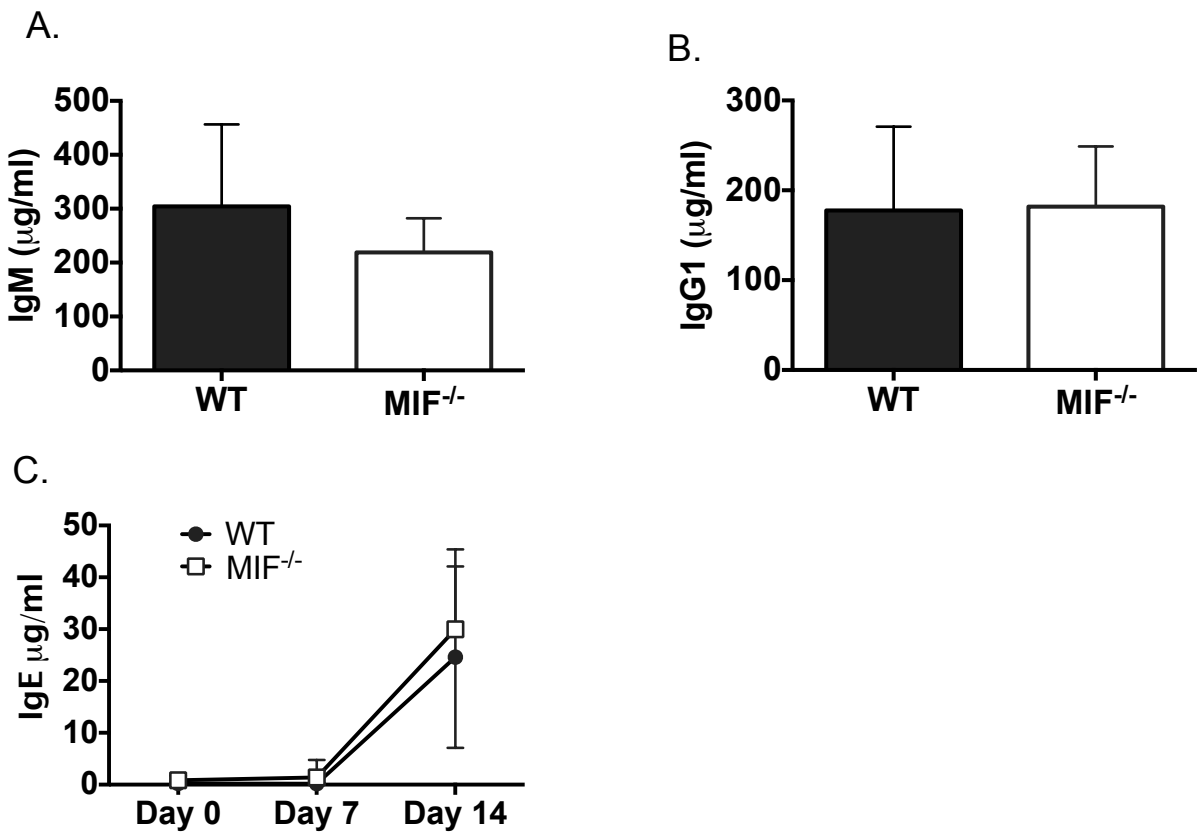

Figure 6: Serum antibodies are similar between WT and MIF$^{-/-}$ mice after *N. brasiliensis* infection.

A. – C. Serum was collected at day 7 (A and B) or days 0, 7, and 14 (C) post infection with *N. brasiliensis*. Indicated immunoglobulin was measured by ELISA. Data is combined from at least three independent experiments and analyzed by unpaired t test.

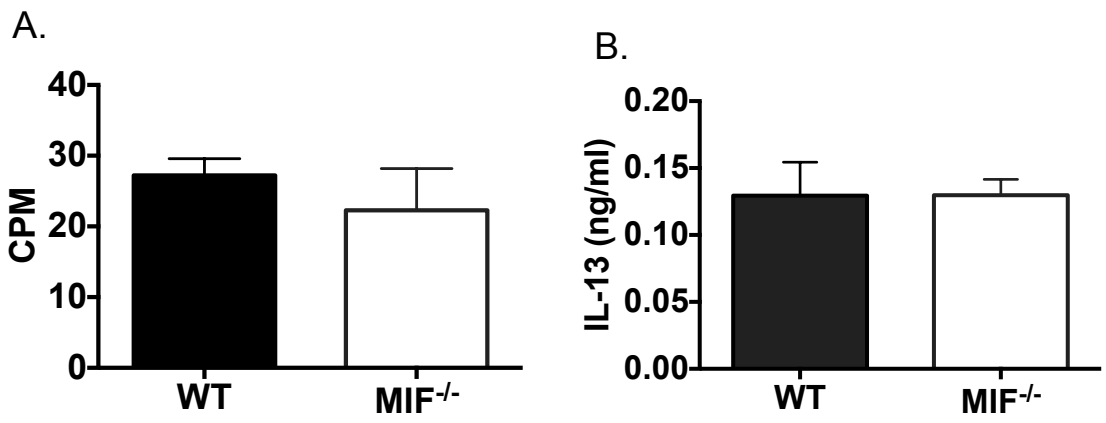

Figure 7: T_H2 response to *N. brasiliensis* in splenocytes is similar in WT and $MIF^{-/-}$ mice.

A. 1.25 x 10^5 cells/mL from the spleen on day 7 post infection were assessed for proliferation by [^{3}H]-thymidine incorporation with anti-CD3ε/anti-CD28 stimulation. B. 5 x 10^5 splenocytes/mL from day 7 infected mice were stimulated with anti-CD3ε/anti-CD28 and IL-13 was measured by ELISA in the culture supernatant. Data is combined from three independent experiments and analyzed by unpaired t test.

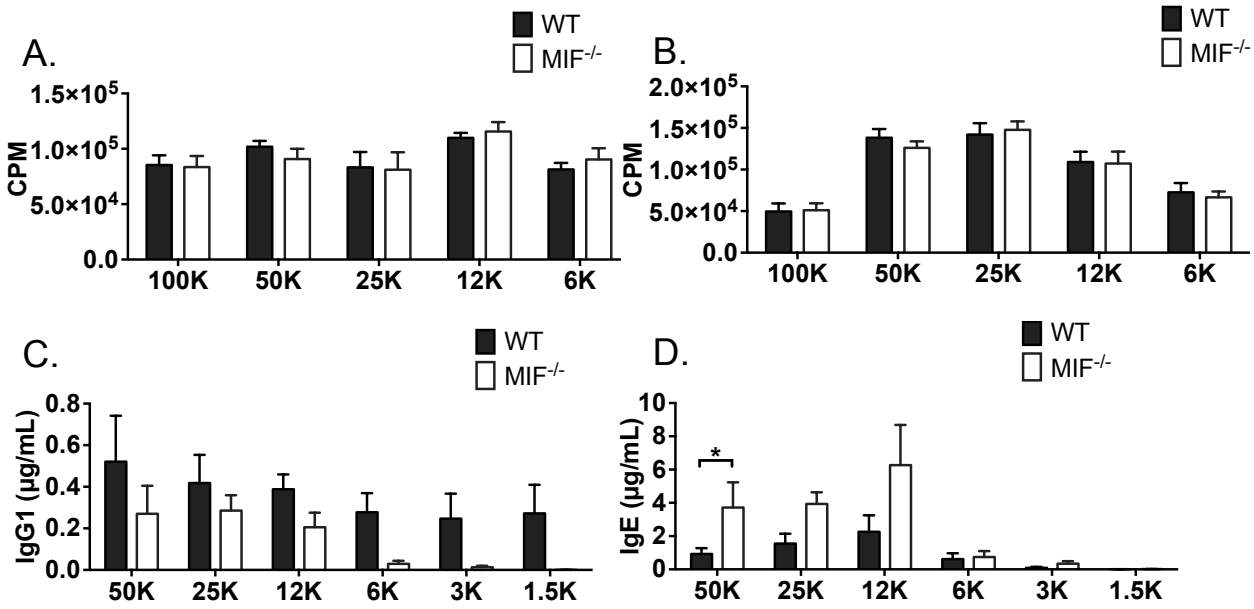

Figure 8: B cell responses in WT and MIF$^{-/-}$ mice are similar.

A. and B. Splenic B cells from WT and MIF$^{-/-}$ mice were cultured at indicated seeding amounts in cRPMI with anti-CD40 and IL-4 (A) or LPS and IL-4 (B). CPM was assessed by [^{3}H]-thymidine incorporation. IgG1 (C) and IgE (D) were measured in cell free supernatants from cultures (A) by ELISA. *$p<0.05$ ANOVA with Tukey's post hoc test.

Enhanced control of N. brasiliensis is dependent on loss of MIF in the hematopoietic compartment

To determine if MIF deficiency in the hematopoietic compartment was responsible for the phenotype observed in the $MIF^{-/-}$ mice, we irradiated WT mice and reconstituted them with $MIF^{-/-}$ bone marrow and compared them to irradiated $MIF^{-/-}$ mice reconstituted with WT bone marrow. After 6 weeks of reconstitution, mice were infected with *N. brasiliensis*. On day 8 post infection, WT mice reconstituted with $MIF^{-/-}$ bone marrow had reduced eggs in the feces compared to $MIF^{-/-}$ mice reconstituted with WT bone marrow (Figure 9A). We confirmed reconstitution by performing flow cytometry on the blood, spleen, peritoneal lavage cells, and MLN after infection. Successful reconstitution was demonstrated by the presence of $CD45.1^{+}$ cells in the $MIF^{-/-}$ mice reconstituted with WT bone marrow and $CD45.2^{+}$ cells in WT mice reconstituted with $MIF^{-/-}$ bone marrow (Figure 11). This suggests that lack of MIF in hematopoietic-derived cells is important for the enhanced clearance of *N. brasiliensis*.

Next, we examined the tissues in WT mice for relative *Mif* message levels before and after infection (day 7). While there was a trend toward increased *Mif* expression in the spleen ($p=0.07$), the only significant induction of *Mif* expression was observed in the proximal small intestine and MLN (Figure 9B). To determine which hematopoietic cell(s) produce MIF in response to *N. brasiliensis* infection, we sorted B, $CD4^{+}$ T, and dendritic cells from the MLNs. Only $CD4^{+}$ T cells ($CD90.2^{+}$ $CD4^{+}$) exhibited an induction of *Mif* expression on day 7 post infection (Figure 9C). Given previous evidence for the role of MIF in macrophages, we also measured *Mif* expression in macrophages from day 7 infected mice, but we found no increase in expression (Figure 10).

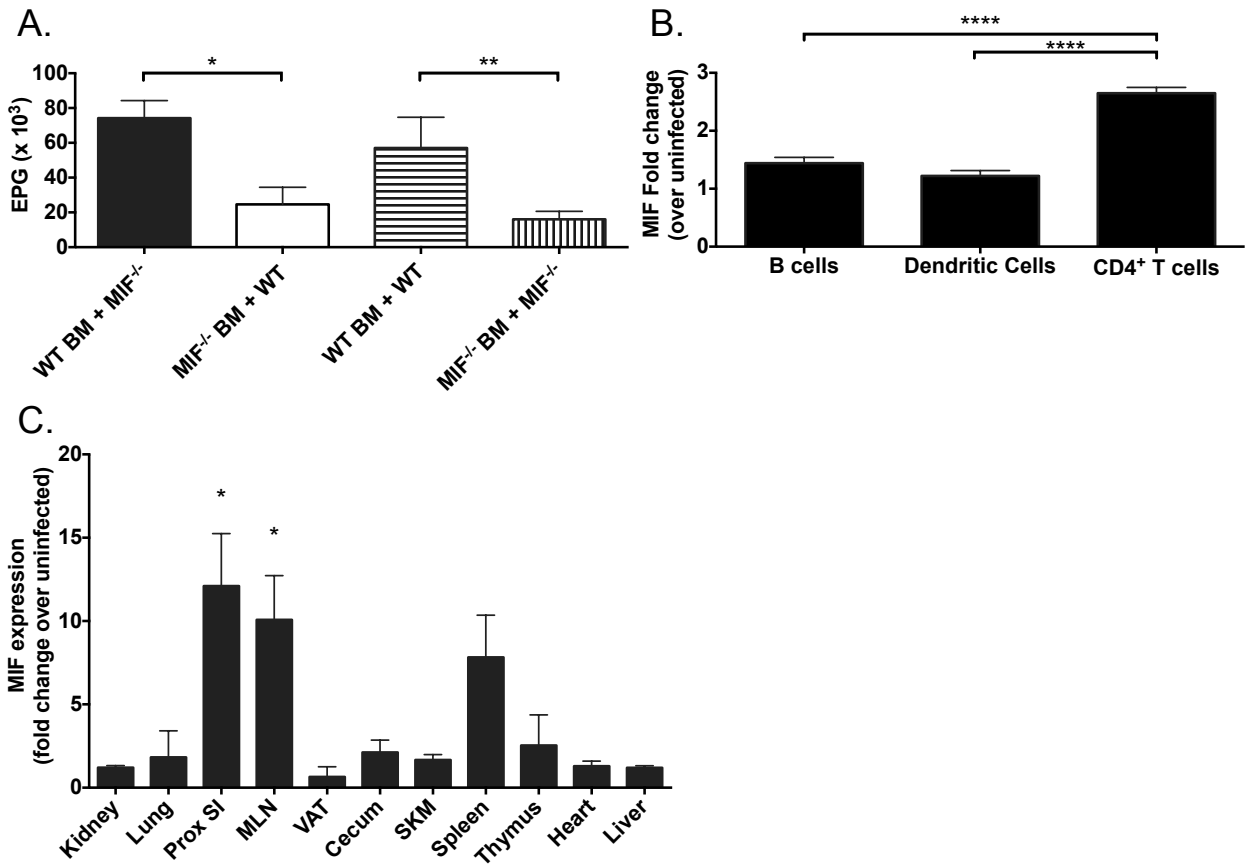

Figure 9: MIF deficiency in the hematopoietic compartment is sufficient for increased parasite clearance.

A. MIF$^{-/-}$ mice reconstituted with WT bone marrow (WT BM + MIF$^{-/-}$) and WT mice reconstituted with MIF$^{-/-}$ bone marrow (MIF$^{-/-}$ BM + WT) were infected with *N. brasiliensis* and EPG was measured at Day 8. B. Tissues from day 7 infected and uninfected mice were flash frozen and total RNA was isolated. *Mif* expression was measured as fold change of infected over uninfected. C. B cells (B220^{+} CD90.2^{-}), dendritic cells (CD90.2^{-} CD11c^{+}), and CD4^{+} T cells (B220^{-} CD90.2^{+} CD4^{+}) were sorted from day 7 infected and uninfected MLNs. *Mif* expression was measured and fold change was calculated. Data is combined from two independent experiments of three mice per group in each experiment. * $p<0.05$, unpaired t test (A and C), one way ANOVA (B).

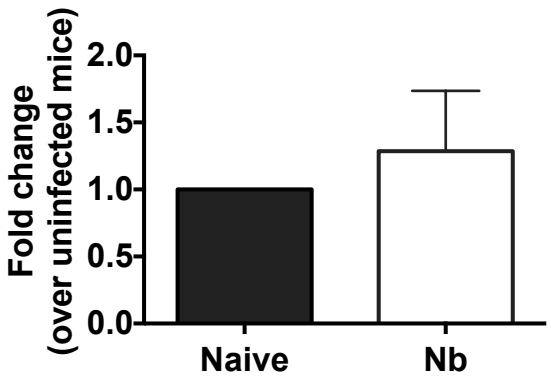

Figure 10: Macrophages do not upregulate MIF after *N. brasiliensis* infection.

Expression of *Mif* in macrophages from naïve and day 7 *N. brasiliensis* infected (Nb) WT mice.

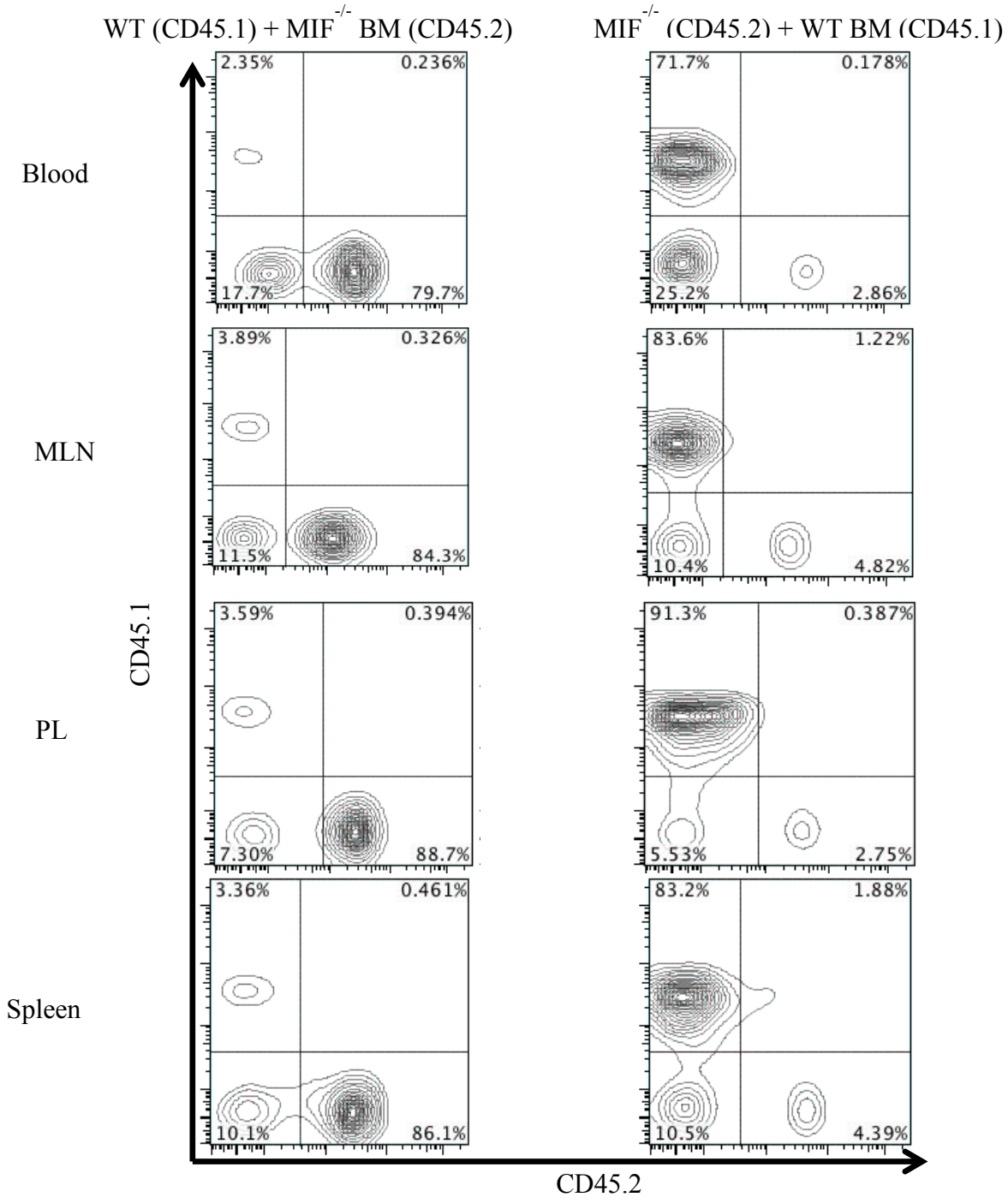

Figure 11: Confirmation of bone marrow reconstitution

On day 14 after *N. brasiliensis* infection, WT + MIF$^{-/-}$ BM and MIF$^{-/-}$ + WT BM groups were analyzed for bone marrow reconstitution. Blood, MLN, peritoneal lavage cells (PL), and splenocytes were analyzed by flow cytometry for CD45.1 and CD45.2.

Taken together, our data indicate that lack of MIF in the hematopoietic compartment, primarily within $CD4^+$ T cells, correlates with increased *Gata3* and IL-13 expression and worm expulsion. We sought to prove that $MIF^{-/-}$ $CD4^+$ T cells mediated the effects demonstrated in the $MIF^{-/-}$ mice. To this end, we reconstituted $Rag1^{-/-}$ mice, which have no mature B or T cells, with WT B cells and either WT or $MIF^{-/-}$ $CD4^+$ T cells. On day 7 after infection with *N. brasiliensis,* non-reconstituted $Rag1^{-/-}$ mice had a severe infection with the helminth. $Rag1^{-/-}$ mice reconstituted with WT $CD4^+$ T cells, where able to mount a response to *N. brasiliensis* as demonstrated by fewer EPG compared to the non-reconstituted $Rag1^{-/-}$. Intriguingly, $Rag1^{-/-}$ mice given $MIF^{-/-}$ $CD4^+$ T cells had significantly reduced EPGs compared to the WT control (Figure 12). These data reinforce the importance of $MIF^{-/-}$ $CD4^+$ T cells in the enhanced T_H2 response in $MIF^{-/-}$ mice.

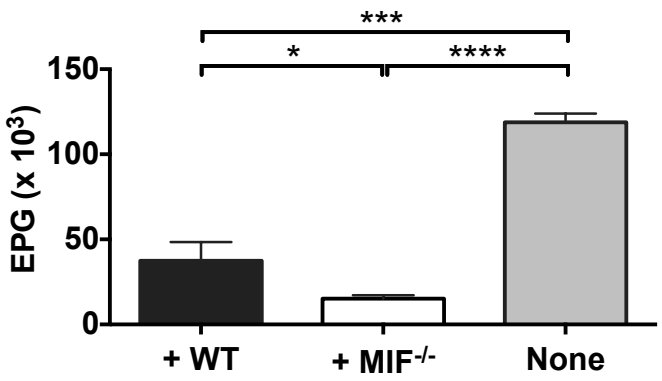

Figure 12: MIF$^{-/-}$ CD4^{+} T cells mediate enhanced clearance of *N. brasiliensis*.

A. Rag1$^{-/-}$ mice reconstituted with 20 x 10^{6} WT B220^{+} B cells and 10 x 10^{6} WT (+ WT) or MIF$^{-/-}$ (+ MIF$^{-/-}$) CD4^{+} T cells or not reconstituted (None) were injected *N. brasiliensis*. EPG were measured on day 7 post infection. Representative data is shown from one of two experiments, n = 3 mice per group per experiment. * $p<0.05$, *** $p<0.001$, **** $p<0.0001$, one way ANOVA with Tukey's multiple comparison test.

MIF$^{-/-}$ CD4^{+} T cells exhibit reduced NF-kB signaling and IL-6 production

Recent literature has demonstrated a regulatory role for IL-6 in T_H2 immune responses to the intestinal helminth *H. polygyrus* in that CD4^{+} T cells from IL-6 deficient mice produced more T_H2 cytokines[51]. Since CD4^{+} T cells had the largest increase in *Mif* message in response to *N. brasiliensis* infection, we investigated the induction of IL-6 in these cells. CD4^{+} T cells isolated from the MLN from MIF$^{-/-}$ mice had a modest increase (5-fold) in *Il6* message expression at day 7 post infection with *N. brasiliensis*. In contrast, *Il6* message was increased 38-fold in the MLN of WT mice (Figure 13A). Additionally, *Il17a* expression was reduced in the MIF$^{-/-}$ CD4^{+} T cells (Figure 13B), which is consistent with in the impaired IL-17 expression observed in IL-6 deficient mice after helminth infection[51].

To understand how MIF deficiency could alter IL-6 production, we examined the pathways on which MIF is known to act. MIF activates mitogen-activated protein kinase (MAPK) pathways[27]. To determine if this pathway was involved in the reduction of IL-6 expression, phosphorylation of ERK1/2 in MIF$^{-/-}$ MLN CD4^{+} T cells on day 7 after infection was measured by western blot. No difference in ERK1/2 phosphorylation between WT and MIF$^{-/-}$ was observed (Figure 13C, D). MIF is also known to act through canonical NF-kB pathways by increasing signaling through TLR4 and other yet to be determined mechanisms leading to the expression of target genes[30]. On day 7 after infection, significantly less phosphorylation of NF-kB component, p65, was observed in MIF$^{-/-}$ CD4^{+} T cells (Figure 13E, F). Since IL-6 is a known NF-kB target gene[52], these results suggest that the reduced induction of IL-6 in the MIF deficient CD4^{+} T cells may be a consequence of impaired NF-kB activation.

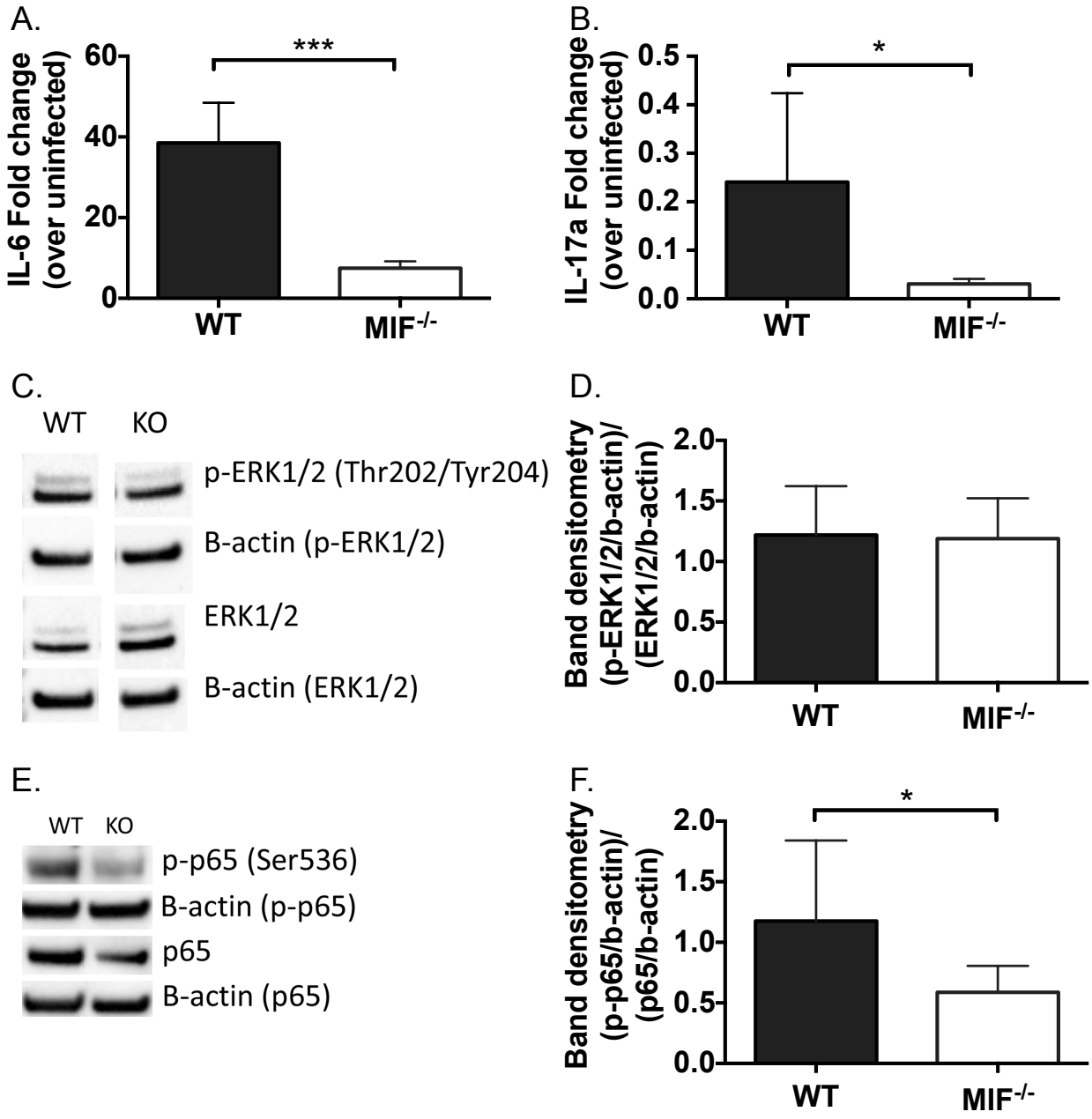

Figure 13: Reduced IL-6 expression and NF-kB activation in MIF$^{-/-}$ CD4^{+} T cells after infection.

A. and B. On day 7 post infection with *N. brasiliensis*, *Il6* (A) and *Il17a* (B) mRNA expression was measured in CD4^{+} T cells from MLNs. Data are expressed as fold change over uninfected. C-F. CD4^{+} T cells isolated from the MLNs of day 7 infected mice were lysed and immunoblots performed for the indicated proteins. C and E. Representative immunoblots D. and F. Quantification of (D) p-ERK1/2 and ERK1/2 and (F) p-p65 and p65. For each, the band densities

were normalized to their respective β-actin controls. The ratios of normalized p-ERK1/2 and p-p65 to normalized total ERK1/2 and p65, respectively, were calculated. Data were combined from one experiment of three mice per group (C and D) and from three independent experiments each with three mice per group (A, B, E, F). *** $p<0.001$, * $p<0.05$, unpaired t test.

Administration of MIF tautomerase inhibitor, SFN, enhances clearance of N. brasiliensis

The cytokine MIF has been characterized as a keto-enol tautomerase[23,25]. While the precise endogenous substrates for this enzymatic activity are unknown, MIF tautomerizes the artificial substrates D-dopachrome and phenylpyruvate, providing the means to assay its activity *in vitro*. Sulforaphane (SFN) is a naturally occurring organosulfur compound found in cruciferous vegetables like broccoli and brussel sprouts[53]. SFN covalently modifies the N-terminal proline of MIF which functions as the catalytic center for its tautomerase activity[31,54,55]. Therefore, SFN is a potent and irreversible inhibitor of MIF.

To determine whether the tautomerase activity of MIF is important for its function during *N. brasiliensis* infection, we administered the tautomerase inhibitor SFN to WT mice daily beginning on the day of infection. Intriguingly, WT mice treated with SFN had fewer eggs in the feces on day 7 of infection relative to the saline controls (Figure 14A) and indeed looked very similar to the $MIF^{-/-}$ animals (Figure 1A). The SFN treated group also had fewer adult worms (L5) in the proximal small intestine on day 7 post infection (Figure 14B). To exclude any effects that SFN may have on the enhanced worm clearance in the $MIF^{-/-}$ mice, we examined SFN treatment in $MIF^{-/-}$ mice and observed no effect of SFN on the clearance of *N. brasiliensis* in the absence of MIF (Figure 14C). To exclude effects of SFN functioning through its ability to induce antioxidant response element (ARE) dependent gene expression, we measured the expression of genes regulated by this transcription factor. We found no significant difference in the expression of these genes in the MLNs of naïve and *N. brasiliensis* infected WT mice with or without SFN treatment (Figure 15), though there was a slight trend upwards ($p=0.06$) for NADPH quinone oxidoreductase (*Nqo1*). We also measured the levels of T_H2 cytokines in day 7 infected saline and SFN treated mice. In agreement with the EPG data, SFN treated mice had a significant

increase in the expression of *Il4* and *Il13* in the MLNs compared to saline treatment (Figure 14D, E). This suggests that the tautomerase activity of MIF is essential for its normal function in the immune response to *N. brasiliensis.*

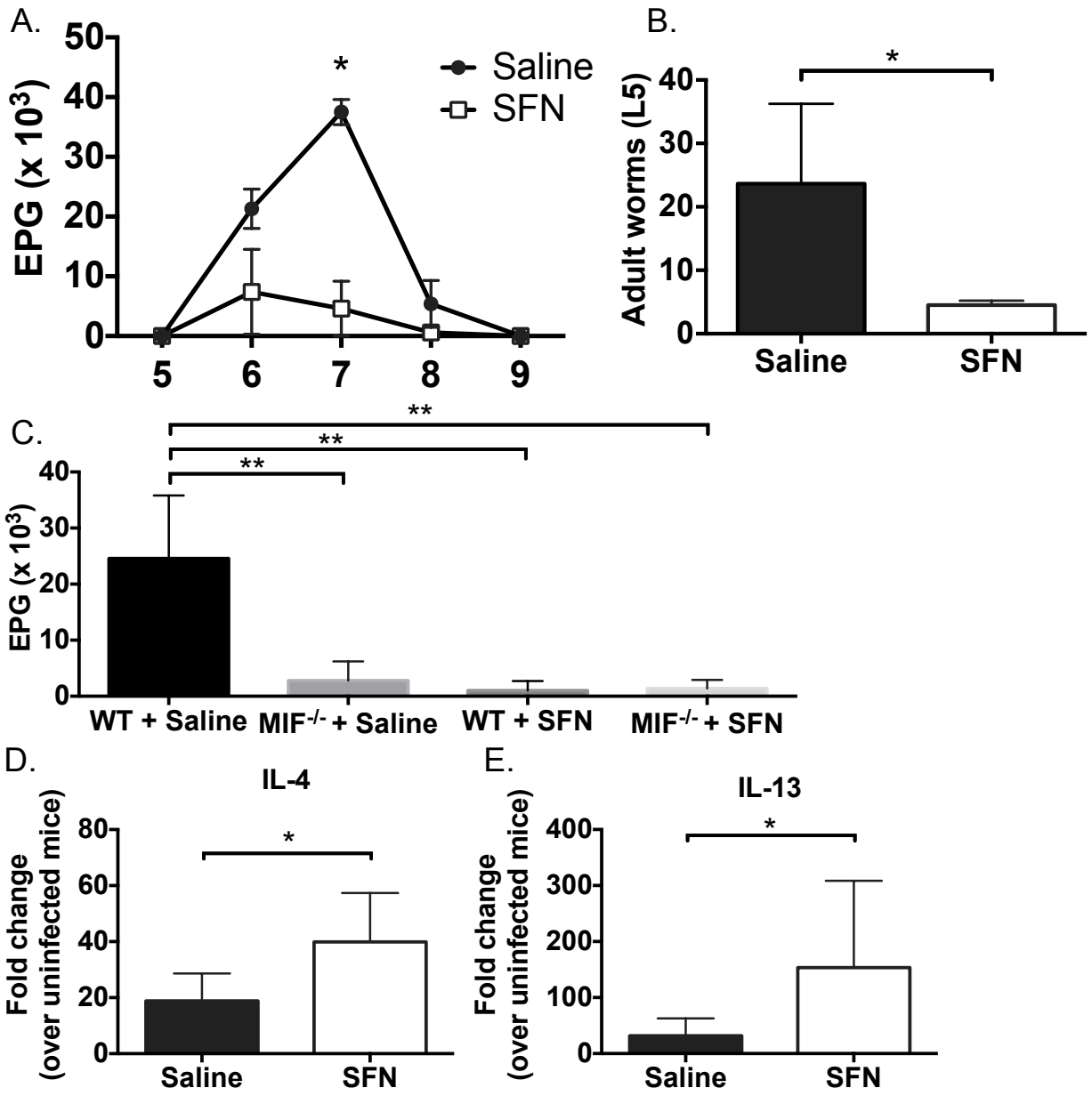

Figure 14: MIF inhibitor and natural product, SFN, promotes clearance of *N. brasiliensis* in WT mice.

A. and B. WT mice were infected with *N. brasiliensis*. Saline or 200µg SFN was administered intraperitoneally into WT mice daily beginning on the day of infection. EPG were enumerated on indicated days (A). On day 7 of infection, adult worms were measured in the proximal small intestine (B). C. WT and MIF$^{-/-}$ mice were infected with *N. brasiliensis* and given either saline or 200µg SFN daily beginning on the day of infection. EPG was measured on day 7 post infection.

D. and E. Fold change of *Il4* and *Il13* were measured in the MLNs of day 7 infected saline and SFN treated WT mice. Data is representative of one experiment of three performed each with three mice per group. ** $p<0.01$, * $p<0.05$, unpaired t test (A, B, D, E) and one way ANOVA with a Dunnett's multiple comparison test to examine differences from WT + saline group (C).

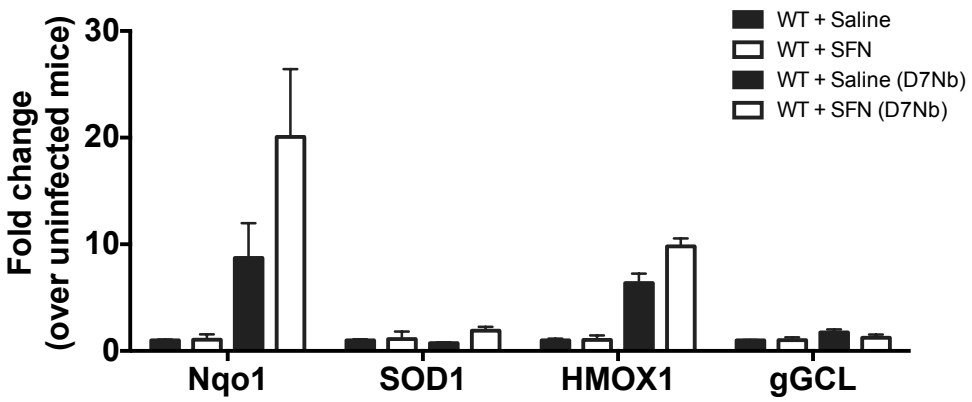

Figure 15: Expression of genes regulated by antioxidant response element (ARE) signaling system.

MLNs from naïve or day 7 infected WT mice treated with saline or SFN were analyzed for expression of genes regulated by the ARE signaling system (NADPH quinone oxidoreductase (*Nqo1*), superoxide dismutase (*Sod1*), hemeoxygenase1 (*Hmox1*), and γ-glutamylycysteine lyase (*γ Gcl*)). Data was analyzed by unpaired Student's t test.

1.1.4 Discussion

MIF has been studied in the context of both the innate and adaptive immune responses in many disease models[56]. T cells were the first identified source of MIF[16,17] and have been extensively studied. Here we describe the role of MIF and, more specifically, its enzymatic tautomerase activity, in the immune response to *N. brasiliensis*. We have demonstrated that MIF deficiency results in decreased induction of IL-6 following infection, correlating with an enhanced T_H2 response and improved control of the infection in $MIF^{-/-}$ mice.

During infection with *N. brasiliensis*, cells isolated from the MLNs of $MIF^{-/-}$ mice exhibited increased T cell proliferation in response to TCR stimulation and produced more IL-13 with a reduction in IFNγ production. While IL-4 induction was not significantly changed, IL-13 alone is sufficient to enhance the "weep and sweep" response that leads to worm expulsion[57]. This was accompanied by increased expression of the T_H2 transcription factor GATA3. In a different helminth infection model, *Taenia crassiceps*[40], which also elicits a T_H2-like immune response[58], $MIF^{-/-}$ mice were shown to be more susceptible to the parasite and had a larger parasite burden despite enhanced IL-13 production. In cysticercosis, it is thought that nitric oxide (NO) from macrophages provides the bulk of protection. Thus in spite of enhanced IL-13 production, it is possible that $MIF^{-/-}$ mice were susceptible to *T. crassiceps* because $MIF^{-/-}$ macrophages are unable to produce the high levels of TNF and NO necessary for parasite clearance[40] in this model. Similarly, in *Schistosoma japonicum* infection, mice given a neutralizing anti-MIF IgG exhibited increased worm burden in the liver. This phenotype was also attributed to the lack of NO and TNF produced by macrophages[59]. This suggests that the impact of MIF on the immune response to a given parasite will vary as a function of the dominant mechanism(s) of worm clearance.

Though many cell types express MIF, we found that MIF deficiency in the hematopoietic compartment was sufficient to recapitulate the enhanced immunity to *N. brasiliensis* that we found in $MIF^{-/-}$ mice. Examining the expression of MIF in many different tissues and cell types indicated that T cells are likely the major source of MIF induced by infection with *N. brasiliensis.* Our $Rag1^{-/-}$ reconstitution data (Figure 12) further support this conclusion. These data provide direct evidence that $MIF^{-/-}$ $CD4^{+}$ T cells confer an advantage in the immune response to *N. brasiliensis* compared to WT. To further investigate the mechanism through which MIF influences worm clearance, we examined the impact of MIF deficiency on infection-induced IL-6. Recently, IL-6 was shown to be detrimental to the T_H2 response and immunity to the intestinal helminth, *H. polygyrus bakeri*[51]. Mice deficient in IL-6 had reduced parasite burden and enhanced T_H2 response. Without IL-6 during this infection, the T helper response was shifted away from T_H17 and toward T_H2 and regulatory T cells but with less Foxp3, Helios, and Gata3 transcription factor expression. MIF has directly or indirectly been shown to influence the production of many molecules important in inflammation including, TNF, IFNγ, IL-1B, IL-2, IL-6, IL-8, MIP2[19–22], NO[18,35], PGE_2, COX_2[27]. MIF deficient macrophages are the most well studied and have been demonstrated to produce fewer inflammatory cytokines upon stimulation or infection[56]. In this study, MIF deficiency resulted in less *Il6* induction in the $MIF^{-/-}$ CD4 T cells (Figure 13A) as well as a decrease in *Il17a* expression following infection (Figure 13B). In the *H. polygyrus* model, it was posited that, without IL-6, the response shifted away from T_H17 and towards T_H2 and an altered Treg phenotype[51]. Our results largely support these conclusions, though we did not see a corresponding increase in IL-10 expression (data not shown). This is likely due to the fact that IL-6 is reduced but not absent in our model as compared to the aforementioned IL-6 deficient mice. It may also possibly reflect differences between *N.*

brasiliensis and *H. polygyrus bakeri* infection models, namely the former is efficiently controlled by the T_H2 response while the latter establishes a more chronic infection.

The tautomerase activity of MIF was first described by Rosengren et al[23]. Several isothiocyanate compounds have been characterized as irreversible inhibitors of this enzymatic activity[31,54,55], including SFN. While the role of MIF's enzymatic activity in its biological functions remains controversial, several published reports have supported the contention that the tautomerase activity is essential for many functions of MIF[49]. Particularly interesting is the study by Simpson et al. in which MIF deficient tumors exhibited reduced growth and impaired ability to attract myeloid derived suppressor cells. They were able to demonstrate that the MIF tautomerase enzyme was critical for this effect using both an enzymatically inactive point mutant of MIF as well as administration of SFN to the mice[49]. While many MIF inhibitors are commercially available, we chose to use the compound SFN because of its status as a natural product with a high concentration in cruciferous vegetables[53]. SFN is also commercially available in nutritional supplements, making it an even more attractive potential solution to reducing worm burden in patients. It is important to note that, in addition to inhibiting MIF enzyme activity, SFN also induces genes associated with cytoprotective responses including the genes regulated by Keap1-Nrf2-ARE signaling system[60]. This system protects against damage by oxidant, electrophile, and inflammatory stresses[61]. However, we did not observe induction of ARE dependent genes in our SFN treated mice (Figure 15). In addition, we observed no additional impact of SFN on parasite clearance in $MIF^{-/-}$ mice, suggesting that MIF inhibition is the predominant target in our model. SFN treatment enhanced T_H2 transcription factor and cytokine expression in MLNs after *N. brasiliensis* infection, mirroring the response seen in MIF

deficiency. These results are the first to show that blockade of the enzyme activity of MIF is sufficient for the enhanced clearance of this helminth infection.

Taken together, our results demonstrate that MIF deficiency leads to an enhanced T_H2 immune response against the helminth parasite, *N. brasiliensis*. While this is not the first example of MIF deficiency resulting in an enhanced T_H2 response, this study shows that, in a pathogen model in which the T_H2 response is able to control the infection, MIF deficiency or inhibition will further enhance this clearance. This enhancement is due to $CD4^+$ T cells, which have the most heightened MIF expression post infection and in our $Rag1^{-/-}$ reconstitution model mediated parasite clearance. The data further show that $CD4^+$ T cells from $MIF^{-/-}$ mice have reduced *Il6* message, potentially due to impaired NF-kB activation. Alternatively, IL-13 has been demonstrated to attenuate NF-kB activation as part of the endogenous regulation of acute inflammatory responses[62]. In conjunction with other reports, this suggests a mechanism for the increased T_H2 response, since IL-6 is known to impede the T_H2 response[51]. Perhaps most excitingly, we were able to show that by blocking the tautomerase enzyme activity of MIF with the inhibitor SFN we could mimic the response seen in MIF deficient mice with *N. brasiliensis* infection, suggesting that this nutritional supplement would enhance resistance to parasitic pathogens in which a T_H2 response is responsible for control.

Chapter 2 Notch1 and ADAM10 on dendritic cells control the development of type 2 immune responses and IgE production.

1.2.1 Introduction

Allergic asthma has become a major disease of the developing world with yearly increases in incidence. Worldwide, the number of people with asthma is estimated to grow by 100 million by the year 2024[63]. Innate and adaptive immune responses lead to the production of T_H2 cytokines, IL-4, IL-5, and IL-13, which in turn cause many of the clinical symptoms seen in asthma including eosinophil infiltration, mucus overproduction, and airway constriction[64]. IgE plays a role in many, but not all T_H2-mediated allergic diseases, and specific control of IgE production has not been successful to date. These effectors of disease have been well studied, but precisely how these pathways are triggered is less well understood. As dendritic cells (DCs) are the most potent activators of adaptive immune responses, including T_H2 immunity, we aimed to understand the role of DCs in the development of allergic responses.

ADAM10

A disintegrin and metalloproteinase (ADAM) 10 is a member of a metzincin superfamily of zinc-dependent metalloproteinases, which also includes a disintegrin and metalloproteinase with thrombospondin domain (ADAM-TS) and matrix metalloproteinases (MMPs). ADAM family members are unique as they are active while membrane bound and have several conserved domains: prodomain, metalloproteinase, c-shaped cysteine-rich, transmembrane, and cytoplasmic tail. ADAMs cleave type I and II transmembrane proteins, which releases the extracellular domain in the soluble space. This is the process that mediates ectodomain shedding and regulated intramembrane proteolysis (RIP). These cleavage events lead to several different events: receptor downregulation, release of receptors leading to paracrine and autocrine signals,

and the release of soluble mediators. Many receptors undergo RIP constitutively but ligand-induced RIP is also common[65,66].

The ADAM family of proteins has approximately 40 members in mammals. Mice have 27 different ADAMs, and humans have 22[67]. ADAM10 was originally characterized in *Drosophila melanogaster* and was named Kuzbanian (Kuz). Kuz-deficiency in *Drosophila* led to several peripheral and central nervous system (CNS) defects[68]. After cloning the Kuz gene, it was found to be similar to bovine metalloproteinase (BMP). Through this comparison, the α-secretase activity of Kuz was discovered, which lead to it being heavily studied in the cleaving of amyloid precursor protein and in Alzheimer's disease[68]. Kuz was determined to be critical for the RIP of Notch receptors, and thus the neurological defects observed in Kuz-deficiency were due to lack of Notch signaling[69].

ADAM10-deficient murine embryos only survive until E9.5 due to severe cardiovascular and CNS defects. It was observed that these development effects of ADAM10 deficiency were similar to the Notch knockout embryos. Controversy as to which ADAM, 10 or 17, was responsible for Notch S2 cleavage existed until ADAM10 and ADAM17 deficient embryos were examined. Only the ADAM10KOs resembled the Notch knockout embryo, lending further support that ADAM10 was the primary sheddase and not ADAM17[70–74]. Knockout murine embryonic fibroblasts (MEFs) helped further elucidate that ADAM10 mediated ligand-induced cleavage, whereas several other proteases could shed in a ligand-independent manner[75–77]. Given its important role in cell-cell and cell-matrix interactions, ADAM10 has been studied in many physiological and disease processes including neuron homeostasis and development, Alzheimer's disease, and allergy[78,79].

Notch signaling

Ligands for ADAMs include growth factors and cytokines as well as their receptors, including Notch receptors. Notch receptors 1 – 4 and the Notch ligands delta like ligand (Dll) 1 – 4 and Jagged 1 and 2 are all substrates for ADAM10[74,80]. Upon Notch receptor–ligand engagement a conformational shift occurs revealing the S2 cleavage site for ADAMs. This step is required for the next cleavage by γ-secretase, releasing the Notch-intracellular domain (N-ICD), which translocates to the nucleus and with binding partners initiates transcription of Notch target genes[81]. ADAM10 is required for the cleavage of Notch as is evident in the global ADAM10 knockout, which displays typical loss of function Notch defects[75]. Within the immune system, lack of ADAM10 in T cells results in no T cell development[82]. We have examined the effects of ADAM10 deletion in B cells, which leads to inhibition of humoral immunity[50,83] and absence of marginal zone B cells[84]. Prior to this study, the role of ADAM10 in DCs has not been explored.

Dendritic cells

DCs are specialized immune cells, which initiate adaptive immune responses by processing and presenting antigen to T cells. DCs take up antigen in the periphery and when they receive appropriate signals travel to the draining lymph node. Conventional DCs (cDCs) are separated into two subsets: IRF8-dependent cDC1s and IRF4-dependent cDC2s. cDC1s cross present antigen to $CD8^+$ T cells and cDC2s stimulate $CD4^+$ T cell responses[85]. In the T cell zone, cDC2s interact with T cells via peptide loaded MHCII. Upon cognate T cell engagement, the DC directs priming of the T cells through costimulatory molecules and DC-derived cytokines[85].

In model antigen (ovalbumin (OVA) and aeroallergen (house dust mite (HDM)) models of allergic airway inflammation in mice, DCs have been extensively studied as initiators of T_H2 immunity. Specific cytokine milieus generated by DCs are important for initiating T_H2

responses, particularly expression of IL-6 and lack of IL-12p70. Recently, the transcription factor KLF4 has also been shown to be important for T_H2 immunity[86]. Further, certain costimulatory molecules, OX40L, CD86, PDL2, and cell surface proteins, CD301b (MGL2), Jagged 1, and Jagged 2, on DCs also influence the priming of T cells toward T_H2[87].

Here we show new evidence for the role of Notch signaling in DCs for the development of T_H2 immune responses in murine allergic airway inflammation and IgE production. The loss of antigen-specific IgE in the ADAM10 deficient DC ($ADAM10^{DC-/-}$) mouse protected against anaphylaxis in an ovalbumin model. We were able to recover IgE production and anaphylaxis in the $ADAM10^{DC-/-}$ mice by expressing the Notch1-intracellular domain (N1-ICD). The phenotype of mice in which Notch1 was deleted from DCs suggested that Notch1 expression was particularly critical. Deletion of ADAM10 on DCs led to changes in the costimulatory molecule OX40L and cytokine IL-6, both of which are critical for the generation of T_H2 responses. Overall, we demonstrate the importance of the expression of ADAM10 on DCs for T_H2 immunity and IgE production.

1.2.2 Materials and Methods

1.2.2.1 Mice

All animal experiments were performed with the approval of the Virginia Commonwealth University Institutional Animal Care and Use Committee. Mice were maintained in the Virginia Commonwealth University animal facility in accordance with guidelines for the humane treatment of laboratory animals set forth by the National Institutes of Health and the American Association for the Accreditation of Laboratory Animal Care. C57Bl/6 $ADAM10^{flox}$ mice were generated as previously described[84] and were bred to B6.Cg-Tg(Itgax-cre)1-1Reiz/J (CD11c-cre,

Stock No. 008068) to generate ADAM10$^{DC-/-}$ mice. Notch1^{flox} (Stock No. 006951) and Notch2^{flox} (Stock No. 010525) were bred to the CD11c-cre mouse (all from The Jackson Laboratory, Bar Harbor, ME). N1-ICD Gt(ROSA)26Sor$^{tm1(Notch1)Dam}$/J (Stock No. 8159) was purchased from Jackson lab and bred to ADAM10$^{DC-/-}$ mice to generate ADAM10$^{DC-/-\ N1-ICD+}$. 4C13RTg mice, which express AmCyan and DsRed with the expression of IL-4 and IL-13, respectively were a kind gift from Dr. Xi Chen at NIH/NIAID. The 4C13RTg mice were bred to OT-II mice to generate 4C13R-OT-II mice. All mice were on the C57Bl/6 background, and healthy male and female 6-12 week old mice were used for experiments. Table 3 lists genotyping primers used to identify mice.

Table 3: Genotyping Primers

Mouse Colony		Primer Name	Sequence (5' – 3')
ADAM10$^{DC-/-}$	Flox and WT	Intron9	CAGTGTAAATGTGAACTCACCC
		Exon9	CGTATCTCAAAACTACCCTCCC
	YFP	oMIR316	GGAGCGGGAGAAATGGATATG
		oMIR883	AAAGTCGCTCTGAGTTGTTAT
		oMIR4982	AAGACCGCGAAGAGTTTGTC
Notch1$^{DC-/-}$	Flox and WT	oMIR6748	TGCCCTTTCCTTAAAAGTGG
		oMIR6749	GCCTACTCCGACACCCAATA
Notch2$^{DC-/-}$	Flox and WT	10084	TAGGAAGCAGCTCAGCTCACAG
		10085	ATAACGCTAAACGTGCACTGGAG
N1-ICD	WT	21306	CTGGCTTCTGAGGACCG
		21309	AATCTGTGGGAAGTCTTGTCC
		21310*FAM/BHQ3	TAACCTGGTGTGTGGGCGTTGT
	Mutant	21306	CTGGCTTCTGAGGACCG
		21307	CGAAGAGTTTGTCCTCAACCG
		21308*FAM/BHQ3	ACCCTGGACTACTGCGCCC
4C13R	DsRed	DsRedEXINTSEQ 5'	GCTCCAAGGTGTACGTGAAG
		DsRedEXINTSEQ 3'	GCTTGGAGTCCACGTAGTAG
	β-actin	ms β-actin F	AGAGGGAAATCGTGCGTGAC
		ms β-actin R	CAATAGTGATGACCTGGCCGT
OT-II	Transgene	oMIR1880	AAAGGGAGAAAAAGCTCTCC
		oMIR1881	ACACAGCAGGTTCTGGGTTC
	Internal positive control	oMIR7338	CTAGGCCACAGAATTGAAAGATCT
		oMIR7339	GTAGGTGGAAATTCTAGCATCATCC
CD11c-Cre	Transgene	oMIR7841	ACTTGGCAGCTGTCTCCAAG
		oMIR7842	GCGAACATCTTCAGGTTCTG
	Internal positive control	oMIR8744	CAAATGTTGCTTGTCTGGTG
		oMIR8745	GTCAGTCGAGTGCACAGTTT

1.2.2.2 NP-KLH immunization

10μg 4-hydroxy-3-nitrophenylacetyl hapten conjugated to keyhole limpet hemocyanin (NP_{31}-KLH, Biosearch Technologies) was emulsified in 4mg alum (Imject, Sigma) and injected *i.p.* into mice. At days 7, 14, and 21 mice were bled by tail vein nick and serum was isolated. NP_4- and NP_{25}-BSA (15 μg/mL Biosearch Technologies) were used to coat ELISA plates in PBS for high and low affinity NP-specific IgG1 and IgG2a[50]. On day 21, mice were injected with 10μg NP_{31}-KLH and alum as above for recall antibody responses. For footpad injections, 10μg NP_{31}-KLH emulsified in 4mg alum was injected into the footpad of mice and after 7 or 14 days, popliteal lymph nodes were isolated and analyzed by flow cytometry for germinal center B cells (BUV395 anti-mouse CD45R/B220 (clone RA3-6B2), PE anti-mouse CD95 (clone SA367H8), and APC anti-GL7 (clone GL7)) and T follicular helper (T_{FH}) cells (FITC anti-mouse CD4 (clone GK1.5), BV421 anti-mouse PD-1 (clone 29F.1A12), Biotin anti-mouse CXCR5 (clone L138D7), and PE-Cy7 Streptavidin) (all from Biolegend).

1.2.2.3 HDM model

Mice were immunized to HDM extract (Stallergenes Greer, Lenoir, NC) as previously described[88]. Briefly, mice were anesthetized with 3.5% isoflurane in O_2 and 15μg HDM extract in saline was i.n. administered. Injections were repeated daily for five days, followed by two rest days, and then five days. 24h after the last i.n. injection, mice were deeply anesthetized with ketamine and xylazine (100mg/kg and 10mg/kg, respectively) intraperitoneal (*i.p.*) injection and subjected to forced oscillations using the Flexivent apparatus (Scireq Inc., Montreal, Canada). Mice were given increased doses of methacholine (0, 2.5, 5, 10, 12.5, 25, 50, and 100mg/mL) through a nebulizer attachment and maximum resistance was calculated. Bronchoalveolar lavage fluid (BALF) was collected, stained for eosinophils ($B220^-$ $CD3^-$ $MHCII^-$ $CCR3^+$), macrophages

(B220$^-$ CD3$^-$ MHCII$^+$ CD11b$^+$), neutrophils (B220$^-$ CD3$^-$ MHCII$^-$ CCR3$^-$), lymphocytes (B220$^+$ and/or CD3$^+$) with APC anti-mouse CD45R/B220 (clone RA3-6B2), APC anti-mouse CD3 (clone 17A2), BV421 anti-mouse I-A/I-E (clone M5/114.15.2), PE anti-mouse CCR3 (clone J073E5) and PE-Cy7 anti-mouse/human CD11b (clone M1/70), and collected on a BD LSRFortessa X-20 flow cytometer with Diva8 (BD Biosciences). FCS files were analyzed using FlowJo software (FlowJo, LLC, Ashland, OR). Lung lobes were snap frozen in liquid N_2 for RNA isolation or fixed in 10% formalin for hematoxylin and eosin staining. Serum was collected for total IgG1 and IgE and HDM-specific IgG1 ELISAs as described previously[89].

1.2.2.4 qPCR

RNA was isolated using TRIzol Reagent (LifeTech) according to manufacturer's instructions. RNA was reverse transcribed into cDNA using SuperScript IV and oligo dTs (LifeTech). qPCR reactions were run using Taqman probes and gene expression master mix (Applied Biotech) or primers (LifeTech) and PowerUp SYBR green master mix (LifeTech) on a QuantStudio3 system (LifeTech). Primers and probes are listed in Table 4.

1.2.2.5 Active systemic anaphylaxis (ASA)

Mice were immunized with 100µg ovalbumin (OVA), 10µg pertussis toxin, and 10mg/ml $AlK(SO_4)_2$ $12H_2O$ in saline[90]. Three weeks later mice were bled by tail vein nick and total and OVA-specific IgG1 and total IgE were measured in the serum. OVA-specific IgE was measured by coating Immunolon 4HBX plates (Thermo Scientific) with rat anti-mouse IgE (clone R1E4) in borate buffered saline and blocking with SuperBlock (ThermoFisher). After samples were added, OVA conjugated to biotin and dinitrophenol (DNP-X-Biocytin-X, SE kit Thermo Fisher) followed by streptavidin-alkaline phosphatase were added to wells. The ELISA was developed using phosphatase substrate (Sigma) and reading the absorbance at 405nm and 650nm. IgE anti-

DNP was used for the standard curve. On day 25 after immunization, mice were challenged with 500μg of OVA and core body temperature was measured. Anaphylaxis was determined if mice had more than 5°C temperature drop. Passive systemic anaphylaxis was conducted as previously described[91].

1.2.2.6 Alternaria alternata model

50μg *Alternaria alternata* extract was administered i.n. to mice on days 0 and 1. On days 14 – 16, mice were injected with 25μg *A. alternata* extract i.n. 24h after the last administration, mice were euthanized and BALF was collected[92]. Eosinophils and neutrophils ($B220^-$ $CD3^-$ $MHCII^-$ $CCR3^-$) were analyzed in the BALF by flow cytometry. Mediastinal lymph nodes (medLNs) were harvested and teased apart to obtain a single cell suspension, which was re-stimulated with plate bound anti-CD3ε (1μg/mL, clone 145-2C11, Biolegend) and monensin (Biolegend) for 4h. PE-Cy7 anti-mouse IL-13 (clone eBio13A, eBioscience), AlexaFluor647 anti-mouse IFNγ (clone XMG1.2, Biolegend), BV650 anti-mouse IL-17A (clone TC11-18H10.1, BD Biosciences), and BV421 anti-mouse CD4 (clone GK1.5, Biolegend) were used to assess intracellular cytokine production. Serum IgG1, IgE, and IgG2b were measured by ELISA.

1.2.2.7 Antigen presentation

For *in vitro* antigen presentation, 1 x 10^4 sorted $CD24^+$ or $CD172^+$ BMDCs were incubated with 0, 1, 10, or 50μg of OVA for 2h in 96h. $CD4^+$ OT-II T cells were isolated by magnetic bead selection with L3T4 beads (Miltenyi Biotec) and labeled with Tag-It Violet Proliferation and Cell Tracking Dye (Biolegend). 1 x 10^5 labeled OT-II were co-cultured with the OVA-loaded BMDCs for 72h after which dilution of the proliferation dye was analyzed by flow cytometry. Percent divided was calculated by dividing the number of cells that had divided at least once by

the total number of cells. For intracellular cytokine expression, monensin (Biolegend) was added 4h before staining.

For *in vivo* antigen presentation, $5x10^6$ labeled $CD4^+$ OT-II T cells were intravenously (*i.v.*) injected into mice. 24h later 25µg OVA and 10µg HDM extract were administered i.n. to mice. 72h later medLN were harvested and analyzed by flow cytometry. For IL-4/IL-13 detection, $CD4^+$ T cells isolated from 4C13R-OT-II mice and labeled with carboxyfluorescein succinimidyl ester (CFSE, Biolegend) were used in the *in vivo* antigen presentation assay described above. AmCyan and DsRed on $CD4^+$ T cells in the medLN were analyzed by flow cytometry as a measure of IL-4 and IL-13 expression.

1.2.2.8 BMDC Cultures

Bone marrow was isolated from mice, and erythrocytes were lysed using ACK Lysis Buffer (Quality Biological Inc.). Cells were cultured at 2 x 10^6 cell/mL with 160ng/mL Flt3L (Peprotech) for 6-8 days. After culture, cells were Fc blocked with anti-mouse CD16/32 (clone 93, Biolegend) and stained with PE-anti-mouse CD11c (clone N418), PE-Cy7 anti-mouse I-A/I-E (MHCII) (clone M5/114.15.2), BV510 anti-mouse CD24 (clone M1/69), and APC anti-mouse CD172 (clone P84). $CD11c^+$ $MHCII^+$ $CD24^-$ $CD172^+$ BMDCs were sorted on a FACS Aria II.

1.2.2.9 Anaplasma phagocytophilum infection

A. phagocytophilum (NCH-1 strain)-infected promyelocytic HL-60 cells (ATCC CCL-224) were cultured as previously described[93]. *A. phagocytophilum* bacteria were isolated via sonication and purified by differential centrifugation as previously described[94]. 10^7 *A. phagocytophilum* organisms were injected *i.p.* and blood was collected by tail vein nick into heparin at indicated days. DNA was isolated from 50µl blood using the DNeasy Blood and Tissue kit (Qiagen)

according to the manufacturer's protocol. Primers for *A. phagocytophilum* 16s DNA and murine Actb (β-actin) are listed in Table 4.

1.2.2.10 Citrobacter rodentium infection

A nalidixic acid-resistant mutant of strain DBS100 (ATCC 51459) of *C. rodentium* ($1x10^{10}$ CFU) was used to infect mice by oral gavage[95]. Dose was confirmed by retrospective plating. Mice were weighed every three days and killed 12 days after infection. Serum was obtained, and total IgG2b antibody was measured by ELISA. Spleens were removed, weighed, and homogenized to assess bacterial load. The terminal 5 cm of the colon was excised, fecal pellets removed, and weighed. The colon was homogenized in LB medium and *C. rodentium* load was determined by plating on LB agar plates with 50μg/mL nalidixic acid. For colon or spleen samples with a colony count of 0 for duplicate plates, colony count value of 0.5 was assigned that represents the limit of detection for statistical and graphical purposes.

1.2.2.11 Antigen uptake

Antigen uptake was measured *in vivo* by administering 25μg OVA conjugated to AlexaFluor647 (OVA-AF647, LifeTech) with 10μg HDM extract i.n. into mice and then isolating medLNs 24h later. MedLNs were tweezed apart with forceps to generate a single cell suspension, which was stained for cDC1 ($CD11c^+$ $MHCII^+$ $CD24^+$ $CD172^-$) and cDC2 ($CD11c^+$ $MHCII^+$ $CD24^-$ $CD172^+$). MedLNs were also frozen in OCT media, sectioned, fixed in acetone, and stained with FITC anti-mouse CD11c (clone N418) and PE anti-mouse CD45R/B220 (clone RA3-6B2). Slides were imaged on a LSM700 confocal and analyzed with Zen Microscopy and Imaging Software (Zeiss).

1.2.2.12 Chromatin Immunoprecipitation

BMDCs from WT and ADAM10$^{DC-/-}$ mice were incubated with 100ng/mL LPS (Sigma Aldrich) for 18h. BMDCs were then fixed in 1% paraformaldehyde at room temperature for 10 mins. Two washes with 0.125M glycine (ice-cold) was added to stop the crosslinking reaction. Cells were spun down at 2,000 rpm at 4°C and cells were resuspended in hypotonic cell lysis buffer (5mM PIPES pH8.0 85mM KCl 0.5% NP-40) and homogenized by douncing. Crude nuclear prep was isolated by centrifuging at 2,000 rpm at 4°C. Nuclear pellet was resuspended in ChIP nuclei lysis buffer (50mM Tris pH8.0, 10mM EDTA, 1% SDS) and samples were sonicated using a Bioruptor Twin (Diagenode) for 15 cycles of 30 seconds on and off. Sonicated mixture was centrifuged at 13,000 rpm at 4°C and supernatant was collected. Supernatants were incubated overnight with anti-cleaved Notch1 (#4147, Cell Signaling) and precipitated using ChIP-grade protein G magnetic beads (#9006, Cell Signaling). Primers used for Hes1 promoter region are found in Table 4.

1.2.2.13 Statistical Analyses

All statistical analyses were performed using Prism6 (GraphPad Software Inc., La Jolla, CA). Statistical significance was assessed by two-tailed, unpaired Student's t test (two groups), Mann-Whitney test, or one-way ANOVA for multiple groups with a Tukey's post hoc test. Unless otherwise indicated differences are not significant. ****$p<0.0001$, *** $p<0.001$, ** $p<0.01$, * $p<0.05$. Samples that were below the limits of detection were assigned a value that the represented the lower limit of detection for purposes of analysis.

Table 4: Primers and probes

Gene	Probe[2]/Primer
Il4	Mm00445259_m1
Il13	Mm00434204_m1
Il12a	Mm00434169_m1
Klf4	Mm00516104_m1
Il6	Mm00446190_m1
Gapdh	Mm99999915_g1
Ap 16s F	TGTAGGCGGTTCGGTAAGTTAAAG
Ap 16s R	GCACTCATCGTTTACAGCGTG
ms β-actin F	AGAGGGAAATCGTGCGTGAC
ms β-actin R	CAATAGTGATGACCTGGCCGT
pHes1 F	CCTAGGGAGAAGGAGCTGGCT
pHes1 R	TGGCCGTCAGGAGCCGGCACC

[2] Product number for Taqman probes purchased from LifeTech.

1.2.3 Results

$ADAM10^{DC-/-}$ mice have reduced high affinity IgG1 and recall responses

To determine if ADAM10 had a role in DC function, we crossed $ADAM10^{flox/flox}$ mice[84] to mice expressing Cre recombinase under the CD11c promoter (CD11c-Cre[96]); thus we generated mice in which ADAM10 is absent in $CD11c^{+}$ cells ($ADAM10^{DC-/-}$ mice). Mice that lack ADAM10 on B cells using CD19-Cre have reduced specific antibody production in all classes examined[50]. To reveal if ADAM10 played a similar role in antibody production in the $ADAM10^{DC-/-}$, $ADAM10^{DC-/-}$ and WT mice were immunized with nitrophenol conjugated to keyhole limpet hemocyanin (NP_{31}-KLH) in alum. High affinity and total affinity antibody were measured by coating with NP_4-BSA and NP_{25}-BSA, respectively. At day 21, WT and $ADAM10^{DC-/-}$ mice have similar levels of total affinity NP-specific IgG1, but $ADAM10^{DC-/-}$ have significantly less high affinity NP-specific IgG1 compared to WT (Figure 16A, B). This difference is further exacerbated 5 days after boosting with NP_{31}-KLH in alum, in which $ADAM10^{DC-/-}$ have less total and high affinity NP-specific IgG1 (Figure 16A, B). Total IgG1 levels were not significantly different at all time points (Figure 16C). Interestingly, these differences are restricted to the IgG1 antibody class, as WT and $ADAM10^{DC-/-}$ had no significant difference between total and high affinity NP-specific IgG2a (Figure 16D-F). As germinal center (GC) B and T_{FH} cells are critical in high affinity antibody responses, we utilized footpad immunization with NP_{31}-KLH in alum. In contrast to the reduced numbers of both populations observed in the $ADAM10^{B-/-}$ mice, neither were significantly changed[50]. WT and $ADAM10^{DC-/-}$ had similar levels of germinal center B cells ($B220^{+}$ $CD95^{+}$ $GL\text{-}7^{+}$) and T_{FH} cells ($CD4^{+}$ $PD\text{-}1^{hi}$ $CXCR5^{hi}$) in draining popliteal lymph nodes (popLNs) 7 (Figure 16G, H) and 14 days after immunization (Figure 16I, J). These results demonstrate that despite the generation of germinal centers and T_{FH}

cells, ADAM10$^{DC-/-}$ mice have a selective defect in the production of high affinity NP-specific IgG1 and recall responses of both total and high affinity NP-specific IgG1 antibody. While insufficient antigen-specific IgE was available even in WT mice, alum injection also causes an increase in total IgE and as seen in Figure 16K, total IgE levels were lower in the ADAM10$^{DC-/-}$ mice.

Recent findings from our lab have implicated ADAM10 as the physiological sheddase of inducible costimulatory ligand (ICOSL). ADAM17 was also found to cleave ICOSL, but to a lesser extent. These results suggest that when ADAM10 is absent and ICOSL cannot be cleaved that it causes the downregulation of ICOS on T cells, which prevents them from becoming T follicular helper (T_{FH}) cells and leads to antibody defects (submitted for publication). Though in the NP-KLH footpad model we did not see differences in T_{FH} levels, we sought to see if ICOSL or ICOS levels were altered on DCs or T cells. On all total cDCs and CD11b^{+} and CD8^{+} DCs in popLNs at days 7 and 14 after NP-KLH footpad immunization we found no significant difference in ICOSL surface expression between WT and ADAM10$^{DC-/-}$ mice (Figure 17A-C). This was also true for mice that have ADAM10 and ADAM17 deleted from CD11c^{+} cells (ADAM10/17$^{DC-/-}$). While we did not see differences in GC B cells or T_{FH} levels between ADAM10$^{DC-/-}$ and WT mice, we did observe that ADAM10/17$^{DC-/-}$ mice had fewer of both 14 days after immunization (Figure 17D-G). T_{FH} cells from each genotype displayed similar ICOS surface expression (Figure 17H, I). Interestingly, non-T_{FH} cells in general had lower ICOS expression than T_{FH} cells and, those from ADAM10/17$^{DC-/-}$ and to a lesser extent ADAM10$^{DC-/-}$ mice had less ICOS expression than WT (Figure 17H, J), suggesting that when both ADAMs are absent some altered ICOS regulation may occur. This idea is supported by data from treating WT bone marrow derived DCs (BMDCs) with an ADAM10 inhibitor and examining ICOSL

expression. Only at the two highest concentrations is an increase in ICOSL expression over baseline seen (Figure 18). At these concentrations both ADAM10 and ADAM17 are likely inhibited. The increase in ICOSL was not seen in BMDCs stimulated with LPS.

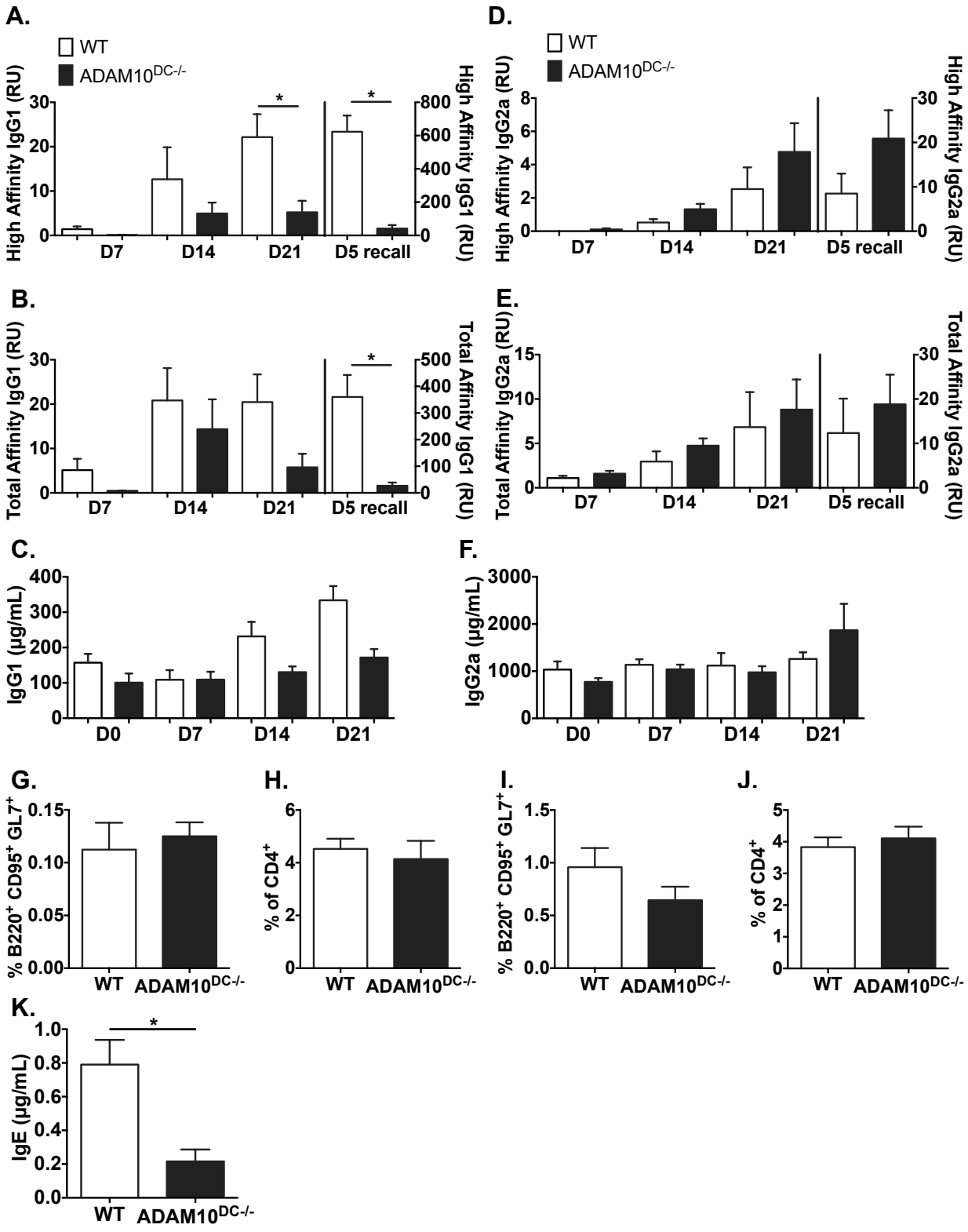

Figure 16: ADAM10$^{DC-/-}$ mice have reduced high affinity IgG1 and recall responses.

Mice were immunized with NP_{31}-KLH in alum and bled on indicated days. NP_4-BSA and NP_{25}-BSA coated ELISAs were used to measure high affinity (A) and total affinity (B) NP-specific IgG1 in the serum. Total IgG1 was measured in the serum (C). High affinity (D) and total affinity (E) NP-specific IgG2a was also measured as well was total IgG2a (F). GC B cells ($B220^+$ $CD95^+$ $GL7^+$) and T_{FH} cells ($CD4^+$ $PD\text{-}1^+$ $CXCR5^+$) were analyzed by flow cytometry in day 7 (G and H) and day 14 (I and J) draining popliteal LNs (popLN) from NP-KLH footpad injections. K. Total IgE was measured in the serum 7 days after boost NP-KLH injection. Data is combined from two independent experiments with n = 6 mice per group. Data is presented as mean ± SEM. *$p<0.05$ unpaired Student's t test.

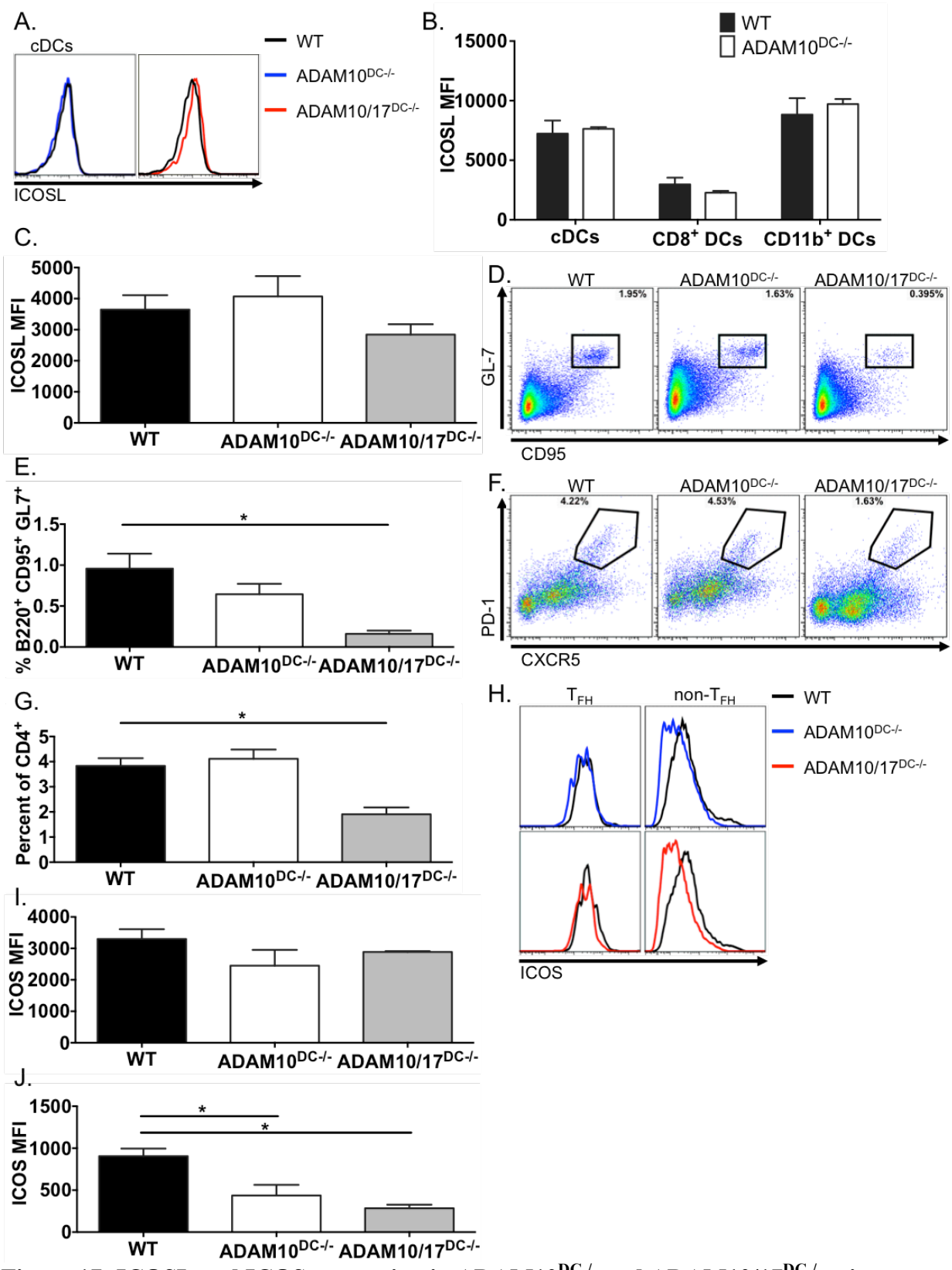

Figure 17: ICOSL and ICOS expression in ADAM10$^{DC-/-}$ and ADAM10/17$^{DC-/-}$ mice.

A. Representative histograms of ICOSL expression on cDCs from WT, ADAM10$^{DC-/-}$, and ADAM10/17$^{DC-/-}$ mice on day 14 after NP-KLH footpad immunization. B. and C. ICOSL surface expression (mean fluorescence intensity, MFI) on DC subsets in the popLN on day 7 (B) and cDCs on day 14 (C) after NP-KLH footpad immunization. D. Representative dot plots for GC B cells gated on B220^{+} cells and summary data for GC B cells in the popLN day 14 after immunization (E). F. and G. Representative dot plot and summary data for T_{FH} cells (% of CD4^{+}) (as in Figure 16) in popLN from WT, ADAM10$^{DC-/-}$, and ADAM10/17$^{DC-/-}$ mice day 14 after NP-KLH footpad immunization. H. Representative histogram of ICOS expression on T_{FH} and non-T_{FH} populations (G) at day 14 after immunization. I. and J. ICOS MFI on T_{FH} and non-T_{FH} from popLN in (G). *$p<0.05$, one –way ANOVA with Tukey's post hoc test.

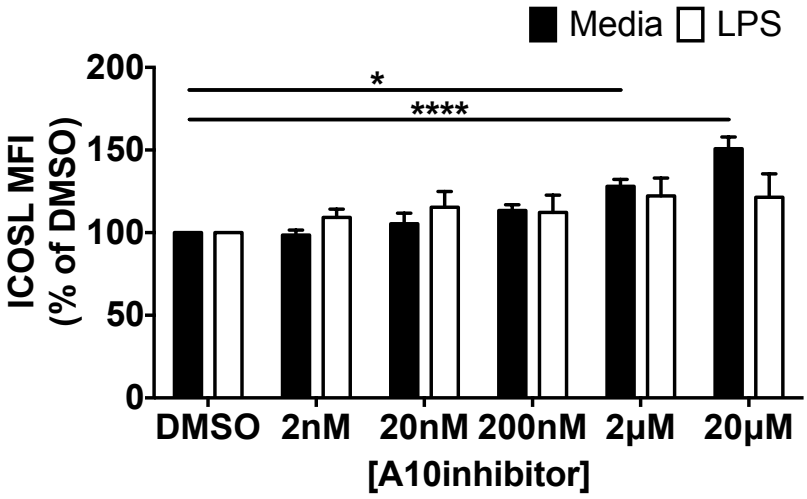

Figure 18: ADAM10 inhibitor treated BMDCs have increased expression of ICOSL.

WT BMDCs were cultured with indicated doses of ADAM10 inhibitor ± LPS for 48h. ICOSL MFI was assessed by flow cytometry. n = 3 mice, *$p<0.05$, ****$p<0.001$, two-way ANOVA with Dunnett's multiple comparison test.

ADAM10$^{DC-/-}$ mice have reduced T_H2 immune response to house dust mite (HDM) extract

The effects on IgG1 and total IgE suggest that ADAM10$^{DC-/-}$ mice have a more restricted defect in humoral immunity than when ADAM10 is deleted from B cells[50]. To examine the effects of ADAM10 deletion from DCs on the course of a T_H2-type immune responses, we administrated HDM i.n. in a 14 day model[88]. We measured airway resistance upon challenge with increasing doses of methacholine, which stimulates M_3 muscarinic acetylcholine receptors on airway smooth muscle cells leading to contraction. We found that compared to WT mice, ADAM10$^{DC-/-}$ mice had significantly less airway hyperresponsiveness with maximum resistance not significantly different than saline controls (Figure 19A). Further, ADAM10$^{DC-/-}$ had fewer eosinophils in the bronchoalveolar lavage fluid (BALF) (Figure 19B) and less *Il4* and *Il13* mRNA expression in the lung tissue compared to WT (Figure 19C, D). By H&E staining, ADAM10$^{DC-/-}$ lungs had dramatically less inflammatory infiltrate than WT (Figure 19E). Serum HDM-specific IgG1 (Figure 19F) and total IgG1 (Figure 19G) were reduced in ADAM10$^{DC-/-}$ mice and most strikingly, serum total IgE was almost completely absent (Figure 19H). These results indicate that ADAM10$^{DC-/-}$ mice have a diminished T_H2 response to HDM, particularly with respect to IgE production.

We also examined the function of innate cells to recruit eosinophils. Deficiency in this function could explain lack of response to HDM. We administered recombinant IL-33 (rIL-33) i.n. daily for three days and then assessed eosinophil recruitment into the BALF. IL-33 acts on cells containing the IL-33R (ST2), which includes innate lymphoid cells type 2 (ILC2s). In response to IL-33, ILC2s release IL-5 leading to eosinophil recruitment. We found equivalent eosinophil levels in the BALF between WT and ADAM10$^{DC-/-}$ mice upon rIL-33 administration

(Figure 20A). Further we found similar percentage and number of ILC2s in the lungs of WT and ADAM10$^{DC-/-}$ mice (Figure 20B, C).

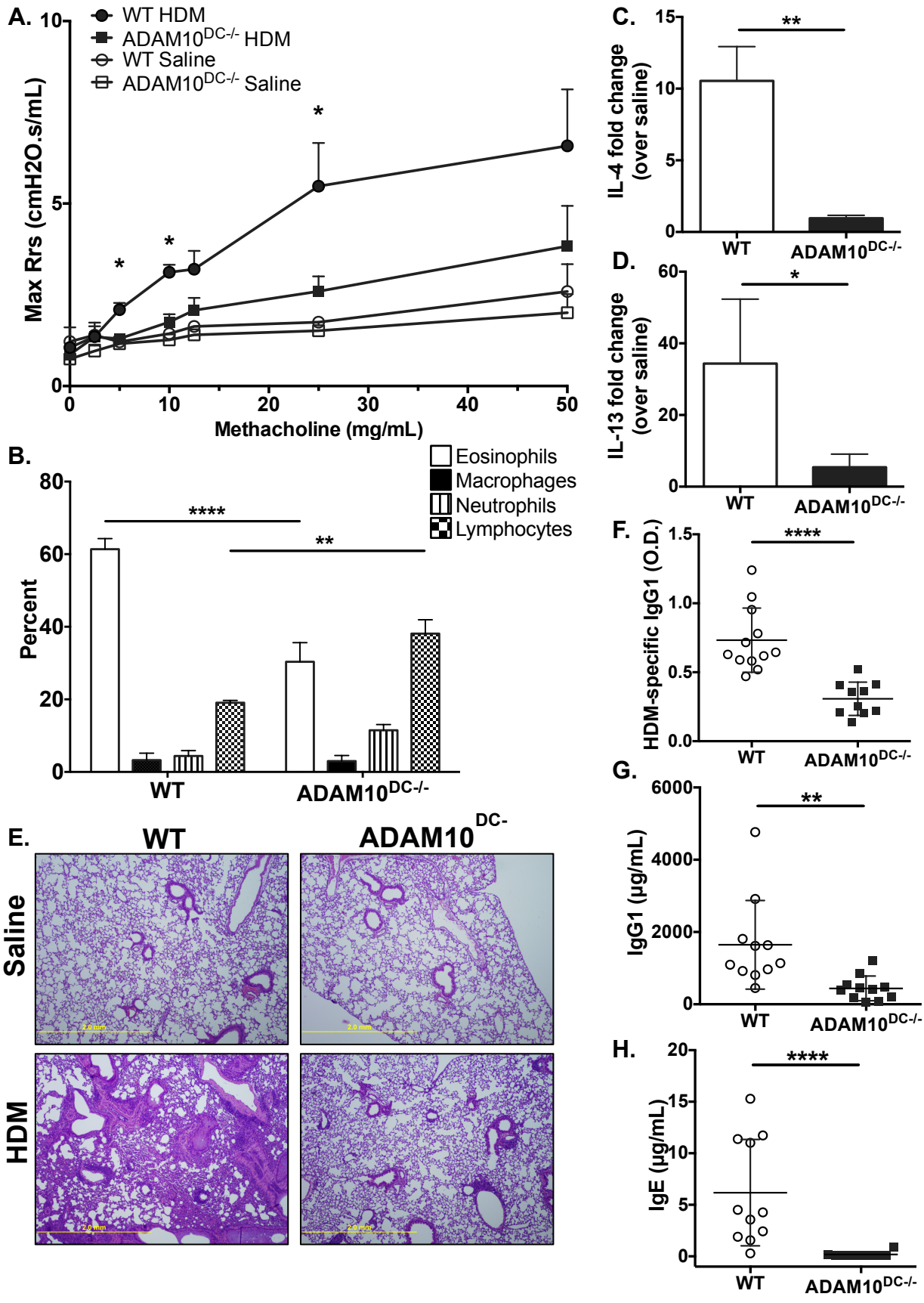
A.
WT HDM
ADAM10DC-/- HDM
WT Saline
ADAM10DC-/- Saline
Max Rrs (cmH2O.s/mL)
Methacholine (mg/mL)
B.
Eosinophils
Macrophages
Neutrophils
Lymphocytes
Percent
WT
ADAM10DC-/-
C.
IL-4 fold change (over saline)
D.
IL-13 fold change (over saline)
E.
WT
ADAM10DC-
Saline
HDM
F.
HDM-specific IgG1 (O.D.)
G.
IgG1 (µg/mL)
H.
IgE (µg/mL)

Figure 19: **ADAM10$^{DC-/-}$ mice have diminished T_H2 responses to HDM.**

ADAM10$^{DC-/-}$ and WT mice were subjected to HDM or saline sensitization and challenge. A. Airway hyperresponsivness was assessed by nebulizing increasing doses of methacholine and measuring resistance. B. Bronchoalveolar lavage fluid (BALF) was harvested and analyzed by flow cytometry. C. and D. *Il4* and *Il13* mRNA expression was measured in lung tissue relative to *Gapdh*. E. Formalin fixed lung sections were stained with H&E. F. – H. HDM-specific IgG1, total IgG1, and total IgE were measured in serum by ELISA. Symbols represent individual mice. Data is combined from three independent experiments with n = 10 per HDM group and n = 3 per saline group. Data is presented as mean ± SEM. ****p<0.0001, ***p<0.001, **p<0.01, *p<0.05, ANOVA with Tukey's post hoc test (A, B), unpaired Student's t test (C, D, F, G), and Mann-Whitney test (H).

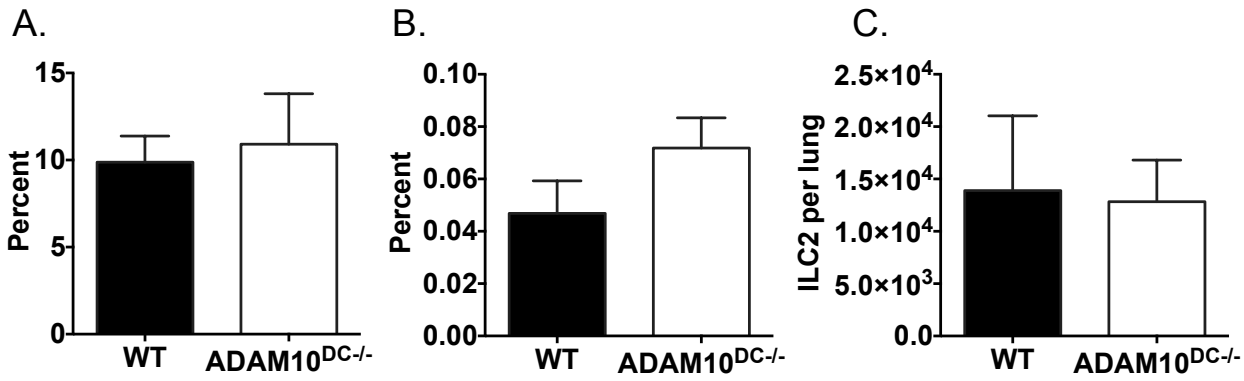

Figure 20: Innate T_H2 responses in ADAM10$^{DC-/-}$ are intact.

WT and ADAM10$^{DC-/-}$ mice were administered i.n. 0.1μg recombinant IL-33 daily for three days and euthanized 24h after the last dose. A. Eosinophils in the BALF were assessed by flow cytometry. B. and C. Percentage (B) and cell number (C) of ILC2s (Lin$^-$ CD90.2$^+$ ST2$^+$) were assessed in the lung by flow cytometry. Data is from one experiment with n = 3 mice per group.

ADAM10$^{DC-/-}$ mice are resistant to active systemic anaphylaxis

House dust mite sensitivity is a significant health issue in human asthma, as well as an established T_H2 model in mice, the degree to which it is IgE dependent is somewhat controversial. In order to examine a model that is highly IgE dependent, we turned to a model of active systemic anaphylaxis (ASA) which is exquisitely sensitive for the presence of antigen specific IgE. First, we immunized WT and ADAM10$^{DC-/-}$ mice with ovalbumin (OVA) and after three weeks measured total and OVA-specific IgG1 and IgE in the serum. On day 25 after immunization, the mice were injected *i.p.* with OVA and core body temperature was measured. As expected, WT mice displayed severe temperature drop after challenge indicating anaphylaxis. Remarkably, ADAM10$^{DC-/-}$ mice were completely resistant to anaphylaxis, exhibiting little temperature change after OVA challenge (Figure 21A). Total and OVA-specific IgG1 levels were similar between WT and ADAM10$^{DC-/-}$ (Figure 21B, C). However, ADAM10$^{DC-/-}$ mice had significantly less total IgE and almost absent OVA-specific IgE in the serum (Figure 21D, E) consistent with the lack of anaphylaxis. To demonstrate that mast cells were functioning properly in the ADAM10$^{DC-/-}$ mice, they were subjected to passive systemic anaphylaxis, in which antigen specific IgE (IgE anti-DNP) is *i.p.* injected into mice, and 24h later, the mice are challenged with the antigen (DNP-BSA). WT and ADAM10$^{DC-/-}$ mice displayed a similar degree of temperature drop after challenge indicating no defect in mast cell function (Figure 21F).

To confirm that the phenomenon exhibited by ADAM10$^{DC-/-}$ mice in the ASA model was distinct to the low antibody levels found in the ADAM10$^{B-/-}$ mice[50], we subjected ADAM10$^{B-/-}$ and ADAM10$^{B\ DC-/-}$ mice to the ASA protocol. Surprisingly, we found that ADAM10$^{B-/-}$ mice had severe temperature drop after challenge, similar to WT (Figure 22A). Mice that lacked ADAM10 from both B cells and DCs (ADAM10$^{B\ DC-/-}$) behaved like ADAM10$^{DC-/-}$ mice and

were resistant to anaphylaxis (Figure 22A). Interestingly, ADAM10$^{B-/-}$ had low levels of all immunoglobulin examined, but still anaphylaxis whereas the ADAM10$^{B\ DC-/-}$ also had low antibody levels, but did not undergo anaphylaxis like the ADAM10$^{DC-/-}$ mice (Figure 22B-D, Figure 21). ADAM10$^{B-/-}$ mice have been previously published to have increased levels of TNF[83], which may make them more susceptible to anaphylaxis.

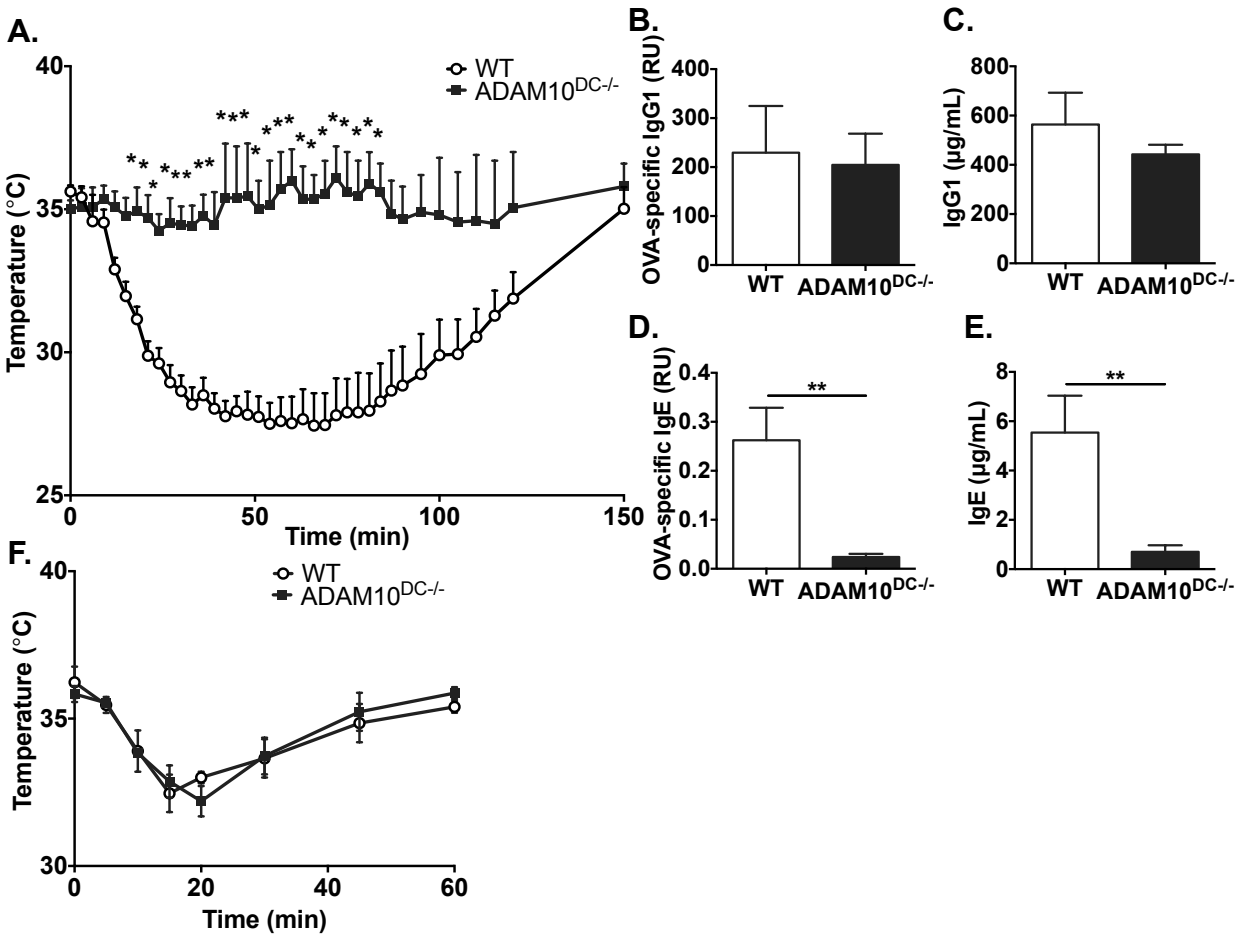

Figure 21: ADAM10$^{DC-/-}$ mice are resistant to active systemic anaphylaxis.

WT and ADAM10$^{DC-/-}$ mice were immunized for the ASA protocol and then challenged with OVA on day 25 after immunization. A. After challenge, core body temperature was measured. B. – E. Mice were bled on day 21 after immunization. OVA-specific and total IgG1 and IgE were measured in the serum by ELISA. F. Mice were subjected to passive systemic anaphylaxis. IgE anti-DNP was injected *i.p.* into mice and then 24h later mice were challenged *i.p.* with DNP-BSA and core body temperature was measured. Data is from three independent experiments with n = 11 mice per group. Data is presented as mean ± SEM. **p<0.01, *p<0.05, unpaired Student's t test.

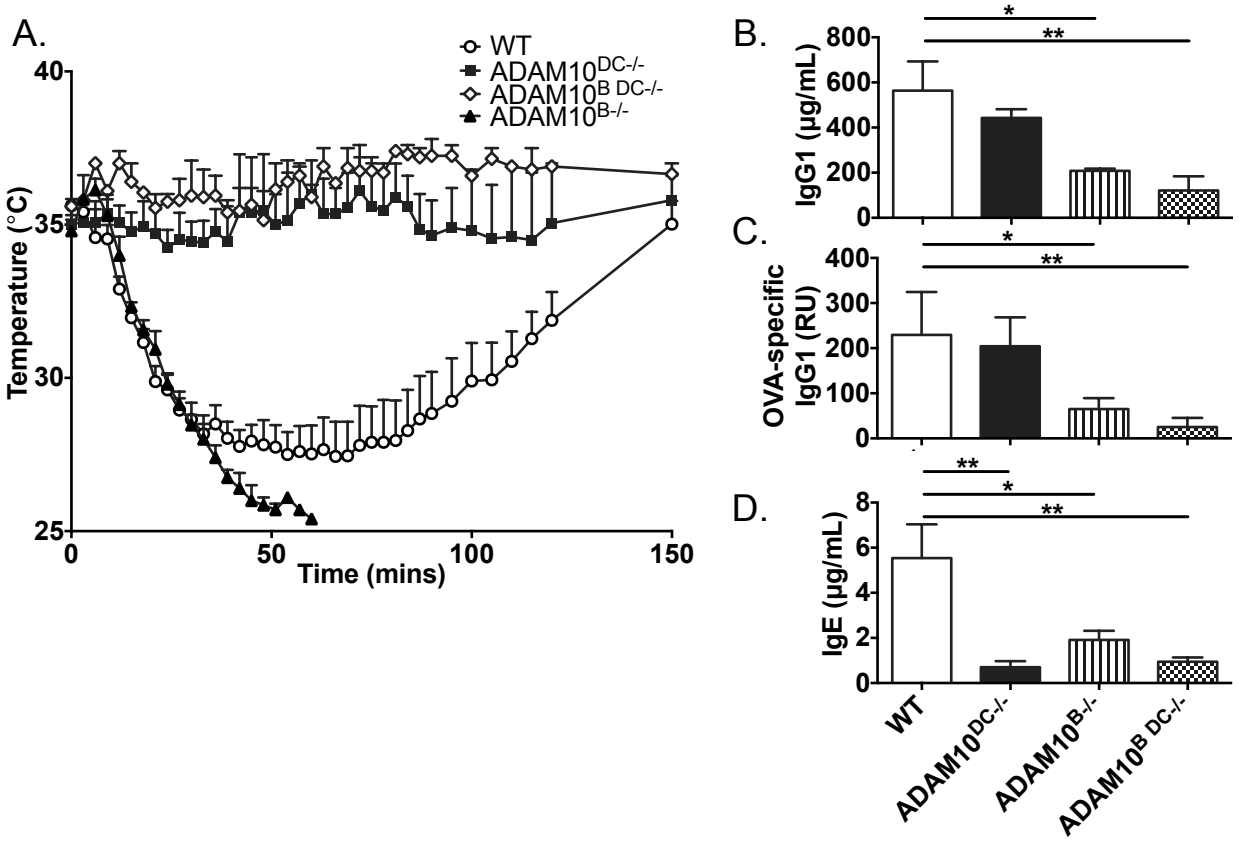

Figure 22: Anaphylaxis in ADAM10$^{B-/-}$ and ADAM10$^{B\ DC-/-}$ mice.

A. ADAM10$^{B-/-}$ and ADAM10$^{B\ DC-/-}$ mice were subjected to the ASA protocol as previously described. Historical controls of WT and ADAM10$^{DC-/-}$ included for reference. B. – D. Total and OVA-specific IgG1 and total IgE were measured by ELISA in the serum. n = 6 mice per group, two independent repeats. *$p<0.05$, **$p<0.01$, one-way ANOVA with Tukey's post hoc test.

ADAM10$^{DC-/-}$ mice have intact T_H17 response to a fungal aeroallergen and T_H1 response to intracellular bacteria

We tested responses to a fungal aeroallergen, *Alternaria alternata*, which stimulates both T_H2 and T_H17 immune responses[92,97]. After intranasal sensitization and challenge with *A. alternata*, we found that ADAM10$^{DC-/-}$ mice had reduced eosinophils in the BALF compared to WT, consistent with the HDM model (Figure 23A). Interestingly, ADAM10$^{DC-/-}$ mice had equivalent levels of neutrophils in the BALF to WT (Figure 23B). Further when we re-stimulated T cells from the mediastinal lymph nodes (medLN) with plate bound anti-CD3ε and analyzed intracellular cytokine production, ADAM10$^{DC-/-}$ mice had fewer CD4$^+$ IL-13$^+$ cells, but similar levels of CD4$^+$ IFNγ$^+$ and CD4$^+$ IL-17$^+$ cells to WT (Figure 23C). As with the HDM model, we found reduced amount of IgG1 and IgE in the serum of ADAM10$^{DC-/-}$ mice, but we did not see any reduction in IgG2b (Figure 23D-F). These data reinforce the selective defect in T_H2 immunity present in ADAM10$^{DC-/-}$ mice. Thus, in two animal models that utilize T_H2 and IgE responses, ADAM10$^{DC-/-}$ mice exhibit minimal if any response in contrast to WT controls. In the *A. alternata* model, T_H2 dependent responses were again reduced, but T_H1 and T_H17 cytokine and antibody responses were similar to WT controls.

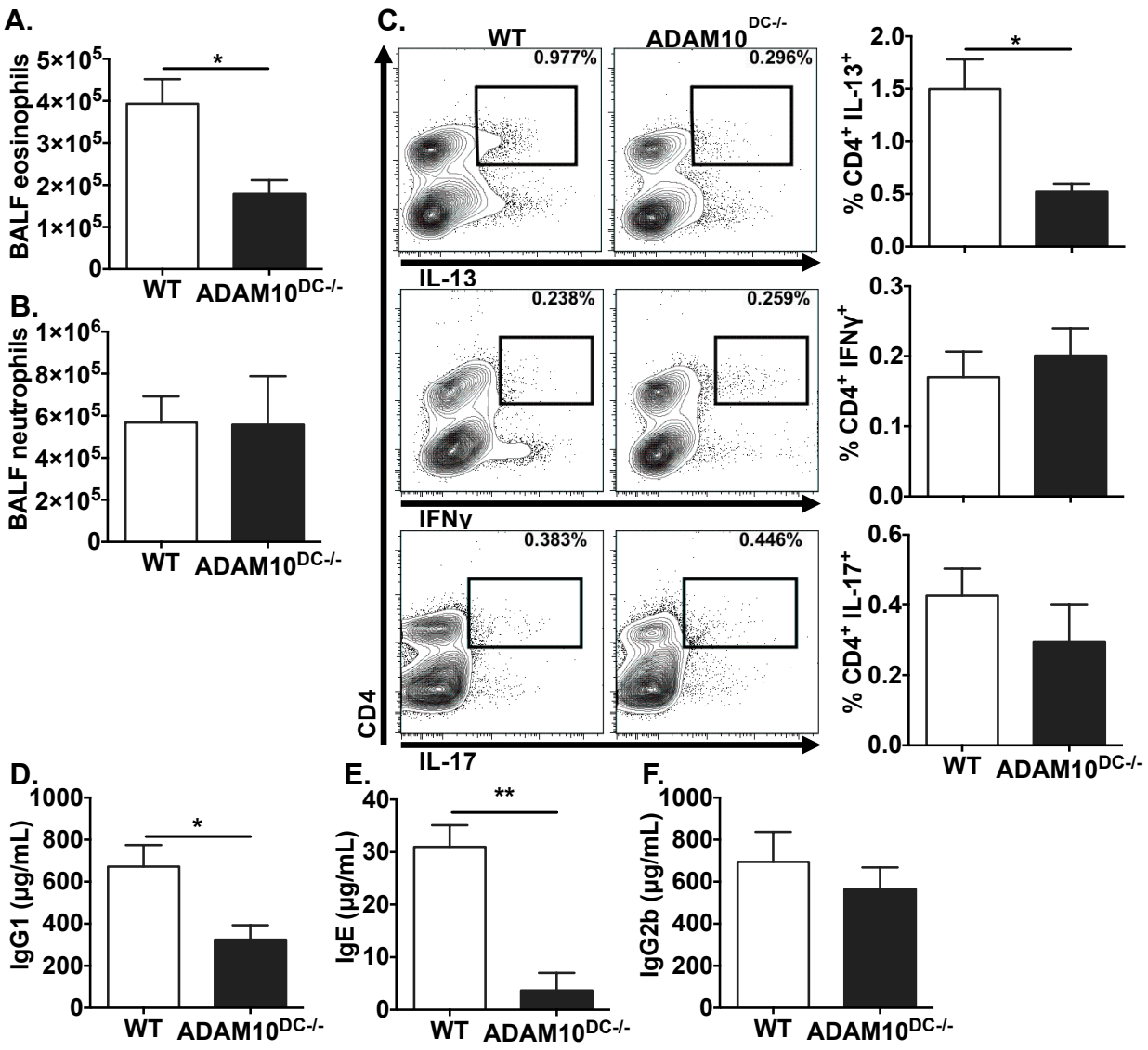

Figure 23: ADAM10$^{DC-/-}$ mice have impaired T_H2, but intact T_H17 responses.

WT and ADAM10$^{DC-/-}$ mice were sensitized and challenged with intranasal administration of *A. alternata* extract. A. and B. BALF eosinophils and neutrophils were analyzed by flow cytometry. C. Total medLN cells were stimulated with plate bound anti-CD3ε for 4h with monensin. Intracellular cytokine expression in $CD4^+$ T cells was assessed by flow cytometry. Representative contour plots and combined results are shown. D. – F. Total IgG1, IgE, and IgG2b were measured in the serum by ELISA. Data shown is from two independent experiments

with n = 5 mice per group. Data is presented as mean ± SEM. **p<0.01, *p<0.05, unpaired Student's t test.

Given the dramatic defect in T_H2 responses and IgE production in the ADAM10$^{DC-/-}$ mice, but not other antibody classes, we wanted to further examine the development of T_H1 and T_H17 immune responses. For T_H1 immunity, we infected ADAM10$^{DC-/-}$ and WT mice with the obligate intracellular bacterium *Anaplasma phagocytophilum,* as CD4$^+$ T cells and IFNγ drive the elimination of this pathogen[98,99]. *A. phagocytophilum* burden was measured by qPCR for *A. phagocytophilum* 16s DNA relative to mouse β-actin in the blood of WT and ADAM10$^{DC-/-}$ mice at indicated days after infection. At all time points, WT and ADAM10$^{DC-/-}$ had equivalent levels of *A. phagocytophilum* and both groups had cleared the infection by day 28 (Figure 24A). We then utilized an infection model with the extracellular bacterium *Citrobacter rodentium* that elicits innate lymphocyte type 3 and T_H17 responses, which are critical for clearance of the bacteria[100]. ADAM10$^{DC-/-}$ mice exhibited a larger drop in body weight over the course of infection compared to WT (Figure 24B). ADAM10$^{DC-/-}$ mice were also more likely to succumb to infection with *C. rodentium* than WT (Figure 24C). Adaptive responses to *C. rodentium* lead to the production of IgG2b antibodies. We found a trend toward less total IgG2b in the ADAM10$^{DC-/-}$ mice and similar levels of CR-specific IgG2b (Figure 24D, E). While the overall infection level of the bacterium in the colon was not different as measured by colony-forming units (CFUs) (Figure 24F), ADAM10$^{DC-/-}$ mice had significantly more disseminated infection as determined by CFUs in the spleen (Figure 24G). These data indicate that ADAM10$^{DC-/-}$ mice had more substantial breakdown of barrier function in the colon allowing the bacteria to spread systemically.

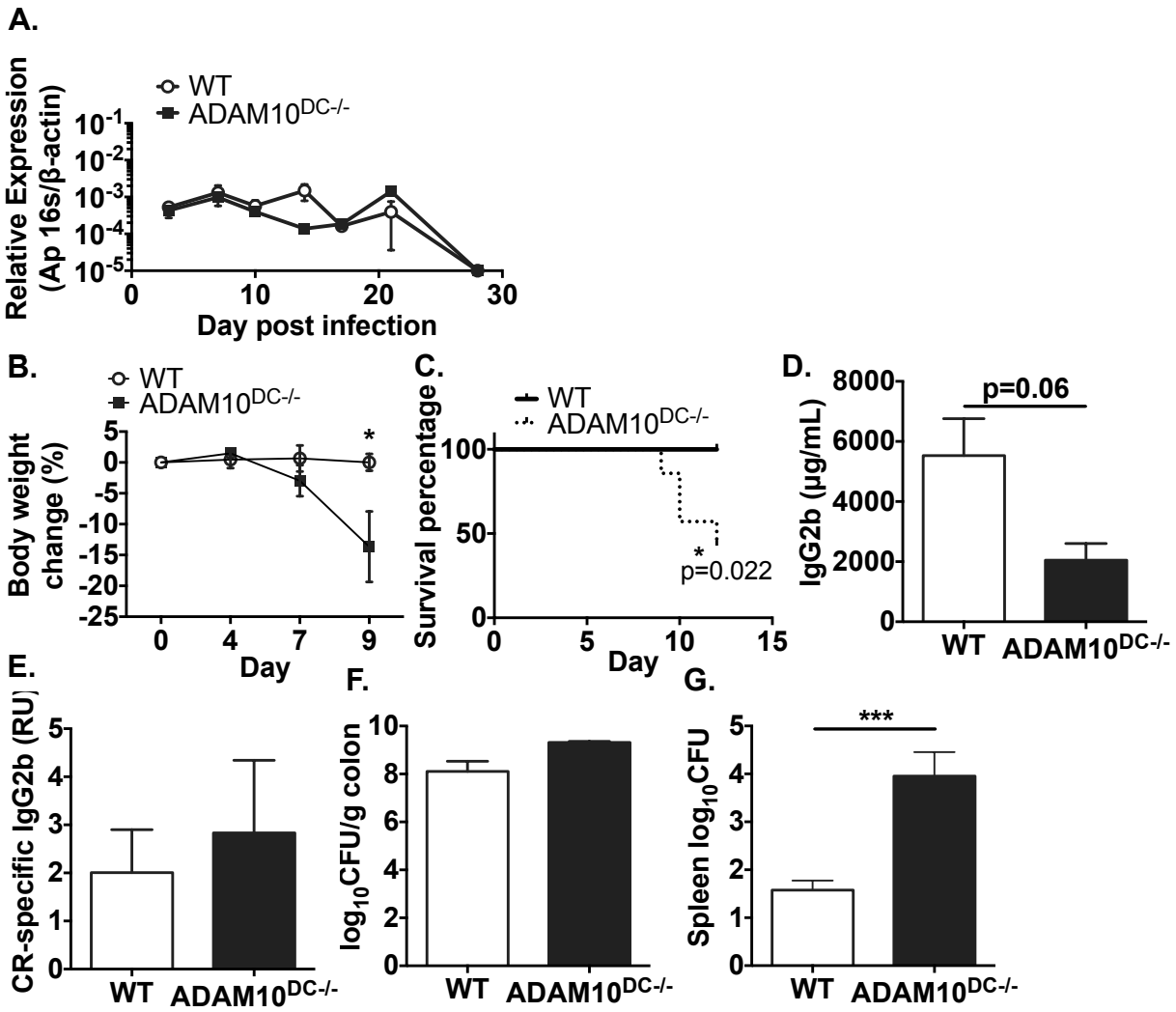

Figure 24: Immune responses to *A. phagocytophilum* and *C. rodentium* infections.

A. ADAM10$^{DC-/-}$ and WT were inoculated *i.p.* with 10^7 *A. phagocytophilum* bacteria. Mice were bled on days 3, 7, 10, 14, 17, 21, and 28. DNA was isolated and qPCR run with primers for *A. phagocytophilum* 16s DNA and mouse β-actin. Data is from two independent experiments with n = 6 mice per group. B. WT and ADAM10$^{DC-/-}$ mice were infected by oral gavage with 10^{10} CFU of *C. rodentium* suspension. Body weight was measured over the course of infection and reported as change from initial body weight. C. Kaplan-Meier survival analysis. D. and E. Total and CR-specific IgG2b was measured in the serum by ELISA. F. and G. Colon and spleen were

homogenized and bacterial load were determined. Data is from two independent experiments with n = 7 mice per group. ***$p<0.001$, *$p<0.05$, unpaired Student's t test.

Unimmunized ADAM10$^{DC-/-}$ and WT mice

When examining ADAM10$^{DC-/-}$ mice in the unimmunized state, we found that they had less IgM present in serum, but similar levels of IgG1 and IgG2b (Figure 25A-C). The latter two findings would suggest that the antibody differences seen in the other immunizations are not due to basal differences in these immunoglobulins. We also found that the ADAM10$^{DC-/-}$ mice were lacking marginal zone B cells (B220^{+} CD23$^{lo/-}$ CD21/35^{hi} IgM^{hi}) (Figure 25D, F), which could explain low baseline IgM levels. Marginal zone macrophages were also surrounding B cell areas as expected (Figure 25E).

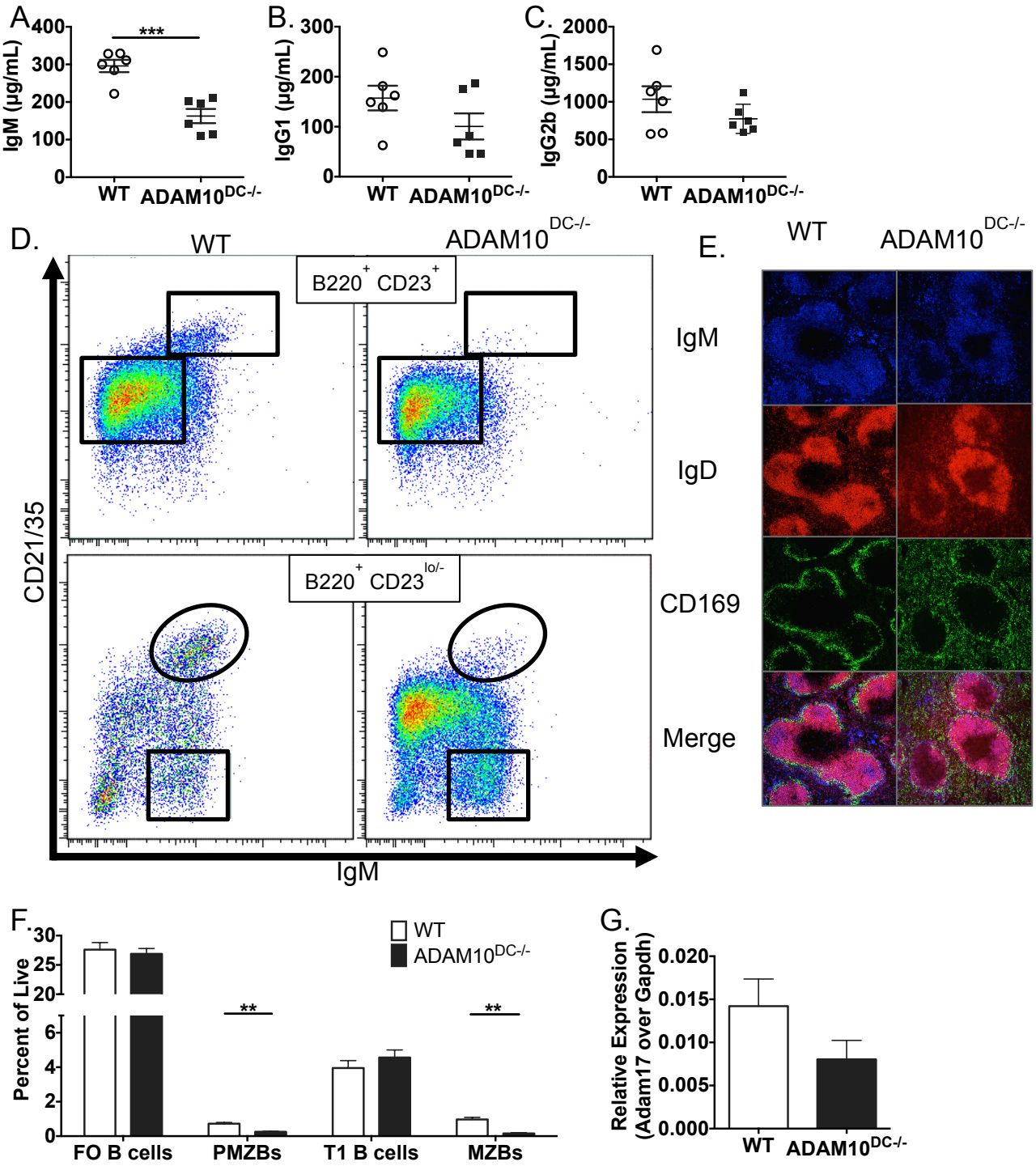

Figure 25: Unimmunized WT and ADAM10$^{DC-/-}$.

A. – C. IgM, IgG1, and IgG2b levels were measured by ELISA in unimmunized WT and ADAM10$^{DC-/-}$. D. Representative flow diagram with the gating strategy for B cell subsets in the spleen. E. Immunofluorescence images of frozen spleen sections using antibodies against IgM

(blue), IgD (red), and CD169 (green). F. Percentage of follicular B cells (FO B cells, $B220^{+}$ $CD23^{+}$ $CD21/35^{int}$ IgM^{int}), pre-marginal zone B cells (PMZBs, $B220^{+}$ $CD23^{+}$ $CD21/35^{hi}$ IgM^{hi}), marginal zone B cells (MZBs, $B220^{+}$ $CD23^{lo/-}$ $CD21/35^{hi}$ IgM^{hi}), and transition 1 B cells (T1 B cells, $B220^{+}$ $CD23^{lo/-}$ $CD21/35^{lo}$ IgM^{hi}) in the spleen. G. *Adam17* mRNA expression relative to *Gapdh* in BMDCs from WT and $ADAM10^{DC-/-}$ mice. **p<0.01, ***p<0.001. Unpaired Student's t test (A – C, F), ANOVA with Tukey's post hoc test (E).

Role of Notch1 and Notch2 in the immune defects of ADAM10$^{DC-/-}$ mice

The most well known ADAM10 substrates are Notch receptors[78]. Notch receptors have been studied on DCs, and mice that lack Notch2 on DCs have deficient innate immunity during infection with *C. rodentium*, which results in a similar phenotype to the ADAM10$^{DC-/-}$ mice[101]. ADAM10$^{DC-/-}$ mice have defects in DC populations similar to the Notch2$^{DC-/-}$ mice including fewer splenic cDCs and CD172^{+}ESAM^{+} DCs as well as CD103^{+} CD11b^{+} DCs in MLNs[96,102] (Figure 26A-C). However, ADAM10$^{DC-/-}$ did not have differences in number or percentage of CD24^{+} DCs in the spleen as Notch2$^{DC-/-}$ mice or in cDCs subsets in other lymph nodes (Figure 26C, D). Thus alterations in DC subsets in the ADAM10$^{DC-/-}$ mice were similar, but not identical to mice in which DCs lack Notch2.

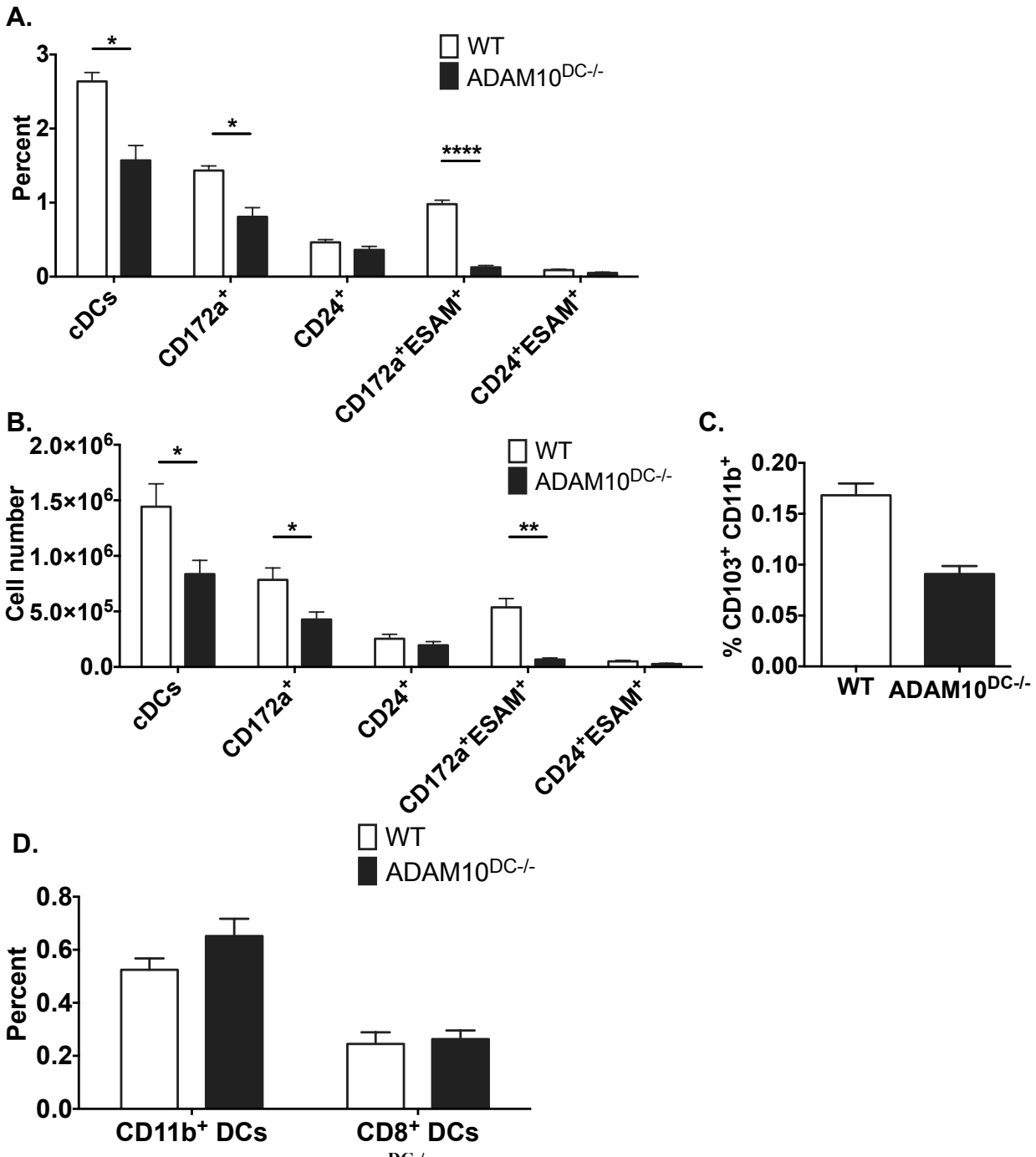

Figure 26: DC subsets in ADAM10$^{DC-/-}$ mice.

Percent (A) and number (B) of DC subsets in spleens from naïve ADAM10$^{DC-/-}$ and WT mice were analyzed by flow cytometry. C. CD103^{+} CD11b^{+} DCs in mesenteric lymph nodes were assessed by flow cytometry. D. CD11b^{+} and CD8^{+} DCs were assessed in mediastinal lymph nodes by flow cytometry.

To determine if the anaphylaxis phenomenon in the ADAM10$^{DC-/-}$ is due to lack of Notch signaling, we subjected Notch2$^{DC-/-}$ mice to the ASA protocol as in Figure 21. Notch2$^{DC-/-}$ produced a similar level of temperature drop as the WT controls (Figure 28A). Serum total and OVA-specific IgG1 and IgE were also not significantly different than WT control (Figure 28B-E). We then subjected Notch1$^{DC-/-}$ mice to the ASA protocol. A total of nine mice were utilized in the experiment – six of nine had essentially no anaphylaxis while three had similar temperature drops as the controls (Figure 28A, B). The combined data is shown in Figure 28F. Due to the aforementioned variability, there is not a significant difference in temperature drop with the Notch1$^{DC-/-}$ mice compared to WT. Notch1$^{DC-/-}$ had less OVA-specific IgE levels compared to WT but had no significant differences in total IgE, total IgG1, and OVA-specific IgG1 (Figure 28G-J). To confirm involvement of Notch signaling in the lack of anaphylaxis in the ADAM10$^{DC-/-}$ mice, we crossed the ADAM10$^{DC-/-}$ mice to the ROSA^{N1-ICD} mice, which have a lox-stop-lox before the Notch1-ICD (N1-ICD) inserted into the ROSA locus. With Cre recombinase expression driven by the CD11c promoter, the stop codon is removed allowing for expression of the N1-ICD in CD11c^{+} cells. Thus, we have mice that have DCs deficient in ADAM10 with expression of N1-ICD, bypassing the need for ADAM10 to cleave the Notch receptor (ADAM10$^{DC-/- N1-ICD+}$)[103]. We proceeded with the ASA and observed that after challenge with OVA the ADAM10$^{DC-/- N1-ICD+}$ mice had anaphylaxis similar to WT mice, indicating that expression of the N1-ICD restores anaphylaxis in ADAM10$^{DC-/-}$ mice (Figure 27K). Thus, overall the data demonstrate the importance of Notch signaling in the anaphylaxis response as well as in production of total and OVA-specific IgE as these were at WT levels in ADAM10$^{DC-/-N1-ICD+}$ mice (Figure 27L-O). Particularly antigen specific IgE is lower in the Notch1$^{DC-/-}$ mice,

suggesting that for the IgE response Notch1 has more importance than Notch2. High levels of N1-ICD clearly restore the anaphylactic response.

We also sought to determine if expression of N1-ICD would also restore the response to HDM immunization in ADAM10$^{DC-/-}$ mice. As in Figure 19, we administered HDM extract to WT, ADAM10$^{DC-/-}$, and ADAM10$^{DC-/- \ N1-ICD+}$ mice and then measured airway resistance in response to increasing doses of nebulized methacholine with the Flexivent apparatus. ADAM10$^{DC-/- \ N1-ICD+}$ and WT resistances appear similar and greater than ADAM10$^{DC-/-}$ mice (Figure 29A). We also see restoration of serum IgE levels in ADAM10$^{DC-/- \ N1-ICD+}$ back to WT levels (Figure 29B) Indicating that in the HDM airway inflammation model, overexpression of the N1-ICD can restore the T_H2 immune response in ADAM10$^{DC-/-}$ mice.

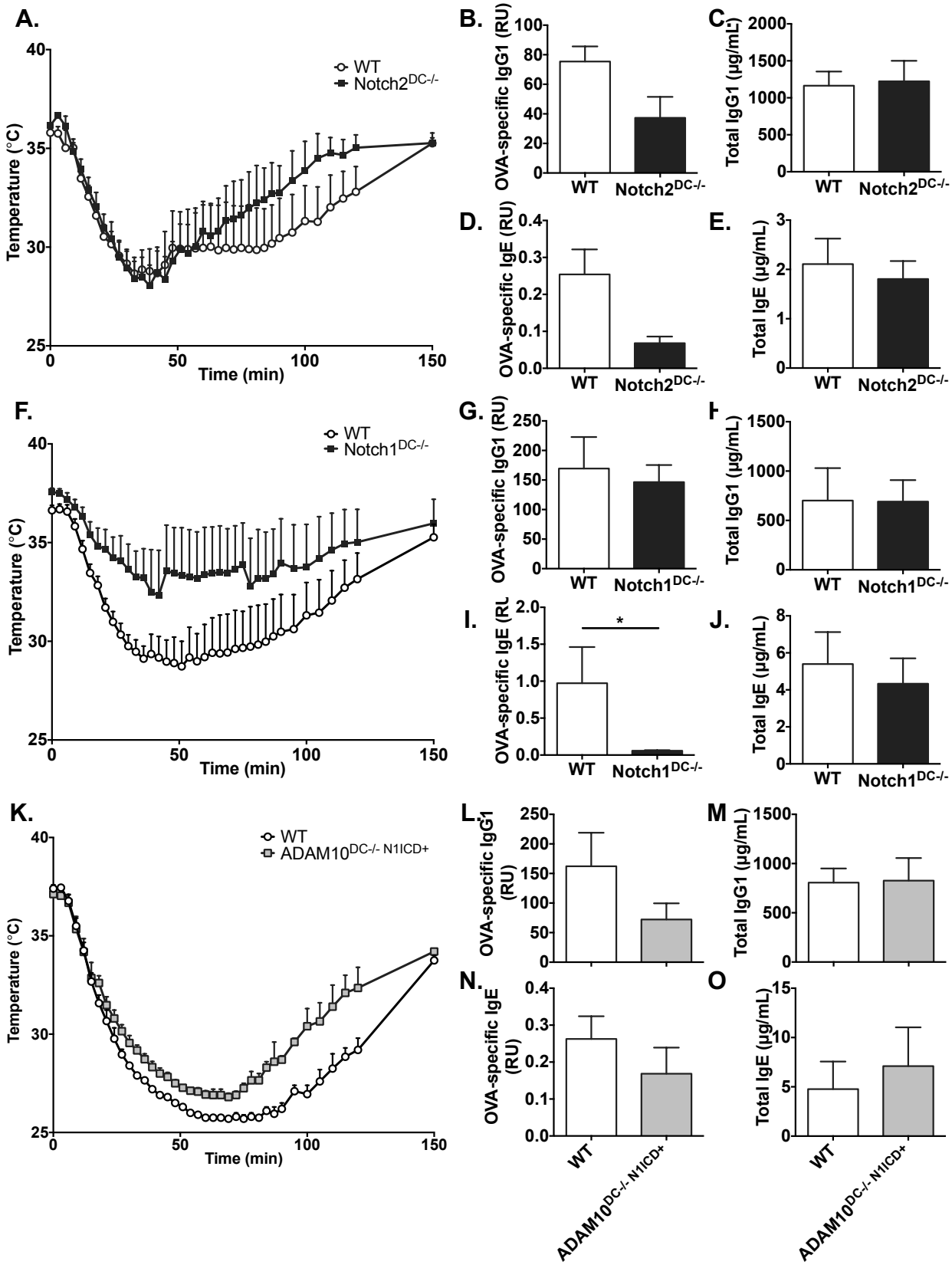

Figure 27: Notch signaling is critical for anaphylaxis responses.

Notch2$^{DC-/-}$ (A), Notch1$^{DC-/-}$ (F), and ADAM10$^{DC-/-\ N1\text{-}ICD+}$ (K) mice were subjected to the active systemic anaphylaxis protocol and core body temperature was measured after challenged with OVA. OVA-specific and total IgG1 and IgE were measured in the serum of Notch2$^{DC-/-}$ (B–E), Notch1$^{DC-/-}$ (G–J), and ADAM10$^{DC-/-\ N1\text{-}ICD+}$ (L–O) mice on day 21 after immunization. Data are from two independent experiments with n = 6-9 mice per group. Data is presented as mean ± SEM. *$p<0.05$, unpaired Student's t test.

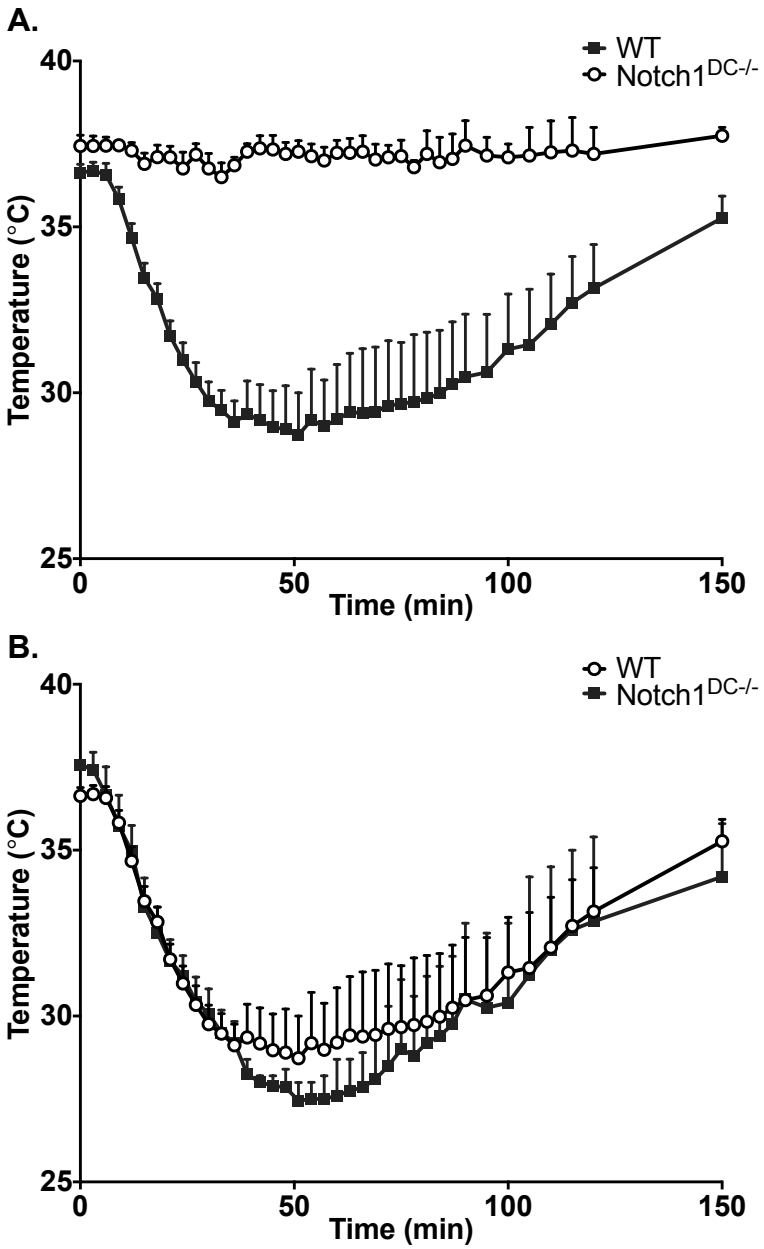

Figure 28: Notch1$^{DC-/-}$ active systemic anaphylaxis.

Active systemic anaphylaxis (ASA) in Notch1$^{DC-/-}$ and WT mice. A. 6 of 9 Notch1$^{DC-/-}$ were resistant to ASA. B. 3 of 9 Notch1$^{DC-/-}$ mice exhibited temperature drop after challenge similar to WT.

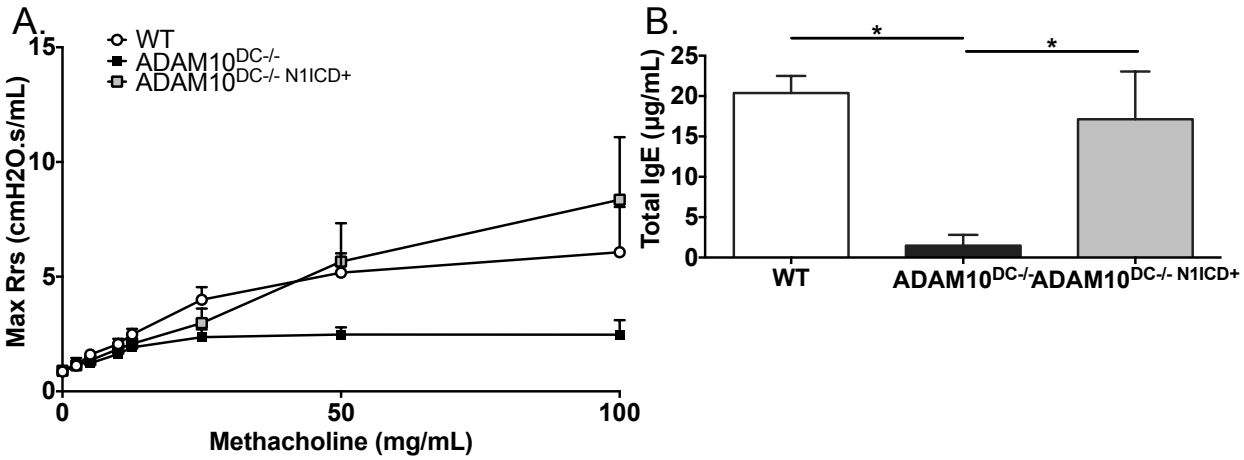

Figure 29: ADAM10$^{DC-/- N1-ICD+}$ mice have restored HDM induced IgE in serum.

WT, ADAM10$^{DC-/-}$, and ADAM10$^{DC-/- N1-ICD+}$ mice were subjected to HDM protocol as in Figure 19. A. Max airway resistance (Rrs) was assessed with increasing doses of methacholine with the Flexivent Apparatus. B. Serum IgE was measured by ELISA. Data represents two independent experiments with n = 6 mice per group. *$p<0.05$ one-way ANOVA with Tukey's post hoc test.

ADAM10-deficient DCs exhibited similar antigen uptake and presentation capacities as WT, but less stimulation of T_H2 cytokine expression in T cells

To understand how ADAM10 deficient DCs were mediating differences in T helper responses, we examined DC functions including antigen uptake, antigen presentation, and stimulation of T cell cytokine production. We first studied the ability of lung DCs to take up antigen and migrate to the medLN. We administered 25μg OVA conjugated to AlexaFluor647 (OVA-AF647) and 10μg HDM extract i.n. and 24h later analyzed DCs in the medLN and lungs for OVA-AF647 by flow cytometry and by immunofluorescence (IF) on frozen medLN sections. In WT and ADAM10$^{DC-/-}$ medLNs and lungs, cDC1s and cDC2s were responsible for the majority of the OVA-AF647 positive staining as determined by flow cytometry (Figure 31A). The percentage of OVA-AF647 positive cDC2s in the medLN and lungs was similar between WT and ADAM10$^{DC-/-}$ mice (Figure 31A). OVA-AF647 levels were also similar between WT and ADAM10$^{DC-/-}$ cDC1s in the medLN (Figure 31A). The OVA-AF647 (blue) co-localized with CD11c (red) immunostaining by IF and was not present in the B cell zone of medLNs from WT and ADAM10$^{DC-/-}$ mice (Figure 31B). We also found that adoptively transferred CFSE-labeled CD4$^+$ OVA TCR transgenic OT-II T cells (green) were present in the T cell zone (Figure 31B). Thus, antigen is being trafficked successfully to the lymph node and is present in the correct area for stimulation of CD4$^+$ T cells in ADAM10$^{DC-/-}$ mice.

We then examined the ability of ADAM10 deficient and WT DCs to present antigen to T cells and stimulate T helper cytokines, *in vitro* and *in vivo*. We first sorted CD172$^+$ and CD24$^+$ DCs from the spleens of naïve WT and ADAM10$^{DC-/-}$ mice and then incubated them with increasing doses of OVA protein for 2 hours. We co-cultured antigen loaded DCs with CD4$^+$ OT-II T cells, which were labeled with a violet cell tracking and proliferation dye. After three

days, co-cultures were analyzed by flow cytometry for dilution of the proliferation dye and percent divided was calculated. $CD172^{+}$ DCs from WT and $ADAM10^{DC-/-}$ stimulated similar levels of T cell proliferation at all antigen doses, as did $CD24^{+}$ DCs but at lower level of division (Figure 30A, B) (Figure 31C, D). Additional wells were treated with monensin in the final four hours of culture in order to analyze expression and IL-13 by intracellular cytokine flow cytometry. We found a trend toward lower levels of $IL\text{-}13^{+}$ in $CD4^{+}$ OT-II T cells (Figure 31E). No difference in T cell proliferation was detected between WT and $ADAM10^{DC-/-}$ $CD172^{+}$ or $CD24^{+}$ BMDCs and $OVA_{323\text{-}339}$ peptide (Figure 32A, B). We next tested *in vivo* antigen presentation by adoptively transferring violet tracer labeled $CD4^{+}$ OT-II T cells by *i.v.* injection into WT and $ADAM10^{DC-/-}$ mice followed by i.n. administered 25µg of OVA and 10µg HDM extract 24h later. After three days, mice were euthanized and medLN were examined for dilution of the proliferation dye. WT and $ADAM10^{DC-/-}$ mice had similar $CD4^{+}$ OT-II T cell proliferation (Figure 30C, D). We tested several OVA/HDM dosing strategies and tested several organs to determine the spread of antigen. None of the doses (Figure 33A-B – 10µg OVA/3x10µg HDM, C-D – 25µg OVA/3x 10µg HDM, E-H – 25µg OVA/10µg HDM) we examined demonstrated differences in the extent of proliferation between WT and $ADAM10^{DC-/-}$ in the medLN (Figure 33A, C, E). However, we did find differences in the proliferation of the OT-II cells found in the spleen. In the lowest OVA dose we surprisingly found a slight increase in the percent divided in the $ADAM10^{DC-/-}$ mice compared to WT (Figure 33B). There was no difference at the 25µg OVA dose with 3x 10µg HDM, but a slight decrease at 25µg OVA/10µg HDM (Figure 33D, F). This proliferation is likely due to escape of antigen from the local environment and how meaningful these splenic differences are to the airway phenotype is unclear. We found no difference in proliferation in the lungs or MLN of WT and medLN at the dosage we chose to use

(25μg OVA/10μg HDM) (Figure 33G, H). We also examined the costimulatory molecule expression on $CD172^+$ $ESAM^+$ splenic DCs after each set of OVA/HDM immunization protocols. Interestingly, we found increased expression of ICOSL (Figure 34A, D, G) and OX40L (Figure 34B, E, H) in $ADAM10^{DC-/-}$ mice in all models. We see a trend toward increase expression of CD86 in $ADAM10^{DC-/-}$ in each case (Figure 34C, F, I). The functional relevance of the increased expression is yet unknown and warrants further investigation.

Interestingly, cDC2s in the medLN of $ADAM10^{DC-/-}$ mice expressed less of the costimulatory molecule OX40L, which has been associated with T_H2 responses (Figure 30E) [104,105]. Expression of CD86 did not differ on these cDC2s as was also true for Notch ligands Jagged1 and Jagged2, though expression of these were low for both WT and $ADAM10^{DC-/-}$ mice (Figure 31F, G). We crossed OT-II mice to the 4C13R IL-4/IL-13 dual reporter mice, express AmCyan and DsRed with IL-4 and IL-13 expression, respectively[106]. CFSE-labeled 4C13R OT-II $CD4^+$ T cells were transferred into WT and $ADAM10^{DC-/-}$ mice followed 24h later with intranasal administration of OVA and HDM extract as above. Three days later, 4C13R OT-II T cells in the medLN were examined for expression of IL-4 and IL-13 by flow cytometry. While IL-4 levels were too low for accurate measurement, $ADAM10^{DC-/-}$ mice had dramatically fewer $CD4^+$ $IL\text{-}13^+$ T cells in the medLN than WT mice (Figure 30F-H). Overall these data suggest that though ADAM10-deficient DCs are able to stimulate antigen-specific T cell proliferation similar to WT DCs, they are not able to stimulate $CD4^+$ T cells to make the T_H2 cytokine, IL-13.

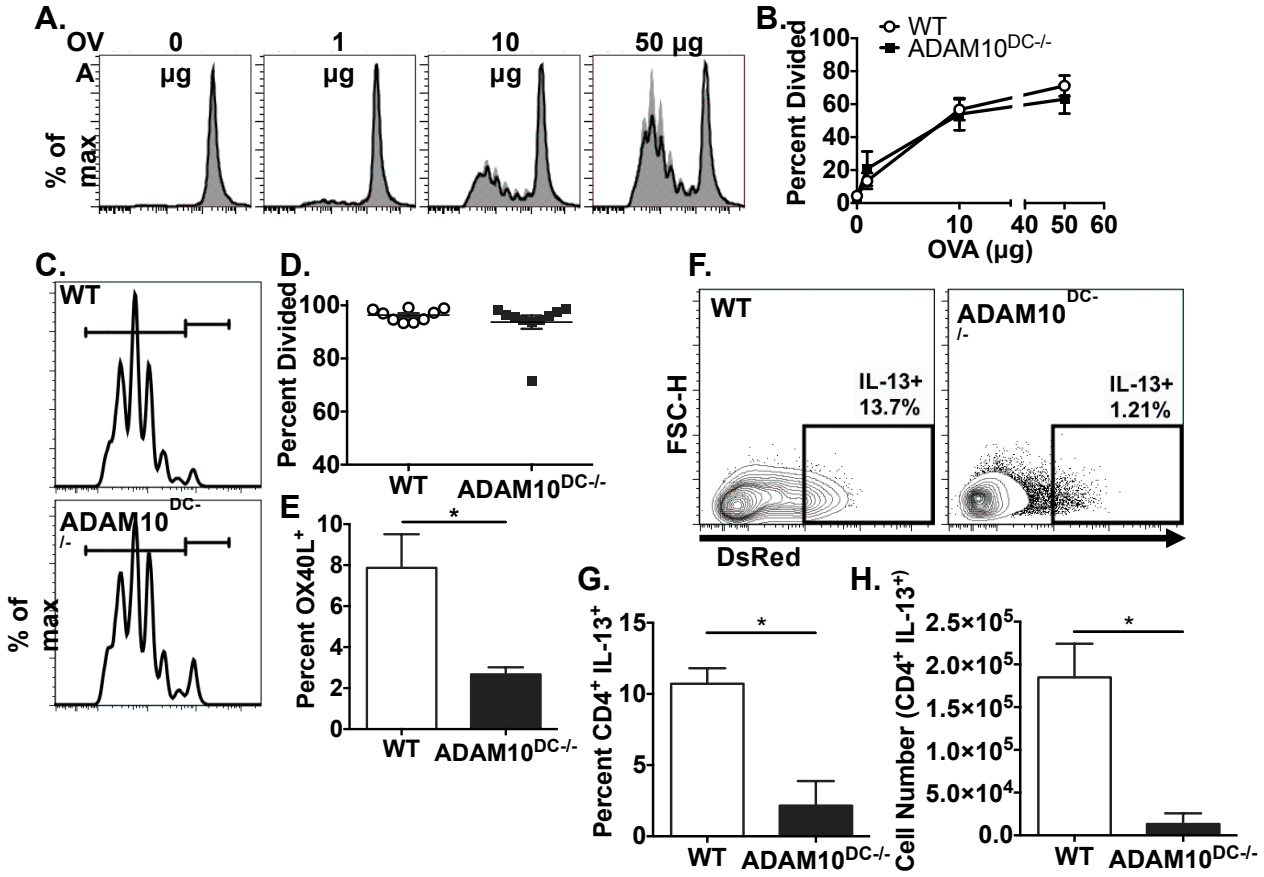

Figure 30: ADAM10-deficient DCs have intact antigen presentation, but stimulate fewer T_H2 cells.

A. CD172$^+$ BMDCs were sorted from ADAM10$^{DC-/-}$ and WT mice and incubated with indicated quantity of OVA protein. 1x10^5 violet cell tracer labeled CD4$^+$ OT-II T cells were co-cultured with 1 x 10^4 OVA-loaded DCs for 72h. Co-cultures were analyzed by flow cytometry for dilution of the tracer dye and percent divided was calculated. Representative histogram is shown for ADAM10$^{DC-/-}$ (solid black) and WT (filled gray) mice. B. Combined data from A. representing three independent experiments with n = 5 mice per group. C. 5x10^6 violet cell tracer labeled CD4$^+$ OT-II T cells were *i.v.* injected into WT (upper panel) and ADAM10$^{DC-/-}$ (lower panel) mice and 24h later 25µg OVA and 10µg HDM were administered i.n. After 72h medLN were harvested and dilution of the dye was analyzed by flow cytometry and shown in a representative histogram. D. Combined data from three independent experiments with n = 9 mice

per group. E. OX40L expression on $CD172^+$ DCs (cDC2s) in the medLN was examined by flow cytometry and shown as percent $OX40L^+$. F. 5 x 10^6 CFSE-labeled $CD4^+$ OT-II T cells were *i.v.* injected into WT and $ADAM10^{DC-/-}$ mice, followed by OVA/HDM (as in C). After 72h, medLNs were harvested and percent (G) and number (H) of $CFSE^+$ $CD4^+$ $IL\text{-}13^+$ was assessed by flow cytometry. Data is from two independent experiments with n = 6 mice per group. Data is presented as mean ± SEM. *$p<0.05$, unpaired Student's t test.

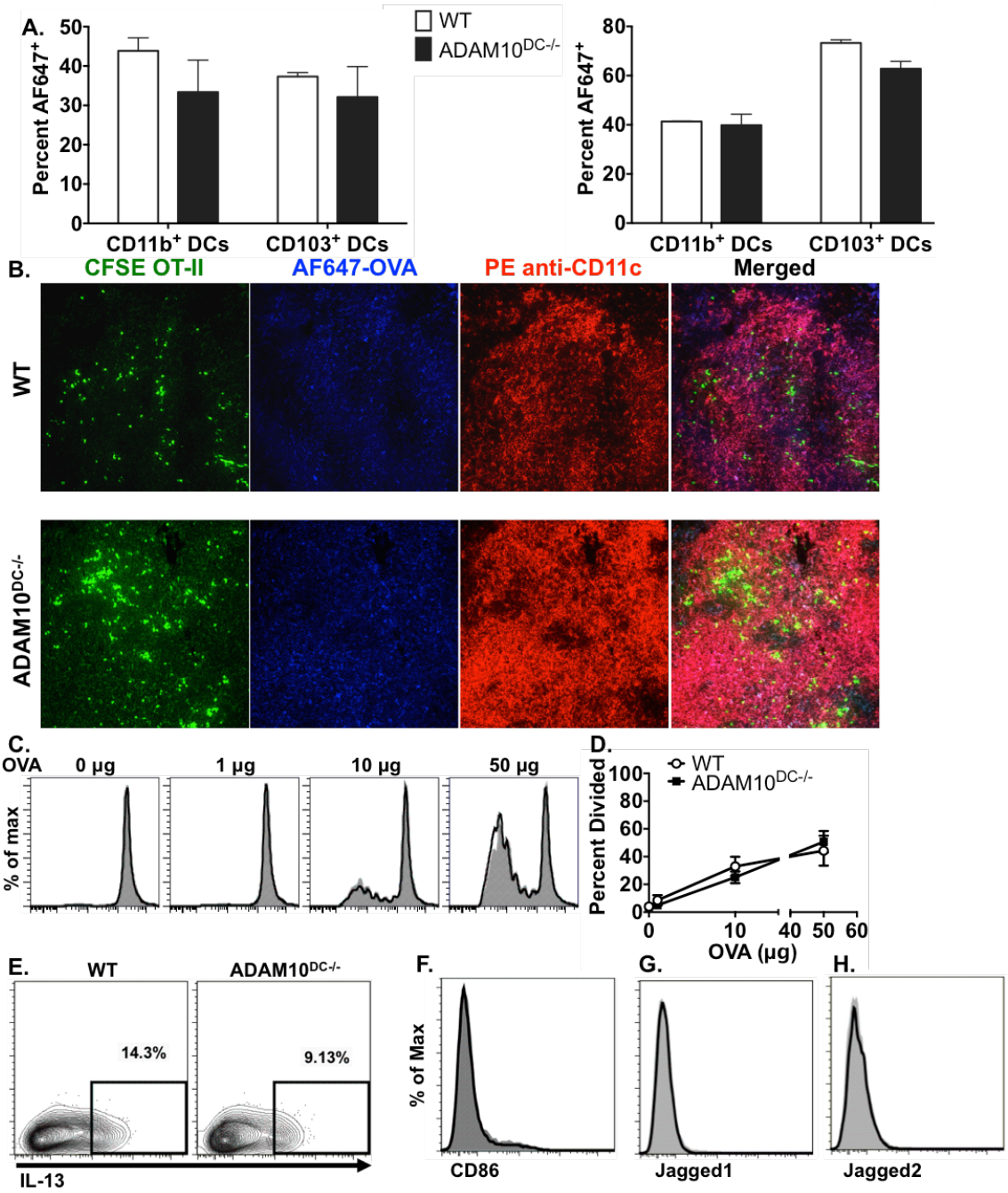

Figure 31: Antigen uptake and presentation is unchanged in ADAM10$^{DC-/-}$ mice.

A. 25µg OVA-AF647 and 10µg HDM were administered i.n. to WT and ADAM10$^{DC-/-}$ mice. MedLNs (left) and lungs (right) were analyzed 24h later by flow cytometry. B. Immunofluorescence images of medLN from mice that were given CFSE-labeled OT-II followed by OVA-AF647 and HDM. C. Violet tracer labeled CD4^{+} OT-II T cells were co-cultured with

OVA-loaded $CD24^+$ DCs. D. Percent divided was analyzed after 72h of culture. E. OT-II T cells co-cultured with OVA-loaded $CD172^+$ DCs were analyzed for intracellular IL-13 expression. F.-H. CD86, Jagged1, and Jagged2 expression was assessed on $CD172^+$ DCs in the medLN 72h after OVA and HDM administration i.n.

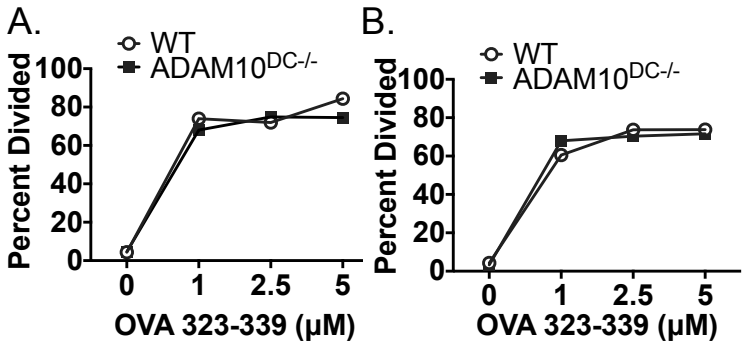

Figure 32: Antigen presentation with OVA peptide.

WT and ADAM10$^{DC-/-}$ BMDCs (CD172^{+} (A) and CD24^{+} (B)) were incubated with indicated concentrations of $OVA_{323-339}$ peptide and then co-cultured with violet tracer labeled CD4^{+} OT-II T cells for 72h. Dilution of the proliferation dye was assessed by flow cytometry, and percent divided was calculated.

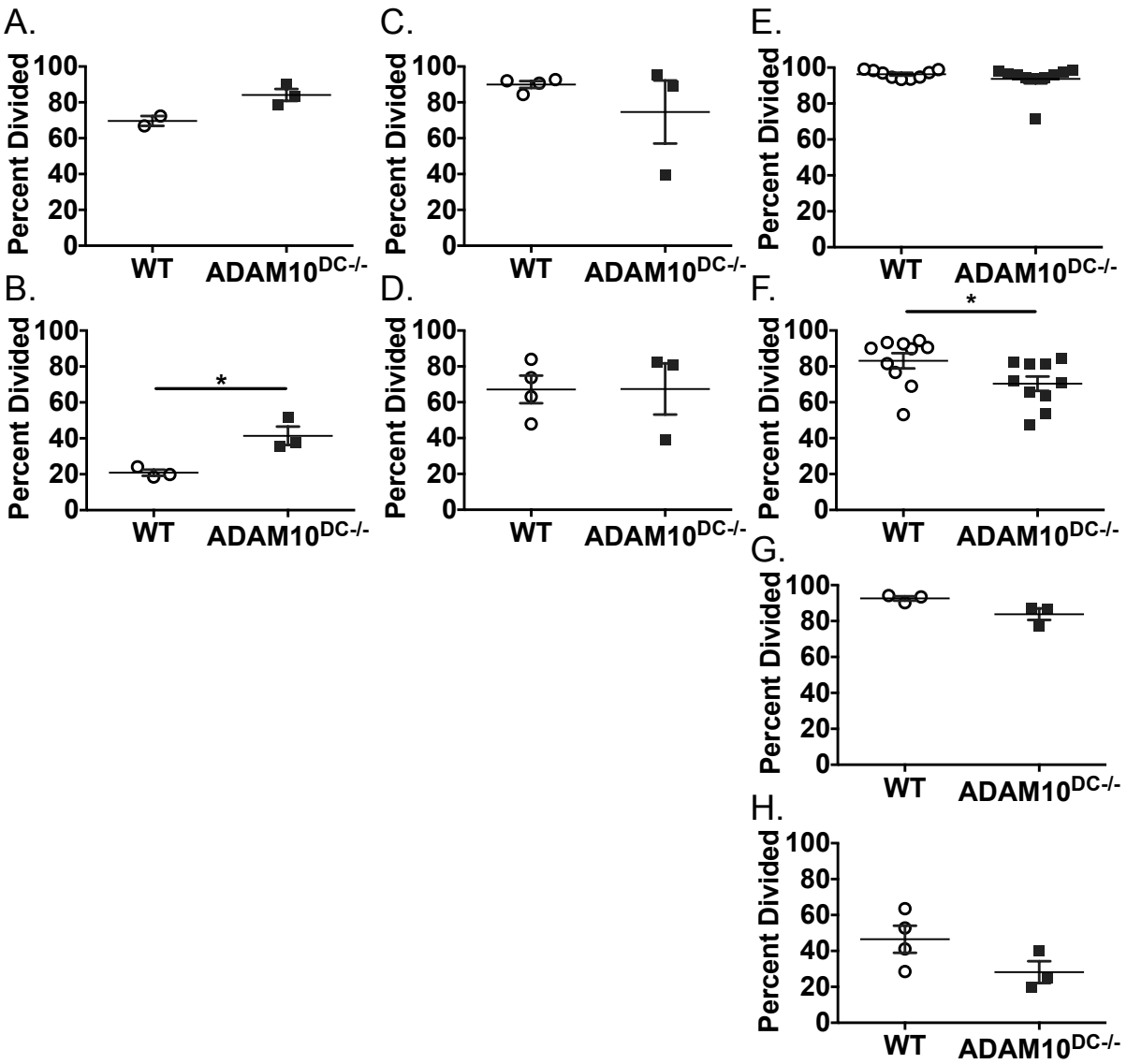

Figure 33: OVA/HDM immunization scheme.

Mice were immunized as in Figure 30C and D except that 10µg OVA/3x 10µg HDM (A, B), 25µg OVA/3x 10µg HDM (C, D), and 25µg OVA/10µg HDM (E-H) were used. Mice were euthanized 72h after last dose and medLN (A, C, E), spleen (B, D, F), lung (G), and MLN (H) were examined by flow cytometry for dilution of the proliferation dye. Symbols indicate individual mice. *$p<0.05$, unpaired Student's t test.

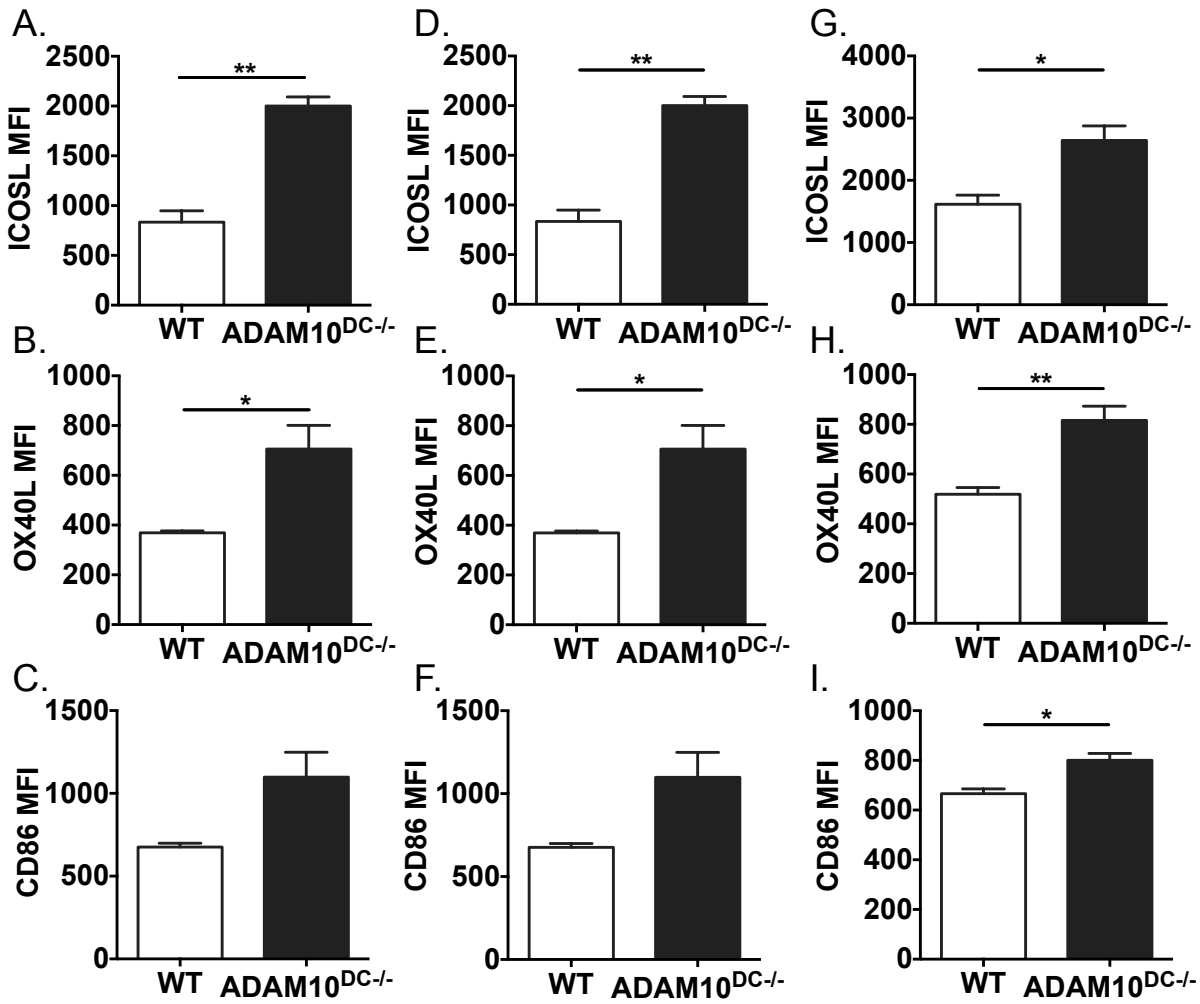

Figure 34: Costimulatory molecule expression on splenic DCs after OVA/HDM i.n.

Mice were immunized as in Figure 33 in which A-C received 10μg OVA/3x 10μg HDM, D-F received 25μg OVA/3x 10μg HDM, and G-I received 25μg OVA/10μg HDM. 72h after the last dose, expression of indicated costimulatory molecules on $CD172^+$ $ESAM^+$ splenic DCs was assessed by flow cytometry. **$p<0.01$, *$p<0.05$ unpaired Student's t test.

ADAM10$^{DC-/-}$ DCs have reduced Klf4 and Il6 expression

Several DC-produced cytokines and transcription factors have been implicated in skewing T helper responses toward T_H2. Lack of IL-12 and high IL-6 expression have been cited as promoting T_H2 cell development[87]. We examined the expression of *IL-12* and found no difference between WT and ADAM10 deficient bone marrow derived DCs (BMDCs) (Figure 35A). A recent report has identified Kruppel like factor 4 (*Klf4*) as being critical for conventional DCs to stimulate T_H2 responses[86]. We examined the expression of *Klf4* in BMDCs from WT and ADAM10$^{DC-/-}$ mice. We found that CD172$^+$ DCs deficient in ADAM10 expressed less *Klf4* than WT (Figure 35B). A potential target of KLF4 is *Il6*, a cytokine important for both T_H2 and T_H17 immune responses[107]. We also found a dramatic reduction in *Il6* mRNA expression in ADAM10$^{DC-/-}$ CD172$^+$ BMDCs compared to WT (Figure 35C). While both of these factors are vital for T_H2 immunity, only *Il6* expression was restored in ADAM10 deficient CD172$^+$ BMDCs when Notch signaling was recovered (ADAM10$^{DC-/-N1-ICD+}$) (Figure 35C). As a control, we also examined the expression of the Notch target gene *Hes1* and indeed found that ADAM10$^{DC-/-}$ BMDCs had less expression of *Hes1* than WT (Figure 36A). *Hes1* expression is additionally recovered with constitutive N1-ICD expression (Figure 36A). We also analyzed ADAM10 deficient and WT CD172$^+$ BMDCs for the presence of cleaved Notch1 by western blot. ADAM10$^{DC-/-}$ BMDCs had less cleaved Notch1 than WT BMDCs (Figure 35D), indicating less activation of Notch1. We found less binding of N1-ICD to the Hes1 promoter by ChIP (Figure 36B). These findings further underscore the importance in Notch signaling in the ability of DCs to stimulate T_H2 responses.

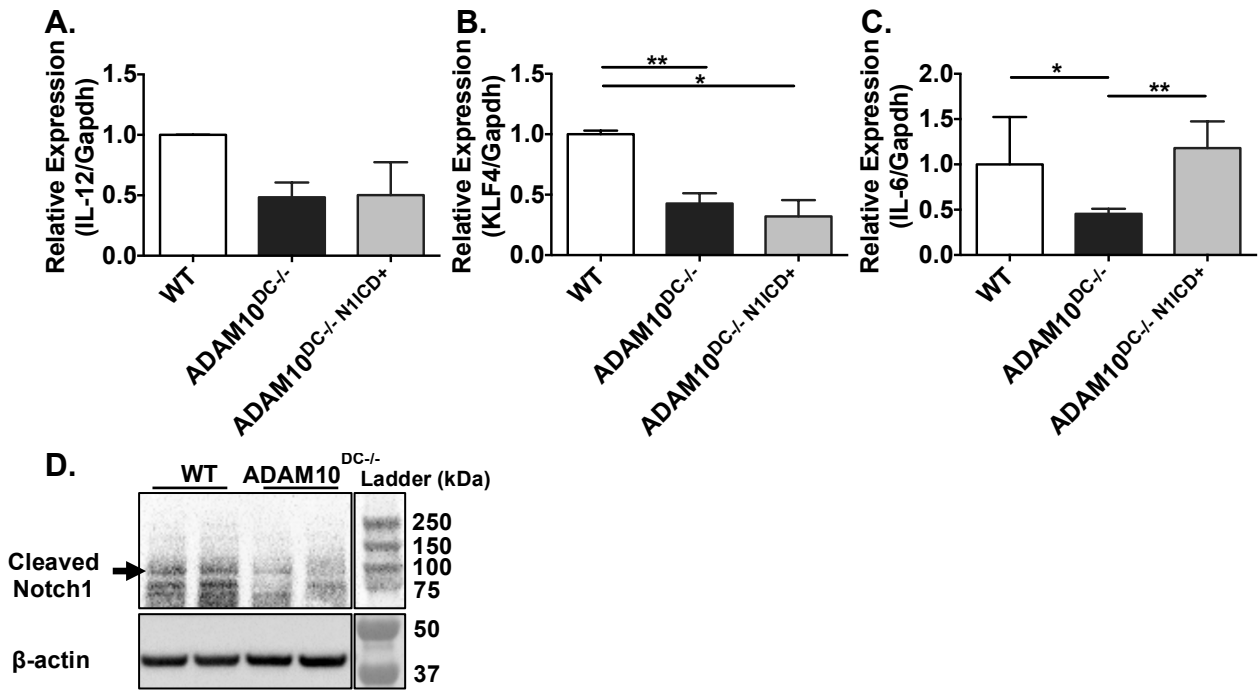

Figure 35: N1-ICD expression restores DC *Il6*, but not *Klf4* message levels.

$CD172^+$ BMDCs were sorted from WT, $ADAM10^{DC-/-}$, and $ADAM10^{DC-/-\ N1\text{-}ICD+}$ mice. A. mRNA expression of *Il12* (A), *Klf4* (B), and *Il6* (C) relative to *Gapdh* was measured by qPCR. Data shown is from three independent experiments with n = 5 mice per group. Data is presented as mean ± SEM. D. WT and $ADAM10^{DC-/-}$ $CD172^+$ BMDCs were examined by western blot for cleaved Notch1 and β-actin. Data shown is representative of two experiment with n = 5 mice per group. **p<0.01, *p<0.05, ANOVA with Tukey's post hoc test.

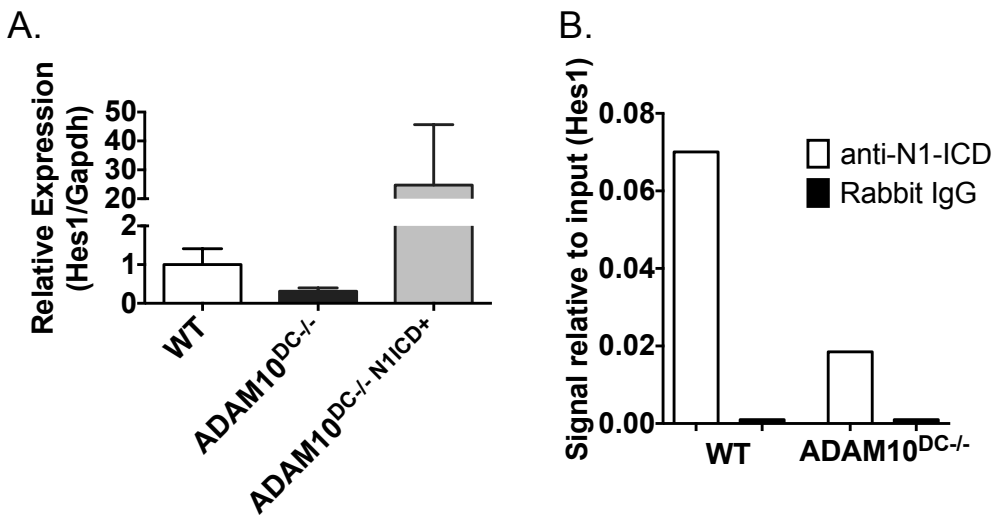

Figure 36: Notch target gene expression.

A. *Hes1* expression relative to *Gapdh* in BMDCs from WT, ADAM10$^{DC-/-}$, and ADAM10$^{DC-/- N1-ICD+}$ mice. B. ChIP with anti-N1-ICD and PCR for the presence of Hes1 in WT and ADAM10$^{DC-/-}$ BMDCs.

1.2.4 Discussion

The role of DCs in the initiation of T_H2 immune responses has been well studied, but the function of ADAM10 on DCs has not yet been investigated. Here we demonstrate that deletion of ADAM10 from DCs results in diminished T_H2/IgE-mediated pathology using several T_H2 models. HDM sensitivity was reduced to essentially the saline control when lung resistance was measured. While eosinophil levels were not at control levels, there was clear, significant reduction of eosinophils in the BALF (Figure 19B). HDM is an important aeroallergen in humans. Eosinophil increases are commonly seen in human patients, however treatment with anti-IL-5 has revealed that many do not achieve reductions in clinical symptoms by blocking this cellular infiltration[108]. Nevertheless reduction in lung resistance parameters is clearly important in all asthma scenarios. There is some controversy whether HDM-sensitized asthma is always IgE-mediated, but the relevance of T_H2 immunity is unquestioned[109]. To that end our demonstration of a reduction in T_H2 cytokines in the lungs supports this conclusion (Figure 19C, D). A T_H2 selective defect is further supported by our results using NP_{31}-KLH immunization and *A. alternata* (Figure 23). In the NP-KLH studies we found less high affinity NP-specific IgG1, but no differences in other isotypes (Figure 16). This is most pronounced in the recall response. The *A. alternata* model causes a strong increase in eosinophils and neutrophils[92], as well as the induction of both T_H2 and T_H17 associated cytokines. We showed fewer eosinophils and IL-13^+ $CD4^+$ T cells, both T_H2 specific indicators (Figure 23A, C). IgE production was also dramatically reduced (Figure 23E). Few IL-17 or IFNγ positive cells were seen in the *A. alternata* model we used, but this was similar between WT and $ADAM10^{DC-/-}$ mice (Figure 23C). This result is in contrast to the infection with *C. rodentium*, in which $ADAM10^{DC-/-}$ mice exhibited impaired immunity. Decreased body weight, survival, and trending less total IgG2b levels were seen, as

well as increased bacterial load in the spleen, indicating loss of barrier function (Figure 24B-G). Interestingly, *C. rodentium-specific* IgG2b was not different. Notch2 is a known target of ADAM10 protease activity and this connection is evident in that others have shown that Notch2$^{DC-/-}$ mice have compromised immunity to this infection[101]. Interestingly, Notch2$^{DC-/-}$ mice are even more severely affected infection as Notch2 controlled the development of the DC subset in the intestine (CD103^{+} CD11b^{+}), which produces the IL-23 necessary for early, innate protection against the bacterium. Loss of early defenses may increase the likelihood of epithelial breakdown and increased disseminated disease in both Notch2$^{DC-/-}$ and ADAM10$^{DC-/-}$ mice. ADAM10$^{DC-/-}$ mice have some reduction in this DC subset, as well as some others seen in the Notch2$^{DC-/-}$, such as the CD172^{+} ESAM^{+} subset in the spleen (Figure 26A-C). This difference may explain the disparity in survival between ADAM10$^{DC-/-}$ and Notch2$^{DC-/-}$ mice in infection with *C. rodentium*[101]. Similar CR-specific IgG2b levels between WT and ADAM10$^{DC-/-}$ mice also support a defect in local innate rather than adaptive responses. DC migration to lymph nodes was required for antibody responses, but not for protection against the bacterium which was mediated by lamina propria DC production of IL-23[101]. For examination of T_H1 defects, ADAM10$^{DC-/-}$ and WT mice with the obligate intracellular bacterium *A. phagocytophilum,* where, as mentioned, T cell production of IFNγ is crucial for pathogen elimination[98,99]. No defects were seen with respect to the control of this infection in the ADAM10$^{DC-/-}$ mice as compared to WT animals (Figure 24A). Thus we conclude that the primary impairment is seen with T_H2 disease models. A defect in the innate responses to infection with *C. rodentium* was also evident, albeit a less severe impairment as seen in Notch2$^{DC-/-}$ mice.

In order to further examine the role of DC Notch expression in the T_H2 impairment seen, we turned to mice in which Notch DC expression was altered. Notch2$^{DC-/-}$ mice exhibited the

same response in the ASA model as WT animals, indicating that lack of Notch2 expression on DCs was not responsible for the loss of T_H2 function. However, Notch signaling was clearly implicated in our results using the $ROSA^{N1\text{-}ICD}$ mice; these animals have overexpression of the nuclear signaling component of Notch (N1-ICD) in cells that have Cre expression. Intriguingly, this restored the temperature drop in the $ADAM10^{DC-/-}$ animals (Figure 27K). This was then further explored by using $Notch1^{DC-/-}$ mice. These animals fell into two groups; 6 of 9 no longer showing evidence of anaphylaxis while 3 of 9 responded the same as WT controls (Figure 28A, B). With $ADAM10^{DC-/-}$ mice, 10 of 11 exhibited no temperature drop. The reason for the two groupings is not known, though the amount of antigen-specific IgE made in $Notch1^{DC-/-}$ mice may be right at the threshold required for anaphylaxis. Thus, most of the $Notch1^{DC-/-}$ mice do not undergo anaphylaxis, but a few do. Mice also exhibit IgG-mediated anaphylaxis with macrophages as the major players, instead of mast cells[110]. However, the model used in this study primarily induces IgE-mediated anaphylaxis so this is unlikely the explanation[90] and the data from the HDM model is not consistent with a macrophage-mediated response. This finding warrants further investigation. Overall the results obtained indicate that the ADAM10 substrate that is important for mediating T_H2 immunity is indeed Notch, with Notch1 exhibiting a higher level of importance than Notch2. The activation of Notch signaling requires the Notch receptor to bind to a Notch ligand, typically on adjacent cells. Several Notch ligands on DCs have been studied in the context of T_H2 immunity. Jagged 1 and 2 on DCs have been shown to promote T_H2 response[87], but we did not find alterations in either of these on ADAM10-deficient DCs (Figure 31G, H). While the role of Notch1 has previously been studied in DCs, the studies found no alterations in DC subsets[102]. While we agree that the DC subset proportion is not altered, our results do indicate an important role for DC Notch1 expression, which is supported by Figure

35D demonstrating less cleaved Notch1 in ADAM10-deficient $CD172^+$ DCs. Further studies will be required to determine if Notch1 expression levels explain this phenomenon.

Deletion of ADAM10 from B cells resulted in the loss of Notch2-dependent marginal zone B cells[84]. $ADAM10^{B-/-}$ mice also have globally reduced humoral immunity, including IgG1 and IgE[50,111–113]. This defect is distinct from the reduction in T_H2 immunoglobulin seen in the $ADAM10^{DC-/-}$ mice, though marginal zone B cells are absent both. The CD11c promoter drives ADAM10 deletion in $ADAM10^{DC-/-}$ mice, and there exists a small subset of B cells, which express CD11c. The difference in humoral response in the $ADAM10^{B-/-}$ and $ADAM10^{DC-/-}$ does not support that the $ADAM10^{DC-/-}$ mouse phenotype is caused by ADAM10 deletion from the $CD11c^+$ B cell population. Alveolar macrophages also express CD11c. Results from studies deleting ADAM10 from myeloid cells using the LysM-Cre would suggest a defect in macrophage migration[114]. As we demonstrate in Figure 19B, we have equivalent levels of macrophage migration into the BALF, further supporting a DC-specific phenotype.

T_H2 priming DCs have been described as being IRF4- and KLF4-dependent[86,115]. IRF4-expression DCs are also responsible for producing T_H17 responses[116]. The precise targets of these transcription factors are unknown, but likely are cytokines or cell surface receptor on DCs. We find that OX40L on DCs in the medLN from $ADAM10^{DC-/-}$ mice is greatly reduced compared to WT (Figure 30E). OX40L has been demonstrated to be important for the induction of T_H2 responses[104,105]. The cytokine IL-6 from DCs has also been shown to be critical for the development of T_H2 responses as DCs from IL-6KO mice are unable to stimulate T_H2 cytokine and Der p-specific IgG1[117]. $ADAM10^{DC-/-}$ mice have reduced IL-6, HDM-specific IgG1, and IgE (Figure 19C) (Figure 35F, H). The transcription factor KLF4 is able to bind to and activate the *Il6* promoter in DCs[107]. We show that both *Klf4* and *Il6* expression is reduced in ADAM10-

deficient DCs (Figure 35B, C). Interestingly, only *Il6* expression was restored with N1-ICD expression (Figure 35C), indicating that it may be responsible for the phenotype observed in ADAM10$^{DC-/-}$ mice. In further support of this is that IL-6 has been demonstrated to be upregulated by non-canonical Notch signaling and is dependent on N1-ICD[118].

Ever since IgE was discovered in the 1960s and the recognition of its importance in Type 1 hypersensitivity, specific reduction in IgE synthesis has been a long sought mechanism to control these diseases. This has proven to be a difficult task, as this needs to be accomplished without significantly reducing protective immunoglobulin. Based on the results presented here, inhibition of ADAM10 on DCs would represent a method to achieve this difficult overall objective. Our current studies are examining whether similar results are seen when ADAM10 inhibitors are targeted to DCs. If successful, this would have the potential of being a general therapy for T_H2-mediated diseases.

Chapter 3: ADAM17 deletion from dendritic cells gives a distinct phenotype.

1.3.1 Introduction

ADAM10 and ADAM17

ADAM10 and ADAM17 have many structural and functional similarities, including an overlapping group of substrates. Both have metalloproteinase domains, disintegrin domain with C-shaped cysteine-rich region, transmembrane region, and a cytoplasmic tail[78]. Both enzymes share similar transmembrane substrates and have constitutive and inducible shedding, but each has its favored substrates. ADAM10 is best known for its ligand-induced cleavage of Notch receptors, amyloid precursor protein, and ligands for epidermal growth factor receptor (EGFR)[75,119,120]. ADAM17 was originally known as TNF converting enzyme (TACE) and also sheds junctional adhesion molecule and vascular endothelial cadherin[121–123].

ADAM17 in the immune system

ADAM17's most well known substrate is TNF, which is critical to many aspects of the immune system[78]. ADAM17 also cleaves other proinflammatory cytokines and their receptors, regulating leukocyte adhesion and migration[124]. L-selectin (CD62L) regulates the rolling phase of diapedesis, which controls leukocyte recruitment toward chemokine signals. ADAM17 cleaves L-selectin in response to activation by chemotactic signals[124]. ADAM17 has also been implicated in cleaving ICOSL on the surface of B cells, which regulates humoral immune responses[125].

Several substrates of ADAM17 are known to be expressed by cDCs, including TNF, TGFα, amphiregulin, Mer tyrosine kinase, FcγRIII (CD16), and IL-6R. Further, L-selectin is used by pDCs to migrate to sites of inflammation.

Given the large number of potential targets, we sought to understand how deletion of ADAM17 from DCs affects their function and overall immune responses. We show that

ADAM17$^{DC-/-}$ have no apparent defect in humoral immunity or T_H2 response to HDM. Interestingly, when both ADAM10 and ADAM17 are knocked out of DCs, we see a phenotype that is unlike the single knockouts (ADAM10$^{DC-/-}$ or ADAM17$^{DC-/-}$) including reduced IL-13 and IFNγ expression in CD4$^+$ T cells after fungal allergen exposure. This indicates two possible hypotheses: either different substrates of ADAM10 and ADAM17 need to be removed for these phenomena to occur or ADAM10 and ADAM17 are cleaving a single substrate, which is required for immune responses.

1.3.2 Materials and Methods

1.3.2.1 Mice

All animal experiments were performed with the approval of the Virginia Commonwealth University Institutional Animal Care and Use Committee. Mice were maintained in the Virginia Commonwealth University animal facility in accordance with guidelines for the humane treatment of laboratory animals set forth by the National Institutes of Health and the American Association for the Accreditation of Laboratory Animal Care. C57Bl/6 ADAM10^{flox} mice were generated as previously described[84] and were bred to B6.Cg-Tg(Itgax-cre)1-1Reiz/J (CD11c-cre, Stock No. 008068) to generate ADAM10$^{DC-/-}$ mice. ADAM17^{flox} were purchased from Jackson lab (Stock No. 009597). ADAM17^{flox} and ADAM10/17^{flox} were bred to the CD11c-cre mouse to generate ADAM17$^{DC-/-}$ and ADAM10/17$^{DC-/-}$ mice. All mice were on the C57Bl/6 background, and healthy male and female 6-12 week old mice were used for experiments. Genotyping primers used for ADAM10$^{DC-/-}$ mice are described in Table 3 and ADAM17$^{DC-/-}$ mice in Table 5.

Table 5: Genotyping Primers

Mouse Colony		Primer Name	Sequence (5' – 3')
$ADAM17^{DC-/-}$	Flox and WT	13799	TCCCCCAGCTAGATTGTTTG
		13800	AGGACCCAGGTTCAGTTCCT

1.3.2.2 Antigen presentation

Antigen presentation assays were conducted using ADAM17$^{DC-/-}$ and ADAM10/17$^{DC-/-}$ mice as described in Section 1.2.2. Antibodies used for flow cytometry that are not previously mentioned are PE-Cy7 anti-mouse MerTK (Clone DS5MMER) (eBioscience) and Biotin-anti-mouse CD16/32 (Clone 2.4G2).

1.3.2.3 HDM

Intranasal administration of HDM and subsequent analysis were performed as described in Section 1.2.2.

1.3.2.4 NP-KLH

Immunization with NP_{31}-KLH in alum and ELISAs were performed as described in Section 1.2.2.

1.3.2.5 A. alternata

Intranasal administration of *A. alternata* and subsequent analysis were performed as described in Section 1.2.2.

1.3.2.6 Aspergillus fumigatus

Mice were sensitized and challenged with *A. fumigatus* as previously described[126]. Briefly, mice were sensitized with 10μg of *A. fumigatus* extract (Stallergenes Greer) in alum (Sigma) on days 0 and 7. On days 14, 15, and 16 mice were given 15μg *A. fumigatus* extract i.n. Mice were euthanized on day 17.

1.3.2.7 IgG1 Immune complexes

$CD4^+$ T cells were isolated from OT-II mice by L3T4 magnetic bead isolation and labeled with Tag-it Violet cell tracer (Biolegend). Labeled $CD4^+$ OT-II T cells were *i.v.* injected into mice. The following day, OVA and anti-OVA IgG1 antibody were mixed in 1:10 ratio with each

mouse getting 2μg OVA and 20μg anti-OVA-DNP IgG1 (in house). The mixture was nutated at room temperature for 30min prior to *i.v.* injection. 72h later mice were euthanized and examined.

1.3.3 Results

Deletion of ADAM17 does not affect DC antigen presentation

Given the striking results with the ADAM10$^{DC-/-}$ mice, we wanted to examine the effect of removing the related metalloproteinase ADAM17 from DCs. We first assessed the ability of the DCs pick up antigen and present it to CD4$^+$ T cells as we had been done with the ADAM10$^{DC-/-}$. We adoptively transferred in labeled CD4$^+$ OT-II T cells into ADAM17$^{DC-/-}$, ADAM10/17$^{DC-/-}$, or WT mice and then administered OVA/HDM i.n. In the medLN of WT, ADAM17$^{DC-/-}$, and ADAM10/17$^{DC-/-}$ mice, almost 100% of the transferred T cells had proliferated (Figure 37A). Deletion of ADAM10 from DCs affected the presence of certain DC subsets in the spleen and LNs due to abrogation of Notch signaling (Figure 26). We wanted to see if the absence of ADAM17 and ADAM10/17 from DCs alters the prevalence of any medLN DC subsets. We examined total cDCs, CD24$^+$, and CD172$^+$ DCs after the antigen presentation assay and found neither group was different than WT (Figure 37B). Previously we had also observed differences in costimulatory molecule expression on ADAM10-deficient DCs, which likely affected their ability to stimulate T_H2 responses (Figure 34). We analyzed costimulatory molecule expression on CD172$^+$ DCs in the medLNs of WT, ADAM17$^{DC-/-}$, and ADAM10/17$^{DC-/-}$ mice. We did not see any differences in CD86, ICOSL, and OX40L (Figure 37C). We also examined the tyrosine kinase MerTK, which is known to help DCs recognize apoptotic cells and is cleaved by ADAM17, but found a trend toward increased expression on ADAM17$^{DC-/-}$, but not ADAM10/17$^{DC-/-}$ mice. (Figure 37C). Overall, antigen presentation, DCs subsets in the medLN, and costimulatory molecule expression are unchanged in ADAM17$^{DC-/-}$ and ADAM10/17$^{DC-/-}$ mice.

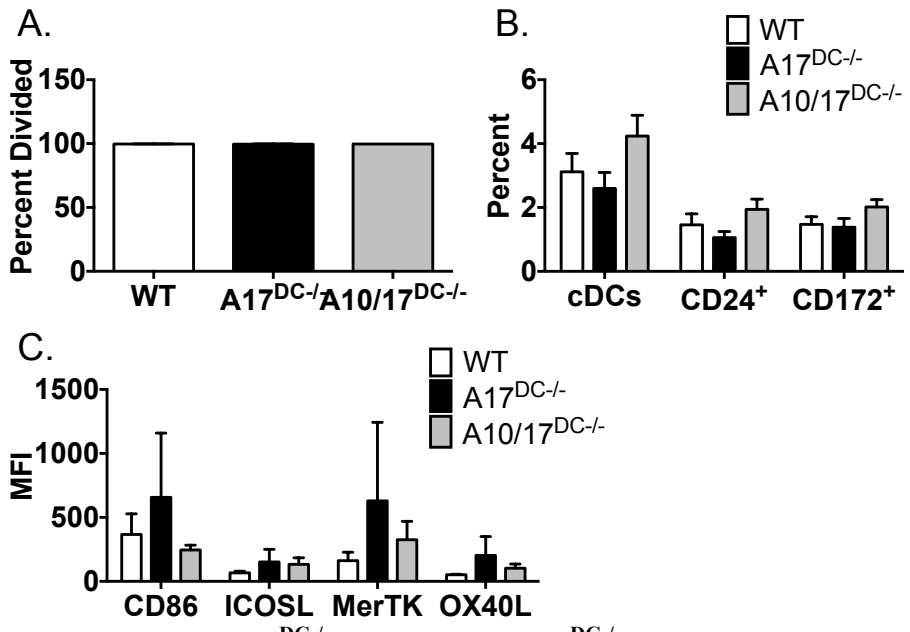

Figure 37: ADAM17$^{DC-/-}$ and ADAM10/17$^{DC-/-}$ mice do not have defects in antigen presentation.

A. *In vivo* antigen presentation assay as was performed in Figure 30 with violet dye-labeled CD4$^+$ OT-II cells and i.n. administration of OVA/HDM. B. DC subsets (cDCs (CD11c$^+$ MHCII$^+$), CD24$^+$ (CD11c$^+$ MHCII$^+$ CD24$^+$ CD172$^-$), and CD172$^+$ (CD11c$^+$ MHCII$^+$ CD24$^-$ CD172$^+$)) in medLN after antigen presentation assay were assessed by flow cytometry. C. Costimulatory molecule expression on CD172$^+$ DCs was examined by flow cytometry.

NP-specific antibody responses are intact in ADAM17$^{DC-/-}$

After determining antigen presentation was intact in the ADAM17$^{DC-/-}$, we wanted to examine if T dependent antibody responses were affected by deletion of ADAM17 from DCs. ADAM10$^{DC-/-}$ had a class-specific reduction in high affinity IgG1 antibody (Figure 16). We immunized ADAM17$^{DC-/-}$ with NP_{31}-KLH in alum as previously described and measured high and total affinity antibody. For both IgG1 and IgG2b antibody classes, ADAM17$^{DC-/-}$ mice made equivalent levels of both high and total affinity as well as total antibody levels (Figure 38A-D). We also examined the presence of GC B and T_{FH} cells in the spleen after boost immunization. ADAM17$^{DC-/-}$ mice had trending higher levels of GC B cells (Figure 38E) and similar levels of T_{FH} cells compared to WT (Figure 38F). We also measured the expression of costimulatory molecules (CD86, ICOSL, and OX40L) and MerTK on CD172^{+} DCs in the spleen. As we found in the antigen presentation assay, ADAM17-deficient DCs expressed these surface molecules similarly to WT DC (Figure 38G).

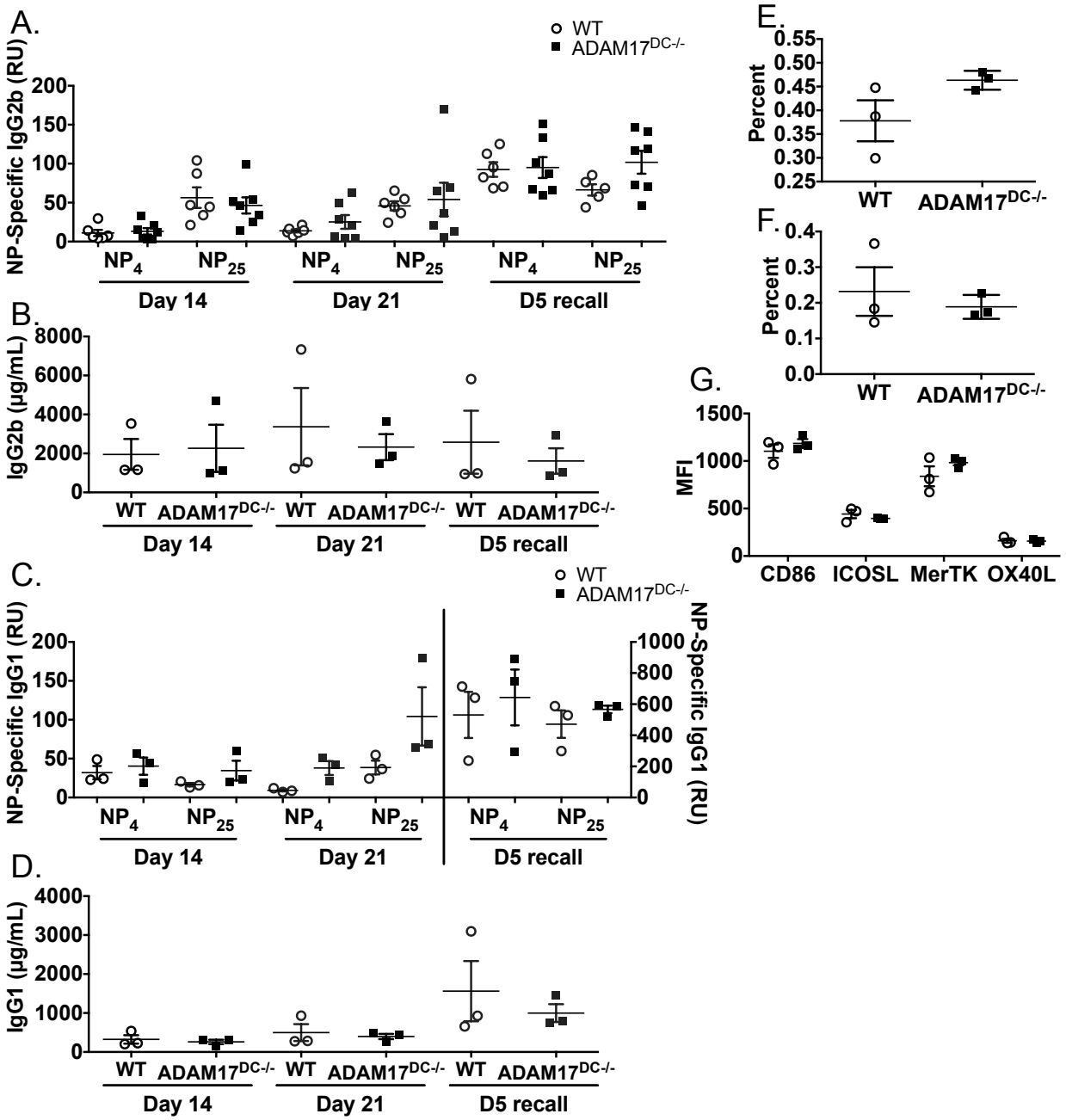

Figure 38: NP-specific antibody responses are intact in ADAM17$^{DC-/-}$.

WT and ADAM17$^{DC-/-}$ mice were immunized with NP-KLH as previously described. High (NP_4) and total (NP_{25}) affinity antibody in serum were measured at indicated days by ELISA. A. IgG2b. B. Total IgG2b. C. IgG1. D. Total IgG1. E. Day 7 after boost, GC B cells ($B220^+$ $CD95^+$ $GL\text{-}7^+$) (E) and T_{FH} cells ($CD4^+$ $PD\text{-}1^+$ $CXCR5^+$) (F) were analyzed in the spleen by flow

cytometry. G. Levels of costimulatory and surface molecules were assessed on $CD172^{+}$ DCs in the spleen day 7 after boost.

ADAM10/17$^{DC-/-}$ mice have diminished T_H2 response to HDM

Though we did not see differences in T_H2 antibody levels in ADAM17$^{DC-/-}$ mice, we wanted to see how these mice would perform in model of allergic airway inflammation. We subjected ADAM17$^{DC-/-}$, ADAM10/17$^{DC-/-}$, ADAM10$^{DC-/-}$, and WT i.n. administration of HDM extract as previously described. After sensitization and challenge with HDM, we used the Flexivent apparatus to measured airway resistance at increasing doses of methacholine. WT mice demonstrate increasing resistance through the 50mg/mL dose. ADAM10$^{DC-/-}$ mice had minimal increases in resistance as shown in Figure 19A. ADAM17$^{DC-/-}$ mice behaved similar to WT, albeit with much variability. Airway resistance in ADAM10/17$^{DC-/-}$ mice increased little with each methacholine dose (Figure 39A). When we examined the BALF for cell infiltrate, we found that both ADAM17$^{DC-/-}$ and ADAM10/17$^{DC-/-}$ mice had high levels of eosinophils, comparable to WT mice (Figure 39B). No significant differences in neutrophils, macrophages, or lymphocytes were found between groups (Figure 39B). Consistent with the lack of airway resistance, ADAM10/17$^{DC-/-}$ had nominal levels of total and HDM-specific IgG1 as well as total IgE in the serum (Figure 39C-E). We observed no difference in the percentage of GC B cells (B220$^+$ CD95$^+$ GL-7$^+$) or CD4$^+$ IL-13$^+$ cell in the medLN (Figure 39F, G). These results indicate that ADAM17$^{DC-/-}$ mice do not have an altered response to HDM, in contrast to ADAM10/17$^{DC-/-}$ mice. Interestingly, this defect results in reduced airway hyperresponsiveness and immunoglobulin, but no reduction in eosinophils or GC B cells.

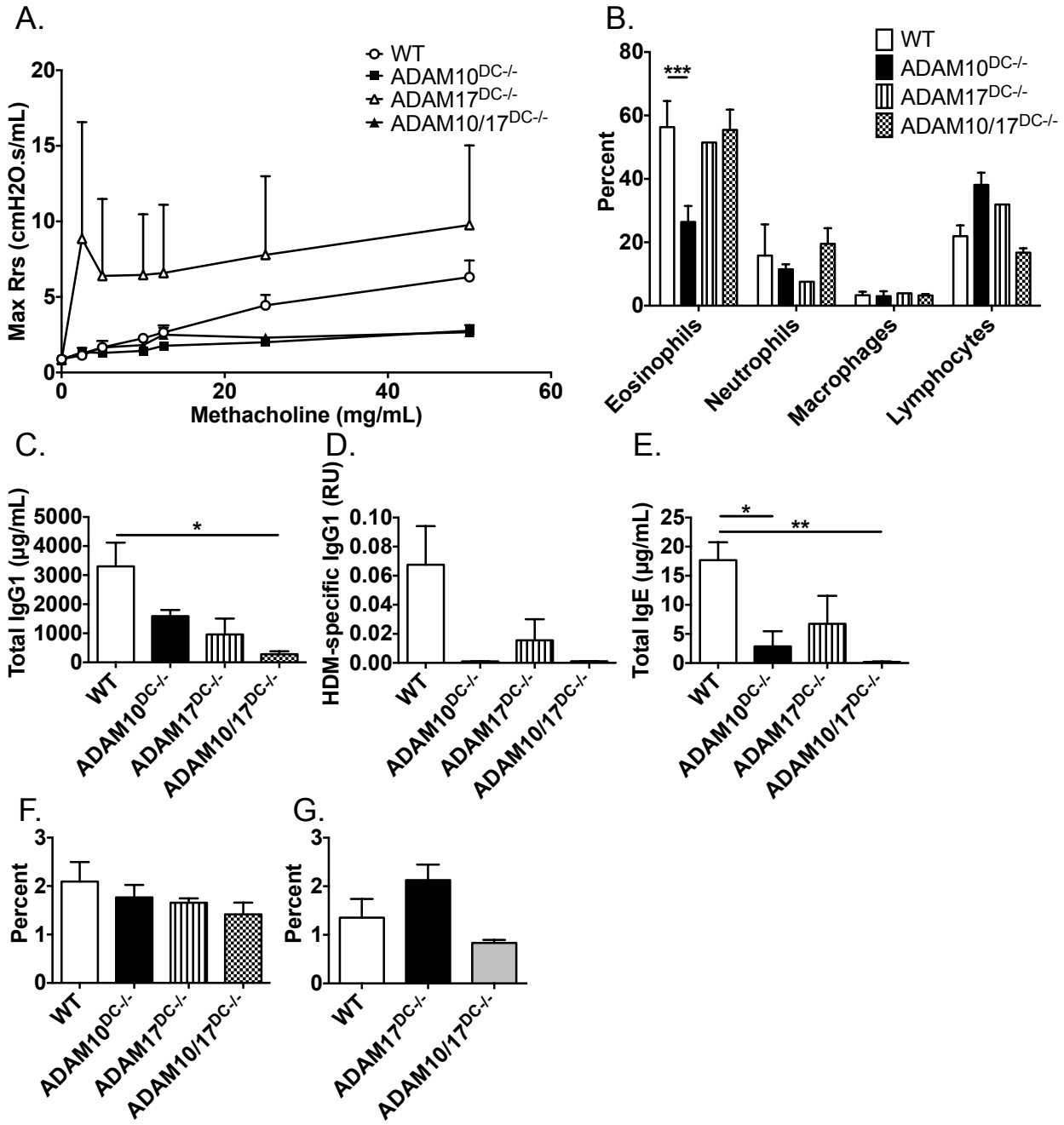

Figure 39: ADAM10/17$^{DC-/-}$, but not ADAM17$^{DC-/-}$ mice have reduced T_H2 response to HDM.

ADAM10$^{DC-/-}$, ADAM17$^{DC-/-}$, ADAM10/17$^{DC-/-}$, and WT mice were subjected to the HDM protocol as previously described. A. Maximum airway resistance (max Rrs) was assessed at increasing doses of methacholine. B. Eosinophils, neutrophils, macrophages, and lymphocytes in the BALF were analyzed by flow cytometry. C. – E. Total and HDM-specific IgG1 and total IgE

were measured in the serum by ELISA. F. and G. GC B ($B220^+$ $CD95^+$ $GL\text{-}7^+$) and $CD4^+$ $IL\text{-}13^+$ cells in the medLN were analyzed by flow cytometry. ***$p<0.001$, **$p<0.01$, *$p<0.05$, one-way ANOVA with Tukey's post hoc test.

Alternaria alternata model in ADAM17$^{DC-/-}$ and ADAM10/17$^{DC-/-}$ mice

Given the intriguing results from the HDM model of allergic airway inflammation, we wanted to examine the response of ADAM17$^{DC-/-}$ and ADAM10/17$^{DC-/-}$ mice with a fungal aeroallergen. *Alternaria alternata* is a common household allergen, which elicits both T_H2 and T_H17 immune responses in the airways[92,97]. We administered *A. alternata* as previously described in Figure 23 and found no difference in eosinophils, macrophages, and lymphocytes in the BALF of WT, ADAM17$^{DC-/-}$, and ADAM10/17$^{DC-/-}$ mice (Figure 40A). We did observe trending higher neutrophils in ADAM17$^{DC-/-}$ compared to WT (Figure 40A). We examined GC B cells in the medLN and found similar percentage between WT, ADAM17$^{DC-/-}$, and ADAM10/17$^{DC-/-}$ mice (Figure 40B). We found fewer T_{FH} cells (CD4$^+$ PD-1$^+$ CXCR5$^+$) in the medLN of ADAM17$^{DC-/-}$ and ADAM10/17$^{DC-/-}$ compared to WT (Figure 40C). When we re-stimulated medLN cells on anti-CD3ε coated plates and then analyzed intracellular cytokine production by flow cytometry, we found that the ADAM10/17$^{DC-/-}$ had fewer CD4$^+$ IL-13$^+$ and CD4$^+$ IFNγ$^+$ cells compared to WT and ADAM17$^{DC-/-}$ (Figure 40D, E). This suggests that there are fewer T_H1 and T_H2 cells present in the medLN of ADAM10/17$^{DC-/-}$ mice after exposure to *A. alternata*.

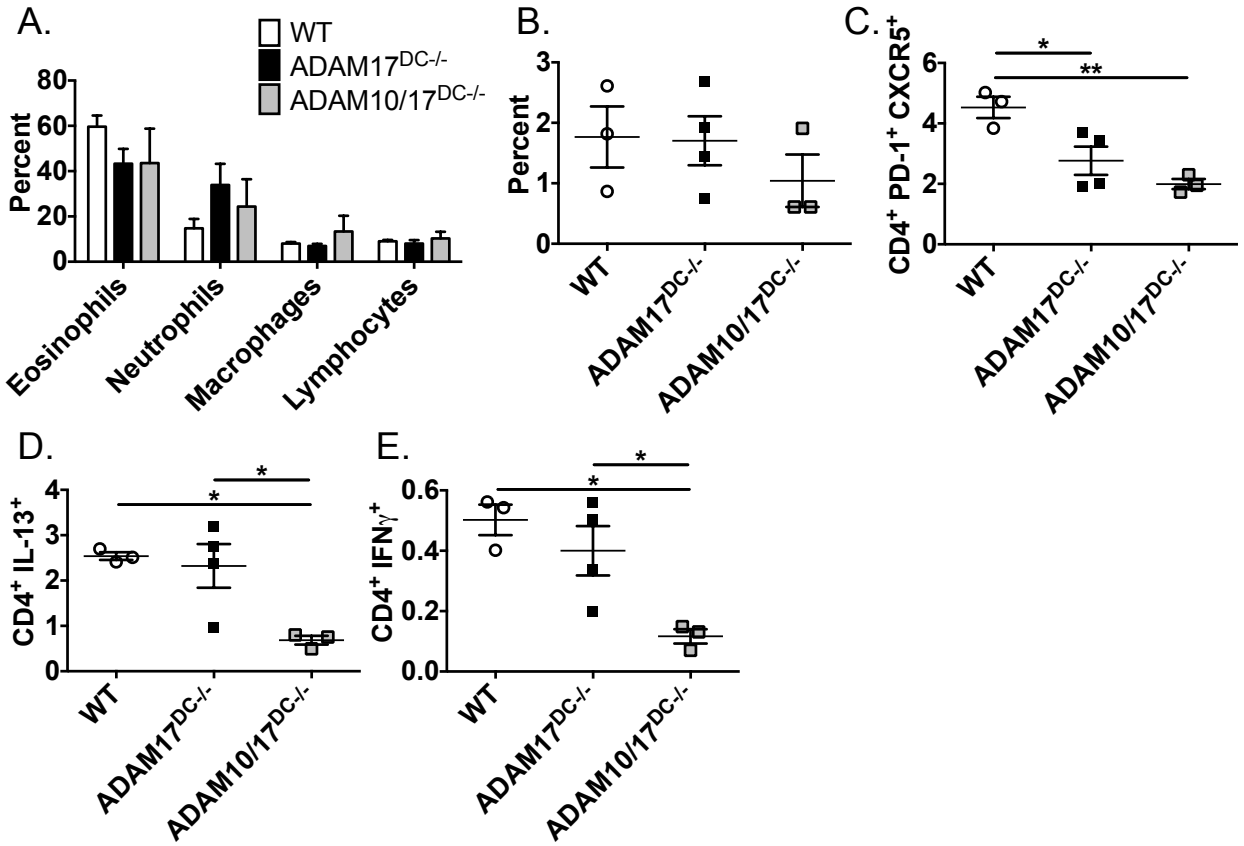

Figure 40: ADAM17$^{DC-/-}$ and ADAM10/17$^{DC-/-}$ with *A. alternata*.

WT, ADAM17$^{DC-/-}$, and ADAM10/17$^{DC-/-}$ mice were given *A. alternata* as previously described. A. BALF was analyzed by flow cytometry for indicated cell types. B. GC B cells (B220^{+} CD95^{+} GL-7^{+}) in the medLN were assessed. C. T_{FH} cells (CD4^{+} PD-1^{+} CXCR5^{+}) were measured in the medLN. D. and E. Cells from medLN were re-stimulated on anti-CD3ε coated plates and intracellular cytokine expression (IL-13 and IFNγ) was assessed by flow cytometry. **p<0.01, *p<0.05, one-way ANOVA with Tukey's post hoc test.

Aspergillus fumigatus model

To extend on the results from the *A. alternata* induced airway inflammation, we utilized another fungal aeroallergen, *A. fumigatus*, which is often associated with severe asthma phenotypes. TNF from inflammatory DCs were found to be critical for T_H17 responses to this fungal allergen[85,127]. As ADAM17 is the principal sheddase of TNF, we might expect this response to be affected. We subjected ADAM17$^{DC-/-}$ and WT mice to an *A. fumigatus* model of airway inflammation[127]. WT and ADAM17$^{DC-/-}$ exhibited similar cell infiltration in the BALF (Figure 41A) and similar GC B cell expansion (Figure 41B). We also did not observe any differences in the percentage of $CD4^+$ T cells that expressed IL-13 or IFNγ after re-stimulation (Figure 41C, D). From these data and Figure 40, we concluded that T_H17 immunity in the airways is not affected by deletion of ADAM17 in DCs.

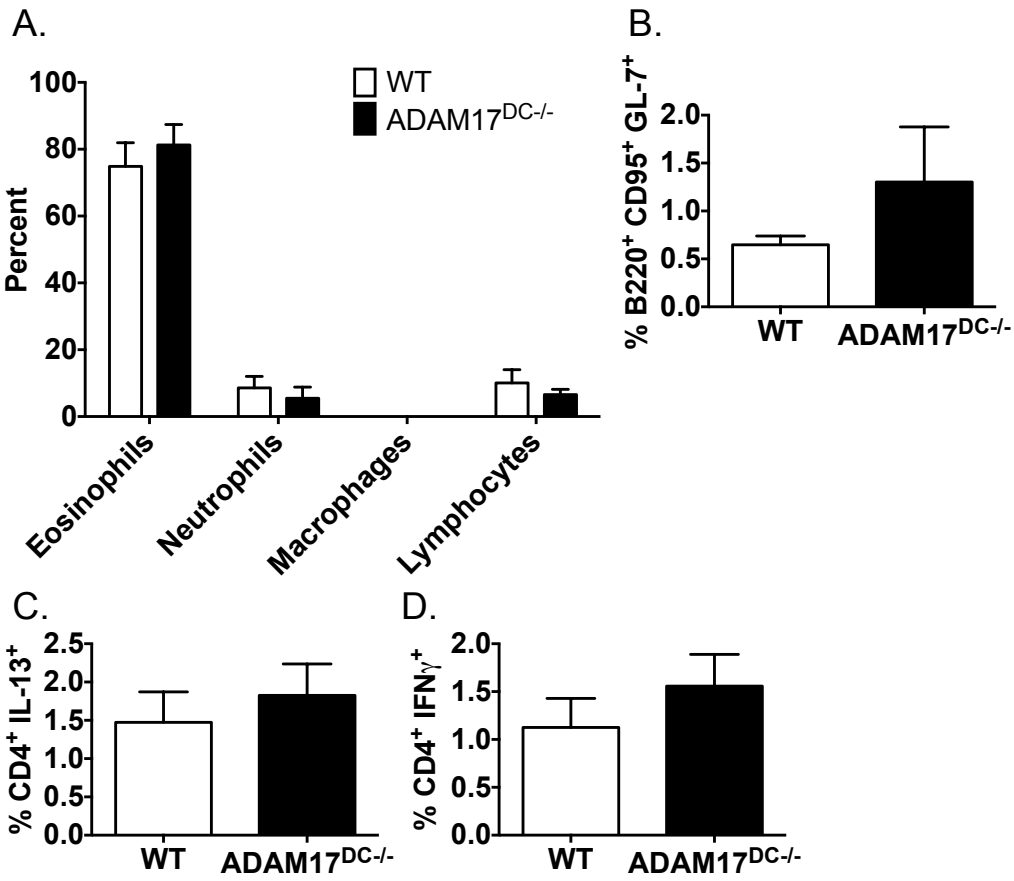

Figure 41: *Aspergillus fumigatus* model in WT and ADAM17$^{DC-/-}$ mice.

WT and ADAM17$^{DC-/-}$ mice were subjected to *A. fumigatus* protocol. A. BALF was examined for eosinophils, neutrophils, macrophages, and lymphocytes by flow cytometry. B. GC B cells (B220^{+} CD95^{+} GL-7^{+}) levels were assessed in the medLN. C. and D. MedLN cells were re-stimulated on anti-CD3ε coated plates and expression of intracellular cytokines, IL-13 (C) and IFNγ (D), were analyzed on CD4^{+} T cells by flow cytometry.

IgG1 immune complex stimulation

Antigen-antibody immune complexes are a critical step in host protection responses to clear pathogens. Immune complexes are also implicated in several human diseases. IgG immune complexes are formed when antigen-specific IgG are bound to antigen, typically with an excess of antibody. These complexes bind to Fcγ receptors (FcγR) on leukocytes, leading to the crosslinking of the FcγR and effector responses. Three classes of FcγRs have been described in mice: FcγRI, FcγRII, and FcγRIII. FcγRI is considered to be a high affinity receptor, whereas FcγRII and FcγRIII are low affinity[128]. IgG1 immune complexes interact almost exclusively with FcγRIII. ADAM17 has been demonstrated to cleave FcγRIII, which is also known as CD16[129,130]. DCs express all three FcγRs, and FcγRIII on DCs has been implicated in increasing antigen presentation to both $CD4^+$ and $CD8^+$ T cells and maturation of DCs[131]. To examine the effect of ADAM17 deletion from DCs on their ability to respond to IgG1 immune complexes, we adoptively transferred violet tracer labeled $CD4^+$ OT-II T cells into WT, $ADAM17^{DC-/-}$, and $ADAM10/17^{DC-/-}$ mice. The next day, we *i.v.* injected OVA-anti-OVA IgG1 immune complexes. After 72h, we assessed the extent of proliferation of the $CD4^+$ OT-II T cells in the spleen as well as the maturation of DCs in the spleen. We found that $ADAM17^{DC-/-}$ and WT had similar proliferation indices, which is estimates the number of cells that have divided disregarding the undivided population. Interestingly, $ADAM10/17^{DC-/-}$ had an increased proliferation index compared to both WT and $ADAM17^{DC-/-}$ (Figure 42A). A representative histogram demonstrated the dilution of the violet tracer in the divided $CD4^+$ OT-II T cells (Figure 42B). We also examined the percentage of cDCs, $CD24^+$ DCs, and $CD172^+$ DCs in the spleen and found a reduction in cDCs in both $ADAM17^{DC-/-}$ and $ADAM10/17^{DC-/-}$ mice compared to WT (Figure

42C). Further, ADAM10/17$^{DC-/-}$ mice had fewer CD24^{+} DCs than WT mice (Figure 42C, D), which was not seen in the ADAM10$^{DC-/-}$ mice (Figure 26).

We then assessed alterations in maturation of the DC subsets or in the expression of other ADAM17 substrates. We found that ADAM17$^{DC-/-}$ had reduced expression of costimulatory molecules CD86 and ICOSL on CD172^{+} DCs as well as less MerTK expression (Figure 43A). ADAM10/17$^{DC-/-}$ had similar levels of costimulatory molecules, but trending reduction in CD16 expression (Figure 43A). Similar trends were found when examining CD24^{+} DCs, but they were more exaggerated in some cases. ADAM17$^{DC-/-}$ had a greater reduction in CD86 and ICOSL (Figure 43B). These results are intriguing, but further study is necessary to understand if the alterations seen are biologically significant. Also, assessing the stimulation of CD8^{+} OT-I T cells may reveal additional consequences of ADAM17 deletion from DCs.

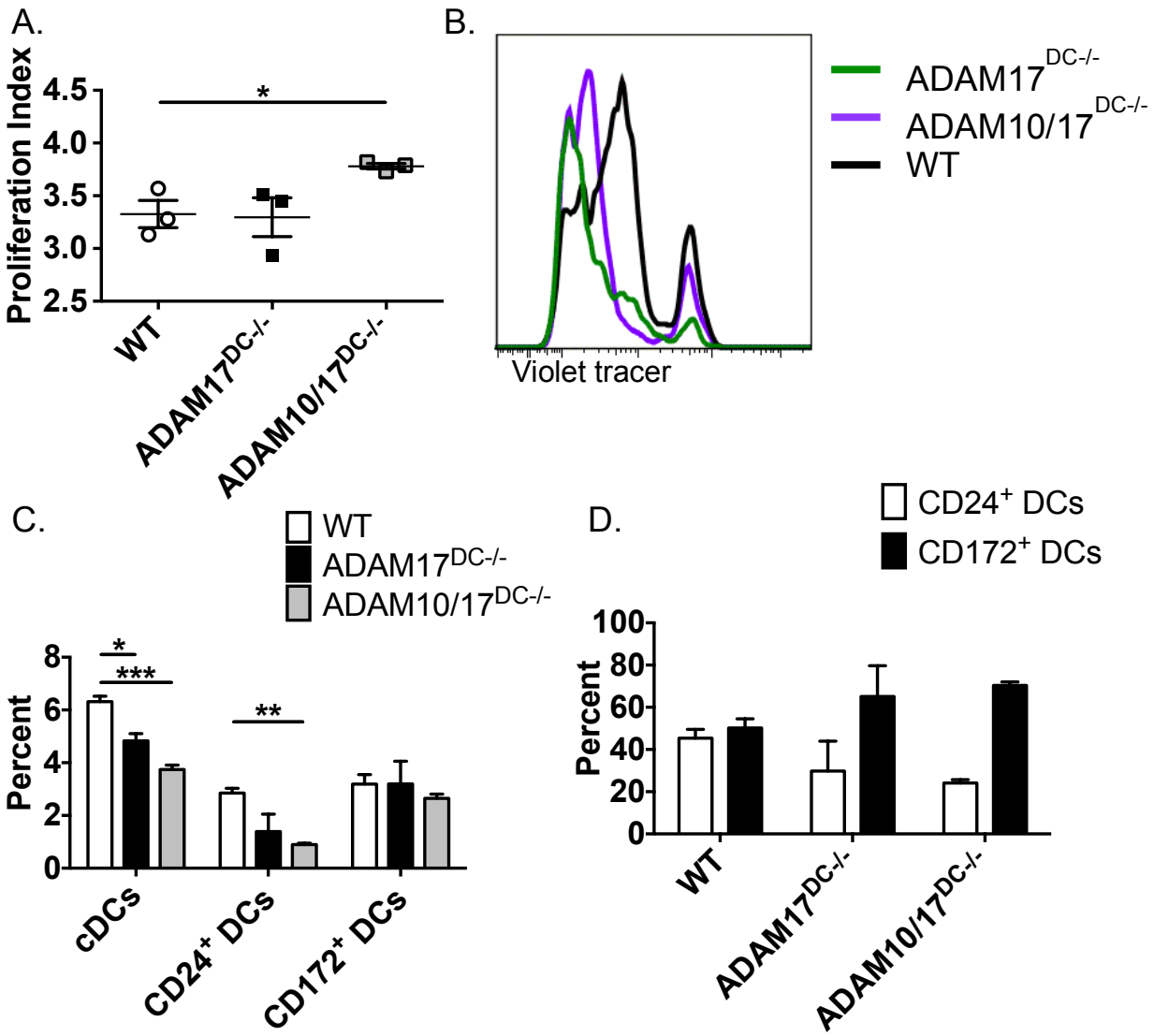

Figure 42: IgG1 immune complexes stimulation is enhanced in ADAM10/17$^{DC-/-}$ mice.

Violet tracer labeled CD4^{+} OT-II T cells were adoptively transferred into WT, ADAM17$^{DC-/-}$, or ADAM10/17$^{DC-/-}$ mice followed by OVA-anti-OVA IgG1 immune complexes *i.v.* A. Dilution of the proliferation dye in transferred cells in the spleen was assessed by flow cytometry. Proliferation index was calculated. B. Representative histogram for violet cell trace on CD4^{+} OT-II T cells in the spleen. C. and D. cDCs, CD24^{+} DCs, and CD172^{+} DCs were examined in the spleen as percent of live cells (C) and as percent of cDCs (D). ***p<0.001, **p<0.01, *p<0.05, two way ANOVA with Tukey's post hoc test.

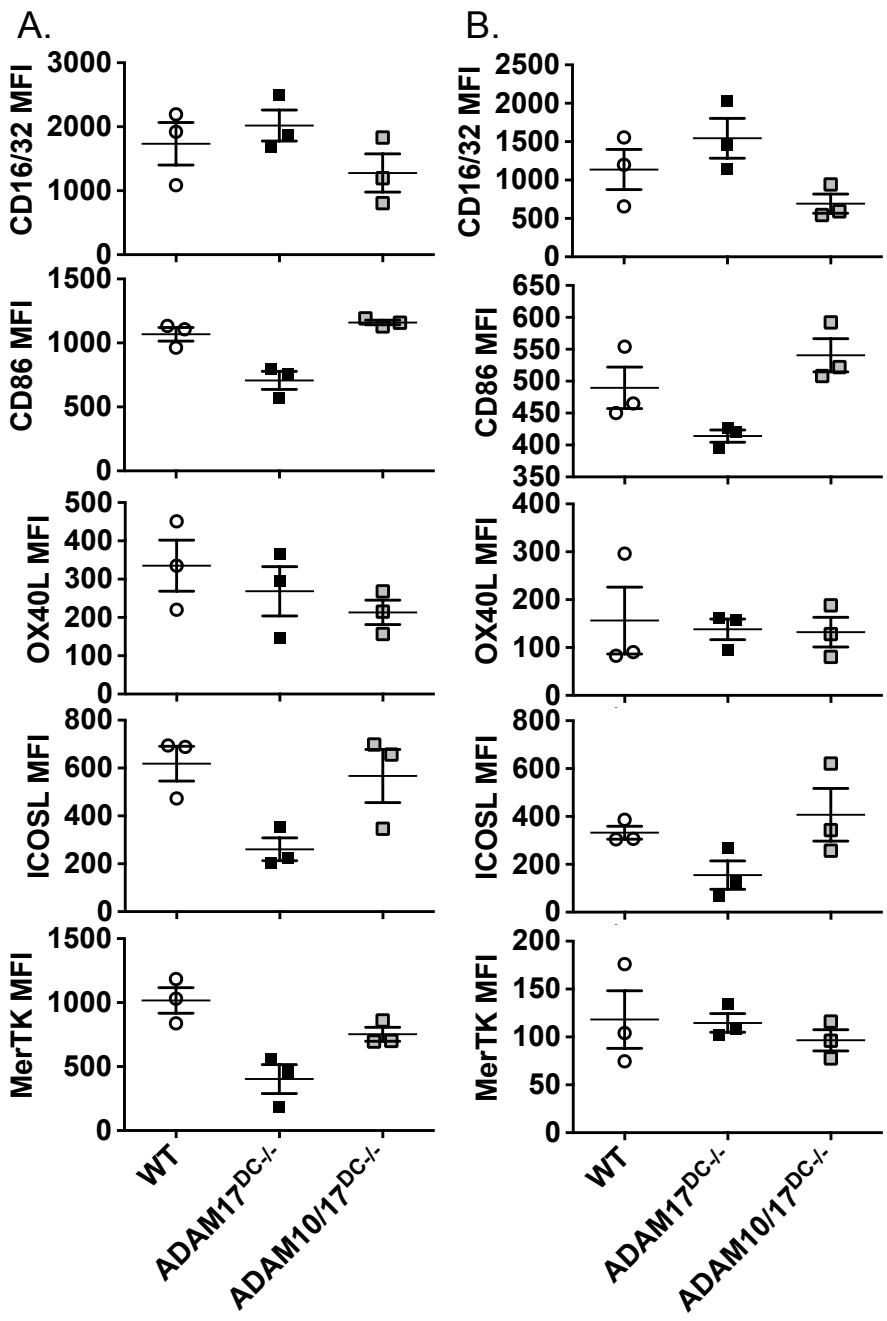

Figure 43: Expression of surface and costimulatory molecules on DCs is altered in ADAM17$^{DC-/-}$ and ADAM10/17$^{DC-/-}$ mice.

Indicated surface molecule expression on CD172^{+} (A) and CD24^{+} (B) DCs from WT, ADAM17$^{DC-/-}$, and ADAM10/17$^{DC-/-}$ mice after immune complex stimulation.

1.3.4 Discussion

ADAM17 is a member of the ADAM family of metalloproteinases and is expressed in many tissues and cell types. It is best known for its cleavage of inflammatory molecules, including TNF. In the immune system, when ADAM17 is deleted from DCs, we see a subtle phenotype. However, when ADAM10 and ADAM17 are both removed from DCs, we find decrease in the activation of several immune responses. In humoral immunity, we see fewer GC B and T_{FH} cells in ADAM10/17$^{DC-/-}$. And in cellular immunity, we demonstrate fewer IL-13^{+} and IFNγ^{+} CD4^{+} T cells after exposure to the environmental fungal allergen, *A. alternata*. Interestingly, these phenotypes are distinct from the ADAM10$^{DC-/-}$ and the ADAM17$^{DC-/-}$ mice.

When we examined antigen presentation in ADAM17$^{DC-/-}$ and ADAM10/17$^{DC-/-}$ mice we found similar levels of proliferation of antigen specific CD4^{+} T cells in the medLN of all genotypes (Figure 37A). These results are similar to the ADAM10$^{DC-/-}$ mice; however, we did not observe any alterations in costimulatory molecules on DCs in the ADAM17$^{DC-/-}$ and ADAM10/17$^{DC-/-}$ mice (Figure 37C). ADAM10-deficient DCs expressed less OX40L compared to WT (Figure 30E). Though we did not assess cytokine production in T cells in the antigen presentation assay as we had done with the ADAM10$^{DC-/-}$. We did analyze cytokine expression in CD4^{+} T cells in re-stimulated medLN after *A. alternata* immunization. Similar to the reduced CD4^{+} IL-13^{+} population in the ADAM10$^{DC-/-}$ mice both in antigen presentation (Figure 30F-H) and *A. alternata* (Figure 23C) models, ADAM10/17$^{DC-/-}$ mice had fewer CD4^{+} IL-13^{+} cells after *A. alternata*. ADAM17$^{DC-/-}$ mice had levels equivalent to WT (Figure 40D). Interestingly, ADAM10/17$^{DC-/-}$ also had fewer CD4^{+} IFNγ^{+} cells, which is in contrast to both ADAM10$^{DC-/-}$ (Figure 23C) and ADAM17$^{DC-/-}$ (Figure 40E).

Given the similarity in IL-13-producing $CD4^+$ T cells between $ADAM10^{DC-/-}$ and $ADAM10/17^{DC-/-}$ mice, we expected that the eosinophils in the BALF would also be comparable. However, $ADAM10/17^{DC-/-}$ did not have a reduction in eosinophils (Figure 40A) with *A. alternata* as $ADAM10^{DC-/-}$ mice did (Figure 23A). In a model of acute allergic airway inflammation, ADAM17 inhibitors blocked neutrophil and eosinophil recruitment into the BALF[132], thus it would be expected that $ADAM17^{DC-/-}$ and $ADAM10/17^{DC-/-}$ would have reductions in these populations as well. However, the ADAM17 inhibitor was administered i.n. and acted on epithelial cells and other leukocytes. ADAM17 in these cells has both pro and anti-inflammatory action in the lungs. ADAM17 activity in epithelial cells increases their chemokine expression[133]. In contrast, ADAM17 *in vitro* acted as a negative regulator of airway inflammation[134].

Overall we have evidence that ADAM17 is important in immune responses though the precise mechanisms are not well understood. We have observed unique phenotypes of $ADAM10^{DC-/-}$, $ADAM17^{DC-/-}$, and $ADAM10/17^{DC-/-}$ mice using several different immunization models. These data indicate that further study is required to understand the ADAM17 substrates and the role they play in immune responses.

Chapter 4: B1 cell IgE impedes B2 cell IgE-mediated mast cell degranulation and parasite expulsion.

1.4.1 Introduction

IgE is an evolutionarily conserved immunoglobulin that is well known for causing the symptoms of atopic disease. This antibody class, despite having a half-life of less than a day in plasma, can persist for weeks to months when bound to cell surface FcεRI, making it a long-lasting "gate-keeper" particularly with respect to triggering mast cells (MCs) or basophils[135]. Specific IgE responses directed against innocuous particles, such as pollen, cat dander, or peanut proteins, can result in allergic disease. IgE-mediated responses range from mild to severe. They can be either site-directed such as allergic rhinitis, atopic dermatitis, urticaria, and asthma, or systemic, as in anaphylactic shock. IgE^+ plasma cells generated in the GCs that produce high affinity IgE to antigens are purported to come from bone marrow (BM) derived B cells or B2 cells through immunoglobulin class switch recombination (CSR) and somatic hyper mutation (SHM). In contrast, memory IgE responses are generated from $IgG1^+$ memory B cells[135,136].

The importance of parasite specific IgE in controlling infection is controversial, yet there is evidence to support IgE-mediated clearance of phylogenetically distinct helminths such as *Schistosoma mansoni* and *Trichnelia spiralis*[135,137,138]. These parasites strongly promote IgE synthesis[139]. Despite high levels of IgE in helminth infected individuals, the prevalence of allergic disease is reduced in some populations with endemic helminth infection[140–143]. In this work, we showed that poly-specific IgE made by B1 cells was responsible for reduced MC degranulation by mechanism of IgE saturation of FcεRI that was first proposed by Bazaral et al.[144].

B1 cells develop early in ontogeny, prior to the first hematopoietic stem cell (HSC), and are derived initially from the fetal yolk sac and then from the fetal liver[145]. They are delineated from B2 cells by the expression of CD11b and absence of CD23 on cells that reside primarily in the pleural and peritoneal body cavities of mice and that traffic to the draining LNs, spleen, and mucosal sites upon activation[145–148]. B1 cells are important immune effectors and regulators of adaptive immunity like other lymphocytes that bridge the innate and adaptive immune systems, such as ILCs, MZBs, and γδ T cells[145,148–152]. The B cell receptor (BCR) repertoire in these cells is enriched for poly-specific receptors with low-affinities to a broad range of antigens encoded in the germline[153]. B1 cells are essential IgM secretors, and have additionally been shown to be the definitive source of 'natural' IgM. As immune effectors, they secrete IgA at mucosal sites. However, only a few reports have demonstrated IgE production by B1 cells[145,154–156].

N. brasiliensis and *H. polygyrus bakeri* are T_H2 inducing helminth parasites of mice similar to the human hookworms, *Necator americanus* and *Ancylostoma duodenale*[157]. WT mice are able to clear these infections in a T cell-dependent manner, relying on the cytokines IL-13 and IL-4 for the 'weep and sweep' of intestinal helminth clearance[45,158]. This refers to the increased mucus production, goblet cell hyperplasia, and enteric nerve stimulation associated with intestinal parasite expulsion[45,158]. Utilizing these intestinal helminths, we demonstrated that B1 cells are capable of CSR to IgE and synthesis of large amounts of polyclonal IgE. In addition, the signals that drive B1 cells to IgE production and the functional relevance of B1 cell IgE in parasite-host interactions were examined.

1.4.2 Materials and Methods

1.4.2.1 Design

Research Subjects-Each experiment was performed in a controlled laboratory environment. Mice were utilized equally from barrier and non-barrier mouse vivaria. Sex was randomized between groups in all experiments and did not show a differential analysis when analyzed by the sexes (data not shown). Ages of mice used were between 6 and 16 weeks. *Blinding*-The animal caretakers were blinded to the assigned groups. Investigators were not blinded to the interventions, *Replicates*- Each experiment was conducted with two to three independent replicates. *Sample Size*-Sample size was determined by previous work with the helminth *N. brasiliensis* and *H. polygyrus bakeri*.

1.4.2.2 Mice

Mice were kept at VCU in accordance with the humane treatment of laboratory animals sets forth by the National Institutes of Health and the American Association for the Accreditation of Laboratory Animal Care. C57BL/6 ADAM10Tg mice were generated by the VCU Transgenic Mouse Core, as previously described[159]. C57BL/6 WT mice were purchased from The Jackson Laboratory. $Rag1^{-/-}$ mice were purchased from The Jackson Laboratory and maintained as above. $IgE^{-/-}$ mice were a generous gift from Drs. Hans Oettgen and Mitch Grayson and were maintained as above[160]. All mouse protocols were approved by the VCU Institutional Animal Care and Use Committee.

1.4.2.3 Flow Cytometry and Cell Sorting

Peritoneal lavage was collected and washed in FACS buffer (PBS, 0.1% BSA, and 2mM EDTA). Mesenteric lymph nodes were collected, pulled apart with tweezers, and flushed through a 40µm mesh cell strainer. Samples were blocked on ice for 10 minutes with Fc block (2.4G2, in house).

Anti-mouse antibodies were then added at concentrations according to manufacturer's protocol. Samples were then washed with FACS buffer. For flow cytometry analysis, samples were run on the BD LSRFortessa (BD Biosciences, San Jose, CA) and for cell sorting, the BD FACSAria II (BD Biosciences, San Jose, CA), both with Diva software in the VCU Flow Cytometry Core. Data was analyzed with Flowjo v7.6.5 software (FlowJo, LLC, Ashland, OR). Anti-mouse antibodies used were Pe-Cy7 conjugated anti-CD11b (M1/70), BV421 conjugated anti-CD23 (B3B4), APC conjugated anti-B220 (RA3-6B2), PE conjugated anti-CD4 (GK1.5) or anti-CD138 (281-2), and FITC conjugated anti-CD3ε (500A2), all from Biolegend, San Diego, CA.

1.4.2.4 Cell Culture and Reagents

Cells were counted and plated in cRPMI 1640 containing 10% FBS, 2mM L-glutamine, 50μM 2-mercaptoethanol, 100 U/mL penicillin, 100g/mL streptomycin, 1mM HEPES (Quality Biological, Gaithersburg, MD), and 1mM sodium pyruvate (Corning Cellgro, Tewksbury, MA). Cells were cultured with or without 10ng/mL rIL-4 (PeproTech, Rocky Hill, NJ), 2μL/mL anti-CD40 (HM40-3) (Biolegend, San Diego, CA), 300ng/mL rIL-5, 50 ng/mL IL-33[161,162], and the indicated concentrations of rIL-25 (PeproTech, Rocky Hill, NJ). Depending on the experiment, cell-free supernatants were harvested at days 5, 7, or 9 or cells were harvested at day 4 or 5. For *in vivo* experiments with IL-33, rIL-33 was injected *i.p.* daily at 2μg/mouse for 7 days prior to sorting.

1.4.2.5 ELISA

ELISA for total IgE, IgG1 and IgM levels was done as described previously[163]. Briefly, plates were coated with 5μg/mL of rat anti-mouse IgE (clone B1E3, in house) in BBS (0.15 sodium chloride, 0.01M borate buffer, pH 9.5), blocked (PBS with 0.02% Tween-20 and 2% FBS), detected with biotinylated rat anti-mouse IgE (R1E4, in house) and streptavidin-alkaline

phosphatase (Southern Biotech, Birmingham, AL). Plates were developed with phosphate tablets (Sigma-Aldrich, St. Louis, MO) dissolved in substrate buffer (0.1g $MgCl_2.6H_2O$, 0.2 NaN_3, 50mL diethanolamine, pH to 9.8 per 500mL). Absorbance was measured at 405nm-650nm[163]. For total IgG1 levels, plates were coated with 5μg/mL of goat-anti mouse IgG1 and detected with goat anti-mouse IgG1-AP (Southern Biotech, Birmingham, AL)[50]. For total IgM levels, plates were coated with 5μg/mL of goat-anti mouse IgM and detected with goat anti-mouse IgM-AP (Southern Biotech, Birmingham, AL). For NP-specific ELISAs, plates were coated with NP_{25}BSA for total affinity and NP_4BSA for high affinity antibody measurement (Biosearch Technologies, Petaluma, CA) and detected as with total immunoglobulin assays[164,165]. Fold IgE (Figure 50) was calculated for each replicate by dividing the condition with anti-CD40, IL-4, ± IL-5, and IL-25 (for each dose) by the cells sorted from the same mouse without IL-25.

1.4.2.6 qRT-PCR

Cells were isolated and total RNA was extracted using TRIzol reagent (Invitrogen, Waltham, MA). RNA was reverse-transcribed using Superscript IV (Invitrogen, Waltham, MA). Control RNA samples were made without adding Superscript IV, but utilizing the same temperature protocol to account for contaminating DNA. 20ng of RNA were used per reaction in duplicate. Each sample was run and compared to its control sample. Primers used with Power Up SYBR Green (Invitrogen, Waltham, MA) qRT-PCR assay were purchased from Integrated DNA Technologies. Primers and Taqman probes (LifeTech) are listed in Table 6. The qPCR was run using QuantStudio 3 real-time PCR system and software (ThermoFischer Scientific).

1.4.2.7 Nippostrongylus brasiliensis, Heligmosomoides polygyrus bakeri infection models, and T cell depletion

N. brasiliensis and *H. polygyrus bakeri* were maintained and mice were inoculated as described in Section 1.1.2. Mice were monitored for eggs per gram of feces (EPG) as described[158,166,167]. For T cell depletion, mice were injected *i.p.* with 200µg anti-CD4 (GK1.5-in house) and anti-CD8 (2.43-in house) antibodies on days -3, -2, -1, 0, 5, and 10[166].

Anaphylaxis models and N. brasiliensis excretory-secretory extract (NES)

Active cutaneous anaphylaxis (ACA)[168] and passive cutaneous anaphylaxis (PCA)[169] models were performed as previously described with the following modifications: intradermal spotting was done on the pre-shaven flank, spot size was measured on the back, and back skin was collected for formamide extraction[168]. NES extract was generated from adult worms as previously described[45].

1.4.2.8 Rag1$^{-/-}$ Reconstitution

Naïve Rag1$^{-/-}$ mice were maintained in a barrier vivarium[163]. All mice were *i.v.* reconstituted with 5 x 10^6 CD4$^+$ T cells isolated by B220$^+$ depletion, followed by STEM Sep Mouse CD4$^+$ T cell enrichment kit (StemCell Technologies, Vancouver, BC) per manufacturer's instructions from the spleens of WT C57Bl/6 mice. Indicated mice were *i.v.* reconstituted with 10 x 10^6 naïve B2 cells isolated by depletion with anti-mouse CD43 Miltenyi microbeads (Miltenyi Biotec, San Diego, CA) or with biotinylated anti-mouse CD43 (Biolegend, San Diego, CA) followed by anti-biotin microbeads (Miltenyi Biotec, San Diego, CA) from the spleens of WT C57Bl/6 mice. Indicated mice were *i.p.* injected with 2 x 10^5 to 4 x 10^5 (indicated in individual experiments) isolated from the peritoneal and pleural cavities of WT C57Bl/6 mice according to described protocol. First, the peritoneal cells were Fc blocked on ice for ten mins (2.4G2, in house)

followed by biotinylated anti-mouse CD23 (B3B4), anti- mouse CD49b (DX5), anti-mouse F4/80 (BM8), anti-mouse CD90.2 (30-H12), and anti-mouse Gr-1 (RB6-8C5), (Biolegend, San Diego, CA) for 30 min on ice. Cells were washed and anti-biotin microbeads (Miltenyi Biotec, San Diego, CA) were added and B1 enrichment was performed according to manufacturer's instructions. At least one week after reconstitution, mice were bled and cells evaluated by flow cytometry to verify reconstitution of T cells, B2 cells, or the absence of B2 cells and then experiments were performed.

1.4.2.9 Statistical analysis

Error bars represent the standard error of the mean (SEM). A horizontal line with a symbol representing the p value indicates statistical comparison. For pairwise comparisons, Mann-Whitney tests were performed for non-normally distributed data, and Student's t-tests were performed for normally distributed data. For multiple comparisons, Kruskal-Wallis tests with Dunn's post hoc were performed for non-normally distributed data, and one-way ANOVA test with Tukey's post hoc were performed for normally distributed data. All tests are noted in figure legends. A p value of <0.05 was considered significant. All statistical analysis was performed with GraphPad Prism 6.

Table 6: Primers and probes

Primer/Probe	**Sequence/Product #**[3]
secreted IgE F	GTCGCCTAGAGGTCGCCAAG
secreted IgE R	CATCCACCTTCCCCACCACAGC
secreted IgG1 F	TGCACAACCACCATACTGAGA
secreted IgG1 R	GGGTGGAGGTAGGTGTCAGA
Actb (β-actin) F	CAATAGTGATGACCTGGCCGT
Actb (β-actin) R	AGAGGGAAATCGTGCGTGAC
Adam10	Mm00545742_m1
Actb (β-actin)	Mm99999915_m1

[3] Product number for Taqman probes purchased from LifeTech.

1.4.3 Results

B1 cells make large amounts of IgE in response to helminth infection

In our laboratory, we generated mice that lack bone marrow (BM) derived B cells, or B2 cells[159]. This is due to overexpression of ADAM10 at the common lymphoid progenitor stage that leads to improper Notch signaling and loss of B cell development[159]. Because this defect is restricted to the BM, the B1 cell compartment is intact[159]. To study the B1 cell antibody response during a helminth-induced T_H2 response, ADAM10Tg and WT control mice were inoculated with 650 *N. brasiliensis* or 200 *H. polygyrus bakeri* infective third-stage larvae (L3). We measured the amount of IgE and IgG1 antibody in the serum. Interestingly, there was no significant difference in IgE production between WT and ADAM10Tg mice infected with either helminth, despite the ADAM10Tg mice lacking B2 cells (Figure 44A, B). This suggested B1 cells were able to produce significant levels of IgE post helminth infection in the absence of B2 cells. Interestingly, IgE production was seen even though significantly less serum IgG1 was measured in ADAM10Tg mice (Figure 44A). ADAM10Tg mice, have an increased number of immature myeloid cells throughout the organs and circulation due to the defect in hematopoiesis[159]. These cells were selectively depleted utilizing Gemcitabine (GEM) to assess if they played a role in enhancing B1 cell IgE[166,170,171]. *N. brasiliensis*-infected and GEM treated mice exhibited no change in IgE levels (Figure 44A), indicating an inconsequential role of immature myeloid cells on B1 cell IgE antibody production. To ensure that this difference was not due to ADAM10 overexpression, B1 cells were sorted from the peritoneal cavity of WT or ADAM10Tg mice (Figure 45A) and *Adam10* message was measured by qPCR. *Adam10* expression in B1 cells does not differ between WT and ADAM10Tg mice indicating that this was not a reason for the significant levels of IgE made by B1 cells (Figure 45B).

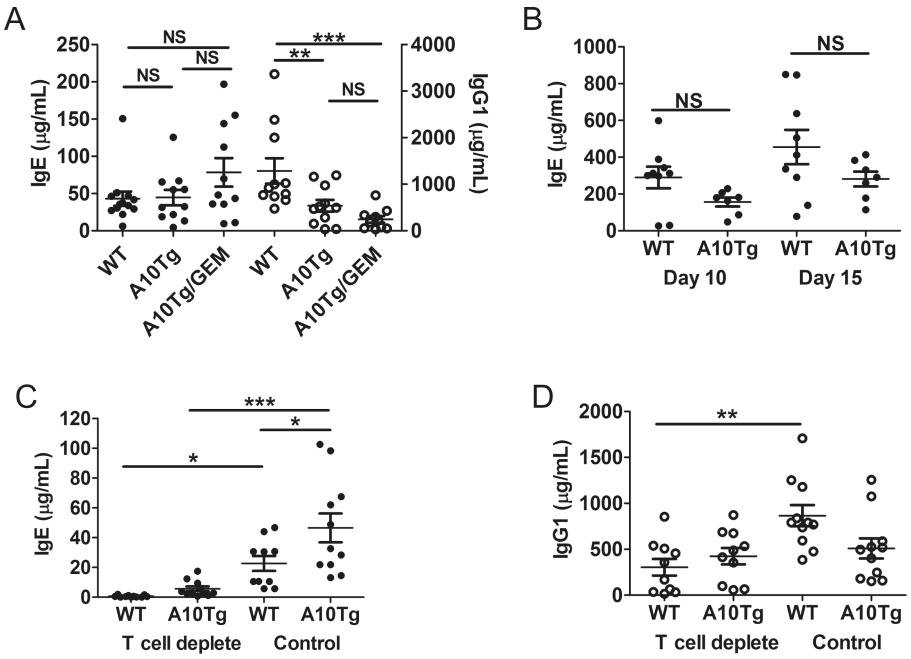

Figure 44: B1 cell IgE is induced with T cell help during helminth infection.

A. Total serum IgE and IgG1 was measured on day 14 post *N. brasiliensis* inoculation and (B) total serum IgE was measured by ELISA on days 10 and 15 after *H. polygyrus bakeri* inoculation in ADAM10Tg (A10Tg) and wild type (WT) mice. Gemcitabine (GEM) drug treatment was used to deplete MDSCs every 5 days. Closed circles are measured on the left Y-axis and open circles are measured on the right Y-axis. C. and D. Mice were T cell depleted using anti-CD4 (GK1.5) and anti-CD8 (2.43) (both 200μg/injection *i.p.*) on days -2, -1, 0, 5, and 10 of *N. brasiliensis* infection or control IgG. Serum was collected on day 14 post inoculation. Total serum IgE (A) and IgG1 (B) were measured by ELISA. NS=not significant, *$p<0.05$. **$p<0.01$, ***$p<0.001$. The error bars represent ± SEM. (A) is representative of three independent experiments. (B), (C), and (D) are representative of two independent experiments. Significance was determined using a one-way ANOVA with Tukey's post hoc test.

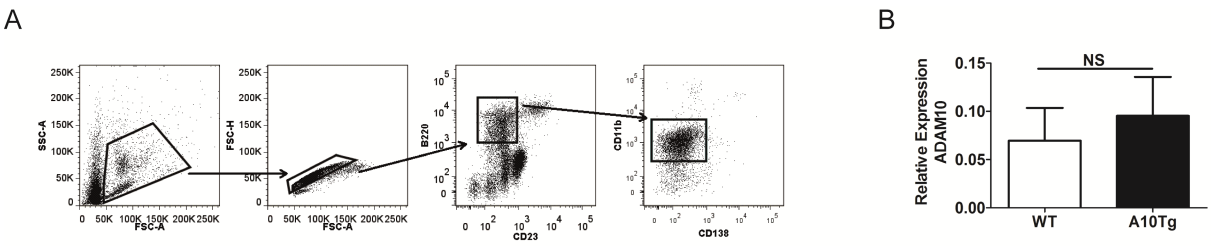

Figure 45: ADAM10 message is not overexpressed on ADAM10Tg B1 cells.

B1 cells were sorted from the peritoneal lavage fluid of mice utilizing the gating strategy illustrated in (A). B. *Adam10* message was measured in WT and ADAM10Tg (A10Tg) B1 cells from mice infected with *N. brasiliensis* directly after sorting. ADAM10 message is normalized to *Gapdh*. n=4 pooled experiments/group and statistical comparison was performed with a Man-Whitney non-parametric analysis. NS=not significant. Error bars represent ± SEM.

B1 cell IgE production during helminth is T cell dependent

To assess whether helminth-induced B1 cell IgE production required T cells, we depleted both $CD8^+$ and $CD4^+$ T cells with injection of GK1.5 and 2.43 antibodies, respectively, starting 5 days prior to inoculation with *N. brasiliensis* and confirmed the cell depletion by flow cytometry[166]. Both WT and ADAM10Tg mice had significantly reduced IgE and IgG1 production after T cell depletion (Figure 44C, D). A baseline level of IgE and IgG1 remained in both WT and ADAM10Tg mice despite the loss of T cells (Figure 44C, D).

B1 cell antibody production induced after NP-KLH immunization is poly-specific

We next examined the antigen specificity of B1 cell IgG1 in the ADAM10Tg mouse. Mice were immunized *i.p.* with NP_{31}-KLH in alum and both high affinity IgG1 antibody (NP_4) and total affinity IgG1 antibody (NP_{25}) were assessed in serum by ELISA[164,165]. On day 14 post immunization, ADAM10Tg mice have almost undetectable high or total affinity IgG1 antibody specific for the NP hapten despite having measurable total IgG1, though significantly less than in WT mice (Figure 46A). An antigen boost at 28 days after the original immunization induced high affinity IgG1, total affinity IgG1, and total IgG1, in WT but not ADAM10Tg mice (Figure 46B, C).

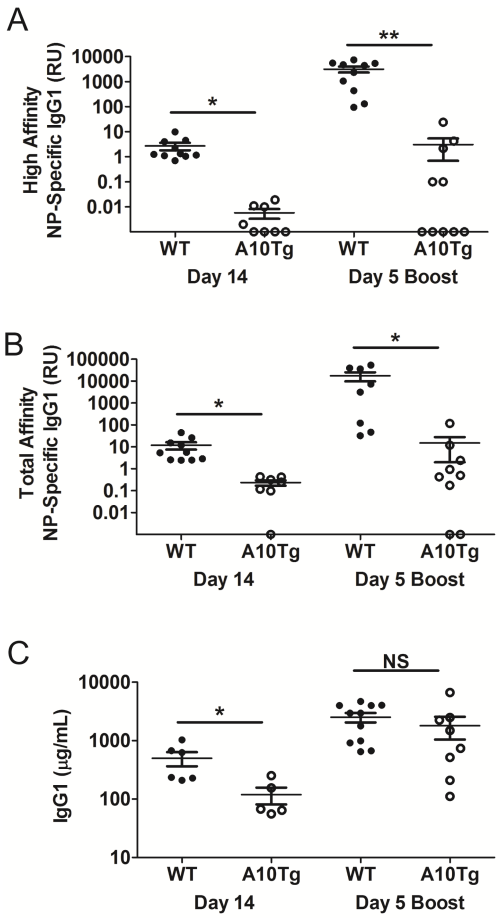

Figure 46: B1 cell antibody responses to NP-KLH are poly-specific.

ADAM10Tg (A10Tg) and WT mice were immunized *i.p.* with NP_{31}-KLH in alum. High affinity (NP_4-specific IgG1) (A), total affinity (NP_{25}-specific IgG1) (B), and total IgG1 (C) were measured in the serum by ELISA on day 14 and day 5 post boost. NS=not significant, *$p<0.05$, **$p<0.01$. Error bars represent ± SEM. Significance was determined using Student's t test between WT and A10Tg. This is data from three independent experiments.

B1 cell-derived IgE blocks MC degranulation post-helminth infection

A major function of antigen specific IgE is to induce degranulation through FcεRI on primarily MCs and to lesser extents, basophils. To measure the antigen specificity of B1 cell IgE, as well as examine the ability of B1 cell antibody to induce degranulation, we used a model of active cutaneous anaphylaxis (ACA). Both ADAM10Tg and WT mice were immunized[168] and challenged intradermally (i.d.) with ovalbumin (OVA) followed by *i.v.* injection of Evan's blue dye solution. MC degranulation was induced by the circulating OVA crosslinking antigen specific IgE molecules bound to FcεRI on skin MCs, resulting in vasodilation and leakage of the dye from vessels creating a blue spot. Measurement of the area of the spot in WT mice indicated significantly increased MC degranulation compared to ADAM10Tg mice (Figure 47A, B) despite robust and equivalent total IgE and IgG1 (Figure 47C, D) in the serum of both groups of mice. This indicated that the B1 cell IgE induced with this antigen in alum is not OVA-specific. Next, blocking of specific IgE to FcεRI by helminth-induced B1 cell antibody was tested in a model of passive cutaneous anaphylaxis (PCA). ADAM10Tg and WT mice were inoculated with *N. brasiliensis* and injected i.d. with IgE anti-DNP 21 days later. This was followed 24 hours later with a challenge *i.v.* of OVA-DNP mixed in an Evan's blue dye solution to measure DNP-specific degranulation (Figure 47E, F). All uninfected control mice had equivalent degranulation indicating that skin MC activation was normal, but the amount of MC degranulation seen in both ADAM10Tg and WT mice was significantly reduced by helminth infection (Figure 47E, F), reinforcing the ability of poly-specific B1 cell IgE to block specific IgE. Total IgE levels in these mice were equivalent and increased during helminth infection (Figure 47G). Total IgG1 levels were elevated in WT mice after helminth infection, but not significantly in ADAM10Tg mice (Figure 47H).

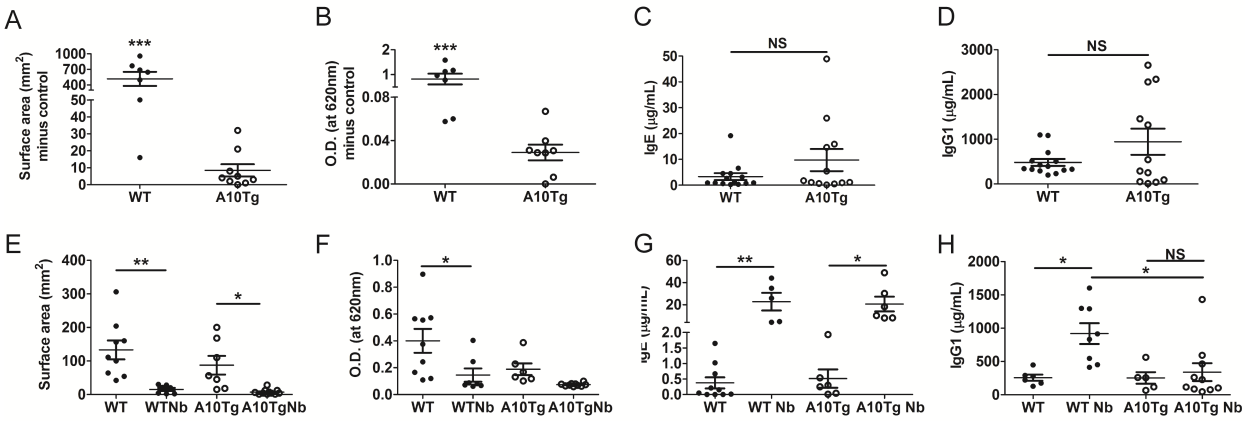

Figure 47: B1 cell antibody blocks mast cell degranulation by specific IgE.

ADAM10Tg (A10Tg) and WT were immunized with OVA in alum in an Active cutaneous anaphylaxis (ACA) model. After intradermal (i.d.) challenge, mast cell degranulation was measured by dye release into the back skin as surface area of the (A) spot and (B) dye extraction from the spot, both minus the negative control spot. Total (C) serum IgE and (D) serum IgG1 antibody as measured at the time that mice were exposed to ACA. Passive cutaneous anaphylaxis (PCA) model was run on day 21 post *N. brasiliensis* (Nb) inoculation of mice or naïve mice. (E) Surface area of the spot or (F) dye extraction from the spot was measured. Total (G) serum IgE and (H) serum IgG1 antibody as measured at the time that mice were exposed to PCA. ***p<0.001, **p<0.01, *p<0.05. Error bars represent ± SEM. Significance was determined using a one-way ANOVA with Tukey's post hoc test.

B1 cells are primed to make IgE during helminth infection

To investigate the signals necessary to help B1 cells switch to IgE, B1 cells were sorted from the peritoneal cavities of WT mice in the naïve state or 14 days after inoculation with *N. brasiliensis* (Figure 45). Both IL-4 and anti-CD40, which simulate CD40L stimulation, were required for B1 cell IgE production (Figure 48A). Naïve B1 cells make little IgE when treated with anti-CD40 and IL-4, but the addition of IL-5 significantly increased IgE production, and the proliferation of these cells[172,173]. Interestingly, B1 cells from mice infected with *N. brasiliensis* made significantly more IgE with anti-CD40 and IL-4 that was independent of cell proliferation compared to B1 cells sorted from naïve mice (Figure 48A, B). In addition, B1 cells from mice infected with *N. brasiliensis* had increased sensitivity to IL-5 induced proliferation and IgE production (Figure 48A, B). Overall, this indicated that B1 cell IgE was stimulated *in vitro* by similar signals as B2 cell-induced IgE, however, other signals may be priming B1 cells for increased IgE production during infection with *N. brasiliensis*. Since B1 cells are known to secrete large amounts of IgM, IgM production by both B1 and B2 cells was compared in culture. B1 cells from *N. brasiliensis* infected mice treated with anti-CD40, IL-4, and ± IL-5 made significantly more IgM than similarly treated B2 cells from infected mice, supporting the notion that B1 cells were being examined (Figure 49).

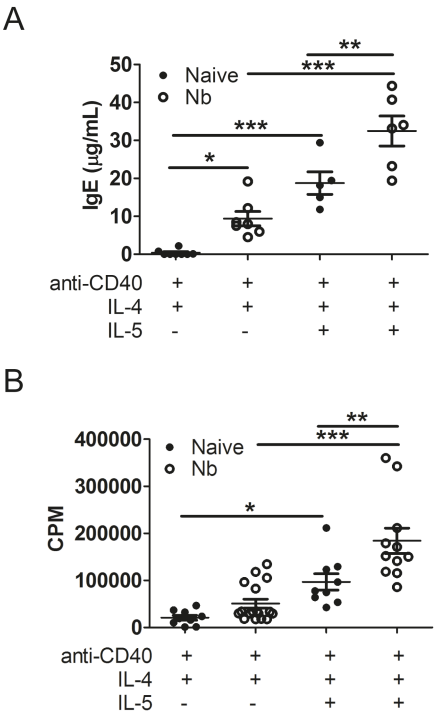

Figure 48: IL-5 induced B1 cell IgE production after helminth infection.

B1 cells were sorted ($CD23^{-}B220^{int}$ $CD11b^{int}$ $CD138^{-}$) (Figure 45 shows gating) from the peritoneal lavage of mice infected with *N. brasiliensis* (day 14) or naïve WT mice. A. 30,000 cells/mL were cultured with anti-CD40, IL-4, and/or IL-5. Supernatants were harvested on day 9 of culture for total IgE ELISA. B. 60,000 cells/mL were cultured as above for 72 hours, followed by the addition of 1µCi/mL [^{3}H]-thymidine, and after 24 hours later these cells were harvested onto GFC plates and read on a TopCount plate reader. CPM=counts per minute. *$p<0.05$ **$p<0.01$ ***$p<0.001$. Error bars represent ± SEM. Significance was determined using a one-way ANOVA with Tukey's post hoc test.

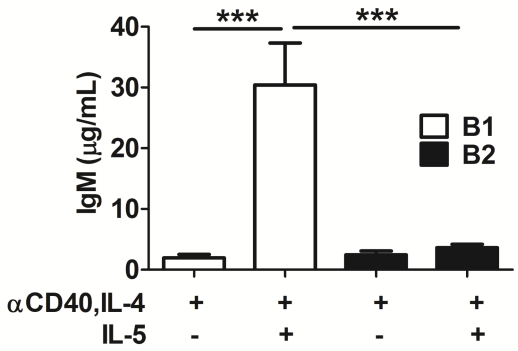

Figure 49: B1 cells from mice infected with *N. brasiliensis* make more IgM in response to IL-5.

B1 cells and B2 cells were sorted from mice infected with *N. brasiliensis* and cultured for 9 days with anti-CD40, IL-4, and ± IL-5. An ELISA was performed to detect total IgM in cell-free supernatants. ***$p<0.001$. Error bars represent ± SEM. $n>7$ mice and statistical comparisons were performed using a one-way ANOVA with Tukey's post hoc test.

The alarmin IL-25, but not IL-33, enhanced B1 cell IgE production during helminth infection

IL-25 production by ILC2s was shown to be important for induction of the T_H2 response[174,175]. Fort et al. reported that *i.p.* IL-25 injection induced IgE production at 10 days[176]. These data, as well as the demonstrated importance of IL-25 release by intestinal tuft cells during helminth infection, led to an examination of the effects of IL-25 on B1 cell IgE[174,175]. Isolated B1 cells from *N. brasiliensis* infected mice made significantly more IgE when treated with anti-CD40, IL-4, and IL-25 (in the range of 1 to 100ng/mL) compared to B1 cells treated with anti-CD40 and IL-4 alone (Figure 50A, B). IL-25 did not significantly increase IgE in B1 cells from naïve mice (Figure 50A, B). IL-25 did not further increase B1 cell IgE production from either naïve or *N. brasiliensis* infected mice when treated with IL-5 (Figure 50C), which was also reflected in the fold IgE (Figure 50A). In addition, IL-25 induced a moderate amount of proliferation in B1 cells treated with anti-CD40 and IL-4 (Figure 50D), but was not further augmented with IL-5 (Figure 50E). The increase in IgE seen after treatment with IL-25 in B1 cells from *N. brasiliensis* infected mice was on a per cell basis and not due to proliferative changes, as demonstrated by qRT-PCR analysis of secreted IgE expression (Figure 50F). RNA was isolated from B1 cells sorted from *N. brasiliensis* infected WT mice that were cultured for four days with anti-CD40, IL-4, and 30ng/mL IL-25 or anti-CD40 and IL-4 alone. Additional controls show that IL-25 alone did not induce detectable levels of B1 cell IgE in culture (Figure 51).

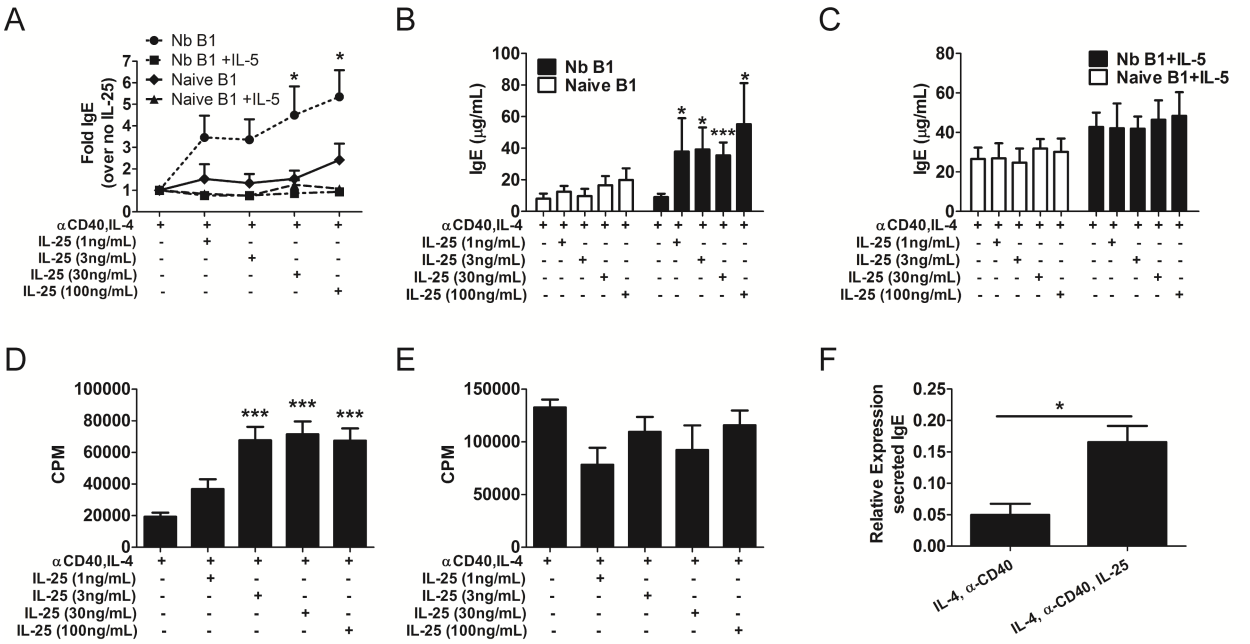

Figure 50: IL-25 enhanced B1 cell IgE production.

B1 cells were sorted as Figure 45 from mice infected with *N. brasiliensis* or naïve mice. They were then cultured with anti-CD40, IL-4, ± IL-5, and with increasing doses of IL-25. A. Fold change in IgE as compared to no IL-25 was assessed. Statistical comparison was made between naïve B1 cells (black diamond, solid line) and B1 cells from mice infected with *N. brasiliensis* (Nb) (Black circle, dotted line) by unpaired Student's t test. Total IgE production in supernatants is represented from (B) no IL-5 in cultures and (C) IL-5 added to cultures. Statistical comparison is made between no IL-25 in culture and dosages of IL-25 added to culture using a Student's t test. Proliferation of B1 cells from mice infected with *N. brasiliensis* was examined as in Fig 4 to IL-25, (D) without or (E) with IL-5 added to culture. CPM = counts per minute. F. Secreted IgE message was assessed after culture in B1 cells and normalized to *Actb* (β-actin). Statistical comparisons were done by a Mann-Whitney, non-parametric comparison. *$p<0.05$, ***$p<0.001$. $n>7$ mice/group in A-E, $n=3$ pooled samples/group in F. Error bars represent ± SEM. Experiments are the products of at least two independent repeats for all groups.

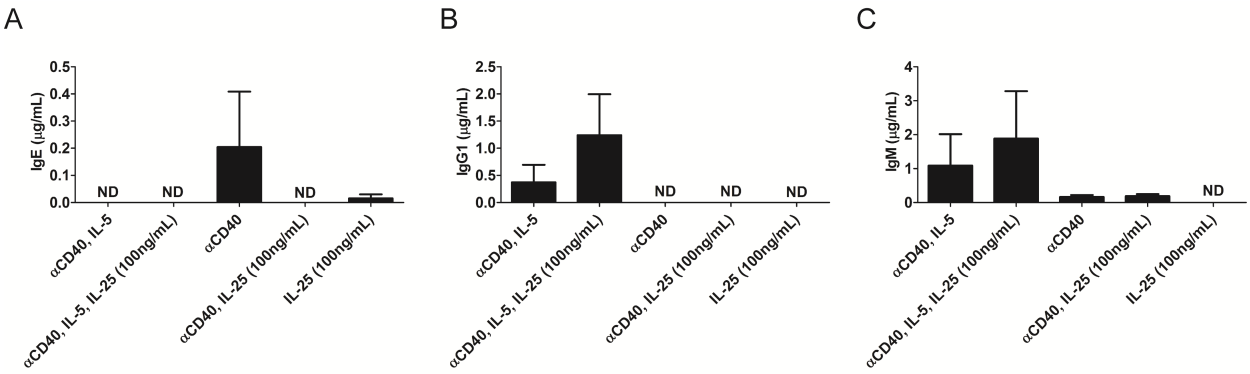

Figure 51: B1 cells require anti-CD40 to make IgE *in vitro*.

Controls for B1 cells sorted from mice infected with *N. brasiliensis*, as in Figure 50. A. Total IgE, B. IgG1, and C. IgM were measured from cell-free supernatants. Cells were cultured with anti-CD40 alone, IL-25 alone, or anti-CD40 in combination with IL-25 and/or IL-5. ND=none detected.

Since IgM is typically secreted by B1 cells, the regulation of IgM levels by IL-25 was examined by ELISA. B1 cells from naïve mice treated with anti-CD40 and IL-4 produced IgM that was not affected by the addition of IL-25 (Figure 51A). IgM production was increased by treatment with IL-5, but not further increased by adding IL-25 (Figure 51B). Inversely, B1 cells from mice infected with *N. brasiliensis* and treated with anti-CD40 and IL-4 had lower IgM when treated with IL-25 compared to without IL-25. IgG1 levels in similarly treated B1 cells were not different by ELISA (Figure 51C, D) or qRT-PCR in B1 cells (Figure 51E). To see if this pathway was active only in B1 cells, we examined IgE production in B2 cells sorted from both naïve and *N. brasiliensis* infected mice and cultured under the same conditions. IgE, IgG1, and IgM were not significantly altered beyond the addition of anti-CD40 and IL-4 (Figure 52A-F). Additionally, IL-25 alone did not induce IgE, IgG1, or IgM (Figure 51A-C).

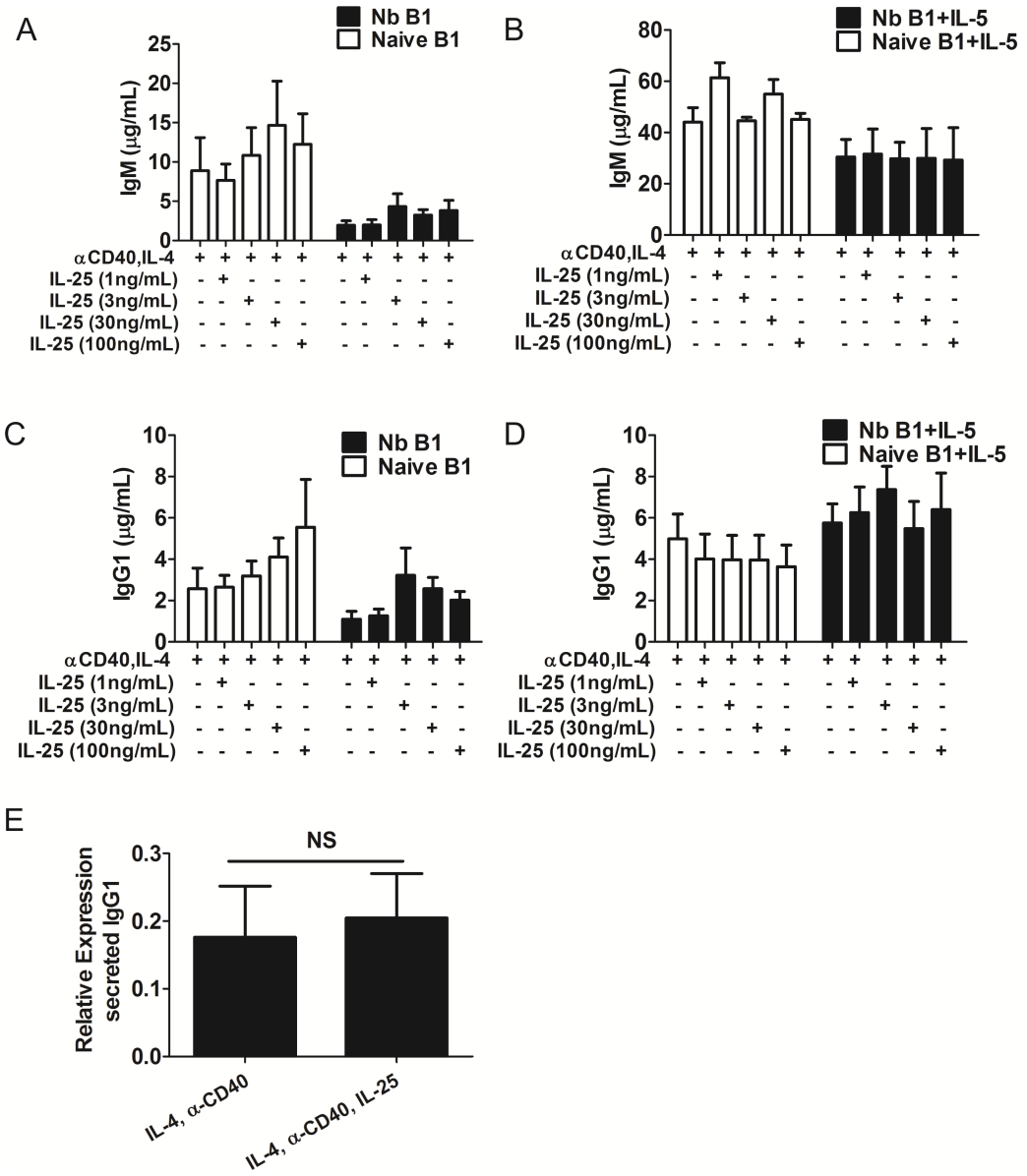

Figure 52: B1 cells do not make increased IgM or IgG1 in response to IL-25.

B1 cells from naïve mice were sorted and treated with anti-CD40 and IL-4 in culture. Cell supernatants were examined for total IgM in the (A) absence or (B) presence of IL-5 added to culture, as well as total IgG1 in the (C) absence or (D) presence of IL-5 added to culture, all with increasing doses of IL-25. Relative expression of secreted IgG1 message (E) was assessed in cells cultured with or without added IL-25, normalized to *Actb* (β-actin) message. NS = not significant. In A-D, n>7 mice/ group and is inclusive of three independent experiments. In E, n = 3 pooled experiments/ group.

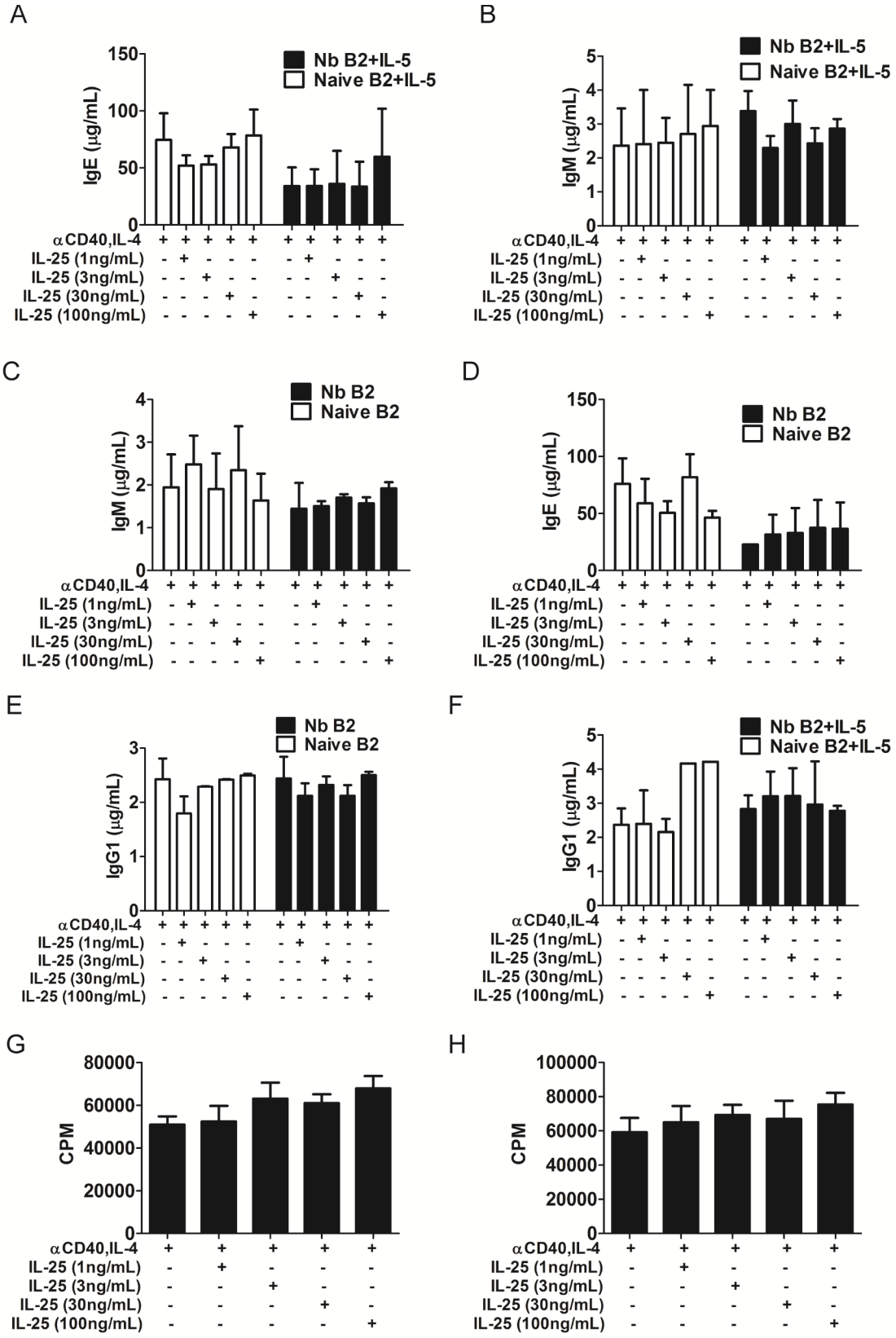

Figure 53: B2 cells from mice infected with *N. brasiliensis* or naïve mice do not have increased antibody or proliferation in response to IL-25.

B2 cells were sorted from the peritoneal lavage of naïve mice or mice infected with *N. brasiliensis* (Nb). They were then cultured with anti-CD40 and IL-4 followed by detection of (A-F) antibody in the cell-free supernatants and (G-H) proliferation. Total IgE, IgM, and IgG1 were measured in the (A, C, E) absence or (B, D, F) presence of IL-5 added to culture. Proliferation was performed as in Figure 5 on B2 cells from mice infected with *N. brasiliensis* with (G) or (H) without IL-5 added to culture. All cells were treated with increasing doses of IL-25. Error bars represent ± SEM. n>7 mice per group and statistical analyses were conducted utilizing Student's t test between IL-25 dose and without IL-25. This is inclusive of three independent experiments.

Komai-Koma et al. recently showed that B1 cells proliferate after daily *i.p.* injection with IL-33[161] through production of IL-5 that upregulated ST2 on B1 cells. This response was replicated *in vitro* by adding IL-5 and waiting for 48 hours before adding IL-33[161]. To test the effect of IL-33 on B1 cell IgE production, IL-33 was injected *i.p.* into WT mice and sorted B1 cells were compared to B1 cells sorted from naïve mice. IL-33 did not increase B1 cell IgE over B1 cells from naïve mice (Figure 54D). In addition, B1 cells from naïve mice treated with IL-5 for 48 hours followed by treatment with IL-33 increased cell proliferation[161,162], but not IgE production (Figure 54D). B1 cells isolated from mice infected with *N. brasiliensis* that are exposed to the infection-induced IL-5[175], did not further increase proliferation or IgE production after treatment with IL-33 (Figure 54A, C). These data suggest that IL-33 does not enhance IgE production by B1 cells.

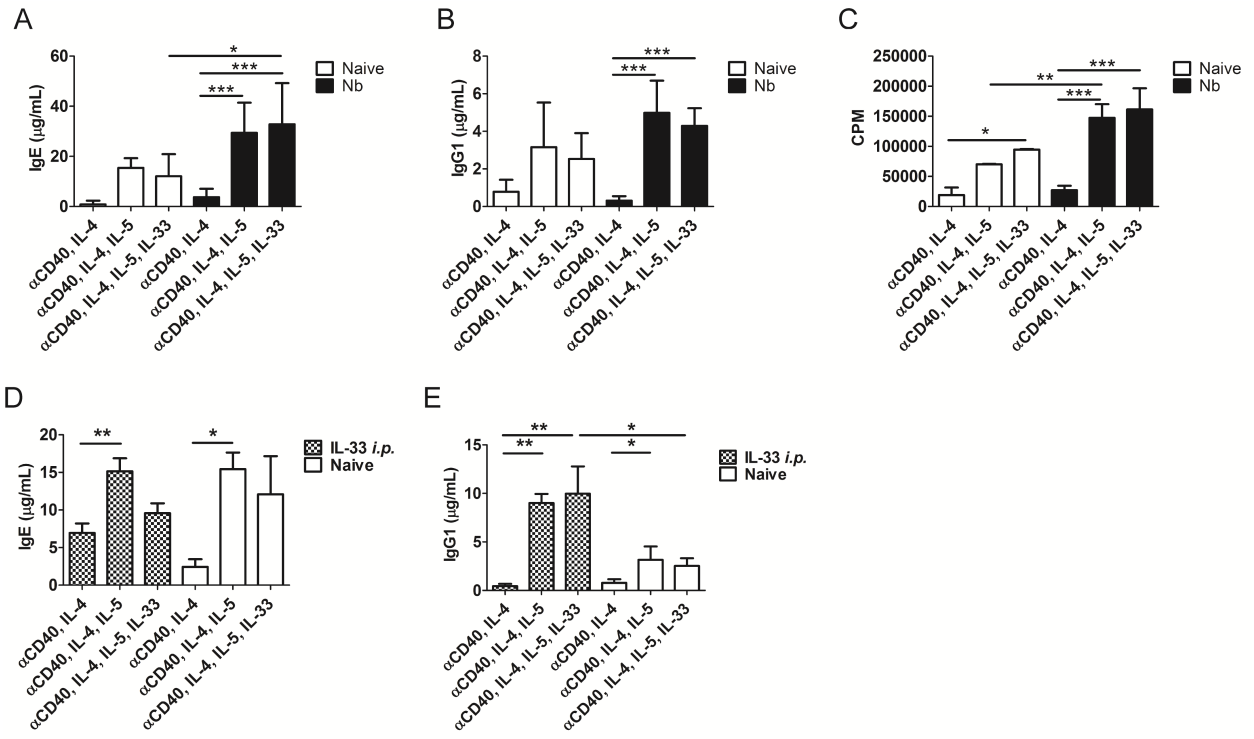

Figure 54: IL-33 does not enhance B1 cell IgE production.

B1 cells from naïve mice and mice infected with *N. brasiliensis* (Nb) were sorted and cultured with anti-CD40, IL-4 and ± IL-5 for 48 hours, followed by the addition of IL-33. After 9 days of culture, cell free supernatants were measured for total IgE (A) and IgG1 (B). Cell proliferation was determined by culturing cells with anti-CD40, IL-4, and ± IL-5 for 48 hours and then adding IL-33. 24 hours later, 1µCi [^{3}H]-thymidine was added and after 24 hours of incubation the plate was harvested onto GFC plates and read on a TopCount plate reader. D. and E. Mice were *i.p.* injected with 2µg/mouse IL-33 daily for 7 days and then B1 cells were sorted from both these mice and naïve mice. After 9 days of culture, total IgE (D) and IgG1 (E) were measured. *p<0.05 **p<0.01 ***p<0.001. Error bars represent ± SEM. Significance was determined using a one-way ANOVA with Tukey's post hoc test.

B1 cell IgE blocks enhanced B2 cell IgE-mediated clearance of N. brasiliensis

To examine the practical application of B1 cell IgE during an infection with *N. brasiliensis*, we turned to a $Rag1^{-/-}$ mouse model. These mice lack functional B and T cells, as well as B1 cells[177]. All mice were reconstituted with $CD4^+$ T cells alone and further reconstituted with B1 cells alone, B2 cells alone, or B1 and B2 cells. One week after reconstitution, mice were inoculated with *N. brasiliensis*. Reconstitution was confirmed by flow cytometry after *N. brasiliensis* infection (Figure 56). The level of infection was monitored by measuring fecal egg burden (Figure 55A, B). Both B1 cell-only and $CD4^+$ T cell-only reconstituted mice had similar infection levels, demonstrating no alteration of parasitic clearance mediated directly by $CD4^+$ T cells by B1 cells (Figure 55A, B). Intriguingly, B2 cell-only reconstituted mice showed significantly augmented parasitic clearance compared to the other groups, and B1/B2 cell-reconstituted mice showed a reduced clearance compared to the B2 cell-only group (Figure 55A, B). This indicated that B1 cells were hindering B2-mediated clearance. To test if this was B1 cell IgE-mediated, mice were reconstituted with B1 cells from $IgE^{-/-}$ mice and WT B2 cells. These $IgE^{-/-}$ B1 cells did not inhibit the B2-mediated clearance (Figure 55A, B). To further show that the B2-mediated clearance was IgE dependent, $Rag1^{-/-}$ mice were reconstituted with $IgE^{-/-}$ B2 cells that proved unable to increase clearance compared to mice given WT B2 cells (Figure 556A, B). The total IgE levels in serum were similar between all three groups and were only significantly reduced in the $IgE^{-/-}$ mice (Figure 55C).

These mice were maintained for 35 days after *N. brasiliensis* inoculation and then i.d. injected with *N. brasiliensis* excretory-secretory extract (NES) in a model of ACA to determine if B1 IgE provided protection against IgE-mediated helminth-specific MC degranulation. We observed that the mice reconstituted with WT B2 cells generated a skin reaction (Figure 55D).

The mice that were reconstituted with WT B1 and WT B2 had reduced ACA, reflective of decreased parasite clearance (Figure 55D, E). $IgE^{-/-}$ B2 cells from *N. brasiliensis*-infected mice failed to induce ACA indicating a lack of IgG1-induced degranulation in the model, and $IgE^{-/-}$ B1 cells in conjunction with WT B2 cells generated ACA, demonstrating the importance of B1 cell-derived IgE in blocking B2 cell-mediated degranulation (Figure 55D, E).

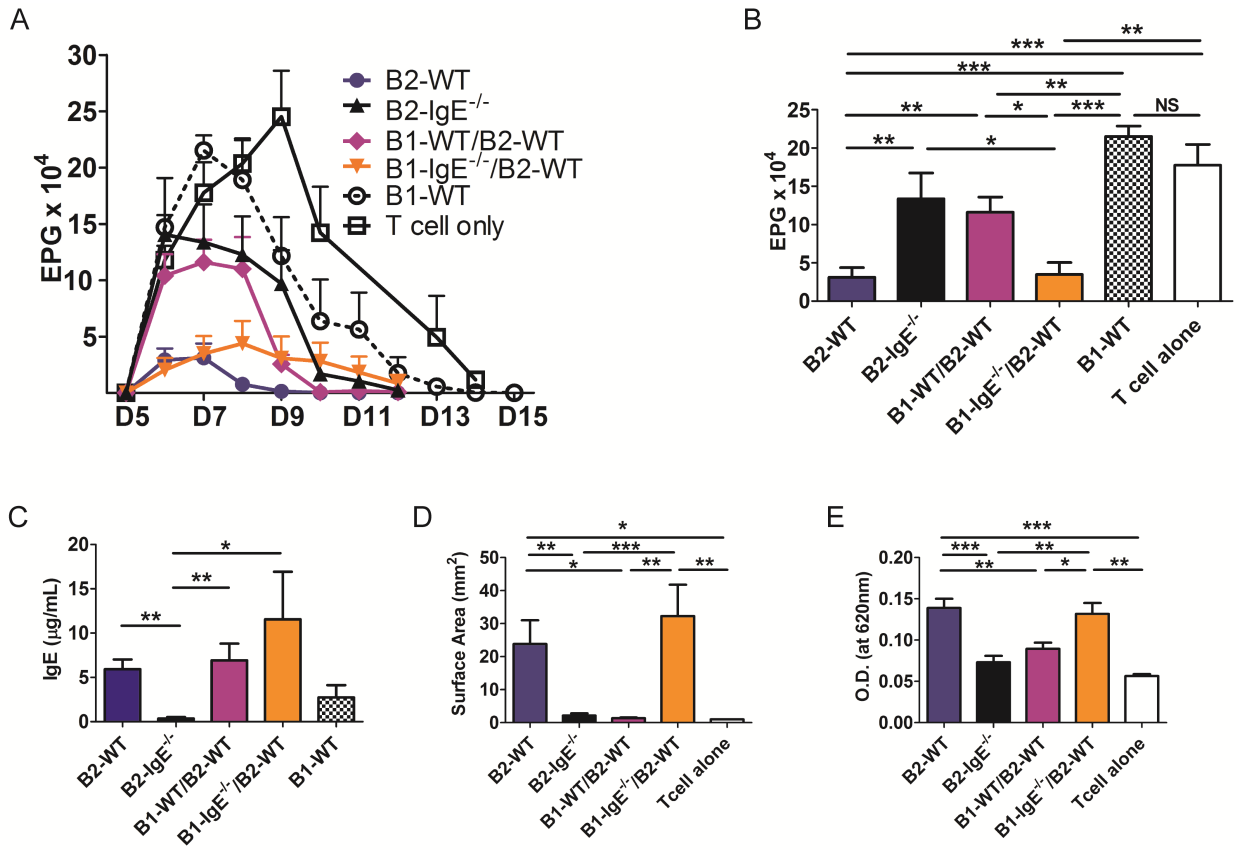

Figure 55: B1 cell IgE blocks parasite clearance by B2 cell IgE in reconstituted mice.

Rag1$^{-/-}$ mice were reconstituted with 5 x 10^6 CD4$^+$ T cells, followed by reconstitution with B1 cells *i.p.* and/or naïve B2 cells *i.v.* from WT or IgE$^{-/-}$ mice. Mice were then infected with 650 *N. brasiliensis* and (A) EPG were determined over the time course of infection and highlighted at day 7 post-inoculation in (B). C. Total serum IgE was measured in serum by ELISA on day 14. Statistical comparison was performed using a Kruskal-Wallis non-parametric test with Dunn's post hoc test. D. 35 days post inoculation with *N. brasiliensis*, an ACA reaction was induced using excretory-secretory extract (NES) derived from *N. brasiliensis* and (D) spot measurement and (E) dye extraction from skin was assessed as in Figure 47. *p<0.05 **p<0.01 ***p<0.001. n>7 mice/group in all groups except T cell alone, which n=4/group. Error bars represent ± SEM. Data is the product of four independent repeats.

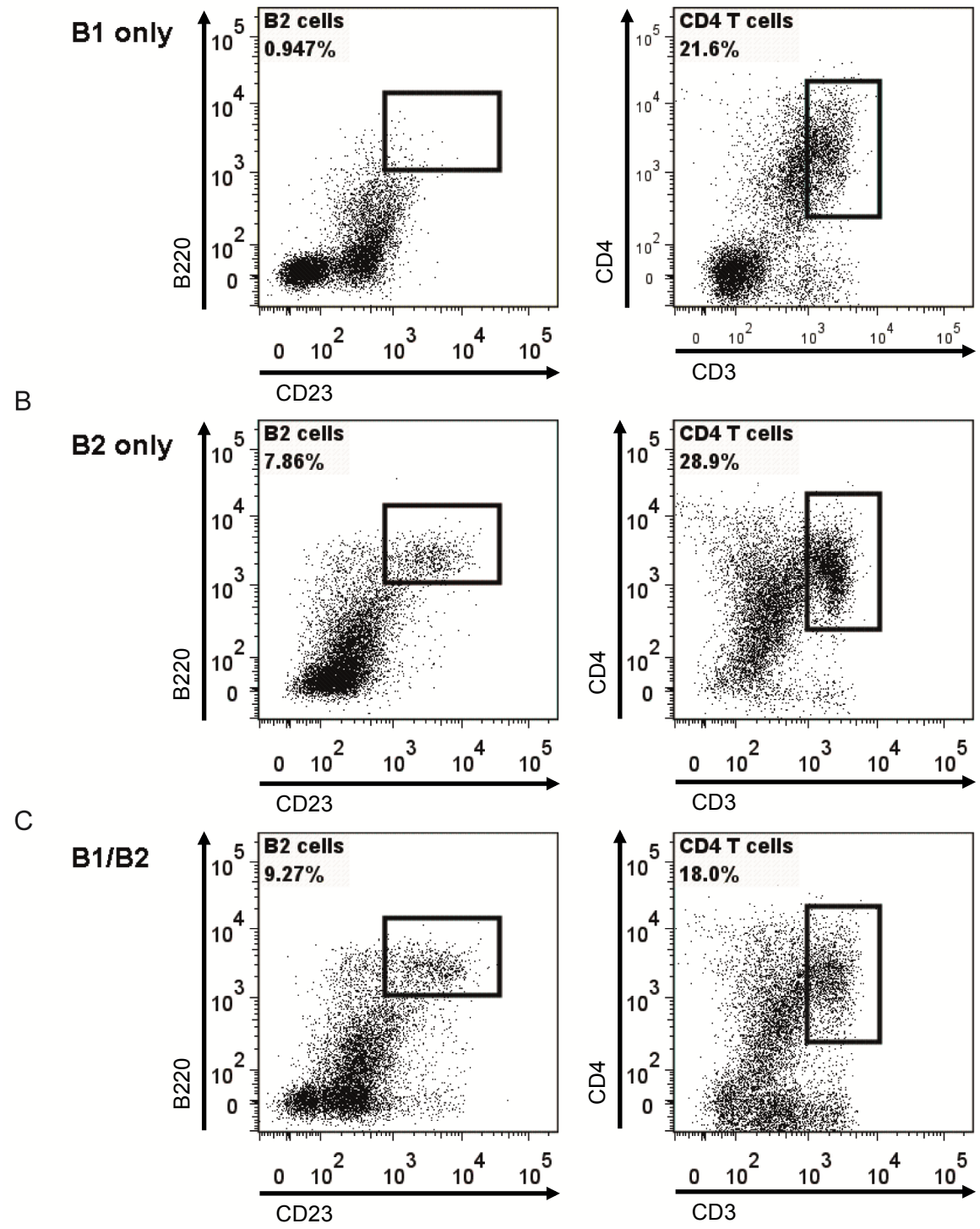

Figure 56: Rag1$^{-/-}$ reconstitution is confirmed by flow cytometry after infection with *N. brasiliensis*.

Flow cytometry was performed on mesenteric lymph node on day 21 after inoculation with *N.*

brasiliensis and reconstitution with $CD4^+$ T cells and either B1 cells alone, B2 cells alone, or B1 and B2 cells. Representative $Rag1^{-/-}$ mice reconstituted with B1 cells from WT mice only is shown in row A, reconstituted with B2 cells from WT mice only is shown in row B, and reconstituted with dual B1/B2 cells from WT mice is shown in row C.

Finally, this same reconstitution model was used to examine mice immunized with NP-KLH in alum. Reconstitution of $Rag1^{-/-}$ mice with B1 cells have significantly reduced total and high affinity IgG1 to the NP antigen, but antigen-specific IgG1 in reconstituted mice given B1/B2 cells was unaffected. Total IgG1 was similar between all groups (Figure 57). This data recapitulated the results observed in the ADAM10Tg mouse model.

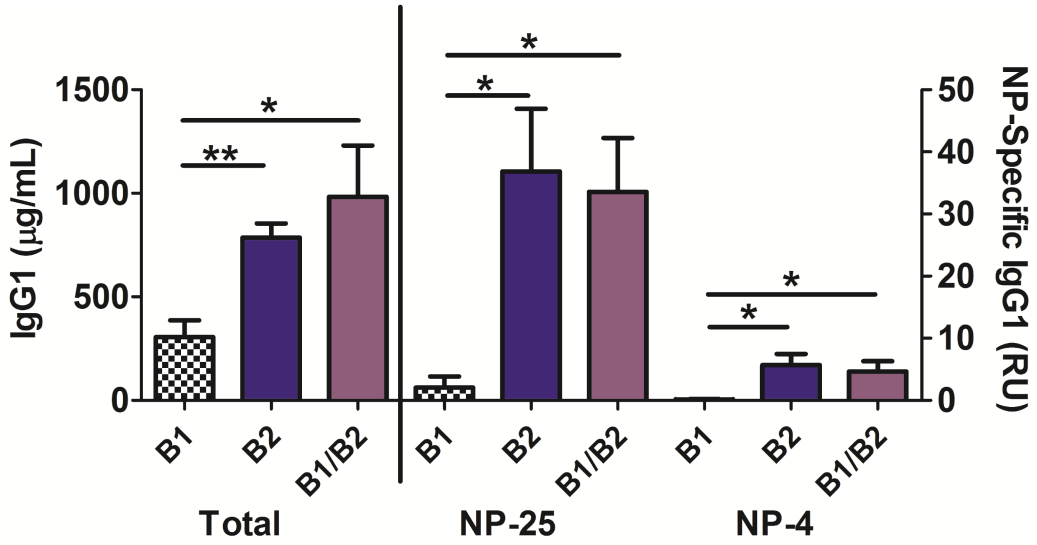

Figure 57: Rag1$^{-/-}$ reconstitution reinforces that B1 cell antibody responses to NP-KLH are poly-specific.

Rag1$^{-/-}$ mice were reconstituted as in Figure 55 with CD4^{+} T cells and B1 cells and/or B2 cells from WT mice and then immunized *i.p.* with NP_{31}-KLH in alum. High affinity (NP_4-specific IgG1), total affinity (NP_{25}-specific IgG1), and total IgG1 were measured in the serum by ELISA on day 14. *p<0.05, **p<0.01. The error bars represent ± SEM. Significance was determined using a one-way ANOVA with Tukey's post hoc test. This is representative of three independent experiments. n>7mice/group.

1.4.4 Discussion

The alarmin IL-25 has been shown to be important regulator of cells that span the adaptive and innate immune system, such as ILC2s. These cells secrete IL-5 in response to IL-25 stimulation, both of which are important for B1 cell IgE production (Figure 50). Although we know from our depletion studies that T cells are important in the B1 cell IgE response to *N. brasiliensis in vivo*, there is a small basal amount of IgE that remains despite this depletion (Figure 44). This residual B1 cell IgE may be stimulated by the cytokines produced directly by ILC2s. The cytokine order and amount may be important for IL-5 to further increase IgE production in conjunction with IL-25. IL-5 induced B1 cell proliferation may increase IgE production by increasing the number of B1 cells (Figure 48)[172]. IL-25, according to qRT-PCR data, increased IgE message on a per cell basis (Figure 50), and thus induced intrinsic signaling that warrants further investigation.

The CSR patterns for low affinity vs. high affinity antibody was elegantly explained by Xiong et al., demonstrating that a direct switch from μ to ε generated antibodies with low to non-affinity for an antigen[178]. This is in contrast to the indirect switch from μ to γ to ε that requires re-entry into germinal center reactions[178]. The indirect mechanism of CSR to IgE is not proven here, but is suggested with the increased IgE and decreased IgG1 seen in helminth infection (Figure 44) (Figure 55). IgG1 levels are only similar to WT when the model is prolonged and includes multiple immunizations, like the ACA model (Figure 47). This suggests that B1 cell IgE is undergoing CSR through a direct μ to ε switch.

B1 cells have long been thought to be important innate immune effectors. They generate critical IgM responses to bacteria, as well as to influenza virus[145,146]. In the past few years more research has described a role for B1 cells in T_H2 disease. Patel et al. demonstrated that B1 cell

IgM blocked the response to HDM, a common aero allergen, with germline anti-phosphorycholine (PC) antibody[179]. Another study suggested that B1 cell IgE might be specific for PC in a HDM model, yet this was never explicitly shown and Patel et al. did not see B1 cell IgE specific for PC in their model[179]. One suggestion is that B1 cell IgE induced by helminth infection may be PC specific, which is interesting, as both *N. brasiliensis* and *H. polygyrus bakeri* have secreted PC epitopes[180,181]. Because anti-PC IgE would likely be able to degranulate MCs and promote clearance of the parasite, the data contained herein argue against PC-specific IgE. In addition, as seen in Figure 55, B1 cell IgE does not enhance parasitic clearance. Nonetheless, it remains possible that B1 cell IgE could be selectively specific to unknown *N. brasiliensis* epitopes that for steric or yet to be determined reasons do not result in MC degranulation. But a poly-specific response that is cytokine enhanced is far more likely when the immunization protocols from Figure 46 and Figure 47 are considered. Unlike a helminth infection that has the potential to activate the germline clones available in the B1 cell repertoire, both NP-KLH and OVA in alum generated robust antibody responses that were not specific for NP or OVA. B1 cell antibody is commonly implicated in autoimmunity, as it is not subjected to any form of negative selection against self-antigen[145]. It would not be surprising if an antigen was revealed during the tissue damage induced by a helminth, but this explanation would not account for the strong B1 cell IgE responses that were observed upon stimulation with several different antigens (Figure 46) (Figure 47). Arguing against the possibility that B1 cell IL-10 may be inhibiting the parasitic clearance seen with the B2 cells in $Rag1^{-/-}$ reconstitution model in Figure 55, is the observation that $IgE^{-/-}$ B1 cells compared to WT B1 cells have reduced inhibition of WT B2 cell-mediated parasite clearance. This supports an IgE-dependent mechanism and not one regulated by cytokines.

Our model demonstrates that IL-25 from the intestinal epithelium initiates the type 2 immune response during helminth infection and along with other signals such as IL-4, IL-5, and CD40L stimulation from T cells causes B1 cells to proliferate and undergo CSR to IgE. This IgE coats MCs and reduces the binding of parasite specific IgE from B2 cells. Traditionally, IgE antibody was not thought to be critical in the clearance of helminth infections since clearance of *N. brasiliensis* was not delayed in $IgE^{-/-}$. With our $Rag1^{-/-}$ mouse cell reconstitution model, we conclusively showed that in the absence of B1 cell IgE, B2 cell IgE is able to more effectively assist in parasite clearance, presumably by enhanced MC degranulation. Late phase mediator release by MCs would also be increased leading to enhanced clearance of the parasite over T cell mediated clearance alone.

The accumulation of immature myeloid cells observed in the ADAM10Tg mice present a limitation to studying B1 cell IgE in these mice[159,166]. To ensure that this was not confounding the data, both an inhibitor of these cells as well as a $Rag1^{-/-}$ mouse reconstitution model using isolated B1 and B2 cell populations was utilized. Due to the inability to reconstitute large numbers of B1 cells as well as reconstitution of mature B cells, no reconstitution model will contain the full clonal repertoire of a WT mouse. But, the power between the two models makes up for some of these faults. No experiment in a mouse model will recapitulate exactly what is happening in the human system, especially with B1 cells, as they are poorly defined in humans[182]. If the epidemiological data is taken into consideration, where polyclonal IgE is seen in individuals protected against atopic disease[142], a role for parasite induced "benign" IgE does emerge.

Based on this data we hypothesize that in the very long evolution between helminths and primates to modern humans, that helminths have developed a mechanism of inducing large of

amounts of B1 cell IgE that provide them with an evolutionary survival advantage. Slower parasite clearance and increased fecundity leads to increased egg output for the parasite and improved evolutionary success[183]. The large amounts of IgE found in helminth-infected humans that is not specific for the parasite may be an indicator of this process at work. Furthermore the epidemiological studies demonstrating decreased rates of allergic disease in helminth endemic countries may be indicative of an additional mechanism in which large amounts of parasite induced polyclonal IgE could combat specific IgE-mediated MC degranulation by diluting it out and competing for receptor occupancy[140–144]. It could also explain the chronic nature of endemic helminth infection in humans. As this poly-specific IgE becomes better understood, its induction would represent an additional alternative for control of IgE-mediated allergic disease.

Section II: Myeloid derived suppressor cells

Chapter 1: Mast cell derived mediators augment the immunomodulatory role of myeloid derived suppressor cells.

2.1.1 Introduction

Myeloid-derived suppressor cells

Myeloid-derived suppressor cells (MDSCs) are a diverse population of immature myeloid cells, which have been found to suppress immune responses. They were originally discovered in patients with cancer and found to suppress anti-tumor immunity. Because this population is heterogeneous, there is some debate as to the precise combination of surface marker expression, but human MDSCs are typically characterized as being HLA-DR$^{-/low}$CD11b^{+}CD33^{+}. MDSCs are divided into two subsets, monocytic (M-MDSCs) and granulocytic (G-MDSCs), characterized by CD14^{+}CD15^{-} and CD14^{-}CD15^{+} expression, respectively[184]. Murine MDSCs have co-expression of the surface markers CD11b^{+}Gr-1^{+}, with the M-MDSCs and G-MDSCs expressing Ly6C^{hi}Ly6G^{-} and Ly6C^{lo}Ly6G^{+}, respectively[185]. Integral to the definition of MDSCs is their ability to suppress immune responses. Several mechanisms have been implicated: depletion of L-arginine[186,187], production of soluble oxidizers[188–191], reduction of T cell migration and viability[192–194], and induction of Tregs[195]. In addition to these functions, MDSCs are also thought to skew the environment to T_H2 type immune responses, which is beneficial in other disease states but detrimental to host anti-tumor reactions. The mechanism of this skew is as of yet unknown, but is potentially the result of interactions of MDSCs with other cell types besides T cells. Our lab demonstrated the novel interaction between MDSCs and mast cells (MCs) in *N. brasiliensis* infection and B16 melanoma (B16) colonization[166]. These studies showed that

MDSCs promoted clearance of *N. brasiliensis* and tumor colonization through amplification of T_H2 immunity and that MCs were critical for this action.

In previous publications, we generated transgenic mice that overexpress ADAM10 (ADAM10Tg), which disrupts Notch signaling in hematopoietic progenitors leading to the accumulation of MDSCs[159]. These MDSCs are functionally similar to those derived from the tumor-derived counterparts as determined by parallel studies using MDSCs from tumor-bearing mice. To study the importance of MCs for MDSC action, we utilized the MC-deficient C57Bl/6 *kit*$^{Wsh/Wsh}$ (Wsh) mice. These mice have a mutation in the white spotting (W) locus gene, which encodes the receptor tyrosine kinase, ckit, and are deficient in MCs but have minimal other hematologic abnormalities. Currently, we use another MC-deficient mouse, C57Bl/6 *Cpa3-Cre;Mcl-1*$^{fl/fl}$, which were a generous gift from Dr. Stephen Galli. The *Cpa3-Cre;Mcl-1*$^{fl/fl}$, named the "Hello *Kit*ty" mice, express Cre recombinase under the carboxypeptidase 3 promoter which removes the anti-apoptotic factor, myeloid cell leukemic factor 1 (Mcl-1), leading to a severe deficiency in MCs and basophils[196]. While our lab has demonstrated that MCs are able to orchestrate MDSC immunoregulatory function, this interaction needs to be further elucidated. Appreciating the communication between MDSCs and MCs may provide functional targets to either enhance or block the skewing of immune responses, which could augment therapeutic regimens in patients with cancer or other diseases.

Mast cells, histamine, and MDSCs

MCs are tissue resident cells, which are found in barrier tissues like skin, gut, and respiratory mucosa. In these tissues, they are important sentinels and coordinate anti-parasitic immune responses[158] via the production cytokines and other molecules and the recruitment of effector cells, like MDSCs[197]. MCs have been consistently demonstrated at the tumor site, and their

presence is correlated with decreased survival and worse prognosis[197,198]. Proinflammatory cytokines secreted by MCs were thought to be the cause; however, MCs secrete factors like 5-lipoxygenase and IL-17, which recruit MDSCs to the tumor microenvironment[199–201]. In addition to these molecules, MCs release histamine, proteases, cytokines, and other lipid-derived mediators[202–204]. Histamine is a major component released by MCs and acts on histamine receptors (HRs) 1 - 4, which are G-protein couple receptors. HRs are present on many cell types including vascular endothelium, enterochromaffin cells, and smooth muscle cells; the resulting effect of histamine depends on which receptor type is present. Actions of histamine include increased vasopermeability, vasodilation, mucus production, and smooth muscle contraction[205]. Myeloid cells express HRs and produce histamine through histidine decarboxylase (HDC)[167,206]. *In vitro*, histamine promoted survival of myeloid cells and supported the M2 phenotype through increased IL-10 and decreased IL-12 production[207,208]. Thus histamine is able to alter the immune environment promoting tumor growth through action on myeloid cells. Histamine has also been shown to enhance growth of human colon cancer cell lines, which was blocked by treatment with the HR2 antagonist, cimetidine (CIM)[209]. Our studies have demonstrated that histamine promotes survival of MDSCs through HR1 and HR2 and alters gene expression of the suppressive enzymes, Arginase 1 (*Arg1*) and inducible nitric oxide synthase (*iNOS*) with different effects on G-MDSCs and M-MDSCs[167]. In response to histamine, M-MDSCs increase mRNA expression of both *Arg1* and *iNOS*, whereas G-MDSCs decrease mRNA expression of both suppressive enzymes. The divergent effects of histamine were also shown *in vivo* where G-MDSC survival in the liver was more susceptible to HR2 antagonism in *N. brasiliensis* infection. MDSCs in the tumor environment can alter the immune response depending on the subtype, G or M.

MC-derived IL-13 on MDSC function

IL-13 is a cytokine made by many different cell types, including MCs[210]. IL-4 and IL-13 are both T_H2 cytokines with many overlapping functions[158,211]. They share a common receptor subunit, IL-4Rα. IL-4 can signal through IL-4Rα by interacting with the common γ chain or IL-13Rα1, whereas IL-13 signals through IL-13Rα1 with IL-4Rα or IL-13Rα2. Despite this commonality, different signaling cascades are activated depending on the ligand bound[211]. IL-13 is responsible for the "weep and sweep" response to intestinal parasites, which consists of enteric nerve stimulation, smooth muscle contraction, and goblet cell hyperplasia[158,210]. The role of IL-13 in tumor progression is controversial. Early reports demonstrated a protective role of IL-4 and IL-13[211–213]. However, these studies were conducted with tumors overexpressing these cytokines, and their biological significance is unclear. Increasing evidence supports the tumor-promoting role of IL-13. Phase I and II trials of IL-13PE38QQR (Cintredikin besudotox), which is IL-13 attached to *Pseudomonas* exotoxin A, are underway for patients with metastatic and locally advanced adrenocortical adenocarcinoma and other advanced tumors expressing high levels of IL-13Rα2[214,215]. Human studies of patients with gastric and pancreatic cancers have demonstrated elevated plasma levels of IL-13, which are correlated with increased MDSCs and worse prognosis[216]. Blockade of IL-4Rα and thus IL-13 signaling, delayed 4T1 tumor progression, increased MDSC apoptosis, and increased $CD8^+$ T cell infiltration into the tumor[217]. Recently, monoclonal antibodies targeting IL-13 have been developed for asthma and allergic disease, but several are currently also in clinical trials for the treatment of solid tumors[218]. While the source of IL-13 is debated, MC-derived IL-13 has been demonstrated to be important in pancreatic ductal adenocarcinoma[219]. Timing, source, dosage, and location are likely to be important for the effect of IL-13. Besides increasing Arg1 expression and activity[220],

understanding the role of IL-13 in cancer is in its infancy. We show preliminary evidence that IL-13 acts as a chemotactic agent to recruit MDSCs to parenchymal sites creating metastatic niches. This novel function of IL-13 is supported by reports that IL-13 can drive chemotaxis in other myeloid cells[221]. The function of MC-derived IL-13 for MDSC-induced tumor promotion is largely unknown and further study in this area is necessary to explain the conflicting views. Given the recent trials targeting IL-13 and IL-13Rα2-expressing cells, we aimed to understand the multi-faceted role of IL-13 in MDSC function and tumor advancement.

2.1.2 Methods

2.1.2.1 Mice

Mice were maintained at VCU animal facility in accordance to guidelines by the National Institutes of Health and American Association for the Accreditation of Laboratory Animal Care. C57BL/6 ADAM10 transgenic mice (A10Tgs) were generated as previously described[159]. C57BL/6 WT mice were purchased from Jackson Laboratories. $Kit^{Wsh/Wsh}$ mice were progeny of breeding pairs purchased from Jackson Laboratories. $Cpa3^{cre}$; $Mcl\text{-}1^{fl/fl}$ mice[205] (C57BL/6 background), were generously provided by Dr. Stephen Galli at Stanford University. $IL\text{-}13^{-/-}$ mice were a generously provided by Dr. Andrew McKenzie at Cambridge University[222]. All mouse protocols were approved by VCU Institutional Animal Care and Use Committee.

Table 7: Genotyping Primers

Mouse Colony		**Primer Name**	**Sequence**
ADAM10Tg	Transgene	A10TgF	CCAACAGTGTTAATTCTGCTCC
		A10TgR	TTCTTTCAGCCAGAGTTGTGCG
Mcl^{flox} Cpa3-Cre	Flox and WT	oMIR5147	GCAGTACAGGTTCAAGCCGATG
		oMIR5148	CTGAGAGTTGTACCGGACAA
	Cpa3-Cre	Cpa3-cre F	CGATGCAACGAGTGATGAGG
		Cpa3-cre R	GCATTGCTGTCACTTGGTCGT
IL-$13^{-/-}$	IL-13	Exon1	AAGAGCCCGAGGCATGATGCG
		Exon2	TCTGGGCGCTATTGCTTGGTCTCTTCTGCC

2.1.2.2 Cell culture

Mouse bone marrow-derived mast cells (BMMCs) were derived from bone marrow from femurs and tibiae of mice and cultured in cRPMI 1640 containing 10% FBS, 2mM L-glutamine, 100 U/mL penicillin, 100µg/mL streptomycin, 1mM HEPES (Quality Biological, Gaithersburg, MD, USA), and 1mM sodium pyruvate (Cellgro, Herndon, VA, USA). Cultures were supplemented with IL-3-containing supernatant from WEHI-3 cells (1ng/mL) and stem cell factor containing supernatant from BHK-MKL cells (10ng/mL). Mature BMMC were used after 28 days culture. B16 melanoma cell line was maintained in DMEM with 10% FBS, 1% penicillin, 1% streptomycin, and 1% L-Glutamine.

2.1.2.3 Isolation of MDSCs, adoptive transfer, and dye labeling

Spleens were harvested from A10Tg mice. They were then dispersed into single cell suspensions. Erythrocytes were lysed using ACK lysing buffer (Quality Biological, Gaithersburg, MD, USA). T cells were depleted using CD90.2 magnetic depletion (Miltenyi Biotec, Inc., Auburn, CA, USA) according to manufacturer's protocol. Gr-1^+, Ly6G^+, or Ly6C^+ cells were purified using Easy Sep PE-selection kit (Stem Cell Technologies, Vancouver, BC, CAN) according to manufacturer's protocol. For AT studies, 10 x 10^6 MDSCs were injected into tail veins every three days. For AT of dye labeled MDSCs, cells were stained with PKH26GL dye linker kit (Sigma-Aldrich, St. Louis, MO, USA) according to manufacturer's protocol.

2.1.2.4 Migration Assays

2 x 10^5 B16, BMMC, or media alone were loaded into the lower well of 8µm trans-well plates (Corning, Herndon, VA, USA). 2x10^5 MDSCs were loaded into the upper well. Plates were incubated for four hours at 37°C and the lower wells were harvested for flow cytometry.

2.1.2.5 T cell suppression assay

T cells were isolated from WT mice by magnetic bead isolation (CD90.2 beads, Miltenyi Biotec) and labeled with 1μM CFSE. Labeled T cells were co-cultured with MDSCs on anti-CD3ε coated plates with anti-CD28 in cRPMI. After 72h of culture, cells were analyzed by flow cytometry for dilution of CFSE. Percent divided was then calculated (# cells divided/total $CFSE^+$ cells).

2.1.2.6 Flow Cytometry

Cell isolation and labeling were conducted as previously described. Antibodies included FITC anti-mouse Gr-1 (RB6-8C5); PE anti-mouse Gr-1 (RB6-8C5); APC anti mouse Ly6C (HK1.4), PERCP/Cy5.5 anti-human CD15 (W6D3); PE/Cy7 anti-mouse CD11b, anti-human CD33 (WM-53) (Biolegend, San Diego, CA, USA); APC anti-human CD11b (ICRF44), and PE anti-human CD14 (61D3) (eBiosciences, Inc., San Diego, CA, USA); and anti-mouse Ly6G-FITC (1A8) (BD Biosciences, San Jose, CA, USA). Flow cytometric analysis was performed using the Canto (BD Biosciences, San Jose, CA, USA). Data analysis was conducted using FlowJo v7.6.5.

2.1.2.7 Tumor cell inoculation

Mice were injected *i.v.* with 2.5 x 10^5 B16 melanoma or Lewis lung carcinoma (LLC) cells, monitored daily, and euthanized after three weeks; lungs were harvested and weighed to determine degree of colonization. Mice were also given flank injections of tumor cells in separate experiments. For LLC flank tumors, firefly luciferase-expressing LLC cells were used for inoculation. D-luciferin (Promega) was injected *i.p.* 5 mins prior to imaging with the IVIS Spectrum In Vivo imaging system (Perkin Elmer).

2.1.2.8 qPCR

Cells were homogenized in TRIzol reagent (LifeTech) and total RNA was isolated according to manufacturer's protocol. cDNA was reverse transcribed with oligodTs and Superscript IV (LifeTech). qPCR was run on a QuantStudio5 (LifeTech) and primers and Taqman probes (LifeTech) used are in Table 8.

2.1.2.9 Cimetidine or Cetirizine administration

For mice treated with cetirizine (CT), 0.5mg/kg was injected *i.p.* starting on day -1 and repeated daily. For mice injected with cimetidine (CIM), 20mg/kg was injected *i.p.* starting on day -1 and repeated every two days.

2.1.2.9 Human Studies

Human studies were conducted under appropriate Institutional Review Board (IRB) approved protocols. All patients gave informed consent for this research. 10 or 20 mLs of blood was collected in EDTA coated vacuum tubes from patients identified as having systemic mastocytosis, chronic urticaria, or seasonal allergy symptoms. Blood from healthy controls was also collected. Peripheral blood mononuclear cells were isolated using Ficoll-Paque separation medium (GE Healthcare, Little Chalfont, Buckinghamshire, UK). Cells were labeled with a live dead cell marker and then stained for flow cytometry as described in Section 2.1.2.6.

2.1.2.10 Statistical analysis

P values were calculated using unpaired Student's t tests in Graphpad Prism v5. Error bars represent the standard deviation between samples. $p<0.05$ is considered statistically significant.

Table 8: Primers and Probes

Primer/Probe	Probe[4]
Ccr2	Mm00438270_m1
Ccl2	Mm00441242_m1
Gapdh	Mm99999915_g1

[4] Product number for Taqman probes purchased from LifeTech.

2.1.3 Results

Histamine and MDSCs

To study the immunoregulatory potential of MDSCs, we have isolated them from ADAM10Tg mice, which accumulate MDSCs in the absence of tumor. As these MDSCs function identically to their tumor-derived analogs[166], we have been able to study the role of MDSCs in different disease states, including *N. brasiliensis* infection and the tumor colonization models, B16 and Lewis lung carcinoma (LLC). In *N. brasiliensis* infection, a robust T_H2 response is elicited which leads to the elimination of adult worms (L5) from the intestine 10 – 12 days after infection. Adoptive transfer of MDSCs into *N. brasiliensis*-infected mice, reduced the fecal egg counts and adult worms in the proximal small intestine compared to wild type C57Bl/6 (WT) controls[166]. Interestingly, WT mice infected with *N. brasiliensis* had increased numbers of MDSCs with G-MDSC and M-MDSC ratios similar to the ADAM10Tg and tumor-bearing mice. To understand different effect of the subsets on clearance of *N. brasiliensis*, G-MDSCs and M-MDSCs were purified from ADAM10Tg mice based on expression of Ly6G and Ly6C and adoptively transferred into *N. brasiliensis*-infected WT mice. The $Ly6G^+$ population (G-MDSCs) had a similar effect as total MDSCs on the immune response to the helminth infection, whereas the $Ly6G^-$ population (M-MDSCs) demonstrated minimal enhancement of anti-*N. brasiliensis* immune response. Further supporting the unequivocal role of MDSCs, depletion of CD8 and CD4 T cells with anti-CD8/CD4 antibodies did not diminish the enhanced expulsion of *N. brasiliensis* by adoptive transfer of MDSCs. Moreover using the adoptive transfer of MDSCs into MC-deficient mice both Wsh and Hello Kitty, we have discovered that MCs are critical for the promotion of anti-helminth immunity by MDSCs (Figure 58A, B)[166]. We then extrapolated the requirement of MCs for MDSCs action to tumor models. We expected that adoptive transfer

of MDSCs would not efficiently promote the metastasis of B16 in MC-deficient mice. To this end we adoptively transferred MDSCs into MC-deficient and WT mice, which received *i.v.* injection of B16. In WT mice, adoptive transfer of MDSCs led to increased number of tumor nodules in the lungs, whereas in MC-deficient mice, MDSC adoptive transfer had almost no effect (Figure 58C)[166,167]. Thus without MCs, MDSC were not able to promote tumor metastasis effectively.

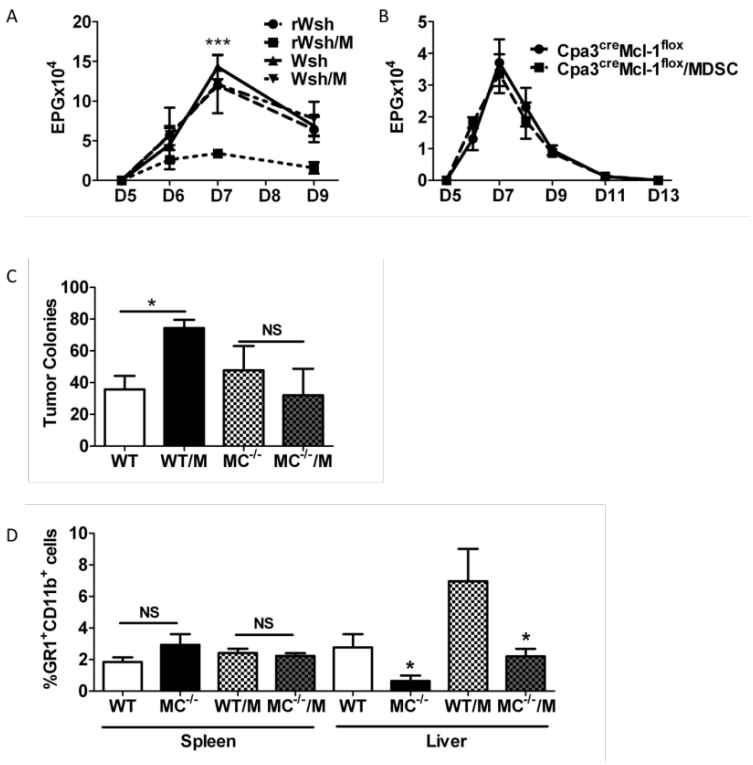

Figure 58: MCs are required for MDSC-mediated *N. brasiliensis* expulsion.

A. $Kit^{Wsh/Wsh}$ mice were reconstituted with BMMC 20 weeks prior to experiment (rWsh). Age matched unreconstituted $Kit^{Wsh/Wsh}$ mice (Wsh) mice were used as controls. Mice were infected with *N. brasiliensis* and *i.v.* AT with A10Tg derived MDSCs on days (-1, 2, 5, and 7) or not. ***$p<0.001$ between rWsh and rWsh/M. B. $Cpa3Cre^{+}$ $Mcl\text{-}1^{fl/fl}$ mice were infected with *N. brasiliensis* and AT with MDSCs (M) as described above or not. Eggs per gram of feces were determined on indicated days. n>5 mice per group. C. $Cpa3Cre^{+}$ $Mcl\text{-}1^{fl/fl}$ ($MC^{-/-}$) or WT Mice were challenged with B16 melanoma with or without adoptive transfer of MDSCs. Mice were euthanized and lung tumor colonies were enumerated. D. Liver and spleen were examined for MDSC accumulation. *$p<0.05$, n>4 mice per group.

Building on the role of histamine in MDSC survival, proliferation, and T_H2 immune responses, we sought to understand the effect of histamine on MDSCs and to determine whether it could be acting as the mediator in MC-MDSC communication. Liver MDSCs express HR 1 – 3, but not 4[167]. We found that *in vitro* exposure to histamine increased survival and proliferation of MDSCs, particularly striking for M-MDSCs. These results were confirmed by utilizing HR1 and HR2 antagonists, cetirizine (CT) and CIM, which abrogated the effects. Expression of enzymes *Arg1* and *iNOS* mediate MDSC suppression of immune responses. Histamine treatment *in vitro* increased the expression of *Arg1* and *iNOS* mRNA in M-MDSCs five-fold and two-fold, respectively. G-MDSCs exhibited five-fold and two-fold decrease in mRNA expression of *Arg1* and *iNOS*. To examine the ability of MDSCs to promote a T_H2 environment in response to histamine, the expression of typical T_H2 cytokines, *Il4* and *Il13* were assessed by quantitative polymerase chain reaction. Histamine treatment caused a four-fold increase in *Il4* and two hundred-fold increase in *Il13* expression in G-MDSCs over M-MDSCs[167]. These data demonstrate the ability of histamine to affect MDSCs *in vitro* and illustrate the differences between the two MDSC subsets.

To understand the role of histamine on the *in vivo* effects of MDSCs, we administered CT and CIM to *N. brasiliensis* infected mice, which were also given MDSCs. Antagonism of HR1 or HR2 abolished the ability of MDSCs to enhance parasite clearance, presumably by inhibition of the T_H2 skew (Figure 59A, B). These results were also correlated with fewer MDSCs in liver and with a higher proportion of G-MDSCs[167]. As we demonstrated that MDSCs, particularly G-MDSCs, increase their expression of suppressive enzymes in response to histamine, we investigated the functional consequence of this suppression in tumor models. We analyzed whether HR2 antagonism would prevent adoptively transferred MDSCs from suppressing anti-

tumor immunity in a B16 colonization model. B16-bearing mice receiving CIM and MDSC adoptive transfer had reduced lung tumor nodules (by weight) compared to B16-bearing mice that did not receive CIM and were similar to levels B16-bearing mice that did not receive any MDSCs (Figure 59C, D). Similar results were shown in an MDSC-accumulating tumor model, LLC, where CIM suppressed tumor growth in the lungs[223].

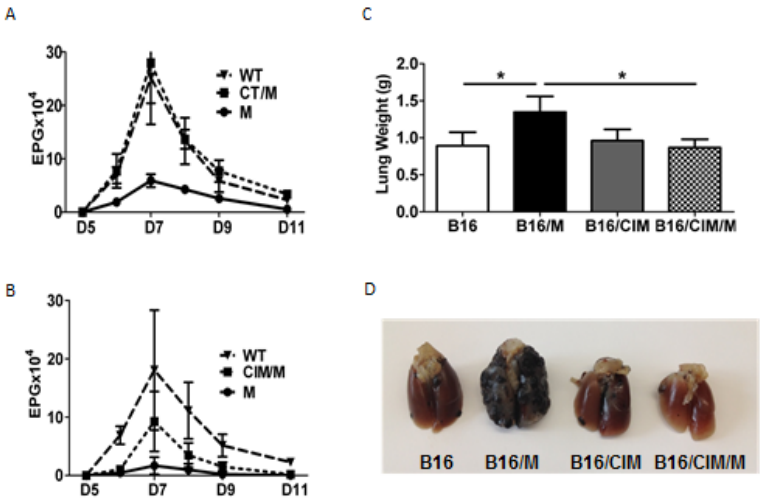

Figure 59: HR1 and HR2 antagonists block MDSC function.

A. and B. EPG in *N. brasiliensis* infected, ± MDSCs (M) every 3 days and ± daily CT treatment (A) or every other day CIM treatment (B). C. and D. Mice were challenged with B16 concomitant with MDSCs ± CIM. Mice were subsequently euthanized, and their lungs weighed for B16 colonization. Mean ± SD. *$p<0.05$, $n>5$ mice/group[167].

MDSCs in human patients

To understand the relevance of MCs in human patients, we examined patients with indolent systemic mastocytosis (ISM), a human disease characterized by clonal expansion of MCs. We found elevated levels of MDSCs in the blood compared to patients with chronic urticaria (CU) and healthy (H) controls (Figure 60A). We confirmed the suppressive function of the MDSCs by T cell suppression assay (as described below) using T cells sorted from the same patient (data not shown). Patients with ISM have symptoms related to MC activation events such as cutaneous skin reactions, gastrointestinal disturbances, and anaphylaxis[224]. Through an IRB in collaboration with Dr. Lawrence Schwartz at VCU, we had access to blood (10mL per patient) from patients with ISM, chronic urticaria (CU) (drug control), and healthy (H) volunteers. Under this protocol, patients answered questions regarding their symptoms and medications (exclusion criteria includes corticosteroid usage as it may confound results). The blood was collected, de-identified, and then provided to us with the questionnaire. We also have published that patients suffering from allergic disease (MC activation) have increased MDSCs in their blood[167] (Figure 60B). While this proposal does not directly aim to examine the MDSCs in human patients further, this data greatly supports the role of MCs in MDSC survival and function in humans.

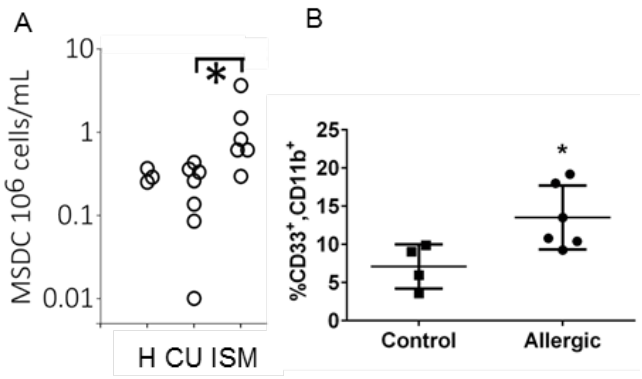

Figure 60: Patients with indolent systemic mastocytosis and allergies have elevated circulating MDSCs.

A. Blood from patients with indolent systemic mastocytosis (ISM), chronic urticaria (CU), and healthy controls (H) was examined for MDSCs (HLA-DR$^-$ CD33$^+$ CD11b$^+$) by flow cytometry. B. Blood from allergic patients and healthy controls were analyzed by flow cytometry for MDSCs (CD34$^-$ CD33$^+$ CD11b$^+$)[167] Mean ± SD. *$p<0.05$.

IL-13 and MDSCs

Given the literature establishing IL-13 as a chemotactic agent for MDSCs and its importance for MDSC recruitment in an effective immune response, we analyzed the trafficking of MDSCs upon adoptive transfer. MDSCs were labeled with the lipid tracking dye, PKH26GL, and injected *i.v.* into naïve mice. Eighteen hours after injection, we found that MDSCs preferentially migrated to the liver[166]. To determine the significance of this localization in *N. brasiliensis* infection, we PKH26GL tracked MDSCs adoptively transferred into *N. brasiliensis*-infected WT and MC-deficient mice (Wsh). In the WT mice, MDSCs again trafficked to the liver. In the MC-deficient mice, the proportion of MDSCs present in the liver was markedly reduced[166], indicating the importance of MCs in MDSC function. We confirmed these results using *in vitro* migration assays; MDSCs displayed a high degree of migration to MCs[167]. Other groups have also demonstrated MDSC trafficking to the liver in tumor models[225,226] in addition to our own data (Figure 61D).

Building on the *in vivo* migration data, we sought to analyze the role of IL-13 using IL-$13^{-/-}$ mice, which were injected s.c. with LLC, generating a primary flank tumor. We demonstrated that MDSCs do exit the bone marrow; however they are reduced in the liver and increased in the PB compared to WT mice with LLC flank tumors. Interestingly, it appears that the MDSCs were unable to escape out of the circulation and travel to the liver, despite being produced from the bone marrow in adequate numbers (Figure 61B and D). The functional consequence of this aberrant migration is evident in the smaller tumor volumes in the IL-$13^{-/-}$ mice compared to WT. Additional data using a LLC colonization model, studying this effect in metastasis, demonstrated that IL-$13^{-/-}$ mice had fewer metastatic colonies compared to WT (Figure 61C). From these results we have crafted a novel hypothesis: MCs secrete IL-13, which

recruits MDSCs from the circulation to MC resident tissues, where they create an immunosuppressive environment via IL-4Rα signaling, facilitating tumor growth and metastasis.

We expanded on the LLC tumor models to explore the effect of IL-13 deficiency on B16 melanoma. Using similar methods as were used with LLC, we inoculated WT and IL-13$^{-/-}$ mice with B16 melanoma. In both colonization and flank tumor models, we found no significant difference in tumor volume or size between WT and IL-13$^{-/-}$ mice (data not shown). When we examined the organs for the presence of MDSCs, IL-13$^{-/-}$ had more MDSCs in the bone marrow and fewer in the spleen (Figure 62A). To establish if the difference in MDSCs in the bone marrow was due to changes in the myeloid progenitors in the bone marrow, we analyzed the common myeloid progenitors (CMP), granulocyte-monocyte progenitors (GMP), and myeloid-erythroid progenitors (MEP) in the bone marrow after tumor. We found similar levels of all progenitors between WT and IL-13$^{-/-}$ mice (Figure 62B), indicating it was likely due to some circulating tumor derived factor that was leading to the alteration in MDSC levels in the bone marrow rather than a change in progenitors. In further support of this is that naïve MDSC levels between WT and IL-13$^{-/-}$ mice are not different (Figure 63). We also measured MDSC levels after B16 flank tumors and found no significant differences in any organs (Figure 62C).

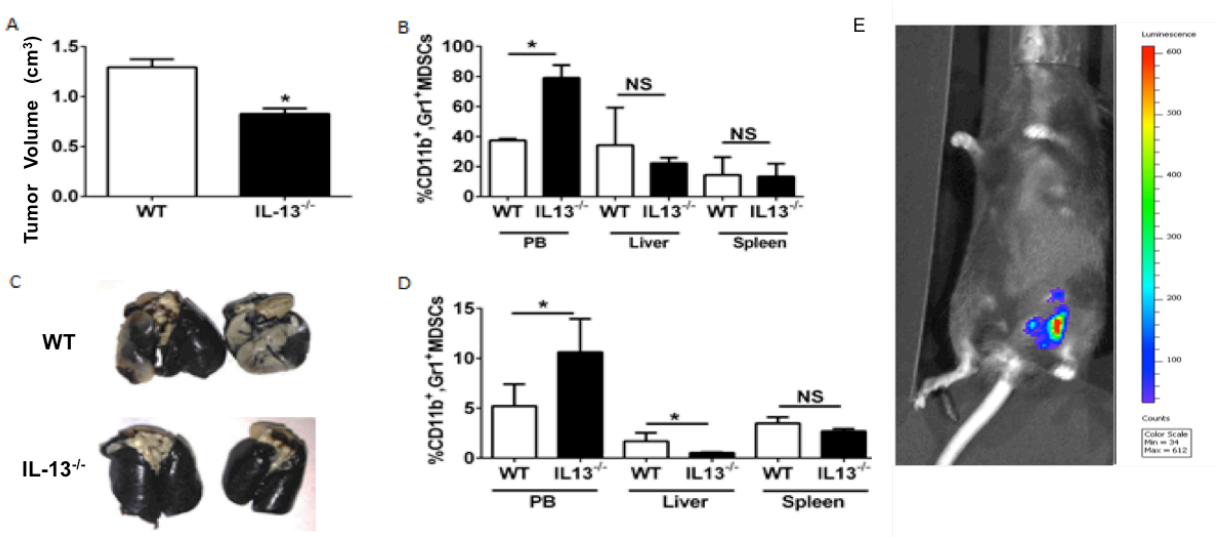

Figure 61: IL-13 is important for MDSC-driven suppression of tumor immunity.

A. and B. IL-13$^{-/-}$ or WT mice were challenged with LLC s.c. tumor. Tumor volume (A) and percent CD11b^{+} Gr1^{+} cells in spleen, liver, and peripheral blood (PB) (B) were assessed. C. Mice were challenged with LLC *i.v.* and lungs were infused with India ink (intra-tracheal) to visualize tumor (representative lungs). D. Percent CD11b^{+} Gr1^{+} cells in spleen, lungs, and PB were analyzed by flow cytometry. E. Representative bioluminescent image overlay of WT with LLC-luciferase s.c. tumor. Mean ± SD. *$p<0.05$. $n>5$, unpaired Student's t test.

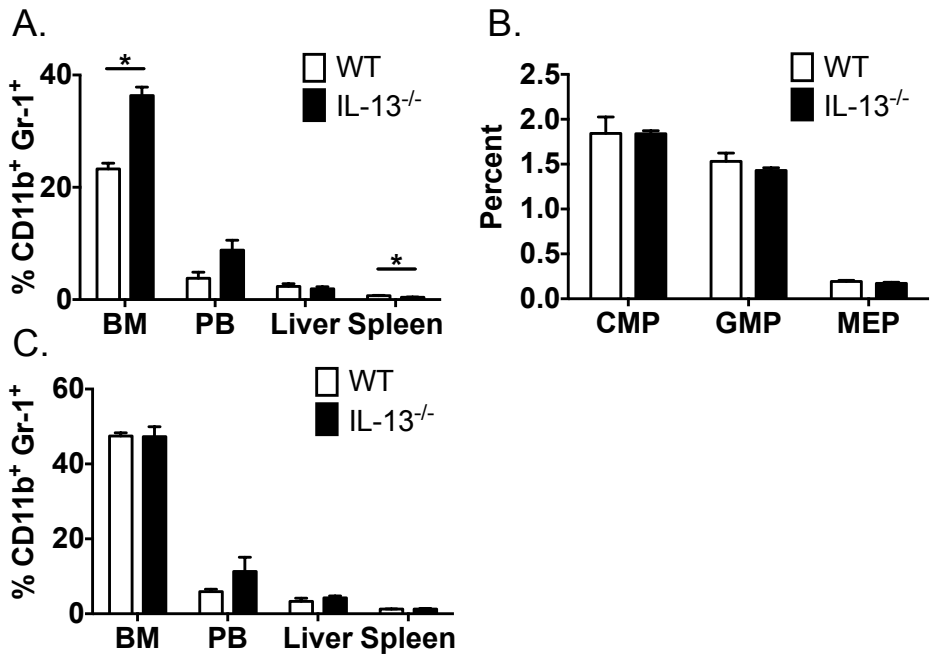

Figure 62: MDSCs levels in B16 melanoma in WT and IL-13$^{-/-}$ mice.

B16 colonization model in WT and IL-13$^{-/-}$ mice. A. Indicated organs were analyzed by flow cytometry for the presence of CD11b^{+} Gr-1^{+} MDSCs 18 days after tumor inoculation (colonization). B. Bone marrow (BM) was assessed for common myeloid progenitors (CMP; Lin^{-} c-Kit^{hi} Sca1^{-} CD34^{+} FcγRII/III^{lo}), granulocytic-monocytic progenitors (GMP; Lin^{-} c-Kit^{hi} Sca1^{-} CD34^{+} FcγRII/III^{hi}), and megakaryocyte-erythroid progenitors (MEP; Lin^{-} c-Kit^{hi} Sca1^{-} CD34^{-} FcγRII/III^{lo}) by flow cytometry. C. B16 melanoma s.c. (flank) tumor model. Percent CD11b^{+} Gr1^{+} cells assessed by flow cytometry.

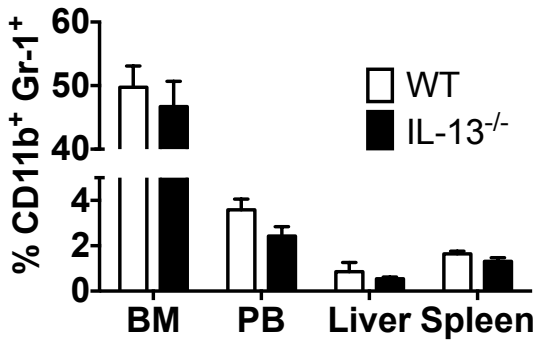

Figure 63: MDSCs in naïve WT and IL-13$^{-/-}$ mice.

CD11b^{+} Gr-1^{+} cells were assessed in indicated organs by flow cytometry.

IL-13$^{-/-}$ MDSCs are less suppressive than A10Tg MDSCs

Given the differences in MDSC levels in WT and IL-13$^{-/-}$ mice in the tumor models, we aimed to understand if the MDSCs generated in IL-13$^{-/-}$ and WT mice functioned similarly. Of note, we did not observe any differences in proportions of G-MDSCs and M-MDSCs between WT and IL-13$^{-/-}$ mice except for a reduction in M-MDSCs in the liver of IL-13$^{-/-}$ mice (). A hallmark of MDSC function is their ability to suppress T cell proliferation. We isolated MDSCs from A10Tg and IL-13$^{-/-}$ A10Tg mice spleens and co-cultured them with CFSE-labeled WT T cells on anti-CD3ε coated plates. Percent divided as assessed after 72h by dilution of CFSE by flow cytometry. A10Tg MDSCs suppressed 50% of T cell proliferation at the ratio of 1:0.25 (T:MDSC) (Figure 65). However, more than twice as many IL-13$^{-/-}$ MDSCs were required to suppress T cell proliferation to the same extent (Figure 65). Interestingly, the addition of rIL-13 to T cell suppression assays with A10Tg or IL-13$^{-/-}$ A10Tg MDSCs did not affect the functional suppression of either cohort (Figure 65). This is in contrast to a report that MDSCs differentiated with IL-13 are more suppressive than those differentiated without IL-13[220]. Less suppressive IL-13$^{-/-}$ MDSCs is consistent with the smaller tumor size seen in the LLC tumor models, which may be the results of better immune control of the tumor.

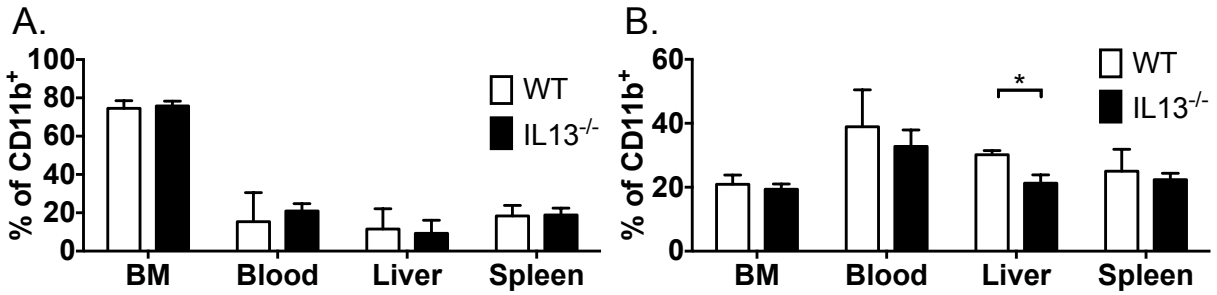

Figure 64: Naïve IL-13$^{-/-}$ mice have similar levels of G-MDSCs and M-MDSCs.

WT and IL-13$^{-/-}$ mice organs were analyzed for G-MDSCs (CD11b^{+} Ly6G^{hi} Ly6C^{lo}) and M-MDSCs (CD11b^{+} Ly6G^{-} Ly6C^{hi}) by flow cytometry. Student's unpaired t test, * $p<0.05$.

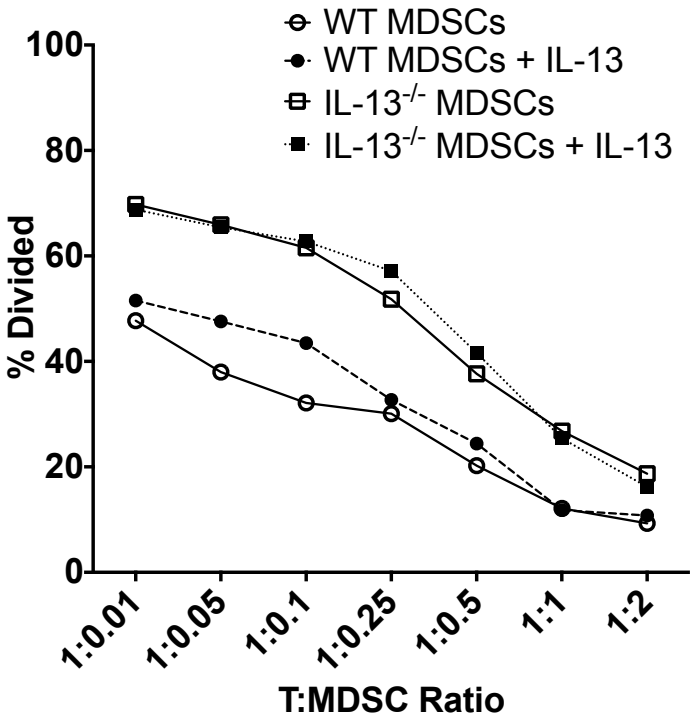

Figure 65: T cell suppression with A10Tg and IL-13$^{-/-}$ A10Tg MDSCs.

CFSE-labeled T cells were co-cultured with WT (A10Tg) or IL-13-deficient (IL-13$^{-/-}$ A10Tg) MDSCs on anti-CD3ε coated plates. Percent divided was assessed after 72h by dilution of the proliferation dye by flow cytometry. rIL-13 (50ng/mL) was added to indicated groups for the entire culture.

MDSCs migration

Given the migration data from our recent publication[167] and the results from tumor models in WT and IL-13$^{-/-}$ mice, we wanted to understand if IL-13 made by the MCs was mediating these effects. We decided to examine migration of MDSCs to WT and IL-13$^{-/-}$ bone marrow derived MCs (BMMCs). As previously published, WT MDSCs migrated efficiently to WT BMMCs; however, these MDSCs migrated to a lesser extent to IL-13-deficient BMMCs (Figure 66). These results may help to explain the findings in tumor models in WT and IL-13$^{-/-}$ mice, which indicated altered trafficking of MDSCs.

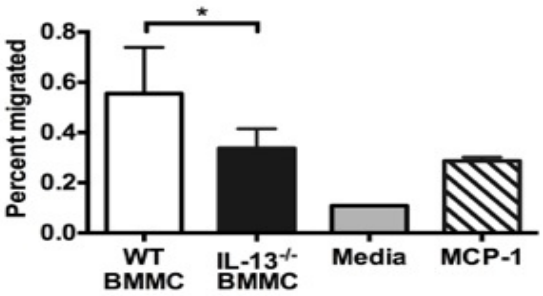

Figure 66: MDSCs migrate less efficiently to IL-13$^{-/-}$ BMMCs.

MDSCs were loaded into trans-well assay plates (8μm pore size) and migrated toward BMMCs from WT or IL-13$^{-/-}$ mice, media only, or MCP-1 (100ng/mL). MDSCs in top and bottom wells were assessed by flow cytometry after 4h to obtain percent migrated. Mean ± SD. n=6 per group, *$p<0.05$, unpaired Student's t test.

MDSCs home less effectively to IL-13$^{-/-}$ liver

The migration results intrigued us, so we explored how MDSCs survive within WT and IL-13$^{-/-}$ mice. To this end, we adoptively transferred PKH26-labeled WT MDSCs into naïve WT and IL-13$^{-/-}$ mice and examined the organs by flow cytometry and confocal microscopy. The lipid labeled dye PKH26 can be detected similarly to phycoerythrin (PE) by flow cytometers, thus we determined the percent of CD11b^{+} Gr-1^{+} MDSCs that were PE^{+} in each organ 24h after adoptive transfer. Bone marrow, peripheral blood, and spleen all had similar levels of PE^{+} MDSCs (Figure 67A). Interestingly, the livers of IL-13$^{-/-}$ mice contained fewer PE^{+} MDSCs than those in WT mice (Figure 67A). Frozen liver sections from these mice were stained for MCs. MDSCs (red) and MCs (green) are seen in both WT and IL-13$^{-/-}$ livers, but the latter contains fewer MDSCs (Figure 67B).

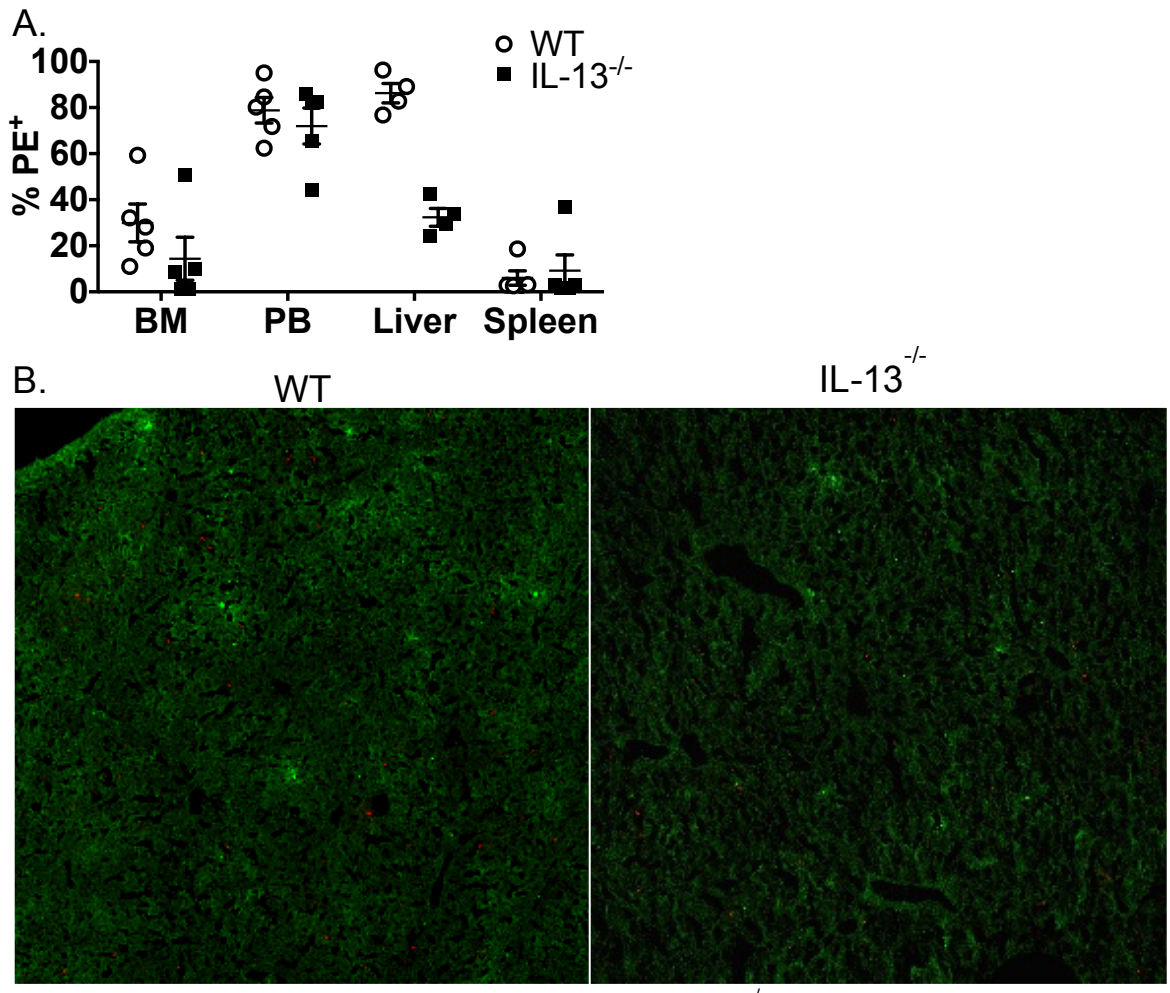

Figure 67: MDSC adoptive transfer into WT and IL-13$^{-/-}$ mice.

PKH26-labeled 10x10^{6} WT MDSCs were adoptively transferred (*i.v.*) into WT and IL-13$^{-/-}$ mice. A. Indicated organs were examined 24h after adoptive transfer for the percent of MDSCs (CD11b^{+} Gr-1^{+}) that were PE^{+} by flow cytometry. B. Livers were frozen in OCT and 5µm sections were cut and stained with anti-mouse mast cell tryptase (green). PKH26-labeled MDSCs are shown in red.

Chemokine expression in WT and IL-13$^{-/-}$ mice

We were intrigued by the difference in migration of MDSCs to both WT and IL-13-deficient BMMCs and within WT and IL-13$^{-/-}$ mice. The liver of these mice was of particular interest as the MDSCs failed to localize here in IL-13$^{-/-}$ mice. In an asthma model, IL-13 was demonstrated to drive the expression of CCL2[227]. We found that the livers of IL-13$^{-/-}$ mice expressed less of the chemokine *Ccl2*, which as been shown to be critical for MDSC trafficking to the tumor site and homeostatic niches[228] (Figure 68A). There was no difference in *Ccl2* expression in the spleens of these mice (Figure 68B). These data are consistent with the adoptive transfer experiments in Figure 67. We did not observe any differences in the expression of the receptor for CCL2, *Ccr2*, between WT and IL-13$^{-/-}$ MDSCs (Figure 68C). We also examined the *Ccl2* expression of the tumor cell lines that were used in previous figures as a way to understand the variability in the results. We found that the control tumor 4T1, which is known for its ability for MDSC accumulation, had the highest *Ccl2* expression. LLC had somewhat less *Ccl2* expression and B16 melanoma had barely detectable levels (Figure 68D). We see the largest disparity in migration between WT and IL-13$^{-/-}$ in the LLC and fewer differences in B16 tumor models. This may be due to the CCL2 expression of each of these tumor lines.

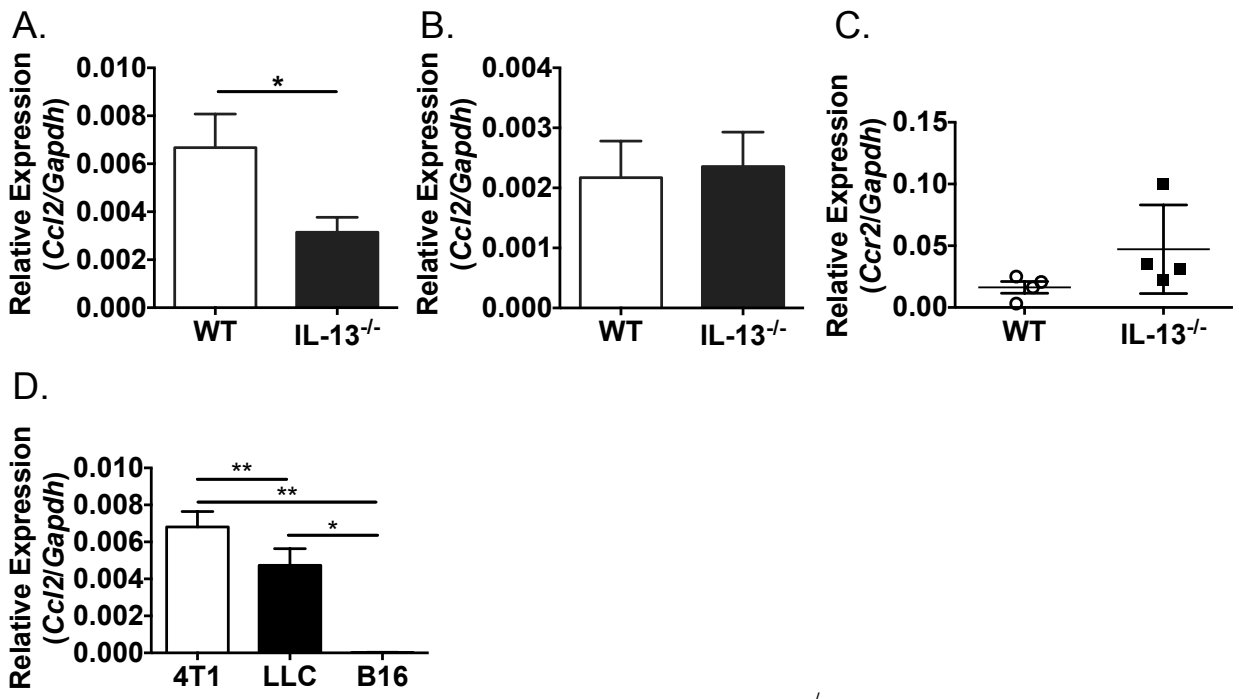

Figure 68: CCL2 and CCR2 expression are altered in IL-13$^{-/-}$ mice.

A. and B. Liver and spleen from WT and IL-13$^{-/-}$ mice were examined for expression of *Ccl2* relative to *Gapdh*. C. Expression of *Ccr2* was measured in MDSCs from WT A10Tg and IL-13$^{-/-}$ A10Tg mice. D. RNA from indicated tumor cells were assessed for expression of *Ccl2* relative to *Gapdh*.

IL-13$^{-/-}$ MDSCs do not enhance N. brasiliensis clearance

Our lab has demonstrated that adoptive transfer of MDSCs increases tumor burden, but also enhances immunity to the helminth parasite *N. brasiliensis*. Given our results with WT and IL-13$^{-/-}$ mice and tumor models in which IL-13$^{-/-}$ had smaller LLC flank tumors and less LLC colonization, we asked if IL-13$^{-/-}$ MDSCs would fail to enhanced clearance of *N. brasiliensis*. We adoptively transferred WT or IL-13$^{-/-}$ MDSCs into WT or IL-13$^{-/-}$ mice and infected them with *N. brasiliensis*. We monitored fecal egg burden over the course of infection. WT mice have peak burden at day 7 and then have cleared the infection by day 10 (Figure 69A). WT MDSC adoptive transfer reduced EPG at days 7 and 8. Transfer of IL-13$^{-/-}$ MDSC into WT mice produced similar parasite burden WT MDSCs. This suggests that the enhanced clearance promoted by MDSCs is not due to IL-13 production (Figure 69A, B). As IL-13 is part of the "weep and sweep" response for parasite clearance, it is unsurprising that IL-13$^{-/-}$ mice have very high level of EPG, which is sustained until euthanasia. WT MDSC adoptive transfer was able to control the parasite in IL-13$^{-/-}$ mice on days 6 and 7, but unable to augment clearance after day 7 (Figure 69A). We also measured IgE in the serum at day 14 after inoculation. IL-13$^{-/-}$ with WT MDSCs produced substantially higher amount of IgE than the rest of the groups (Figure 69C), though the reason for this is yet unknown. This group notwithstanding, IgE levels were similar among groups. (Figure 69C).

Given these results we wanted to see if there were differences in the localization of MDSCs in each of these groups after infection. We examined the liver, peripheral blood, and spleen for total MDSCs as well as the M- and G-MDSC subsets. In contrast to the LLC tumor studies, after *N. brasiliensis* infection we only see trending decreases in MDSCs in the liver between WT and IL-13$^{-/-}$ mice (Figure 70A). We do not see differences in any of the adoptive

transfer groups in total MDSCs in liver or M- or G-MDSCs (Figure 70A-C). In the peripheral blood, we find increased total MDSCs in WT mice given WT MDSCs and IL-13$^{-/-}$ MDSCs. IL-13$^{-/-}$ mice had trending higher level of total MDSCs (Figure 70D) and significantly higher M-MDSCs (Figure 70E), consistent with data Figure 61. WT and IL-13$^{-/-}$ MDSCs transferred into WT mice also had increases in M-MDSCs over WT (Figure 70E). WT MDSCs put in IL-13$^{-/-}$ mice resulted higher M-MDSCs, trending higher than WT + IL-13$^{-/-}$ MDSCs. The prevalence of G-MDSCs followed the same general trend as for M-MDSCs (Figure 70F). In the spleen, adoptive transfer of WT-MDSCs into WT did not results in increased total MDSCs, but the addition of IL-13$^{-/-}$ MDSCs led to higher levels (Figure 70G). Total MDSC levels were also not different between IL-13$^{-/-}$ with or without WT MDSCs. Interestingly, IL-13$^{-/-}$ MDSC injection into WT resulted in more M-MDSCs than WT MDSC transfer (Figure 70H). IL-13$^{-/-}$ mice had more M-MDSCs in the spleen (Figure 70H). G-MDSCs were not remarkable between groups (Figure 70I). Overall, these results indicate that in *N. brasiliensis* infection deletion of IL-13 alters MDSCs both in terms of their function, but also related to their ability to circulate and traffic.

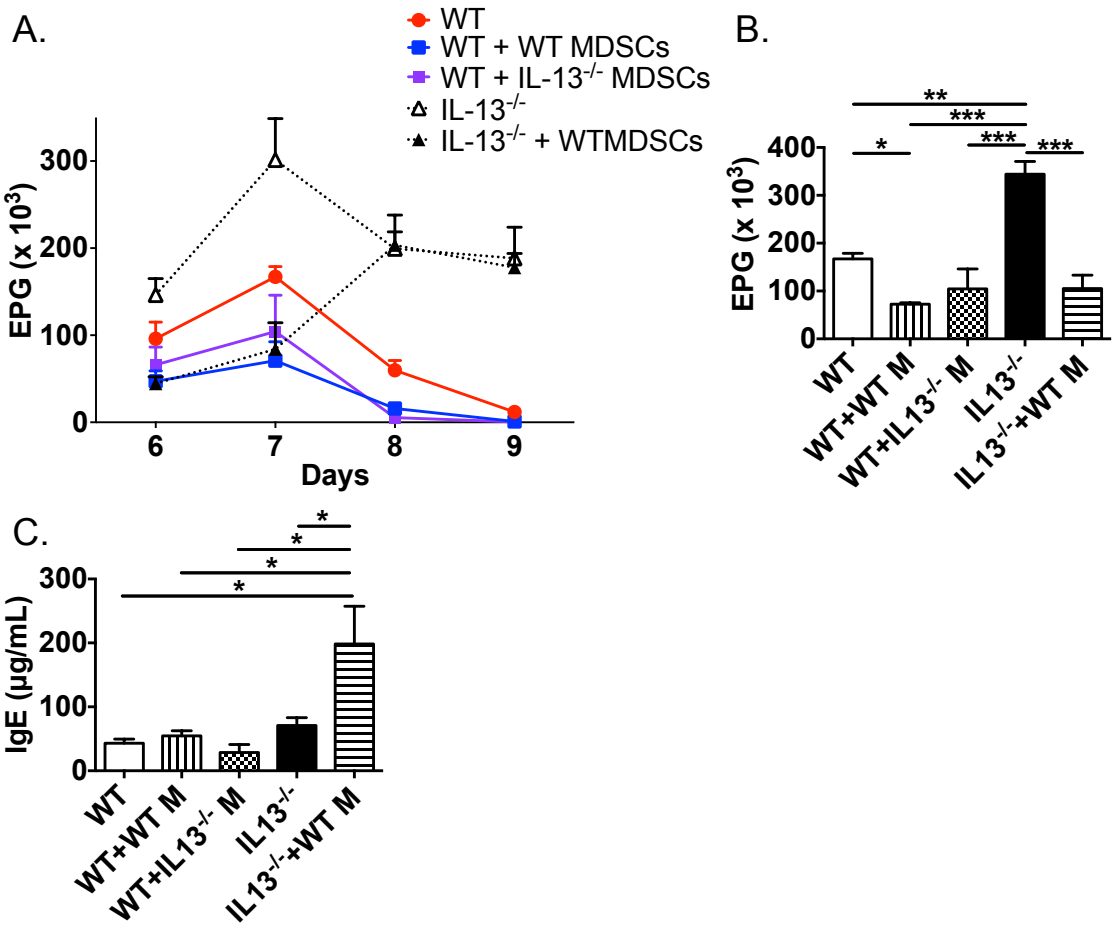

Figure 69: *N. brasiliensis* infection with WT or IL-13$^{-/-}$ MDSC adoptive transfer.

A. WT and IL-13$^{-/-}$ mice were *i.v.* injected with WT or IL-13$^{-/-}$ MDSCs and then inoculated with *N. brasiliensis*. EPG were measured at indicated days. B. Day 7 egg counts. C. IgE was measured in the serum at day 14 after infection. ***p<0.001, **p<0.01, *p<0.05, One-way ANOVA with Tukey's post hoc test.

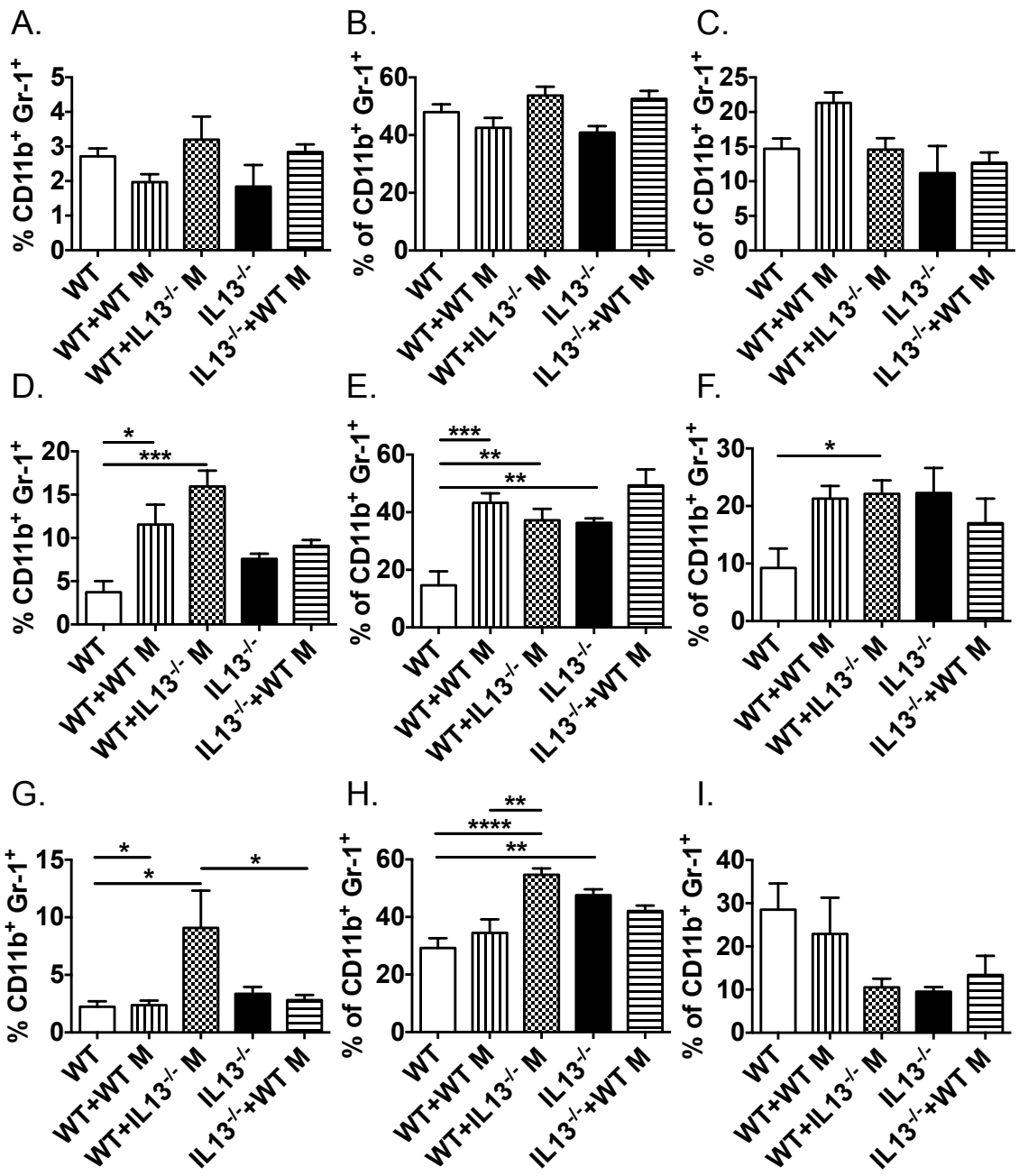

Figure 70: MDSCs levels after adoptive transfer and *N. brasiliensis*.

Liver (A – C), PB (D – F), and Spleen (G – I) from WT and IL-13$^{-/-}$ mice from Figure 69 were examined for total MDSCs (A, D, G), M-MDSCs (B, E, H), and G-MDSCs (C, F, I) by flow cytometry at day 14 after infection. ****p<0.0001, ***p<0.001, **p<0.01, *p<0.05 one-way ANOVA with Tukey's post hoc test.

2.1.4 Discussion

Our lab has demonstrated the substantial connection between MDSCs and MCs particularly with respect to diminishing anti-tumor immunity and enhancing clearance of *N. brasiliensis*. We show that without MCs, MDSCs are unable to perform either of these functions. Precisely how the MC is exerts its influence is still unknown, but we examine two key mediators made by MCs, histamine and IL-13, and their effect on MDSCs. Histamine receptor antagonism blocked enhanced clearance by MDSCs as well as the promotion of tumor growth[167]. We also see that in human patients with indolent systemic mastocytosis and allergies, MDSCs are expanded in the peripheral blood (Figure 60). These data provide strong evidence for the role of histamine in MDSC function. The data with respect to IL-13 has been more difficult to interpret and is likely due to the fact that IL-13 plays a multifactorial role and redundancy of certain functions with IL-4. Environmental loss of IL-13 has clear effects on MDSC trafficking, though intrinsic IL-13-deficiency also affects MDSC function.

In the tumor models we used to study IL-13$^{-/-}$ and WT mice, we found differing results. We found few differences between WT and IL-13$^{-/-}$ mice with B16 tumor models (Figure 62). With LLC flank and colonization models, IL-13$^{-/-}$ mice had more MDSC circulating in the peripheral blood (Figure 61). These results correlated with less tumor burden in the IL-13$^{-/-}$. We hypothesized that IL-13$^{-/-}$ MDSCs were less effective at promoting tumor growth and/or MDSCs in IL-13$^{-/-}$ mice were not receiving the proper signals they needed to traffic to the tumor and other homeostatic niches. We show evidence that IL-13$^{-/-}$ MDSCs are indeed less suppressive than WT MDSCs (Figure 65), though the magnitude of this difference likely is not responsible for changes in tumor burden.

MDSCs egress from the bone marrow and circulate through the blood and spleen to the tumor microenvironment to exert the anti-tumor immune suppression[229]. Stimuli from tumors that govern this migration have been well characterized and are related to the expansion of myeloid cells and as well as inflammatory cytokines. Once generated MDSCs are relatively short-lived, and thus require additional signals to persist[230]. Several groups report that MDSCs accumulate and have a survival advantage within the liver[226,228,231]. We demonstrate that WT MDSCs home less effectively to the liver in IL-13$^{-/-}$ mice compared to WT (Figure 67). This accumulation in the liver is thought to be due CCL2/CCR2 signaling[231]. Liver tissue from IL-13$^{-/-}$ mice had significantly less expression of *Ccl2*, but *Ccr2* levels on IL-13$^{-/-}$ MDSCs were unchanged (Figure 68). Further, we show that different tumor models also express varying levels of *Ccl2*. LLC, the tumor model which we see the largest effect of IL-13 deficiency, expresses more *Ccl2* than B16 melanoma, a model in which we see little effect in IL-13$^{-/-}$ mice (Figure 68). Beyond homeostasis in the liver, Ilkovitch et al. propose that in the liver MDSCs interact with liver macrophages and Kupffer cells, which increase the suppressive capacity of the MDSCs[226]. Without out the interaction in the liver, IL-13$^{-/-}$ MDSCs do not get these cues, potentially explaining the less suppressive capacity observed (Figure 65) and smaller tumor burden (Figure 61).

With histamine receptor antagonism, the MDSCs were unable to enhance parasite clearance (Figure 59). We suspected that IL-13$^{-/-}$ MDSCs might not be able to promote clearance as they were less suppressive of T cell proliferation. However, when IL-13$^{-/-}$ MDSCs were adoptive transferred into WT mice, they improved parasite clearance to a similar extent as WT MDSCs (Figure 69A, B). This indicated that IL-13 made by the MDSCs is responsible for these effects and that different mechanisms were involved suppression of T cell proliferation and

enhancement of *N. brasiliensis* clearance. This was further supported by examining the location of the MDSCs after adoptive transfer. We found that after transfer of IL-13-deficient MDSCs into WT during helminth infection, there were more total and M-MDSCs in the spleen compared to WT given WT MDSCs (Figure 70G, H). However in the liver, we found no differences in the abundance of MDSCs after adoptive transfer (Figure 70A-C). These results are in contrast to the LLC and B16 tumor models, but may represent differences between the signals in parasite infection and tumor growth and metastasis.

We demonstrate that MC mediators, histamine and IL-13, affect the function of MDSCs to enhance *N. brasiliensis* clearance and promote tumor. The interaction between MDSCs and MCs is critical to understanding the tumor microenvironment and how MDSCs exert their anti-tumor effects.

Chapter 2: DNA methyltransferase inhibitor decitabine alters the immunoregulatory function of myeloid derived suppressor cells

2.2.1 Introduction

Despite substantial improvement in breast cancer therapy over the past three decades, invasive disease continues to affect over 200,000 American women each year[232]. Advances in adjuvant therapy have improved outcomes, but for metastatic disease available therapies remain palliative. Current treatments in general are hampered by tumors evading immune mediated attack. Two major strategies employed by tumors are immunoediting and induction of immunosuppressive cells. Immunoediting refers to genetic or epigenetic alterations in tumor antigen expression in order to reduce immunogenicity and occurs normally to aid tumor cells evade immune surveillance. Epigenetic changes can occur through excessive deacetylation of histones or through extensive methylation of genes. Inhibition of the enzymes that catalyze these epigenetic modifications are currently being tested in clinical trials in conjunction with immunotherapies. Recent trials have begun utilizing DNA methyltransferase inhibition (DNAMTi) in conjunction with immunotherapies for squamous cell carcinoma and multiple myeloma[233,234]. Tumor cells can also produce cytokines and growth factors that lead to the expansion of immune cells, which inhibit anti-tumor immune responses. Regulatory T cells (Tregs), tumor associated macrophages (TAMs), and MDSCs are among the suppressive immune cells generated which have been shown to inhibit anti-tumor immunity[229].

Modification of both of these evasion strategies is an attractive supplement to current therapies that may improve outcomes. In recent publications by our group and others have presented evidence for DNA methyltransferase inhibition therapy reversing the downregulation of Her2/Neu[235] on 4T1 murine breast carcinoma cells and MHCII on $CD11b^{+}$ myeloid

cells[236,237]. Both of these studies found an improvement of anti-tumor immune responses. MDSCs are a heterogeneous population of immature myeloid cells, which arise from the bone marrow and have been shown to suppress anti-tumor immunity. Murine MDSCs are defined by surface marker expression of $CD11b^+$ and $Gr\text{-}1^+$, and can be further divided into monocytic (M-MDSCs, $CD11b^+$ $Ly6C^{hi}$ $Ly6G^-$) and granulocytic (G-MDSCs, $CD11b^+$ $Ly6C^{lo}$ $Ly6G^{hi}$) subsets[185]. Integral to the mechanism is their ability to suppress immune responses. Several mechanisms have been implicated: depletion of L-arginine by the enzyme arginase[186,187], generation of soluble oxidizers[188,190,191,238], reduction of T cell migration and viability[170,192,194], and the induction of Tregs[195]. Because MDSCs are immature, with appropriate signals can be stimulated to differentiate[239]. MDSCs, like the other immune suppressive cells, are typically found within the tumor microenvironment as well as in circulation. These circulating MDSCs aggregated with tumor cells may seed and prepare metastatic sites. Given their plasticity and proximity to tumor cells, we propose to alter MDSCs with DNA methyltransferase inhibitors to be less suppressive and promote their ability to generate anti-tumor immune responses.

2.2.2 Materials and Methods

2.2.2.1 Mice

Mice were maintained at VCU animal facility in accordance to guidelines by the National Institutes of Health and American Association for the Accreditation of Laboratory Animal Care. WT Balb/c (Stock No. 000651) and C57BL/6 (Stock No. 000664) were purchased from Jackson Lab. C57BL/6 ADAM10 transgenics (A10Tgs) were generated as previously described[159]. All mouse protocols were approved by VCU Institutional Animal Care and Use Committee.

2.2.2.2 4T1 tumor inoculation

The 4T1 mammary tumor cell line used was provided by Dr. Jane Tsai of the Michigan Cancer Foundation (Detroit, Michigan). Cells were maintained in Dulbecco's Modified Eagle Medium (DMEM) with 10% heat-inactivated fetal calf serum (Hyclone, Logan, UT), 1mM sodium pyruvate, 100U/mL penicillin, and 100µg/mL streptomycin (Sigma, St. Louis MO) (modified DMEM). Tumor cells were harvested for inoculation of mice with 0.05% trypsin–EDTA (Fisher, Pittsburgh, PA). To establish 4T1 flank tumors, 2.5×10^4 4T1 cells were injected in PBS suspension i.d. over the flank[235].

2.2.2.3 Decitabine treatment

For experiments to assess tumor-induced MDSC expansion *in vivo*, tumor-bearing mice were either untreated or treated with decitabine 15µg *i.p.* daily on days 10-13; mice were euthanized on day 15[235].

2.2.2.4 MDSC isolation and in vitro culture with decitabine

MDSCs were isolated from spleens of A10Tg by negative selection using CD90.2 microbeads (Miltenyi Biotec) or positive selection with biotin anti-Gr-1 (clone RB6-8C5)/anti-biotin bead positive selection (Miltenyi Biotec). A10Tg MDSCs were cultured with 10ng/mL GM-CSF (Peprotech) and DMSO (vehicle), 2.5, 5, or 10µM decitabine (EMD Millipore) in cRPMI. Media was changed every two days with fresh GM-CSF and decitabine.

2.2.2.5 Flow cytometry

Antibodies included FITC anti-mouse Gr-1 (RB6-8C5); PE anti-mouse Gr-1 (RB6-8C5); APC anti mouse Ly6C (HK1.4), anti-mouse Ly6G-FITC (1A8), BUV395 anti-mouse CD11b (clone M1/70), PE-Cy7 anti-mouse CD86 (clone GL-1), BV421 anti-mouse I-A/I-E (clone M5/114.15.2), BV510 anti-mouse F4/80 (clone BM8), PE anti-mouse ICOSL (clone HK5.3),

APC anti-mouse OX40L (clone RM134L), and BV711 anti-mouse CD11c (clone N418). Flow cytometric analysis was performed using the LSRFortessa X-20 (BD Biosciences, San Jose, CA, USA). Data analysis was conducted using FlowJo v7.6.5.

2.2.2.6 qPCR

RNA from MDSCs was isolated using TRIzol reagent (LifeTech) according to manufacturer's instructions. cDNA was reversed transcribed using oligodTs and Superscript IV (Lifetech). Taqman probes used are in Table 9.

2.2.2.7 Statistical analysis

Statistical analyses were conducted using Graphpad Prism 6. Error bars represent the standard error of the mean (SEM). A horizontal line with a symbol representing the p value indicates statistical comparison. For pairwise comparisons, Student's t tests were performed for normally distributed data. For multiple comparisons, one-way or two-way ANOVA tests with Tukey's post hoc were performed for normally distributed data. All tests are noted in figure legends.

Table 9: Probes

	Product #[5]
Arg1	Mm00475988_m1
Tgif1	Mm01227699_m1
Il10	Mm01288386_m1
Il4	Mm00445259_m1
Il13	Mm00434204_m1
Gapdh	Mm99999915_g1

[5] Product number for Taqman probes purchased from LifeTech.

2.2.3 Results

4T1 tumor-bearing mice treated with decitabine

A recent publication from our lab demonstrated in a murine 4T1 tumor model that decitabine increased the expression of Her2/Neu and MHCI on tumor cells, enhanced adoptive immunotherapy[235], and reduced MDSC burden in the spleen and circulation (Figure 71). These studies showed the effect of decitabine on increasing tumor immunogenicity, and thus enhancing the anti-tumor immune response. Other groups using combinations of DNAMTi, histone deacetylase (HDAC) inhibition, and immune checkpoint inhibition have also demonstrated reductions in MDSCs.

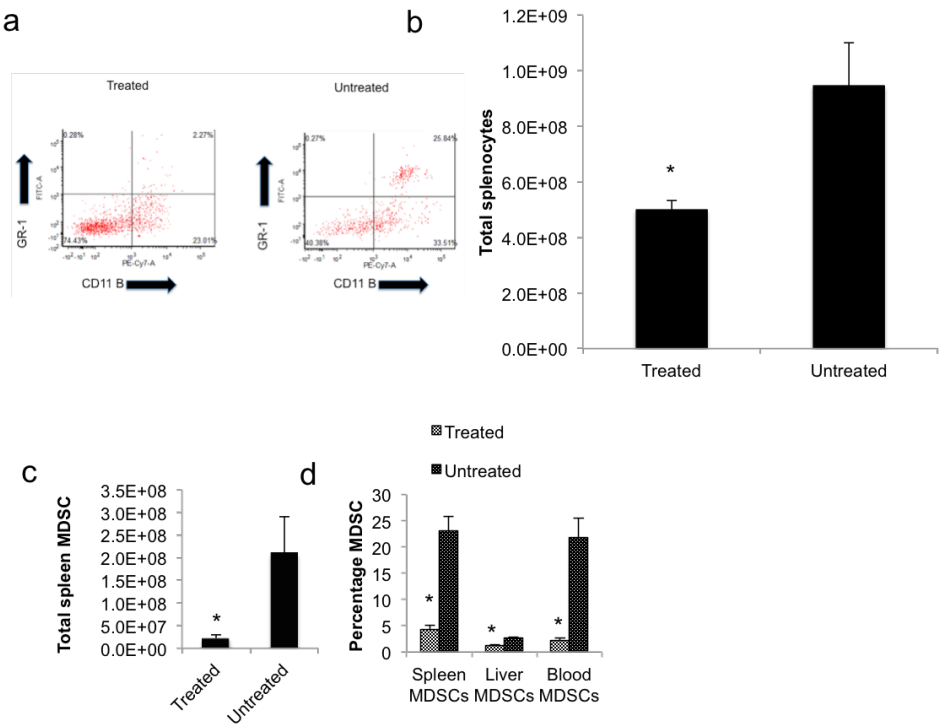

Figure 71: Decitabine treatment *in vivo* reduces MDSC burden in 4T1 tumor bearing mice.

A. Representative dot plot of splenocytes from decitabine treated or untreated 4T1 tumor bearing mice stained with anti-Gr-1 and anti-CD11b. B. Total splenocytes counts from decitabine treated and untreated 4T1 tumor bearing mice. Total number of MDSCs in the spleen (C) and percentages of MDSCs in the spleen, liver, and blood are shown from decitabine treated or untreated 4T1 tumor bearing mice[235].

MDSCs from decitabine-treated tumor bearing mice

As MDSCs are immature myeloid cells that can be differentiated, we aimed to understand if decitabine was affecting the MDSCs in addition to the reduction in numbers. We isolated MDSCs from 4T1 tumor-bearing mice that were treated with decitabine or control and examined their expression of cytokines and enzymes known to be important for MDSC functions[235]. We did not find differences in *Tgfb*, *Il10*, *Il4*, or *Il13* expression between control and decitabine treated MDSCs (Figure 72A). We did see less *Arg1* expression (Figure 72A), which led us to examine the suppressive capacity of these MDSCs. We co-cultured vehicle control and decitabine-treated MDSCs from 4T1 tumor-bearing mice with CFSE-labeled T cells from healthy controls on anti-CD3ε coated plates for 72h. At a low ratio of T:MDSCs, control and decitabine-treated MDSCs did not suppress T cell proliferation (Figure 72B). However at a the higher ratio of 1:5 T:MDSCs, control MDSCs suppressed twice as much T cell proliferation as decitabine-treated (Figure 72B).

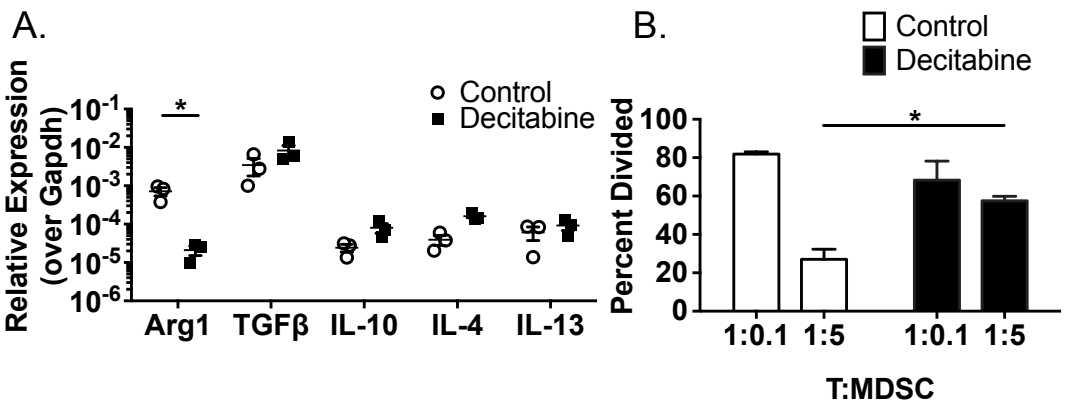

Figure 72: MDSCs from decitabine-treated mice are less suppressive.

MDSCs were isolated from the spleens of control and decitabine-treated 4T1 tumor-bearing mice. A. Expression of indicated genes relative to *Gapdh* was measured in MDSCs. B. CFSE-labeled T cells from healthy control mice were co-cultured with MDSCs from control or decitabine-treated mice at the indicated ratios (T:MDSCs) on anti-CD3ε (1μg/mL) coated plates. After 72h of culture, proliferation was assessed by dilution of CFSE by flow cytometry, and percent divided was calculated. *$p<0.05$, unpaired, Student's t test.

Decitabine-treated MDSCs in vitro

The results of the T cell suppression using MDSCs from *in vivo* decitabine treatment were intriguing, but decitabine treatment causes a drastic reduction in MDSCs and few are left for characterization. We utilized A10Tg mice, which have large numbers of MDSCs without tumor as a source of MDSCs to further study, the effects of decitabine[159]. Thus these mice are a valuable source of MDSCs that are not from tumor-bearing hosts, but have been demonstrated to be equivalent to their tumor-derived counterparts[166]. We cultured MDSCs with 0 (vehicle), 2.5, 5, and 10μM decitabine and 10ng/mL GM-CSF for 1 week and then co-cultured them with violet-labeled T cells on an anti-CD3ε coated plate with anti-CD28 in the media for 96h. Only live cells were used in the T cell suppression assays. At low ratios of T:MDSCs, decitabine- and vehicle-treated MDSCs were unable to block anti-CD3ε/28 stimulated T cell proliferation. Beginning at the 1:0.1 (T:MDSCs) ratio vehicle-treated MDSCs suppressed virtually all T cell proliferation. However, 10 to 50 fold more decitabine treated MDSCs were required to suppress T cell proliferation to a similar extent (Figure 73). These data demonstrate that independent of the reduction of MDSC numbers, decitabine also impairs the suppressive function of MDSCs.

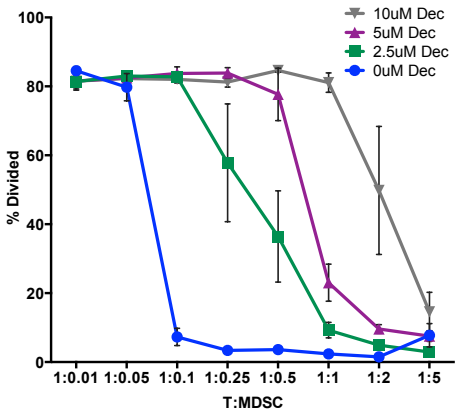

Figure 73: *In vitro* decitabine treatment of MDSCs reduces their ability to suppress T cell proliferation.

MDSCs from ADAM10Tg mice were incubated with indicated concentrations of decitabine for 1 week. MDSCs were washed, counted, and co-cultured with Tag-It Violet labeled T cells with anti-CD3/CD28 stimulation. Percent divided was measured by dye dilution by flow cytometry after 96hrs of culture. Error bars represent SEM.

In vitro decitabine treatment of MDSCs

Given these striking results that treating a tumor-bearing mouse with the DNAMTi decitabine alters both the prevalence and function of MDSCs, we aimed to examine other changes in the MDSCs. We first examined the expression of molecules associated with antigen presentation, MHCII and the costimulatory molecule CD86. As in Figure 73, we cultured ADAM10Tg MDSCs with 0 (vehicle), 2.5, 5, and 10μM decitabine and 10ng/mL GM-CSF. We then analyzed the expression of MHCII and CD86 by flow cytometry. Directly *ex vivo*, the MDSCs did not express MHCII. However, with all doses of decitabine we found a significant increase in the percentage of MDSCs that expressed high levels of MHCII (Figure 74A, B). Further, these $MHCII^{hi}$ MDSCs also expressed CD86 (Figure 74C, D). This was only present when the MDSCs were cultured with decitabine. Interestingly, culturing MDSCs with decitabine did not alter the percentages of cells that were $CD11b^{+}$ $Gr\text{-}1^{+}$ as was seen in with *in vivo* treatment, though these were only 7 day cultures (data not shown). These data suggest that in addition to reducing the suppressive ability of MDSCs, decitabine can potentially make MDSCs into antigen presenting cells.

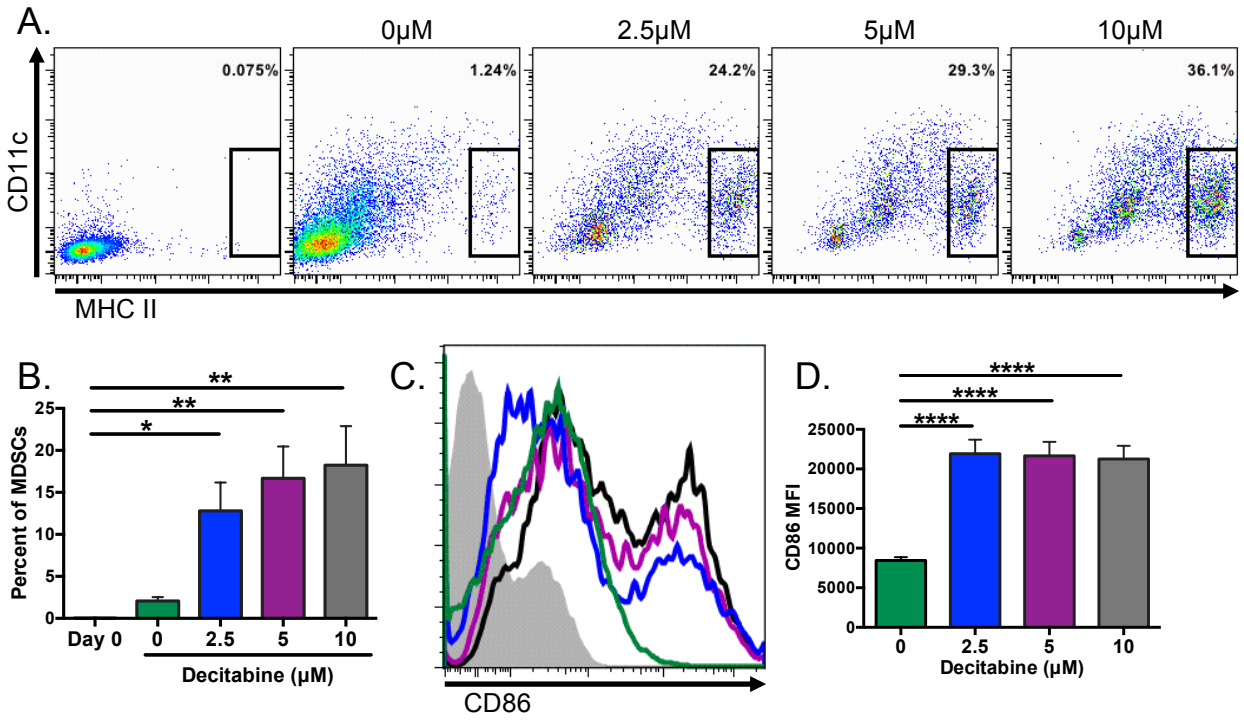

Figure 74: *In vitro* Decitabine treatment of MDSCs increases their expression of MHCII and CD86.

MDSCs from ADAM10Tg mice were incubated with indicated concentrations of decitabine for 1 week with 10mg/mL GM-CSF. A. Representative dot plots are shown for MHCII expression on MDSCs directly *ex vivo* and at each concentration of decitabine. B. Summary data of MHCII expression. C. Representative histogram of CD86 expression on MDSCs is shown and summary data in (D). Error bars represent SEM, ANOVA with Bonferroni multiple comparisons test, **** $p<0.001$, ** $p<0.01$, * $p<0.05$,

Effect of in vivo decitabine treatment of tumor-bearing mice on MDSCs

To confirm the results of *in vitro* treated MDSCs, we treated 4T1 tumor-bearing mice with decitabine and with guadecitabine. Guadecitabine contains an additional guanine compared to decitabine, which increases its half-life in the body and potentially lengthens the exposure to tumor. It is currently in clinical trials for treatment of solid tumors, hematologic malignancies, and lymphomas[240,241]. In addition to testing if decitabine treatment *in vivo* would lead to similar changes in MDSCs as *in vitro* treatment, we also wanted to examine if guadecitabine had similar effects. Consistent with our previous results, we found that treatment of 4T1 tumor-bearing mice with decitabine dramatically decreases the number and percentage of MDSCs. Both guadecitabine groups performed equivalently in terms of MDSC reduction (Figure 75A, B). We then looked at expression of MHCII and CD86, similar to the *in vitro* treatment. Again we found robust increases the expression of both MHCII and CD86 (Figure 75C, D, E). We also examined two other costimulatory molecules, ICOSL and OX40L, which have been shown to promote T_H2 immune responses. Interestingly, only the guadecitabine *i.p.* group had increased expression of ICOSL, and OX40L was increased in all groups compared to no treatment (Figure 75F, G). We also examined the proportions of B, $CD4^+$ T, and $CD8^+$ T cells in the spleen and found that decitabine- and guadecitabine-treated had a larger percentage of B cells. The guadecitabine s.c. group had an increase in $CD4^+$ T cells (Figure 75H). Though these changes may be due to the overall decrease in splenocyte number in the DNAMTi-treated groups. When we examined the type of MDSC was most affected by the various treatments, G-MDSCs were present at a higher percentage of total MDSCs in the no treatment group and decreased by over an order of magnitude with treatment with any of DNAMTi (Figure 75I). M-MDSCs were also reduced by all treatments, but only by approximately half (Figure 75I). These results indicate that decitabine

and guadecitabine treatments *in vivo* reduce MDSCs especially G-MDSCs and increase MDSC expression of MHCII and costimulatory molecules.

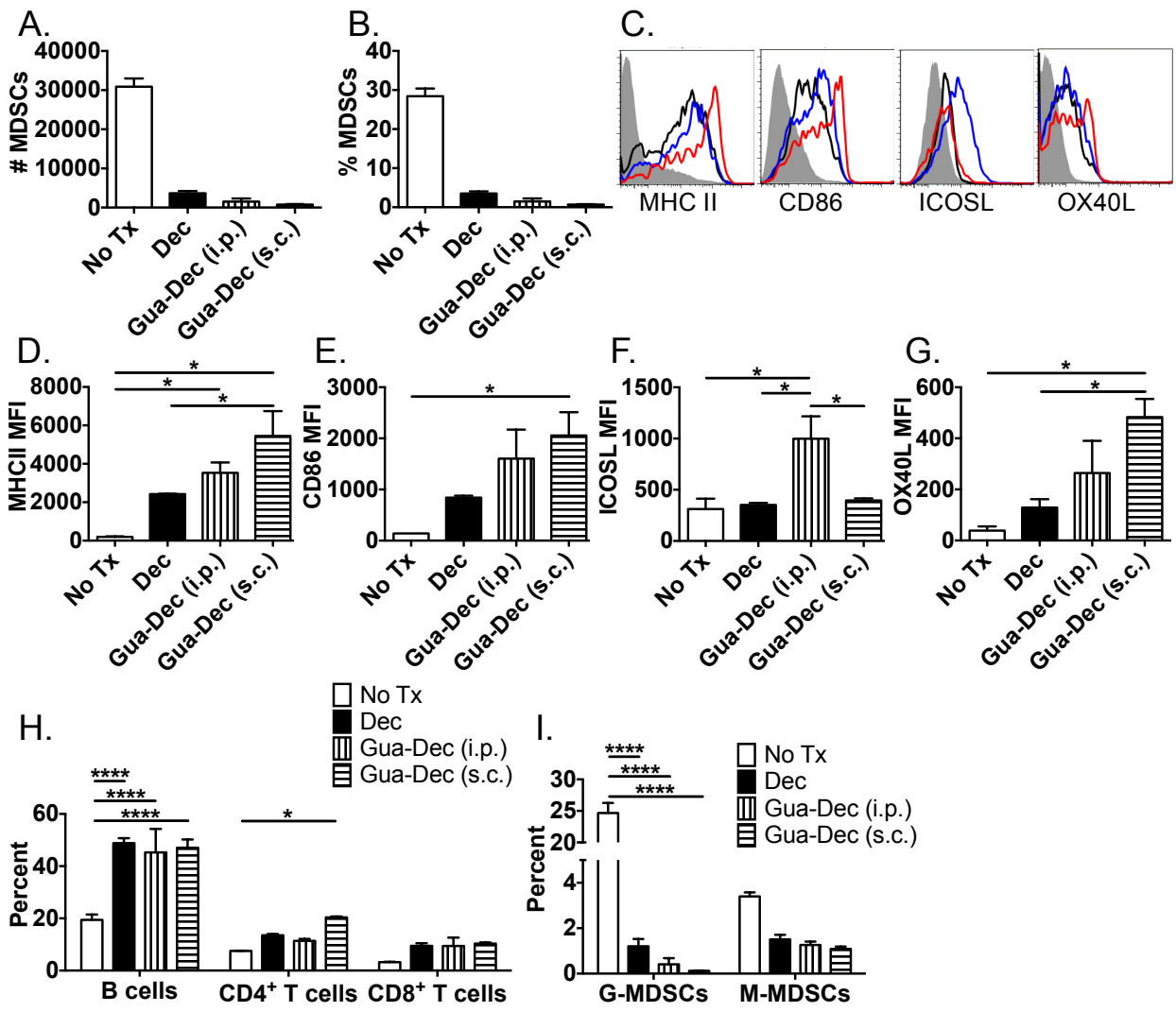

Figure 75: *In vivo* treatment with decitabine and guadecitabine affects MDSC levels and surface molecule expression.

4T1 tumor-bearing mice were treated with decitabine, guadecitabine (*i.p.*), or guadecitabine (s.c.). A. and B. MDSCs in the spleen were assessed by flow cytometry at day 18 after tumor inoculation. C. Representative histograms for the expression of MHCII, CD86, ICOSL, and OX40L on MDSCs in the spleen from treatment groups: no treatment (grey, filled), decitabine (black), guadecitabine *i.p.* (blue), and guadecitabine *s.c.* (red). D. – G. Combined data from (C). H. Relative percentages of splenic B cells ($B220^+$ $CD11b^-$), $CD4^+$ T cells ($B220^-$ $CD11b^-$ $CD4^+$ $CD8^-$), and $CD8^+$ T cells ($B220^-$ $CD11b^-$ $CD4^-$ $CD8^+$). I. Proportions of G- and M-MDSCs in the

spleen. ****$p<0.0001$, *$p<0.05$, one-way ANOVA with Tukey's post hoc test (D-G), two-way ANOVA with Tukey's post hoc test (H, I).

2.2.4 Discussion

Our results demonstrate that treatment of tumor bearing mice with the DNAMTi decitabine reduces MDSC burden and increases expression of MHCII and costimulatory molecules. Further, decitabine treatment also reduced the suppressive capacity of MDSCs. These data represent part of the promise of utilizing epigenetic modification to enhancing anti-tumor immunity and immunotherapy.

Another DNAMTi, azacytidine, has been used to increase tumor antigenicity and was also shown to reduce MDSC in tumor models[242]. Interestingly, azacytidine only decreased MDSC levels when in combination with immune checkpoint inhibitors. Azacytidine alone or with the histone deacetylase (HDAC) inhibitor etinostat were unable to change the percent of MDSCs[242]. Azacytidine and decitabine are remarkably similar and as the mechanism for the MDSC reduction with decitabine is unknown, it is difficult to explain the differing results with the two drugs.

Several strategies have been employed to reduce MDSC numbers as well alter their function. Two main strategies are used to affect MDSC function: inhibiting suppressive enzymes and differentiating MDSCs into non-suppressive cell types[243]. The drug AT38 targeted reactive nitrogen species by downregulating Arg1, iNOS, and peroxynitrite in MDSCs. and nitroaspirin reduced levels of these in MDSCs. Treatment of tumor-bearing mice with a phosphodiesterase-5 inhibitor correlated with less expression of suppressive enzymes in MDSCs, but the mechanism was not elucidated. There have also been reports of differentiating MDSCs to other non-suppressive cell types using various agents, including all-trans retinoic acid[244], low dose IFNγ and TNFα[245], IL-12[245,246], and GM-CSF and IL-4[247]. Each of these groups were able to demonstrate that MDSCs treated with their respective agents became positive for MHC II and in

some cases costimulatory molecules[245]. In several of these studies, MDSCs begin to express CD11c or F4/80, DC and macrophage markers, respectively[246,247]. In our experiments, MDSCs treated with decitabine did increase the expression of MHCII and CD86, but did not express CD11c, F4/80, or NK1.1. The cytokines and growth factors other groups used are often used in to differentiate myeloid lineages from bone marrow cells. Thus, it is unsurprising that these agents are able to alter MDSCs, which are often considered immature in nature. Though the precise mechanism of how decitabine increases the expression, it is likely due to a different mechanism than these growth factors.

Overall the studies presented here demonstrate the promise of using decitabine to reduce MDSCs burden. We demonstrate that *in vivo* and *in vitro* treatment alter MDSC numbers and function in tumor-bearing mice. Further we increase the expression of factors required to present antigen and stimulate adaptive responses.

List of References

List of References

1. Mosmann, T. R.; Coffman, R. L. Th1 AND Th2 CELLS: Different Patterns of Lymphokine Secretion Lead to Different Functional Properties. *Ann. Rev. Immunol* **1989**, *7*, 145–173.
2. Abbas, A. K.; Murphy, K. M.; Sher, A. Functional Diversity of Helper T Lymphocytes. *Nature* **1996**, *383*, 787–93.
3. Urban, J. F.; Noben-Trauth, N.; Donaldson, D. D.; Madden, K. B.; Morris, S. C.; Collins, M.; Finkelman, F. D. IL-13, IL-4Rα, and Stat6 Are Required for the Expulsion of the Gastrointestinal Nematode Parasite Nippostrongylus Brasiliensis. *Immunity* **1998**, *8*, 255–264.
4. Anthony, R. M.; Jr, J. F. U.; Alem, F.; Hamed, H. a; Cristina, T. Mediate Protection Against Nematode Parasites. **2007**, *12*, 955–960.
5. Cliffe, L. J.; Humphreys, N. E.; Lane, T. E.; Potten, C. S.; Booth, C.; Grencis, R. K. Accelerated Intestinal Epithelial Cell Turnover: A New Mechanism of Parasite Expulsion. *Science (New York, N.Y.)* **2005**, *308*, 1463–5.
6. Hasnain, S. Z.; Evans, C. M.; Roy, M.; Gallagher, A. L.; Kindrachuk, K. N.; Barron, L.; Dickey, B. F.; Wilson, M. S.; Wynn, T. a; Grencis, R. K.; Thornton, D. J. Muc5ac: A Critical Component Mediating the Rejection of Enteric Nematodes. *The Journal of experimental medicine* **2011**, *208*, 893–900.
7. Zhao, A.; McDermott, J.; Urban, J. F.; Gause, W.; Madden, K. B.; Yeung, K. A.; Morris, S. C.; Finkelman, F. D.; Shea-Donohue, T. Dependence of IL-4, IL-13, and Nematode-

Induced Alterations in Murine Small Intestinal Smooth Muscle Contractility on Stat6 and Enteric Nerves. *Journal of immunology (Baltimore, Md. : 1950)* **2003**, *171*, 948–54.

8. Palm, N. W.; Rosenstein, R. K.; Medzhitov, R. Allergic Host Defences. *Nature* **2012**, *484*, 465–72.
9. Gocheva, V.; Wang, H. W.; Gadea, B. B.; Shree, T.; Hunter, K. E.; Garfall, A. L.; Berman, T.; Joyce, J. A. IL-4 Induces Cathepsin Protease Activity in Tumor-Associated Macrophages to Promote Cancer Growth and Invasion. *Genes and Development* **2010**, *24*, 241–255.
10. Bronte, V.; Serafini, P.; Santo, C. De; Marigo, I.; Tosello, V.; Mazzoni, A.; Segal, D. M.; Staib, C.; Lowel, M.; Sutter, G.; Colombo, M. P.; Zanovello, P. IL-4-Induced Arginase 1 Suppresses Alloreactive T Cells in Tumor-Bearing Mice. *Journal of immunology (Baltimore, Md. : 1950)* **2003**, *170*, 270–278.
11. Gallina, G.; Dolcetti, L.; Serafini, P.; Santo, C. De; Marigo, I.; Colombo, M. P.; Basso, G.; Brombacher, F.; Borrello, I.; Zanovello, P.; Bicciato, S.; Bronte, V. Tumors Induce a Subset of Inflammatory Monocytes with Immunosuppressive Activity on CD8+ T Cells. *Journal of Clinical Investigation* **2006**, *116*, 2777–2790.
12. World Health Organization *Preventive Chemotherapy in Human Helminthiasis: Coordinated Use of Antihelminthic Drugs in Control Interventions*; World Health Organization Press, 2006.
13. Tchuem Tchuenté, L. a. Control of Soil-Transmitted Helminths in Sub-Saharan Africa: Diagnosis, Drug Efficacy Concerns and Challenges. *Acta Tropica* **2011**, *120*, 4–11.
14. Wills-Karp, M.; Rani, R.; Dienger, K.; Lewkowich, I.; Fox, J. G.; Perkins, C.; Lewis, L.; Finkelman, F. D.; Smith, D. E.; Bryce, P. J.; Kurt-Jones, E. a; Wang, T. C.; Sivaprasad,

U.; Hershey, G. K.; Herbert, D. R. Trefoil Factor 2 Rapidly Induces Interleukin 33 to Promote Type 2 Immunity during Allergic Asthma and Hookworm Infection. *The Journal of experimental medicine* **2012**, *209*, 607–22.

15. Sutherland, T. E.; Logan, N.; Rückerl, D.; Humbles, A. a; Allan, S. M.; Papayannopoulos, V.; Stockinger, B.; Maizels, R. M.; Allen, J. E. Chitinase-like Proteins Promote IL-17-Mediated Neutrophilia in a Tradeoff between Nematode Killing and Host Damage. *Nature Immunology* **2014**, *15*.
16. David, J. R. Delayed Hypersensitivity in Vitro: Its Mediation by Cell-Free Substances Formed by Lymphoid Cell-Antigen Interaction. *Proceedings of the National Academy of Sciences of the United States of America* **1966**, *56*, 72–7.
17. Bloom, B. R.; Bennett, B. Mechanism of a Reaction in Vitro Associated with Delayed-Type Hypersensitivity. *Science (New York, N.Y.)* **1966**, *153*, 80–2.
18. Bernhagen, J.; Calandra, T.; Mitchell, R. A.; Martin, S. B.; Tracey, K. J.; Voelter, W.; Manogue, K. R.; Cerami, A.; Bucala, R. MIF Is a Pituitary-Derived Cytokine That Potentiates Lethal Endotoxaemia. *Nature* **1993**, *365*, 756–9.
19. Calandra, B. T.; Bernhagen, J.; Mitchell, R. A.; Bucala, R. The Macrophage Is an Important and Previously Unrecognized Source of Macrophage Migration Inhibitory Factor. *Journal of Experimental Medicine* **1994**, *179*.
20. Calandra, T.; Bernhagen, J.; Metz, C. N.; Spiegel, L. a; Bacher, M.; Donnelly, T.; Cerami, a; Bucala, R. MIF as a Glucocorticoid-Induced Modulator of Cytokine Production. *Nature* **1995**, *377*, 68–71.
21. Bacher, M.; Metz, C. N.; Calandra, T.; Mayer, K.; Chesney, J.; Lohoff, M.; Gemsa, D.; Donnelly, T.; Bucala, R. An Essential Regulatory Role for Macrophage Migration

Inhibitory Factor in T-Cell Activation. *Proceedings of the National Academy of Sciences of the United States of America* **1996**, *93*, 7849–54.

22. Makita, H.; Nishimura, M.; Miyamoto, K.; Nakano, T.; Tanino, Y.; Hirokawa, J.; Nishihira, J.; Kawakami, Y. Effect of Anti-Macrophage Migration Inhibitory Factor Antibody on Lipopolysaccharide-Induced Pulmonary Neutrophil Accumulation. *American Journal of Respiratory and Critical Care Medicine* **1998**, *158*, 573–579.
23. Rosengren, E.; Aman, P.; Thelin, S.; Hansson, C.; Ahlfors, S.; Björk, P.; Jacobsson, L.; Rorsman, H. The Macrophage Migration Inhibitory Factor MIF Is a Phenylpyruvate Tautomerase. *FEBS letters* **1997**, *417*, 85–8.
24. Swope, M. D.; Lolis, E. Macrophage Migration Inhibitory Factor: Cytokine, Hormone, or Enzyme? *Reviews of physiology, biochemistry and pharmacology* **1999**, *139*, 1–32.
25. Rosengren, E.; Bucala, R.; Aman, P.; Jacobsson, L.; Odh, G.; Metz, C. N.; Rorsman, H. The Immunoregulatory Mediator Macrophage Migration Inhibitory Factor (MIF) Catalyzes a Tautomerization Reaction. *Molecular medicine (Cambridge, Mass.)* **1996**, *2*, 143–149.
26. Grieb, G.; Merk, M.; Bernhagen, J.; Bucala, R. Macrophage Migration Inhibitory Factor (MIF): A Promising Biomarker. *Drug news & perspectives* **2010**, *23*, 257–64.
27. Mitchell, R. a; Metz, C. N.; Peng, T.; Bucala, R. Sustained Mitogen-Activated Protein Kinase (MAPK) and Cytoplasmic Phospholipase A2 Activation by Macrophage Migration Inhibitory Factor (MIF). Regulatory Role in Cell Proliferation and Glucocorticoid Action. *The Journal of biological chemistry* **1999**, *274*, 18100–18106.
28. Roger, T.; David, J.; Glauser, M. P.; Calandra, T. MIF Regulates Innate Immune Responses through Modulation of Toll-like Receptor 4. *Nature* **2001**, *414*, 920–924.

29. Kleemann, R.; Hausser, a; Geiger, G.; Mischke, R.; Burger-Kentischer, a; Flieger, O.; Johannes, F. J.; Roger, T.; Calandra, T.; Kapurniotu, a; Grell, M.; Finkelmeier, D.; Brunner, H.; Bernhagen, J. Intracellular Action of the Cytokine MIF to Modulate AP-1 Activity and the Cell Cycle through Jab1. *Nature* **2000**, *408*, 211–6.

30. Chuang, C.-C.; Chuang, Y.-C.; Chang, W.-T.; Chen, C.-C.; Hor, L.-I.; Huang, A.-M.; Choi, P.-C.; Wang, C.-Y.; Tseng, P.-C.; Lin, C.-F. Macrophage Migration Inhibitory Factor Regulates Interleukin-6 Production by Facilitating Nuclear Factor-Kappa B Activation during Vibrio Vulnificus Infection. *BMC immunology* **2010**, *11*, 50.

31. Cross, J. V; Rady, J. M.; Foss, F. W.; Lyons, C. E.; Macdonald, T. L.; Templeton, D. J. Nutrient Isothiocyanates Covalently Modify and Inhibit the Inflammatory Cytokine Macrophage Migration Inhibitory Factor (MIF). *The Biochemical journal* **2009**, *423*, 315–21.

32. Lubetsky, J. B.; Dios, A.; Han, J.; Aljabari, B.; Ruzsicska, B.; Mitchell, R.; Lolis, E.; Al-Abed, Y. The Tautomerase Active Site of Macrophage Migration Inhibitory Factor Is a Potential Target for Discovery of Novel Anti-Inflammatory Agents. *The Journal of biological chemistry* **2002**, *277*, 24976–82.

33. Mikulowska, A.; Metz, C. N.; Bucala, R.; Holmdahl, R. Macrophage Migration Inhibitory Factor Is Involved in the Pathogenesis of Collagen Type II-Induced Arthritis in Mice. *Journal of immunology (Baltimore, Md. : 1950)* **1997**, *158*, 5514–7.

34. Bernhagen, J.; Krohn, R.; Lue, H.; Gregory, J. L.; Zernecke, A.; Koenen, R. R.; Dewor, M.; Georgiev, I.; Schober, A.; Leng, L.; Kooistra, T.; Fingerle-Rowson, G.; Ghezzi, P.; Kleemann, R.; McColl, S. R.; Bucala, R.; Hickey, M. J.; Weber, C. MIF Is a Noncognate Ligand of CXC Chemokine Receptors in Inflammatory and Atherogenic Cell

Recruitment. *Nature medicine* **2007**, *13*, 587–596.

35. Bozza, M.; Satoskar, a R.; Lin, G.; Lu, B.; Humbles, a a; Gerard, C.; David, J. R. Targeted Disruption of Migration Inhibitory Factor Gene Reveals Its Critical Role in Sepsis. *The Journal of experimental medicine* **1999**, *189*, 341–346.

36. Koebernick, H.; Grode, L.; David, J. R.; Rohde, W.; Rolph, M. S.; Mittrucker, H. W.; Kaufmann, S. H. Macrophage Migration Inhibitory Factor (MIF) Plays a Pivotal Role in Immunity against Salmonella Typhimurium. *Proceedings of the National Academy of Sciences of the United States of America* **2002**, *99*, 13681–13686.

37. Das, R.; Koo, M.-S.; Kim, B. H.; Jacob, S. T.; Subbian, S.; Yao, J.; Leng, L.; Levy, R.; Murchison, C.; Burman, W. J.; Moore, C. C.; Scheld, W. M.; David, J. R.; Kaplan, G.; MacMicking, J. D.; Bucala, R. Macrophage Migration Inhibitory Factor (MIF) Is a Critical Mediator of the Innate Immune Response to Mycobacterium Tuberculosis. *Proceedings of the National Academy of Sciences of the United States of America* **2013**, *110*, E2997-3006.

38. Jüttner, S.; Bernhagen, J.; Metz, C. N.; Röllinghoff, M.; Bucala, R.; Gessner, A. Migration Inhibitory Factor Induces Killing of Leishmania Major by Macrophages: Dependence on Reactive Nitrogen Intermediates and Endogenous TNF-Alpha. *Journal of immunology (Baltimore, Md. : 1950)* **1998**, *161*, 2383–90.

39. Satoskar, a. R.; Bozza, M.; Sosa, M. R.; Lin, G.; David, J. R. Migration-Inhibitory Factor Gene-Deficient Mice Are Susceptible to Cutaneous Leishmania Major Infection. *Infection and Immunity* **2001**, *69*, 906–911.

40. Rodríguez-sosa, M.; Rosas, L. E.; David, J. R.; Bojalil, R.; Satoskar, A. R.; Terrazas, L. I. Macrophage Migration Inhibitory Factor Plays a Critical Role in Mediating Protection

against the Helminth Parasite Taenia Crassiceps. *Infection and immunity* **2003**, *71*, 1247–1254.

41. Martiney, J. a; Sherry, B.; Metz, C. N.; Espinoza, M.; Ferrer, A. S.; Calandra, T.; Hal, E.; Bucala, R. Macrophage Migration Inhibitory Factor Release by Macrophages after Ingestion of Plasmodium Chabaudi -Infected Erythrocytes : Possible Role in the Pathogenesis of Malarial Anemia Macrophage Migration Inhibitory Factor Release by Macrophages after Ingestio. **2000**, *68*, 2259–2267.

42. Chaisavaneeyakorn, S.; Moore, J. M.; Othoro, C.; Otieno, J.; Chaiyaroj, S. C.; Shi, Y. P.; Nahlen, B. L.; Lal, A. a; Udhayakumar, V. Immunity to Placental Malaria. IV. Placental Malaria Is Associated with up-Regulation of Macrophage Migration Inhibitory Factor in Intervillous Blood. *The Journal of infectious diseases* **2002**, *186*, 1371–1375.

43. Rodriguez-Sosa, M.; David, J. R.; Bojalil, R.; Satoskar, A. R.; Terrazas, L. I. Cutting Edge: Susceptibility to the Larval Stage of the Helminth Parasite Taenia Crassiceps Is Mediated by Th2 Response Induced via STAT6 Signaling. *Journal of immunology (Baltimore, Md. : 1950)* **2002**, *168*, 3135–3139.

44. Conine, S. J.; Cross, J. V. MIF Deficiency Does Not Alter Glucose Homeostasis or Adipose Tissue Inflammatory Cell Infiltrates during Diet-Induced Obesity. *Obesity* **2014**, *22*, 418–425.

45. Camberis, M.; Gros, G. Le; Urban, J. Animal Model of Nippostrongylus Brasiliensis and Heligmosomoides Polygyrus. *Current protocols in immunology / edited by John E. Coligan ... [et al.]* **2003**, *Chapter 19*, Unit 19.12.

46. Caven, T. H.; Shelburne, A.; Sato, J.; Yee, C. L.; Becker, S.; Conrad, D. H. IL-21 Dependent IgE Production in Human and Mouse in Vitro Culture Systems Is Cell Density

and Cell Division Dependent and Is Augmented by IL-10. *Cellular Immunology* **2005**, *238*, 123–134.

47. Dussault, A.-A.; Pouliot, M. Rapid and Simple Comparison of Messenger RNA Levels Using Real-Time PCR. *Biological procedures online* **2006**, *8*, 1–10.

48. Gommerman, J.; Gommerman, J.; Rojas, O. Creation of Mixed Bone Marrow Chimeras with Appropriate Controls. *Protoc. Exch.* **2011**.

49. Simpson, K. D.; Templeton, D. J.; Cross, J. V Macrophage Migration Inhibitory Factor Promotes Tumor Growth and Metastasis by Inducing Myeloid-Derived Suppressor Cells in the Tumor Microenvironment. *Journal of immunology (Baltimore, Md. : 1950)* **2012**, *189*, 5533–40.

50. Chaimowitz, N. S.; Martin, R. K.; Cichy, J.; Gibb, D. R.; Patil, P.; Kang, D.-J.; Farnsworth, J.; Butcher, E. C.; McCright, B.; Conrad, D. H. A Disintegrin and Metalloproteinase 10 Regulates Antibody Production and Maintenance of Lymphoid Architecture. *Journal of immunology (Baltimore, Md. : 1950)* **2011**, *187*, 5114–22.

51. Smith, K. A.; Maizels, R. M. IL-6 Controls Susceptibility to Helminth Infection by Impeding Th2 Responsiveness and Altering the Treg Phenotype in Vivo. *European Journal of Immunology* **2014**, *44*, 150–161.

52. Xiao, W.; Hodge, D. R.; Wang, L.; Yang, X.; Zhang, X.; Farrar, W. L. Co-Operative Functions between Nuclear Factors NFkappaB and CCAT/enhancer-Binding Protein-Beta (C/EBP-Beta) Regulate the IL-6 Promoter in Autocrine Human Prostate Cancer Cells. *The Prostate* **2004**, *61*, 354–370.

53. Zhang, Y.; Talalay, P.; Cho, C. G.; Posner, G. H. A Major Inducer of Anticarcinogenic Protective Enzymes from Broccoli: Isolation and Elucidation of Structure. *Proceedings of*

the National Academy of Sciences of the United States of America **1992**, *89*, 2399–2403.

54. Brown, K. K.; Blaikie, F. H.; Smith, R. A. J.; Tyndall, J. D. A.; Lue, H.; Bernhagen, J.; Winterbourn, C. C.; Hampton, M. B. Direct Modification of the Proinflammatory Cytokine Macrophage Migration Inhibitory Factor by Dietary Isothiocyanates. *The Journal of biological chemistry* **2009**, *284*, 32425–33.

55. Ouertatani-Sakouhi, H.; El-Turk, F.; Fauvet, B.; Roger, T.; Roy, D. Le; Karpinar, D. P.; Leng, L.; Bucala, R.; Zweckstetter, M.; Calandra, T.; Lashuel, H. A. A New Class of Isothiocyanate-Based Irreversible Inhibitors of Macrophage Migration Inhibitory Factor. *Biochemistry* **2009**, *48*, 9858–70.

56. Calandra, T.; Roger, T. Macrophage Migration Inhibitory Factor: A Regulator of Innate Immunity. *Nature reviews. Immunology* **2003**, *3*, 791–800.

57. Bancroft, A. J.; Artis, D.; Donaldson, D. D.; Sypek, J. P.; Grencis, R. K. Gastrointestinal Nematode Expulsion in IL-4 Knockout Mice Is IL-13 Dependent. *European Journal of Immunology* **2000**, *30*, 2083–2091.

58. Terrazas, L. I.; Bojalil, R.; Govezensky, T.; Larralde, C. Shift from an Early Protective Th1-Type Immune Response to a Late Permissive Th2-Type Response in Murine Cysticercosis (Taenia Crassiceps). *The Journal of parasitology* **1998**, *84*, 74–81.

59. Stavitsky, A. B.; Metz, C.; Liu, S.; Xianli, J.; Bucala, R. Blockade of Macrophage Migration Inhibitory Factor (MIF) in Schistosoma Japonicum-Infected Mice Results in an Increased Adult Worm Burden and Reduced Fecundity. *Parasite immunology* **2003**, *25*, 369–74.

60. Talalay, P.; Dinkova-Kostova, A. T.; Holtzclaw, W. D. Importance of Phase 2 Gene Regulation in Protection against Electrophile and Reactive Oxygen Toxicity and

Carcinogenesis. *Advances in Enzyme Regulation* **2003**, *43*, 121–134.

61. Healy, Z. R.; Liu, H.; Holtzclaw, W. D.; Talalay, P. Inactivation of Tautomerase Activity of Macrophage Migration Inhibitory Factor by Sulforaphane: A Potential Biomarker for Anti-Inflammatory Intervention. *Cancer epidemiology, biomarkers & prevention : a publication of the American Association for Cancer Research, cosponsored by the American Society of Preventive Oncology* **2011**, *20*, 1516–23.

62. Ward, P. A.; Lentsch, A. B. Endogenous Regulation of the Acute Inflammatory Response. **2002**, 225–228.

63. World Health Organization World Health Organization. Global Surveillance, Prevention and Control of Chronic Respiratory Diseases: A Comprehensive Approach. Geneva, Switzerland. *Chronic respiratory disease* **2007**, 1–146.

64. Wynn, T. a. Type 2 Cytokines: Mechanisms and Therapeutic Strategies. *Nature Reviews Immunology* **2015**, *15*, 271–282.

65. Seals, D. F.; Courtneidge, S. A. The ADAMs Family of Metalloproteases: Multidomain Proteins with Multiple Functions. *Genes & development* **2003**, *17*, 7–30.

66. Weber, S.; Saftig, P. Ectodomain Shedding and ADAMs in Development. *Development (Cambridge, England)* **2012**, *139*, 3693–709.

67. Blobel, C. P.; Wolfsberg, T. G.; Turck, C. W.; Myles, D. G.; Primakoff, P.; White, J. M. A Potential Fusion Peptide and an Integrin Ligand Domain in a Protein Active in Sperm-Egg Fusion. *Nature* **1992**, *356*, 248–252.

68. Rooke, J.; Pan, D.; Xu, T.; Rubin, G. M. KUZ, a Conserved Metalloprotease-Disintegrin Protein with Two Roles in Drosophila Neurogenesis. *Science* **1996**, *273*, 1227–1231.

69. Duojia, P.; Rubin, G. M. Kuzbanian Controls Proteolytic Processing of Notch and

Mediates Lateral Inhibition during Drosophila and Vertebrate Neurogenesis. *Cell* **1997**, *90*, 271–280.

70. Mumm, J. S.; Schroeter, E. H.; Saxena, M. T.; Griesemer, A.; Tian, X.; Pan, D. J.; Ray, W. J.; Kopan, R. A Ligand-Induced Extracellular Cleavage Regulates □-Secretase-like Proteolytic Activation of Notch1. *Molecular Cell* **2000**, *5*, 197–206.

71. Brou, C.; Logeat, F.; Gupta, N.; Bessia, C.; LeBail, O.; Doedens, J. R.; Cumano, A.; Roux, P.; Black, R. A.; Israël, A. A Novel Proteolytic Cleavage Involved in Notch Signaling. *Molecular Cell* **2000**, *5*, 207–216.

72. Saito, T.; Chiba, S.; Ichikawa, M.; Kunisato, A.; Asai, T.; Shimizu, K.; Yamaguchi, T.; Yamamoto, G.; Seo, S.; Kumano, K.; Nakagami-Yamaguchi, E.; Hamada, Y.; Aizawa, S.; Hirai, H. Notch2 Is Preferentially Expressed in Mature B Cells and Indispensable for Marginal Zone B Lineage Development. *Immunity* **2003**, *18*, 675–685.

73. Radtke, F.; Wilson, A.; Mancini, S. J. C.; MacDonald, H. R. Notch Regulation of Lymphocyte Development and Function. *Nature immunology* **2004**, *5*, 247–53.

74. Tetering, G. van; Diest, P. van; Verlaan, I.; Wall, E. van der; Kopan, R.; Vooijs, M. Metalloprotease ADAM10 Is Required for Notch1 Site 2 Cleavage. *Journal of Biological Chemistry* **2009**, *284*, 31018–31027.

75. Hartmann, D.; Strooper, B. de; Serneels, L.; Craessaerts, K.; Herreman, A.; Annaert, W.; Umans, L.; Lübke, T.; Lena Illert, A.; Figura, K. von; Saftig, P. The Disintegrin/metalloprotease ADAM 10 Is Essential for Notch Signalling but Not for Alpha-Secretase Activity in Fibroblasts. *Human molecular genetics* **2002**, *11*, 2615–24.

76. Swiatek, P. J.; Lindsell, C. E.; Amo, F. F. Del; Weinmaster, G.; Gridley, T. Notch 1 Is Essential for Postimplantation Development in Mice. *Genes Dev* **1994**, *8*, 707–719.

77. Peschon, J. J.; Slack, J. l; Reddy, P.; Stocking, K. L.; Sunnarborg, S. W.; Lee, D. C.; Russell, W. E.; Castner, B. J.; Johnson, R. S.; Fitzner, J. N.; Boyce, R. W.; Nelson, N.; Kozolosky, C. J.; Wolfson, M. F.; Rauch, C. T.; Pat Cerretti, D.; Paxton, R. J. An Essential Role for Ectodomain Shedding in Mammalian Development. *Science* **1998**, *282*, 1281–1284.

78. Saftig, P.; Reiss, K. The "A Disintegrin And Metalloproteases" ADAM10 and ADAM17: Novel Drug Targets with Therapeutic Potential? *European journal of cell biology* **2011**, *90*, 527–35.

79. Conrad, D. H.; Ford, J. W.; Sturgill, J. L.; Gibb, D. R. CD23: An Overlooked Regulator of Allergic Disease. *Current allergy and asthma reports* **2007**, *7*, 331–7.

80. Bozkulak, E. C.; Weinmaster, G. Selective Use of ADAM10 and ADAM17 in Activation of Notch1 Signaling. *Molecular and Cellular Biology* **2009**, *29*, 5679–5695.

81. Bray, S. J. Notch Signalling in Context. *Nature reviews. Molecular cell biology* **2016**, *9*, 722–735.

82. Tian, L.; Wu, X.; Chi, C.; Han, M.; Xu, T.; Zhuang, Y. ADAM10 Is Essential for Proteolytic Activation of Notch during Thymocyte Development. *International Immunology* **2008**, *20*, 1181–1187.

83. Folgosa, L.; Zellner, H. B.; Shikh, M. E. El; Conrad, D. H. Disturbed Follicular Architecture in B Cell A Disintegrin and Metalloproteinase (ADAM)10 Knockouts Is Mediated by Compensatory Increases in ADAM17 and TNF-α Shedding. *Journal of immunology (Baltimore, Md. : 1950)* **2013**, *191*, 5951–8.

84. Gibb, D. R.; Shikh, M. El; Kang, D.-J.; Rowe, W. J.; Sayed, R. El; Cichy, J.; Yagita, H.; Tew, J. G.; Dempsey, P. J.; Crawford, H. C.; Conrad, D. H. ADAM10 Is Essential for

Notch2-Dependent Marginal Zone B Cell Development and CD23 Cleavage in Vivo. *The Journal of experimental medicine* **2010**, *207*, 623–35.

85. Mildner, A.; Jung, S. Development and Function of Dendritic Cell Subsets. *Immunity* **2014**, *40*, 642–656.

86. Tussiwand, R.; Everts, B.; Grajales-Reyes, G. E.; Kretzer, N. M.; Iwata, A.; Bagaitkar, J.; Wu, X.; Wong, R.; Anderson, D. A.; Murphy, T. L.; Pearce, E. J.; Murphy, K. M. Klf4 Expression in Conventional Dendritic Cells Is Required for T Helper 2 Cell Responses. *Immunity* **2015**, *42*, 916–928.

87. Lambrecht, B. N.; Galli, S. J. SnapShot: Integrated Type 2 Immune Responses. *Immunity* **2015**, *43*, 408–408.

88. Hirota, J. a; Budelsky, a; Smith, D.; Lipsky, B.; Ellis, R.; Xiang, Y.-Y.; Lu, W.-Y.; Inman, M. D. The Role of Interleukin-4Ralpha in the Induction of Glutamic Acid Decarboxylase in Airway Epithelium Following Acute House Dust Mite Exposure. *Clinical and experimental allergy : journal of the British Society for Allergy and Clinical Immunology* **2010**, *40*, 820–30.

89. Cates, E. C.; Fattouh, R.; Wattie, J.; Inman, M. D.; Goncharova, S.; Coyle, A. J.; Gutierrez-Ramos, J.-C.; Jordana, M. Intranasal Exposure of Mice to House Dust Mite Elicits Allergic Airway Inflammation via a GM-CSF-Mediated Mechanism. *J Immunology* **2004**, *173*, 6384–6392.

90. *Mouse Models of Allergic Disease*; Allen, I. C., Ed.; Methods in Molecular Biology; Humana Press: Totowa, NJ, 2013; vol1032.

91. Metz, M.; Schäfer, B.; Tsai, M.; Maurer, M.; Galli, S. J. Evidence That the Endothelin A Receptor Can Enhance IgE-Dependent Anaphylaxis in Mice. *Journal of Allergy and*

Clinical Immunology **2011**, *128*, 424–426.e1.

92. Valladao, A. C.; Frevert, C. W.; Koch, L. K.; Campbell, D. J.; Ziegler, S. F. STAT6 Regulates the Development of Eosinophilic versus Neutrophilic Asthma in Response to Alternaria Alternata. *The Journal of Immunology* **2016**.

93. Huang, B.; Troese, M. J.; Howe, D.; Ye, S.; Sims, J. T.; Heinzen, R. A.; Borjesson, D. L.; Carlyon, J. A. Anaplasma Phagocytophilum APH_0032 Is Expressed Late during Infection and Localizes to the Pathogen-Occupied Vacuolar Membrane. *Microbial Pathogenesis* **2010**, *49*, 273–284.

94. Troese, M. J.; Carlyon, J. A. Anaplasma Phagocytophilum Dense-Cored Organisms Mediate Cellular Adherence through Recognition of Human P-Selectin Glycoprotein Ligand 1. *Infection and Immunity* **2009**, *77*, 4018–4027.

95. Smith, A. D.; Botero, S.; Shea-Donohue, T.; Urban, J. F. The Pathogenicity of an Enteric Citrobacter Rodentium Infection Is Enhanced by Deficiencies in the Antioxidants Selenium and Vitamin E. *Infection and Immunity* **2011**, *79*, 1471–1478.

96. Caton, M. L.; Smith-Raska, M. R.; Reizis, B. Notch-RBP-J Signaling Controls the Homeostasis of CD8- Dendritic Cells in the Spleen. *The Journal of experimental medicine* **2007**, *204*, 1653–1664.

97. Denis, O.; Vincent, M.; Havaux, X.; Prins, S. De; Treutens, G.; Huygen, K. Induction of the Specific Allergic Immune Response Is Independent of Proteases from the Fungus Alternaria Alternata. *European Journal of Immunology* **2013**, *43*, 907–917.

98. Akkoyunlu, M.; Fikrig, E. Gamma Interferon Dominates the Murine Cytokine Response to the Agent of Human Granulocytic Ehrlichiosis and Helps to Control the Degree of Early Rickettsemia. *Infection and Immunity* **2000**, *68*, 1827–1833.

99. Pedra, J. H. F.; Tao, J.; Sutterwala, F. S.; Sukumaran, B.; Berliner, N.; Bockenstedt, L. K.; Flavell, R. A.; Yin, Z.; Fikrig, E. IL-12/23p40-Dependent Clearance of Anaplasma Phagocytophilum in the Murine Model of Human Anaplasmosis. *FEMS Immunology and Medical Microbiology* **2007**, *50*, 401–410.

100. Collins, J. W.; Keeney, K. M.; Crepin, V. F.; Rathinam, V. a K.; Fitzgerald, K. a; Finlay, B. B.; Frankel, G. Citrobacter Rodentium: Infection, Inflammation and the Microbiota. *Nature reviews. Microbiology* **2014**, *12*, 612–623.

101. Satpathy, A. T.; Briseño, C. G.; Lee, J. S.; Ng, D.; Nicholas, a; Kc, W.; Wu, X.; Thomas, S. R.; Lee, W.; Mcdonald, K. G.; Meredith, M. M.; Song, C.; Guidos, C. J.; Newberry, R. D.; Ouyang, W.; Murphy, T. L.; Stappenbeck, T. S. Immunity Against Attaching and Effacing Bacterial Pathogens. **2014**, *14*, 937–948.

102. Lewis, K. L.; Caton, M. L.; Bogunovic, M.; Greter, M.; Grajkowska, L. T.; Ng, D.; Klinakis, a; Charo, I. F.; Jung, S.; Gommerman, J. L.; Ivanov II; Liu, K.; Merad, M.; Reizis, B. Notch2 Receptor Signaling Controls Functional Differentiation of Dendritic Cells in the Spleen and Intestine. *Immunity* **2011**, *35*, 780–791.

103. Murtaugh, L. C.; Stanger, B. Z.; Kwan, K. M.; Melton, D. A. Notch Signaling Controls Multiple Steps of Pancreatic Differentiation. *Proceedings of the National Academy of Sciences of the United States of America* **2003**, *100*, 14920–5.

104. Jenkins, S. J.; Perona-Wright, G.; Worsley, A. G. F.; Ishii, N.; MacDonald, A. S. Dendritic Cell Expression of OX40 Ligand Acts as a Costimulatory, Not Polarizing, Signal for Optimal Th2 Priming and Memory Induction in Vivo. *Journal of immunology (Baltimore, Md. : 1950)* **2007**, *179*, 3515–23.

105. Ito, T.; Wang, Y. H.; Duramad, O.; Hori, T.; Delespesse, G. J.; Watanabe, N.; Qin, F. X.;

Yao, Z.; Cao, W.; Liu, Y. J. TSLP-Activated Dendritic Cells Induce an Inflammatory T Helper Type 2 Cell Response through OX40 Ligand. *The Journal of Experimental Medicine* **2005**, *202*, 1213–1223.

106. Guo, L.; Huang, Y.; Chen, X.; Hu-Li, J.; Urban, J. F.; Paul, W. E. Innate Immunological Function of TH2 Cells in Vivo. *Nature immunology* **2015**, *16*, 1051–9.

107. Rosenzweig, J. M.; Glenn, J. D.; Calabresi, P. A.; Whartenby, K. A. KLF4 Modulates Expression of IL-6 in Dendritic Cells via Both Promoter Activation and Epigenetic Modification. *Journal of Biological Chemistry* **2013**, *288*, 23868–23874.

108. Mukherjee, M.; Sehmi, R.; Nair, P. Anti-IL5 Therapy for Asthma and Beyond. *The World Allergy Organization journal* **2014**, *7*, 32.

109. Woodruff, P. G.; Modrek, B.; Choy, D. F.; Jia, G.; Abbas, A. R.; Ellwanger, A.; Arron, J. R.; Koth, L. L.; Fahy, J. V. T-Helper Type 2-Driven Inflammation Defines Major Subphenotypes of Asthma. *American Journal of Respiratory and Critical Care Medicine* **2009**, *180*, 388–395.

110. Ishikawa, R.; Tsujimura, Y.; Obata, K.; Kawano, Y.; Minegishi, Y.; Karasuyama, H. IgG-Mediated Systemic Anaphylaxis to Protein Antigen Can Be Induced Even under Conditions of Limited Amounts of Antibody and Antigen. *Biochemical and Biophysical Research Communications* **2010**, *402*, 742–746.

111. Mathews, J. a; Ford, J.; Norton, S.; Kang, D.; Dellinger, a; Gibb, D. R.; Ford, a Q.; Massay, H.; Kepley, C. L.; Scherle, P.; Keegan, a D.; Conrad, D. H. A Potential New Target for Asthma Therapy: A Disintegrin and Metalloprotease 10 (ADAM10) Involvement in Murine Experimental Asthma. *Allergy* **2011**, *66*, 1193–200.

112. Chaimowitz, N. S.; Kang, D.-J.; Dean, L. M.; Conrad, D. H. ADAM10 Regulates

Transcription Factor Expression Required for Plasma Cell Function. *PloS one* **2012**, *7*, e42694.

113. Cooley, L. F.; Martin, R. K.; Zellner, H. B.; Irani, A. M.; Uram-Tuculescu, C.; Shikh, M. E. El; Conrad, D. H. Increased B Cell ADAM10 in Allergic Patients and Th2 Prone Mice. *PLoS ONE* **2015**, *10*, 1–16.

114. Pruessmeyer, J.; Hess, F. M.; Alert, H.; Groth, E.; Pasqualon, T.; Schwarz, N.; Nyamoya, S.; Kollert, J.; Vorst, E. van der; Donners, M.; Martin, C.; Uhlig, S.; Saftig, P.; Dreymueller, D.; Ludwig, A. Leukocytes Require ADAM10 but Not ADAM17 for Their Migration and Inflammatory Recruitment into the Alveolar Space. *Blood* **2014**, *123*, 4077–4088.

115. Gao, Y.; Nish, S.; Jiang, R.; Hou, L.; Licona-Limón, P.; Weinstein, J.; Zhao, H.; Medzhitov, R. Control of T Helper 2 Responses by Transcription Factor IRF4-Dependent Dendritic Cells. *Immunity* **2013**, *39*, 722–732.

116. Persson, E.; Uronen-Hansson, H.; Semmrich, M.; Rivollier, A.; Hägerbrand, K.; Marsal, J.; Gudjonsson, S.; Håkansson, U.; Reizis, B.; Kotarsky, K.; Agace, W. W. IRF4 Transcription-Factor-Dependent CD103+CD11b+ Dendritic Cells Drive Mucosal T Helper 17 Cell Differentiation. *Immunity* **2013**, *38*, 958–969.

117. Lin, Y. L.; Chen, S. H.; Wang, J. Y. Critical Role of IL-6 in Dendritic Cell-Induced Allergic Inflammation of Asthma. *Journal of Molecular Medicine* **2016**, *94*, 51–59.

118. Jin, S.; Mutvei, a P.; Chivukula, I. V; Andersson, E. R.; Ramsköld, D.; Sandberg, R.; Lee, K. L.; Kronqvist, P.; Mamaeva, V.; Ostling, P.; Mpindi, J.-P.; Kallioniemi, O.; Screpanti, I.; Poellinger, L.; Sahlgren, C.; Lendahl, U. Non-Canonical Notch Signaling Activates IL-6/JAK/STAT Signaling in Breast Tumor Cells and Is Controlled by p53 and IKKα/IKKβ.

Oncogene **2013**, *32*, 4892–902.

119. Kuhn, P.-H.; Wang, H.; Dislich, B.; Colombo, A.; Zeitschel, U.; Ellwart, J. W.; Kremmer, E.; Rossner, S.; Lichtenthaler, S. F. ADAM10 Is the Physiologically Relevant, Constitutive Alpha-Secretase of the Amyloid Precursor Protein in Primary Neurons. *The EMBO journal* **2010**, *29*, 3020–32.

120. Sahin, U.; Weskamp, G.; Kelly, K.; Zhou, H. M.; Higashiyama, S.; Peschon, J.; Hartmann, D.; Saftig, P.; Blobel, C. P. Distinct Roles for ADAM10 and ADAM17 in Ectodomain Shedding of Six EGFR Ligands. *Journal of Cell Biology* **2004**, *164*, 769–779.

121. Black, R. A.; Rauch, C. T.; Kozlosky, C. J.; Peschon, J. J.; Slack, J. L.; Wolfson, M. F.; Castner, B. J.; Stocking, K. L.; Reddy, P.; Srinivasan, S.; Nelson, N.; Boiani, N.; Schooley, K. A.; Gerhart, M.; Davis, R.; Fitzner, J. N.; Johnson, R. S.; Paxton, R. J.; March, C. J.; Cerretti, D. P. A Metalloproteinase Disintegrin That Releases Tumour-Necrosis Factor-Alpha from Cells. *Nature* **1997**, *385*, 729–733.

122. Schulz, B.; Pruessmeyer, J.; Maretzky, T.; Ludwig, A.; Blobel, C. P.; Saftig, P.; Reiss, K. ADAM10 Regulates Endothelial Permeability and T-Cell Transmigration by Proteolysis of Vascular Endothelial Cadherin. *Circulation Research* **2008**, *102*, 1192–1201.

123. Koenen, R. R.; Pruessmeyer, J.; Soehnlein, O.; Fraemohs, L.; Zernecke, A.; Schwarz, N.; Reiss, K.; Sarabi, A.; Lindbom, L.; Hackeng, T. M.; Weber, C.; Ludwig, A. Regulated Release and Functional Modulation of Junctional Adhesion Molecule A by Disintegrin Metalloproteinases. *Blood* **2009**, *113*, 4799–4809.

124. Pruessmeyer, J.; Ludwig, A. The Good, the Bad and the Ugly Substrates for ADAM10 and ADAM17 in Brain Pathology, Inflammation and Cancer. *Seminars in Cell and Developmental Biology* **2009**, *20*, 164–174.

125. Marczynska, J.; Ozga, A.; Wlodarczyk, A.; Majchrzak-Gorecka, M.; Kulig, P.; Banas, M.; Michalczyk-Wetula, D.; Majewski, P.; Hutloff, A.; Schwarz, J.; Chalaris, A.; Scheller, J.; Rose-John, S.; Cichy, J. The Role of Metalloproteinase ADAM17 in Regulating ICOS Ligand-Mediated Humoral Immune Responses. *Journal of immunology (Baltimore, Md. : 1950)* **2014**, *193*, 2753–63.

126. Atochina, E. N.; Beers, M. F.; Tomer, Y.; Scanlon, S. T.; Russo, S. J.; Panettieri, R. A.; Haczku, A. Attenuated Allergic Airway Hyperresponsiveness in C57BL/6 Mice Is Associated with Enhanced Surfactant Protein (SP)-D Production Following Allergic Sensitization. *Respiratory research* **2003**, *4*, 15.

127. Fei, M.; Bhatia, S.; Oriss, T. B.; Yarlagadda, M.; Khare, A.; Akira, S.; Saijo, S.; Iwakura, Y.; Fallert Junecko, B. A.; Reinhart, T. A.; Foreman, O.; Ray, P.; Kolls, J.; Ray, A. TNF-Alpha from Inflammatory Dendritic Cells (DCs) Regulates Lung IL-17A/IL-5 Levels and Neutrophilia versus Eosinophilia during Persistent Fungal Infection. *Proceedings of the National Academy of Sciences of the United States of America* **2011**, *108*, 5360–5.

128. Hazenbos, W. L.; Heijnen, I. a; Meyer, D.; Hofhuis, F. M.; Renardel de Lavalette, C. R.; Schmidt, R. E.; Capel, P. J.; Winkel, J. G. van de; Gessner, J. E.; Berg, T. K. van den; Verbeek, J. S. Murine IgG1 Complexes Trigger Immune Effector Functions Predominantly via Fc Gamma RIII (CD16). *Journal of immunology (Baltimore, Md. : 1950)* **1998**, *161*, 3026–3032.

129. Jing, Y.; Ni, Z.; Wu, J.; Higgins, L. A.; Markowski, T. W.; Kaufman, D. S.; Walcheck, B. Identification of an ADAM17 Cleavage Region in Human CD16 (FcγRIII) and the Engineering of a Non-Cleavable Version of the Receptor in NK Cells. *PLoS ONE* **2015**, *10*, 1–14.

130. Romee, R.; Foley, B.; Lenvik, T.; Wang, Y.; Zhang, B.; Ankarlo, D.; Luo, X.; Cooley, S.; Verneris, M.; Walcheck, B.; Miller, J. NK Cell CD16 Surface Expression and Function Is Regulated by a Disintegrin and Metalloprotease-17 (ADAM17). *Blood* **2013**, *121*, 3599–3608.

131. Schuurhuis, D. H.; Ioan-Facsinay, A.; Nagelkerken, B.; Schip, J. J. van; Sedlik, C.; Melief, C. J. M.; Verbeek, J. S.; Ossendorp, F. Antigen-Antibody Immune Complexes Empower Dendritic Cells to Efficiently Prime Specific CD8+ CTL Responses in Vivo. *Journal of immunology (Baltimore, Md : 1950)* **2002**, *168*, 2240–2246.

132. Trifilieff, A.; Walker, C.; Keller, T.; Kottirsch, G.; Neumann, U. Pharmacological Profile of PKF242-484 and PKF241-466, Novel Dual Inhibitors of TNF-Alpha Converting Enzyme and Matrix Metalloproteinases, in Models of Airway Inflammation. *British journal of pharmacology* **2002**, *135*, 1655–64.

133. Hartl, D.; He, C. H.; Koller, B.; Silva, C. A. Da; Homer, R.; Lee, C. G.; Elias, J. A. Acidic Mammalian Chitinase Is Secreted via an ADAM17/epidermal Growth Factor Receptor-Dependent Pathway and Stimulates Chemokine Production by Pulmonary Epithelial Cells. *Journal of Biological Chemistry* **2008**, *283*, 33472–33482.

134. Kuwahara, I.; Lillehoj, E. P.; Koga, T.; Isohama, Y.; Miyata, T.; Kim, K. C. The Signaling Pathway Involved in Neutrophil Elastase-Stimulated MUC1 Transcription. *American Journal of Respiratory Cell and Molecular Biology* **2007**, *37*, 691–698.

135. Oettgen, H. C. Fifty Years Later: Emerging Functions of IgE Antibodies in Host Defense, Immune Regulation, and Allergic Diseases. *The Journal of allergy and clinical immunology* **2016**, *137*, 1631–45.

136. Larché, M.; Akdis, C. A.; Valenta, R. Immunological Mechanisms of Allergen-Specific

Immunotherapy. *Nature reviews. Immunology* **2006**, *6*, 761–71.

137. Gurish, M. F.; Bryce, P. J.; Tao, H.; Kisselgof, A. B.; Thornton, E. M.; Miller, H. R.; Friend, D. S.; Oettgen, H. C. IgE Enhances Parasite Clearance and Regulates Mast Cell Responses in Mice Infected with Trichinella Spiralis. *Journal of immunology (Baltimore, Md. : 1950)* **2004**, *172*, 1139–45.

138. Joseph, M.; Auriault, C.; Capron, A.; Vorng, H.; Viens, P. A New Function for Platelets: IgE-Dependent Killing of Schistosomes. *Nature* **1983**, *303*, 810–2.

139. Wu, L. C.; Zarrin, A. a The Production and Regulation of IgE by the Immune System. *Nature reviews. Immunology* **2014**, *14*, 247–59.

140. Flohr, C.; Quinnell, R. J.; Britton, J. Do Helminth Parasites Protect against Atopy and Allergic Disease? *Clinical and experimental allergy : journal of the British Society for Allergy and Clinical Immunology* **2009**, *39*, 20–32.

141. Yazdanbakhsh, M.; Kremsner, P. G.; Ree, R. van Allergy, Parasites, and the Hygiene Hypothesis. *Science (New York, N.Y.)* **2002**, *296*, 490–4.

142. Capron, M. Effect of Parasite Infection on Allergic Disease. *Allergy* **2011**, *66 Suppl 9*, 16–8.

143. Nutman, T. B. Looking beyond the Induction of Th2 Responses to Explain Immunomodulation by Helminths. *Parasite immunology* **2015**, *37*, 304–13.

144. Bazaral, M.; Orgel, H. a; Hamburger, R. N. The Influence of Serum IgE Levels of Selected Recipients, Including Patients with Allergy, Helminthiasis and Tuberculosis, on the Apparent P-K Titre of a Reaginic Serum. *Clinical and experimental immunology* **1973**, *14*, 117–25.

145. Savage, H. P.; Baumgarth, N. Characteristics of Natural Antibody-Secreting Cells. *Annals*

of the New York Academy of Sciences **2015**, *1362*, 132–42.

146. Waffarn, E. E.; Hastey, C. J.; Dixit, N.; Soo Choi, Y.; Cherry, S.; Kalinke, U.; Simon, S. I.; Baumgarth, N. Infection-Induced Type I Interferons Activate CD11b on B-1 Cells for Subsequent Lymph Node Accumulation. *Nature communications* **2015**, *6*, 8991.

147. Yenson, V.; Baumgarth, N. Purification and Immune Phenotyping of B-1 Cells from Body Cavities of Mice. *Methods in molecular biology (Clifton, N.J.)* **2014**, *1190*, 17–34.

148. Waldschmidt, T.; Snapp, K.; Foy, T.; Tygrett, L.; Carpenter, C. B-Cell Subsets Defined by the Fc Epsilon R. *Annals of the New York Academy of Sciences* **1992**, *651*, 84–98.

149. Soriano, F. G.; Barbeiro, H. V.; Barbeiro, D. F. Inflammatory Response: Role of B1 Cells. *Shock (Augusta, Ga.)* **2013**, *39 Suppl 1*, 5–9.

150. Hayakawa, K.; Hardy, R. R. Normal, Autoimmune, and Malignant CD5+ B Cells: The Ly-1 B Lineage? *Annual review of immunology* **1988**, *6*, 197–218.

151. Förster, I.; Rajewsky, K. Expansion and Functional Activity of Ly-1+ B Cells upon Transfer of Peritoneal Cells into Allotype-Congenic, Newborn Mice. *European journal of immunology* **1987**, *17*, 521–8.

152. Kocks, C.; Rajewsky, K. Stable Expression and Somatic Hypermutation of Antibody V Regions in B-Cell Developmental Pathways. *Annual review of immunology* **1989**, *7*, 537–59.

153. Baumgarth, N.; Tung, J. W.; Herzenberg, L. A. Inherent Specificities in Natural Antibodies: A Key to Immune Defense against Pathogen Invasion. *Springer seminars in immunopathology* **2005**, *26*, 347–62.

154. Takatsu, K.; Takaki, S.; Hitoshi, Y.; Mita, S.; Katoh, S.; Yamaguchi, N.; Tominaga, A. Cytokine Receptors on Ly-1 B Cells. IL-5 and Its Receptor System. *Annals of the New*

York Academy of Sciences **1992**, *651*, 241–58.

155. Vink, A.; Warnier, G.; Brombacher, F.; Renauld, J. C. Interleukin 9-Induced in Vivo Expansion of the B-1 Lymphocyte Population. *The Journal of experimental medicine* **1999**, *189*, 1413–23.

156. Perona-Wright, G.; Mohrs, K.; Taylor, J.; Zaph, C.; Artis, D.; Pearce, E. J.; Mohrs, M. Cutting Edge: Helminth Infection Induces IgE in the Absence of Mu- or Delta-Chain Expression. *Journal of immunology (Baltimore, Md. : 1950)* **2008**, *181*, 6697–701.

157. Silva, N. R. de; Brooker, S.; Hotez, P. J.; Montresor, A.; Engels, D.; Savioli, L.; Silva, N. R. De; Brooker, S.; Hotez, P. J.; Montresor, A.; Engels, D.; Savioli, L. Soil-Transmitted Helminth Infections: Updating the Global Picture. *Trends in parasitology* **2003**, *19*, 547–51.

158. Finkelman, F. D.; Shea-Donohue, T.; Morris, S. C.; Gildea, L.; Strait, R.; Madden, K. B.; Schopf, L.; Urban, J. F. Interleukin-4- and Interleukin-13-Mediated Host Protection against Intestinal Nematode Parasites. *Immunological reviews* **2004**, *201*, 139–55.

159. Gibb, D. R.; Saleem, S. J.; Kang, D.-J.; Subler, M. a; Conrad, D. H. ADAM10 Overexpression Shifts Lympho- and Myelopoiesis by Dysregulating Site 2/site 3 Cleavage Products of Notch. *Journal of immunology (Baltimore, Md. : 1950)* **2011**, *186*, 4244–52.

160. Oettgen, H. C.; Martin, T. R.; Wynshaw-Boris, A.; Deng, C.; Drazen, J. M.; Leder, P. Active Anaphylaxis in IgE-Deficient Mice. *Nature* **1994**, *370*, 367–70.

161. Komai-Koma, M.; Gilchrist, D. S.; McKenzie, A. N. J.; Goodyear, C. S.; Xu, D.; Liew, F. Y. IL-33 Activates B1 Cells and Exacerbates Contact Sensitivity. *Journal of immunology (Baltimore, Md. : 1950)* **2011**, *186*, 2584–91.

162. Ahmed, A.; Koma, M. K. Interleukin-33 Triggers B1 Cell Expansion and Its Release of

Monocyte/Macrophage Chemoattractants and Growth Factors. *Scandinavian journal of immunology* **2015**, *82*, 118–24.

163. Damle, S. R.; Martin, R. K.; Cross, J. V; Conrad, D. H. Macrophage Migration Inhibitory Factor Deficiency Enhances Immune Response to Nippostrongylus Brasiliensis. *Mucosal Immunology* **2016**, 1–10.

164. Smith, K. G.; Light, A.; Nossal, G. J.; Tarlinton, D. M. The Extent of Affinity Maturation Differs between the Memory and Antibody-Forming Cell Compartments in the Primary Immune Response. *The EMBO journal* **1997**, *16*, 2996–3006.

165. Jones, S. A.; White, C. A.; Robb, L.; Alexander, W. S.; Tarlinton, D. M. SOCS3 Deletion in B Cells Alters Cytokine Responses and Germinal Center Output. *Journal of immunology (Baltimore, Md. : 1950)* **2011**, *187*, 6318–26.

166. Saleem, S. J.; Martin, R. K.; Morales, J. K.; Sturgill, J. L.; Gibb, D. R.; Graham, L.; Bear, H. D.; Manjili, M. H.; Ryan, J. J.; Conrad, D. H. Cutting Edge: Mast Cells Critically Augment Myeloid-Derived Suppressor Cell Activity. *Journal of immunology (Baltimore, Md. : 1950)* **2012**, *189*, 511–5.

167. Martin, R. K.; Saleem, S. J.; Folgosa, L.; Zellner, H. B.; Damle, S. R.; Nguyen, G.-K. T.; Ryan, J. J.; Bear, H. D.; Irani, A.-M.; Conrad, D. H. Mast Cell Histamine Promotes the Immunoregulatory Activity of Myeloid-Derived Suppressor Cells. *Journal of leukocyte biology* **2014**, *96*, 1–9.

168. Evans, H.; Killoran, K. E.; Mitre, E. Measuring Local Anaphylaxis in Mice. *Journal of visualized experiments : JoVE* **2014**, e52005.

169. Starkl, P.; Marichal, T.; Gaudenzio, N.; Reber, L. L. L. L.; Sibilano, R.; Tsai, M.; Galli, S. J. S. J.; Berger, B. J.; Bhatti, A. R.; Habermann, E.; Meier, J.; White, J.; Fry, B. G.;

Roelants, K.; Champagne, D. E.; Scheib, H.; Tyndall, J. D.; King, G. F.; al., et; Brodie, E. D.; Perales, J.; Neves-Ferreira, A. G.; Valente, R. H.; Domont, G. B.; Voss, R. S.; Jansa, S. A.; Rowe, A. H.; Xiao, Y.; Rowe, M. P.; Cummins, T. R.; Zakon, H. H.; Galli, S. J. S. J.; Grimbaldeston, M. A.; Tsai, M.; Kitamura, Y.; Galli, S. J. S. J.; Kalesnikoff, J.; Grimbaldeston, M. A.; Piliponsky, A. M.; Williams, C. M.; Tsai, M.; Metz, M.; Grimbaldeston, M. A.; Nakae, S.; Piliponsky, A. M.; Tsai, M.; Galli, S. J. S. J.; Akahoshi, M.; Song, C. H.; Piliponsky, A. M.; Metz, M.; Guzzetta, A.; Abrink, M.; al., et; Higginbotham, R. D.; Higginbotham, R. D.; Karnella, S.; Metz, M.; Piliponsky, A. M.; Chen, C. C.; Lammel, V.; Abrink, M.; Pejler, G.; al., et; Schneider, L. A.; Schlenner, S. M.; Feyerabend, T. B.; Wunderlin, M.; Rodewald, H. R.; Simpson, I. D.; Norris, R. L.; Warrell, D. A.; Wernersson, S.; Pejler, G.; Marichal, T.; Starkl, P.; Reber, L. L. L. L.; Kalesnikoff, J.; Oettgen, H. C.; Tsai, M.; al., et; Profet, M.; Palm, N. W.; Rosenstein, R. K.; Medzhitov, R.; Bilo, B. M.; Rueff, F.; Mosbech, H.; Bonifazi, F.; Oude-Elberink, J. N.; Medeiros, C. R. de; Barbaro, K. C.; Lira, M. S.; Franca, F. O.; Zaher, V. L.; Kokron, C. M.; al., et; Kopp, P.; Dahinden, C. A.; Mullner, G.; et al. IgE Antibodies, FcεRIα, and IgE-Mediated Local Anaphylaxis Can Limit Snake Venom Toxicity. *The Journal of allergy and clinical immunology* **2016**, *137*, 246–57.e11.

170. Sinha, P.; Clements, V. K.; Bunt, S. K.; Albelda, S. M.; Ostrand-Rosenberg, S. Cross-Talk between Myeloid-Derived Suppressor Cells and Macrophages Subverts Tumor Immunity toward a Type 2 Response. *Journal of immunology (Baltimore, Md. : 1950)* **2007**, *179*, 977–83.

171. Le, H. K.; Graham, L.; Cha, E.; Morales, J. K.; Manjili, M. H.; Bear, H. D. Gemcitabine Directly Inhibits Myeloid Derived Suppressor Cells in BALB/c Mice Bearing 4T1

Mammary Carcinoma and Augments Expansion of T Cells from Tumor-Bearing Mice. *International immunopharmacology* **2009**, *9*, 900–9.

172. TAKATSU, K. Interleukin-5 and IL-5 Receptor in Health and Diseases. *Proceedings of the Japan Academy, Series B* **2011**, *87*, 463–485.

173. Erickson, L. D.; Foy, T. M.; Waldschmidt, T. J. Murine B1 B Cells Require IL-5 for Optimal T Cell-Dependent Activation. *Journal of immunology (Baltimore, Md. : 1950)* **2001**, *166*, 1531–9.

174. Moltke, J. von; Ji, M.; Liang, H.-E.; Locksley, R. M. Tuft-Cell-Derived IL-25 Regulates an Intestinal ILC2–epithelial Response Circuit. *Nature* **2015**, *529*, 221–225.

175. Gerbe, F.; Sidot, E.; Smyth, D. J.; Ohmoto, M.; Matsumoto, I.; Dardalhon, V.; Cesses, P.; Garnier, L.; Pouzolles, M.; Brulin, B.; Bruschi, M.; Harcus, Y.; Zimmermann, V. S.; Taylor, N.; Maizels, R. M.; Jay, P. Intestinal Epithelial Tuft Cells Initiate Type 2 Mucosal Immunity to Helminth Parasites. *Nature* **2016**, *529*, 226–30.

176. Fort, M. M.; Cheung, J.; Yen, D.; Li, J.; Zurawski, S. M.; Lo, S.; Menon, S.; Clifford, T.; Hunte, B.; Lesley, R.; Muchamuel, T.; Hurst, S. D.; Zurawski, G.; Leach, M. W.; Gorman, D. M.; Rennick, D. M. IL-25 Induces IL-4, IL-5, and IL-13 and Th2-Associated Pathologies in Vivo. *Immunity* **2001**, *15*, 985–95.

177. Paciorkowski, N.; Porte, P.; Shultz, L. D.; Rajan, T. V B1 B Lymphocytes Play a Critical Role in Host Protection against Lymphatic Filarial Parasites. *The Journal of experimental medicine* **2000**, *191*, 731–6.

178. Xiong, H.; Dolpady, J.; Wabl, M.; Curotto de Lafaille, M. a; Lafaille, J. J. Sequential Class Switching Is Required for the Generation of High Affinity IgE Antibodies. *The Journal of experimental medicine* **2012**, *209*, 353–64.

179. Patel, P. S.; Kearney, J. F. Neonatal Exposure to Pneumococcal Phosphorylcholine Modulates the Development of House Dust Mite Allergy during Adult Life. *Journal of immunology (Baltimore, Md. : 1950)* **2015**, *194*, 5838–50.

180. Péry, P.; Luffau, G.; Charley, J.; Petit, A.; Rouze, P.; Bernard, S. Phosphorylcholine Antigens from Nippostrongylus Brasiliensis. II.--Isolation and Partial Characterization of Phosphorylcholine Antigens from Adult Worm. *Annales d'immunologie* **1978**, *130*, 889–900.

181. Hewitson, J. P.; Filbey, K. J.; Grainger, J. R.; Dowle, A. A.; Pearson, M.; Murray, J.; Harcus, Y.; Maizels, R. M. Heligmosomoides Polygyrus Elicits a Dominant Nonprotective Antibody Response Directed against Restricted Glycan and Peptide Epitopes. *Journal of immunology (Baltimore, Md. : 1950)* **2011**, *187*, 4764–77.

182. Griffin, D. O.; Holodick, N. E.; Rothstein, T. L. Human B1 Cells in Umbilical Cord and Adult Peripheral Blood Express the Novel Phenotype CD20+ CD27+ CD43+ CD70-. *The Journal of experimental medicine* **2011**, *208*, 67–80.

183. Quinnell, R. J.; Bethony, J.; Pritchard, D. I. The Immunoepidemiology of Human Hookworm Infection. *Parasite immunology* **2004**, *26*, 443–54.

184. Poschke, I.; Mougiakakos, D.; Hansson, J.; Masucci, G. V; Kiessling, R. Immature Immunosuppressive CD14+HLA-DR-/low Cells in Melanoma Patients Are Stat3hi and Overexpress CD80, CD83, and DC-Sign. *Cancer research* **2010**, *70*, 4335–45.

185. Movahedi, K.; Guilliams, M.; Bossche, J. Van den; Bergh, R. Van den; Gysemans, C.; Beschin, A.; Baetselier, P. De; Ginderachter, J. a Van Identification of Discrete Tumor-Induced Myeloid-Derived Suppressor Cell Subpopulations with Distinct T Cell-Suppressive Activity. *Blood* **2008**, *111*, 4233–44.

186. Ochoa, A. C.; Zea, A. H.; Hernandez, C.; Rodriguez, P. C. Arginase, Prostaglandins, and Myeloid-Derived Suppressor Cells in Renal Cell Carcinoma. *Clinical cancer research : an official journal of the American Association for Cancer Research* **2007**, *13*, 721s–726s.

187. Rodriguez, P. C.; Hernandez, C. P.; Quiceno, D.; Dubinett, S. M.; Zabaleta, J.; Ochoa, J. B.; Gilbert, J.; Ochoa, A. C. Arginase I in Myeloid Suppressor Cells Is Induced by COX-2 in Lung Carcinoma. *The Journal of experimental medicine* **2005**, *202*, 931–9.

188. Gabrilovich, D. I.; Ostrand-Rosenberg, S.; Bronte, V. Coordinated Regulation of Myeloid Cells by Tumours. *Nature reviews. Immunology* **2012**, *12*, 253–68.

189. Kusmartsev, S. Inhibition of Myeloid Cell Differentiation in Cancer: The Role of Reactive Oxygen Species. *Journal of Leukocyte Biology* **2003**, *74*, 186–196.

190. Kusmartsev, S.; Nefedova, Y.; Yoder, D.; Gabrilovich, D. I. Antigen-Specific Inhibition of CD8+ T Cell Response by Immature Myeloid Cells in Cancer Is Mediated by Reactive Oxygen Species. *Journal of immunology (Baltimore, Md. : 1950)* **2004**, *172*, 989–99.

191. Nagaraj, S.; Gupta, K.; Pisarev, V.; Kinarsky, L.; Sherman, S.; Kang, L.; Herber, D. L.; Schneck, J.; Gabrilovich, D. I. Altered Recognition of Antigen Is a Mechanism of CD8+ T Cell Tolerance in Cancer. *Nature medicine* **2007**, *13*, 828–35.

192. Hanson, E. M.; Clements, V. K.; Sinha, P.; Ilkovitch, D.; Ostrand-Rosenberg, S. Myeloid-Derived Suppressor Cells down-Regulate L-Selectin Expression on CD4+ and CD8+ T Cells. *Journal of immunology (Baltimore, Md. : 1950)* **2009**, *183*, 937–44.

193. Sinha, P.; Clements, V. K.; Fulton, A. M.; Ostrand-Rosenberg, S. Prostaglandin E2 Promotes Tumor Progression by Inducing Myeloid-Derived Suppressor Cells. *Cancer research* **2007**, *67*, 4507–13.

194. Sakuishi, K.; Jayaraman, P.; Behar, S. M.; Anderson, A. C.; Kuchroo, V. K. Emerging

Tim-3 Functions in Antimicrobial and Tumor Immunity. *Trends in immunology* **2011**, *32*, 345–9.

195. Huang, B.; Pan, P.-Y.; Li, Q.; Sato, A. I.; Levy, D. E.; Bromberg, J.; Divino, C. M.; Chen, S.-H. Gr-1+CD115+ Immature Myeloid Suppressor Cells Mediate the Development of Tumor-Induced T Regulatory Cells and T-Cell Anergy in Tumor-Bearing Host. *Cancer research* **2006**, *66*, 1123–31.

196. Lilla, J. N.; Chen, C.-C.; Mukai, K.; BenBarak, M. J.; Franco, C. B.; Kalesnikoff, J.; Yu, M.; Tsai, M.; Piliponsky, A. M.; Galli, S. J. Reduced Mast Cell and Basophil Numbers and Function in Cpa3-Cre; Mcl-1fl/fl Mice. *Blood* **2011**, *118*, 6930–8.

197. Ginderachter, J. a Van; Beschin, A.; Baetselier, P. De; Raes, G. Myeloid-Derived Suppressor Cells in Parasitic Infections. *European journal of immunology* **2010**, *40*, 2976–85.

198. Oldford, S. a; Haidl, I. D.; Howatt, M. a; Leiva, C. a; Johnston, B.; Marshall, J. S. A Critical Role for Mast Cells and Mast Cell-Derived IL-6 in TLR2-Mediated Inhibition of Tumor Growth. *Journal of immunology (Baltimore, Md. : 1950)* **2010**, *185*, 7067–76.

199. Cheon, E. C.; Khazaie, K.; Khan, M. W. Mast Cell 5-Lipoxygenase Activity Promotes Intestinal Polyposis in APC Δ 468 Mice Mast Cell 5-Lipoxygenase Activity Promotes Intestinal. **2011**, 1627–1636.

200. Yang, Z.; Zhang, B.; Li, D.; Lv, M.; Huang, C.; Shen, G.-X.; Huang, B. Mast Cells Mobilize Myeloid-Derived Suppressor Cells and Treg Cells in Tumor Microenvironment via IL-17 Pathway in Murine Hepatocarcinoma Model. *PloS one* **2010**, *5*, e8922.

201. Huang, B.; Lei, Z.; Zhang, G.-M.; Li, D.; Song, C.; Li, B.; Liu, Y.; Yuan, Y.; Unkeless, J.; Xiong, H.; Feng, Z.-H. SCF-Mediated Mast Cell Infiltration and Activation Exacerbate

the Inflammation and Immunosuppression in Tumor Microenvironment. *Blood* **2008**, *112*, 1269–79.

202. El-Agamy, D. S. Targeting c-Kit in the Therapy of Mast Cell Disorders: Current Update. *European journal of pharmacology* **2012**, *690*, 1–3.

203. Hsu, C.-L.; Bryce, P. J. Inducible IL-33 Expression by Mast Cells Is Regulated by a Calcium-Dependent Pathway. *Journal of immunology (Baltimore, Md. : 1950)* **2012**, *189*, 3421–9.

204. Ribatti, D.; Crivellato, E. *The Controversial Role of Mast Cells in Tumor Growth.*; 1st ed.; Elsevier Inc., 2009; vol275.

205. Galli, S. J.; Tsai, M.; Piliponsky, A. M. The Development of Allergic Inflammation. *Nature* **2008**, *454*, 445–54.

206. Yang, X. D.; Ai, W.; Asfaha, S.; Bhagat, G.; Friedman, R. A.; Jin, G.; Park, H.; Shykind, B.; Diacovo, T. G.; Falus, A.; Wang, T. C. Histamine Deficiency Promotes Inflammation-Associated Carcinogenesis through Reduced Myeloid Maturation and Accumulation of CD11b+Ly6G+ Immature Myeloid Cells. *Nature medicine* **2011**, *17*, 87–95.

207. Pouw Kraan, T. C. van der; Snijders, a; Boeije, L. C.; Groot, E. R. de; Alewijnse, a E.; Leurs, R.; Aarden, L. a Histamine Inhibits the Production of Interleukin-12 through Interaction with H2 Receptors. *The Journal of clinical investigation* **1998**, *102*, 1866–73.

208. Elenkov, I. J.; Webster, E.; Papanicolaou, D. a; Fleisher, T. a; Chrousos, G. P.; Wilder, R. L. Histamine Potently Suppresses Human IL-12 and Stimulates IL-10 Production via H2 Receptors. *Journal of immunology (Baltimore, Md. : 1950)* **1998**, *161*, 2586–93.

209. Adams, W. J.; Lawson, J. a; Morris, D. L. Cimetidine Inhibits in Vivo Growth of Human Colon Cancer and Reverses Histamine Stimulated in Vitro and in Vivo Growth. *Gut* **1994**,

35, 1632–6.

210. Elliott, K. a; Osna, N. a; Scofield, M. a; Khan, M. M. Regulation of IL-13 Production by Histamine in Cloned Murine T Helper Type 2 Cells. *International immunopharmacology* **2001**, *1*, 1923–37.

211. Hallett, M. a; Venmar, K. T.; Fingleton, B. Cytokine Stimulation of Epithelial Cancer Cells: The Similar and Divergent Functions of IL-4 and IL-13. *Cancer research* **2012**, *72*, 6338–43.

212. Lebel-Binay, S.; Laguerre, B.; Quintin-Colonna, F.; Conjeaud, H.; Magazin, M.; Miloux, B.; Pecceu, F.; Caput, D.; Ferrara, P.; Fradelizi, D. Experimental Gene Therapy of Cancer Using Tumor Cells Engineered to Secrete Interleukin-13. *European journal of immunology* **1995**, *25*, 2340–8.

213. Rothe, M.; Quarcoo, D.; Chashchina, A. a; Bozrova, S. V; Qin, Z.; Nedospasov, S. a; Blankenstein, T.; Kammertoens, T.; Drutskaya, M. S. IL-13 but Not IL-4 Signaling via IL-4Rα Protects Mice from Papilloma Formation during DMBA/TPA Two-Step Skin Carcinogenesis. *Cancer medicine* **2013**, *2*, 815–25.

214. Jain, M.; Zhang, L.; He, M.; Patterson, E. E.; Nilubol, N.; Fojo, A. T.; Joshi, B.; Puri, R.; Kebebew, E. Interleukin-13 Receptor alpha2 Is a Novel Therapeutic Target for Human Adrenocortical Carcinoma. *Cancer* **2012**, *118*, 5698–708.

215. Hall, B.; Nakashima, H.; Sun, Z.-J.; Sato, Y.; Bian, Y.; Husain, S. R.; Puri, R. K.; Kulkarni, A. B. Targeting of Interleukin-13 Receptor α2 for Treatment of Head and Neck Squamous Cell Carcinoma Induced by Conditional Deletion of TGF-β and PTEN Signaling. *Journal of translational medicine* **2013**, *11*, 45.

216. Gabitass, R. F.; Annels, N. E.; Stocken, D. D.; Pandha, H. a; Middleton, G. W. Elevated

Myeloid-Derived Suppressor Cells in Pancreatic, Esophageal and Gastric Cancer Are an Independent Prognostic Factor and Are Associated with Significant Elevation of the Th2 Cytokine Interleukin-13. *Cancer immunology, immunotherapy : CII* **2011**, *60*, 1419–30.

217. Roth, F.; La Fuente, A. C. De; Vella, J. L.; Zoso, A.; Inverardi, L.; Serafini, P. Aptamer-Mediated Blockade of IL4Rα Triggers Apoptosis of MDSCs and Limits Tumor Progression. *Cancer research* **2012**, *72*, 1373–83.

218. Zhou, R.; Qian, S.; Gu, X.; Chen, Z.; Xiang, J. Interleukin-13 and Its Receptors in Colorectal Cancer (Review). *Biomedical Reports* **2013**, *1*, 687–690.

219. Ma, Y.; Hwang, R. F.; Logsdon, C. D.; Ullrich, S. E. Dynamic Mast Cell-Stromal Cell Interactions Promote Growth of Pancreatic Cancer. *Cancer research* **2013**, *73*, 3927–37.

220. Highfill, S. L.; Rodriguez, P. C.; Zhou, Q.; Goetz, C. a; Koehn, B. H.; Veenstra, R.; Taylor, P. a; Panoskaltsis-Mortari, A.; Serody, J. S.; Munn, D. H.; Tolar, J.; Ochoa, A. C.; Blazar, B. R. Bone Marrow Myeloid-Derived Suppressor Cells (MDSCs) Inhibit Graft-versus-Host Disease (GVHD) via an Arginase-1-Dependent Mechanism That Is up-Regulated by Interleukin-13. *Blood* **2010**, *116*, 5738–47.

221. Magazin, M.; Guillemot, J. C.; Vita, N.; Ferrara, P. Interleukin-13 Is a Monocyte Chemoattractant. *European cytokine network 5*, 397–400.

222. McKenzie, G. J.; Emson, C. L.; Bell, S. E.; Anderson, S.; Fallon, P.; Zurawski, G.; Murray, R.; Grencis, R.; McKenzie, A. N. J. Impaired Development of Th2 Cells in IL-13-Deficient Mice. *Immunity* **1998**, *9*, 423–432.

223. Zheng, Y.; Xu, M.; Li, X.; Jia, J.; Fan, K.; Lai, G. Cimetidine Suppresses Lung Tumor Growth in Mice through Proapoptosis of Myeloid-Derived Suppressor Cells. *Molecular immunology* **2013**, *54*, 74–83.

224. Valent, P.; Akin, C.; Arock, M.; Brockow, K.; Butterfield, J. H.; Carter, M. C.; Castells, M.; Escribano, L.; Hartmann, K.; Lieberman, P.; Nedoszytko, B.; Orfao, A.; Schwartz, L. B.; Sotlar, K.; Sperr, W. R.; Triggiani, M.; Valenta, R.; Horny, H.-P.; Metcalfe, D. D. Definitions, Criteria and Global Classification of Mast Cell Disorders with Special Reference to Mast Cell Activation Syndromes: A Consensus Proposal. *International archives of allergy and immunology* **2012**, *157*, 215–25.

225. Connolly, M. K.; Mallen-St Clair, J.; Bedrosian, A. S.; Malhotra, A.; Vera, V.; Ibrahim, J.; Henning, J.; Pachter, H. L.; Bar-Sagi, D.; Frey, A. B.; Miller, G. Distinct Populations of Metastases-Enabling Myeloid Cells Expand in the Liver of Mice Harboring Invasive and Preinvasive Intra-Abdominal Tumor. *Journal of leukocyte biology* **2010**, *87*, 713–25.

226. Ilkovitch, D.; Lopez, D. M. The Liver Is a Site for Tumor-Induced Myeloid-Derived Suppressor Cell Accumulation and Immunosuppression. *Cancer research* **2009**, *69*, 5514–21.

227. Munitz, a; Brandt, E. B.; Mingler, M.; Finkelman, F. D.; Rothenberg, M. E. Distinct Roles for IL-13 and IL-4 via IL-13 Receptor alpha1 and the Type II IL-4 Receptor in Asthma Pathogenesis. *Proceedings of the National Academy of Sciences of the United States of America* **2008**, *105*, 7240–5.

228. Condamine, T.; Kumar, V.; Ramachandran, I. R.; Youn, J.; Celis, E.; Finnberg, N.; El-deiry, W. S.; Winograd, R.; Vonderheide, R. H.; English, N. R.; Knight, S. C.; Yagita, H.; Mccaffrey, J. C.; Antonia, S.; Hockstein, N.; Witt, R.; Masters, G.; Bauer, T.; Gabrilovich, D. I. ER Stress Regulates Myeloid-Derived Suppressor Cell Fate through TRAIL-R – Mediated Apoptosis. *J Clin Invest* **2014**, *124*, 2626–2639.

229. Gabrilovich, D. I.; Nagaraj, S. Myeloid-Derived Suppressor Cells as Regulators of the

Immune System. *Nature reviews. Immunology* **2009**, *9*, 162–74.

230. Youn, J.-I.; Gabrilovich, D. I. The Biology of Myeloid-Derived Suppressor Cells: The Blessing and the Curse of Morphological and Functional Heterogeneity. *European journal of immunology* **2010**, *40*, 2969–75.

231. Yao, L.; Abe, M.; Kawasaki, K.; Akbar, S. M. F.; Matsuura, B.; Onji, M.; Hiasa, Y. Characterization of Liver Monocytic Myeloid-Derived Suppressor Cells and Their Role in a Murine Model of Non-Alcoholic Fatty Liver Disease. *PLoS ONE* **2016**, *11*, 1–16.

232. Siegel, A. M.; Stone, K. D.; Cruse, G.; Lawrence, M. G.; Olivera, A.; Jung, M.; Barber, J. S.; Freeman, A. F.; Holland, S. M.; O'Brien, M.; Jones, N.; Wisch, L. B.; Kong, H. H.; Desai, A.; Farber, O.; Gilfillan, A. M.; Rivera, J.; Milner, J. D. Diminished Allergic Disease in Patients with STAT3 Mutations Reveals a Role for STAT3 Signaling in Mast Cell Degranulation. *The Journal of allergy and clinical immunology* **2013**, *132*, 1388–96.

233. Odunsi, K.; Matsuzaki, J.; James, S. R.; Mhawech-Fauceglia, P.; Tsuji, T.; Miller, A.; Zhang, W.; Akers, S. N.; Griffiths, E. a; Miliotto, A.; Beck, A.; Batt, C. a; Ritter, G.; Lele, S.; Gnjatic, S.; Karpf, A. R. Epigenetic Potentiation of NY-ESO-1 Vaccine Therapy in Human Ovarian Cancer. *Cancer immunology research* **2014**, *2*, 37–49.

234. Toor, A. A.; Payne, K. K.; Chung, H. M.; Sabo, R. T.; Hazlett, A. F.; Kmieciak, M.; Sanford, K.; Williams, D. C.; Clark, W. B.; Roberts, C. H.; Mccarty, J. M.; Manjili, M. H. Epigenetic Induction of Adaptive Immune Response in Multiple Myeloma: Sequential Azacitidine and Lenalidomide Generate Cancer Testis Antigen-Specific Cellular Immunity. *British Journal of Haematology* **2012**, *158*, 700–711.

235. Terracina, K. P.; Graham, L. J.; Payne, K. K.; Manjili, M. H.; Baek, A.; Damle, S. R.; Bear, H. D. DNA Methyltransferase Inhibition Increases Efficacy of Adoptive Cellular

Immunotherapy of Murine Breast Cancer. *Cancer Immunology, Immunotherapy* **2016**, *65*, 1061–1073.

236. Mikysková, R.; Indrová, M.; Vlková, V.; Bieblová, J.; Símová, J.; Paracková, Z.; Pajtasz-Piasecka, E.; Rossowska, J.; Reinis, M. DNA Demethylating Agent 5-Azacytidine Inhibits Myeloid-Derived Suppressor Cells Induced by Tumor Growth and Cyclophosphamide Treatment. *Journal of leukocyte biology* **2014**, *95*, 1–11.

237. Daurkin, I.; Eruslanov, E.; Vieweg, J.; Kusmartsev, S. Generation of Antigen-Presenting Cells from Tumor-Infiltrated CD11b Myeloid Cells with DNA Demethylating Agent 5-Aza-2???-Deoxycytidine. *Cancer Immunology, Immunotherapy* **2010**, *59*, 697–706.

238. Kusmartsev, S.; Cheng, F.; Yu, B.; Nefedova, Y.; Sotomayor, E.; Lush, R.; Gabrilovich, D. All-Trans-Retinoic Acid Eliminates Immature Myeloid Cells from Tumor-Bearing Mice and Improves the Effect of Vaccination. *Cancer research* **2003**, *63*, 4441–9.

239. Sander, L. E.; Sackett, S. D.; Dierssen, U.; Beraza, N.; Linke, R. P.; Müller, M.; Blander, J. M.; Tacke, F.; Trautwein, C. Hepatic Acute-Phase Proteins Control Innate Immune Responses during Infection by Promoting Myeloid-Derived Suppressor Cell Function. *The Journal of experimental medicine* **2010**, *207*, 1453–64.

240. Savona, M. R.; Odenike, O.; Amrein, P.; Steensma, D.; Dezern, A.; Michaelis, L.; Faderl, S.; Lowder, J.; Taverna, P.; Oganesian, A.; Azab, M.; Garcia-manero, G. Phase 1 Dose-Escalation Study of ASTX727 , a Combination of the Oral Cytidine Deaminase Inhibitor (CDAi) E7727 with Oral Decitabine : Comparable Variability in Pharmacokinetics. **2016**, *126*, 7727.

241. Garcia-manero, G.; Roboz, G. J.; Savona, M. R.; Kropf, P. L.; Connell, C. L. O.; Walsh, K. J.; Lunin, S.; Tibes, R.; Rosenblat, T. L.; Griffiths, E. A.; Mace, J. OVERALL

SURVIVAL (OS) AND SUBGROUP RESULTS FROM A RANDOMIZED PHASE 2 STUDY OF SGI-110 (GUADECITABINE) IN PREVIOUSLY TREATED MYELODYSPLASTIC SYNDROMES (MDS). **2016**, *110*, 2016.

242. Kim, K.; Skora, A. D.; Li, Z.; Liu, Q.; Tam, A. J.; Blosser, R. L.; Diaz Jr., L. A.; Papadopoulos, N.; Kinzler, K. W.; Vogelstein, B.; Zhou, S. Eradication of Metastatic Mouse Cancers Resistant to Immune Checkpoint Blockade by Suppression of Myeloid-Derived Cells. *Proc Natl Acad Sci U S A* **2014**, *111*, 11774–11779.

243. Albeituni, S. H.; Ding, C.; Yan, J. Hampering Immune Suppressors: Therapeutic Targeting of Myeloid-Derived Suppressor Cells in Cancer. *Cancer journal* **2013**, *19*, 490–501.

244. Lee, J.-M.; Seo, J.-H.; Kim, Y.-J.; Kim, Y.-S.; Ko, H.-J.; Kang, C.-Y. The Restoration of Myeloid-Derived Suppressor Cells as Functional Antigen-Presenting Cells by NKT Cell Help and All-Trans-Retinoic Acid Treatment. *International Journal of Cancer* **2012**, *131*, 741–751.

245. Bronte, V.; Apolloni, E.; Cabrelle, A.; Ronca, R.; Serafini, P.; Zamboni, P.; Restifo, N. P.; Zanovello, P. Identification of a CD11b(+)/Gr-1(+)/CD31(+) Myeloid Progenitor Capable of Activating or Suppressing CD8(+) T Cells. *Blood* **2000**, *96*, 3838–46.

246. Narita, Y.; Wakita, D.; Ohkuri, T.; Chamoto, K.; Nishimura, T. Potential Differentiation of Tumor Bearing Mouse CD11b+Gr-1+ Immature Myeloid Cells into Both Suppressor Macrophages and Immunostimulatory Dendritic Cells. *Biomedical Research* **2009**, *30*, 7–15.

247. Caquard, M.; Ferret-Bernard, S.; Haurogné, K.; Ouary, M.; Allard, M.; Jégou, D.; Bach, J.-M.; Lieubeau, B. Diabetes Acceleration by Cyclophosphamide in the Non-Obese

Diabetic Mouse Is Associated with Differentiation of Immunosuppressive Monocytes into Immunostimulatory Cells. *Immunology letters* **2010**, *129*, 85–93.

Vita

Sheela Ruby Damle was born on March 24, 1986 in Fargo, North Dakota. She graduated from Red River High School in Grand Forks, North Dakota in 2004. She attended Cornell University and graduated with a Bachelor of Science in Chemical Engineering in 2008. After graduating, she worked as a research technician at the Hospital for Special Surgery for three years before matriculating in the MD-PhD program at Virginia Commonwealth University in 2011.